pennsylvania
DEPARTMENT OF TRANSPORTATION

Project Title:

Application of Non-Destructive Testing to Evaluate Unknown Foundations for Pennsylvania Bridges

FINAL REPORT

August 13, 2013

By: Joseph T. Coe, Ph.D. (PI)
Jonathan E. Nyquist, Ph.D. (co-PI)
Behnoud Kermani
Lorraine Sybrandy

Temple University

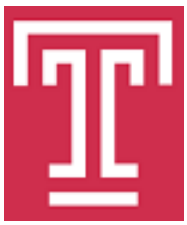

COMMONWEALTH OF PENNSYLVANIA
DEPARTMENT OF TRANSPORTATION

CONTRACT # 510801
WORK ORDER # TEM 002

1. Report No. FHWA-PA-2013-003-TEM 002	**2. Government Accession No.**	**3. Recipient's Catalog No.**
4. Title and Subtitle Application of Non-Destructive Testing to Evaluate Unknown Foundations for Pennsylvania Bridges		**5. Report Date** August 13, 2013 **6. Performing Organization Code**
7. Author(s) Joseph T. Coe (PI), Jonathan Nyquist (co-PI), Behnoud Kermani, Lorraine Sybrandy		**8. Performing Organization Report No.**
9. Performing Organization Name and Address Temple University 1947 N. 12th St. Philadelphia, PA 19122		**10. Work Unit No. (TRAIS)** **11. Contract or Grant No.** 510801, TEM 002
12. Sponsoring Agency Name and Address The Pennsylvania Department of Transportation Bureau of Planning and Research Commonwealth Keystone Building 400 North Street, 6th Floor Harrisburg, PA 17120-0064		**13. Type of Report and Period Covered** Final Report 12/14/2012 – 8/13/2013 **14. Sponsoring Agency Code**

15. Supplementary Notes

16. Abstract

Unknown bridge foundations present a unique challenge to Departments of Transportation (DOT) across the country since foundation characteristics are a necessary input to assess scour vulnerability and to develop appropriate scour countermeasures. A number of non-destructive testing techniques have evolved over time to address this challenge and evaluate unknown foundation type and geometry. The most comprehensive study of NDT methods for unknown foundations was performed as part of National Cooperative Highway Research Program (NCHRP) 21-05 in 2001. Since NCHRP 21-05 other case studies have expanded the literature and further advancements in computer software and hardware have improved NDT capabilities and reliability for unknown foundation evaluation. In particular, P-wave reflection imaging has the potential to provide higher resolution data and significantly more detail regarding the subsurface in both the laboratory and the field.

An ultrasonic P-wave reflection imaging system was investigated in this study as a viable NDT method to assess unknown foundations. The P-wave system was originally developed to image large scale soil models in the laboratory and to image the profile of vertically embedded structural elements such as foundations. The P-wave system was utilized in a field testing program to image the vertical profile of foundations at two bridge sites in southeastern Pennsylvania. Site selection, characteristics of the foundations tested, and the site soil conditions are summarized. The final foundation depths were unknown to the research team at the sites, which resulted in a true blind study and simulated the unknown foundation problem. The ultrasound probe was lowered in a PVC-cased borehole alongside the foundation to generate and record P-wave signals. The resulting data was plotted to construct an image and predict foundation characteristics. Multiple NDT techniques including Parallel Seismic, Borehole Magnetometer, and Borehole Radar were also performed at the sites in conjunction with the P-wave testing. The resulting data and interpretation of foundation characteristics are compared between all methods.

17. Key Words Unknown Foundations, Non-Destructive Testing, NDT, P-wave Reflection, Parallel Seismic, Borehole Radar, Magnetometer, Ground Penetrating Radar, Electrical Resistivity Imaging	**18. Distribution Statement** No restrictions. This document is available from the National Technical Information Service, Springfield, VA 22161

19. Security Classif. (of this report)	**20. Security Classif. (of this page)**	**21. No. of Pages**	**22. Price**
Unclassified	Unclassified	288	**N/A**

DISCLAIMER

This work was sponsored by the Pennsylvania Department of Transportation and the U.S. Department of Transportation, Federal Highway Administration. The contents of this report reflect the views of the authors, who are responsible for the facts and the accuracy of the data presented herein. The contents do not necessarily reflect the official views or policies of the Federal Highway Administration, U.S. Department of Transportation, or the Commonwealth of Pennsylvania at the time of publication. This report does not constitute a standard, specification, or regulation.

ACKNOWLEDGEMENTS

The financial and technical support provided by the Pennsylvania Department of Transportation (PennDOT) for this project is gratefully acknowledged. The authors would like to extend their sincere gratitude to the project manager Ms. Lisa Tarson for all her support throughout the project. The authors also appreciate all the time, helpful comments, and technical oversight offered by the technical advisors from District 6-0, Mr. Peter Berg and Ms. Sarah McInnes. The authors would also like to individually thank Mr. Bob Moyer and Mr. Charles Malson at TRC Drilling, Mr. Dennis Mills at Exploration Instruments in Austin, TX, and Ms. Amber Onufer with MALA Geoscience in Charleston, SC for their kind support of this project.

TABLE OF CONTENTS

LIST OF FIGURES

LIST OF TABLES

EXECUTIVE SUMMARY

Unknown bridge foundations present a unique challenge to Departments of Transportation (DOT) across the country since foundation characteristics are a necessary input to assess scour vulnerability and to develop appropriate scour countermeasures. A number of non-destructive testing techniques have evolved over time to address this challenge and evaluate unknown foundation type and geometry. The most comprehensive study of NDT methods for unknown foundations was performed as part of National Cooperative Highway Research Program (NCHRP) 21-05 in 2001. Since NCHRP 21-05 other case studies have expanded the literature and further advancements in computer software and hardware have improved NDT capabilities and reliability for unknown foundation evaluation. In particular, P-wave reflection imaging has the potential to provide higher resolution data and significantly more detail regarding the subsurface in both the laboratory and the field.

An ultrasonic P-wave reflection imaging system was investigated in this study as a viable NDT method to assess unknown foundations. The P-wave system was originally developed to image large scale soil models in the laboratory and to image the profile of vertically embedded structural elements such as foundations. The P-wave system was utilized in a field testing program to image the vertical profile of foundations at two bridge sites in southeastern Pennsylvania. The final foundation depths were unknown to the research team at the sites, which simulated the unknown foundation problem. The ultrasound probe was lowered in a PVC-cased borehole alongside the foundation to generate and record P-wave signals. The probe was successful in recording reflections from the piles, but the results were inconsistent and could not predict foundation characteristics. Multiple NDT techniques were also performed in conjunction with the P-wave testing. Of these methods, Parallel Seismic proved the least useful due to high traffic noise. Borehole Magnetometer obtained highly reproducible results. Borehole Radar was capable of imaging foundations that were farther than the one immediately adjacent to the PVC-cased borehole. Foundation depth predictions from these methods were negatively affected by inadequate depth of the borehole constructed at the two sites. GPR provided estimates of the foundation dimensions that were reasonable but not as accurate as had been anticipated due to clayey soils at the test sites. Finally, ERI showed tremendous promise as the only surface method capable of imaging the subsurface below the pile cap.

1. LITERATURE REVIEW

1.1 BRIDGE SCOUR AND UNKNOWN FOUNDATIONS

Proper design of bridge structures requires an appreciation for the possible failure mechanisms that can develop over the lifetime of the bridge. Many of these failure mechanisms are directly related to natural hazards. Due to the uncertainty associated with these natural hazards, regular inspection of bridge components is necessary to ensure long term integrity. This is especially true when considering the long-term effects of scour, which is the most common cause of bridge failures (Deng and Cai 2010). In a 30 year period prior to 1991, it was estimated that more than 1,000 bridges collapsed in the United States, and about 60% of those failures were related to scour of the bridge foundations (Shirhole and Holt 1991). In another study, bridge failures across the United States were compiled for the period of 1989 to 2000 from multiple sources, including the New York Department of Transportation (NYDOT) Bridge Safety Assurance Unit database, engineering journals and magazines, the websites of the Federal Highway Administration (FHWA) and multiple state Departments of Transportation (DOT), personal communications, and email contacts (Wardhana and Hadipriono 2003). During this time period 503 bridge failures were documented, of which more than 50% were attributed to flood and scour. In the past, the annual cost for scour-related bridge failures in the United States has been estimated at $30 million (Lagasse et al. 1997).

Scour is an erosion process that results from the flow of water along a stream, tidal waterway, or river (Figs. 1-1 – 1-3) (Arneson et al. 2012). The rate and total amount of scour depend on many factors related to depth of channel, water flow rate, soil erodibility, and geometry of any bridge substructure components. Typically, the total amount of scour at a bridge crossing is the sum of three primary components: (1) Degradation Scour, (2) Contraction Scour, and (3) Local Scour (Fig. 1-4). Degradation scour is the long-term drop in the overall streambed elevation due to a deficit in upstream sediment. Contraction scour results from constriction of the water flow in the vicinity of the bridge structure, which removes sediment material across all or most of the channel width. Local scour involves removal of sediment material from the immediate area around bridge piers, abutments, and embankments due to the vortices induced by these flow obstructions (Fig. 1-5). The scour process is cyclic in nature due to the dynamic processes involved (i.e. sediment shear stress equilibrium, flow continuity, etc.) (Haas et al. 1999). Thus

the total magnitude of scour can vary before, during, and after a flood event, and estimating this magnitude presents unique challenges to hydraulic engineers.

The FHWA implemented the National Bridge Inspection Standards (NBIS) in 1967 in response to the collapse of the Silver Bridge over the Ohio River near Gallipolis, Ohio and Point Pleasant, West Virginia (Olson 2005a). The resulting Federal-Aid Highway Act of 1968 established the NBIS as a means to ensure the safety of the traveling public (FHWA 2004). The NBIS sets federal requirements for bridge owners (typically state DOTs) to maintain an inspection program to evaluate, rate, and manage operations of highway bridges. The resulting information is tabulated as part of the National Bridge Inventory (NBI) (FHWA 1995). According to data compiled in the NBI, approximately 500,000 bridges are located over waterways across the United States. Since it statistically likely that hundreds of these bridges may be subject to major flood events on a given year, scour is a major design concern for these bridges. As a result, a scour evaluation program was incorporated into the NBIS (FHWA 1988). The FHWA technical advisory (TA) that established this scour evaluation program provides guidance on new bridge designs, evaluation of scour vulnerability for existing bridges, scour countermeasures, and improving estimates of scour at bridges. Over 90% of state DOT bridges have been evaluated for scour in compliance with the NBIS (Arneson et al. 2012). These scour evaluations have been conducted based on interdisciplinary studies by bridge, hydraulic, and geotechnical engineers. The resulting ratings for each bridge are cataloged under Item 113, Scour Critical Bridges, in the NBI. A risk-based Plan of Action (POA) must be developed by the state DOT for any bridges categorized as “Scour Critical” under Item 113 (e.g. Stein and Sedmera 2006). The POA establishes guidelines for bridge-specific inspection type and frequency, monitoring of scour, potential installation of scour countermeasures, and instructions for bridge closures if necessary.

A key input for evaluation of scour potential is information regarding the bridge substructure (i.e. piers, abutments, foundations, etc.). However, there are more than 40,000 bridges across United States with unknown foundations as of 2011 (Arneson et al. 2012). Generally for these bridges there are no design plans or as-built plans available to reveal foundation type, depth, or geometry. In some cases there is limited knowledge concerning the structural and geotechnical load capacity or the long-term condition of the foundation elements. Many of these bridges are

categorized as “off-system” bridges, which were constructed and owned by county and local municipalities, and were later state-owned (Briaud et al. 2012). The distribution of unknown foundation bridges varies widely by state as does the percentage of bridges with unknown foundations supporting principal arterials (i.e. high traffic roads) (Stein and Sedmera 2006).

Bridges with unknown foundations present a unique challenge to state DOTs as the foundation characteristics are a necessary input to assess scour vulnerability and to develop appropriate scour countermeasures. Initially these bridges were exempt from being directly assessed for their scour vulnerability and were coded as “U” under Item 113 in the NBI. However, the FHWA released a series of memorandums in 2008 and 2009 that altered this policy to reduce the number of unknown foundation bridges (Gee 2008, Lwin 2009a, and Lwin 2009b). As of November 2010, any bridges coded as “U” in the NBI is considered “Scour Critical” and subject to development of an appropriate POA. The bridge can be re-categorized if the foundation properties are determined (e.g. field reconnaissance, review of bridge reports, etc.), if properly designed scour countermeasures are implemented, or if the bridge is closed.

1.2 UNKNOWN FOUNDATIONS IN THE COMMONWEALTH OF PENNSYLVANIA

Based on information provided by District 6-0 of the Pennsylvania Department of Transportation (PennDOT), there are 31,645 bridges in the Commonwealth of Pennsylvania (Abboud and Kaiser 2012). Of these bridges 27,036 are located over water and 11,409 are considered scour critical. Of the scour critical bridges, 11,201 have insufficient information regarding bridge substructure and can be classified as unknown foundation bridges. For example, in District 6-0 there are 1,087 bridges with unknown foundations (325 in Bucks county, 339 in Chester County, 268 in Montgomery County, and 28 in Philadelphia County) (Abboud and Kaiser 2012). Thus unknown foundation bridges pose a significant concern for PennDOT in light of the FHWA policies to treat unknown foundations as scour critical.

1.3 EVALUATION OF UNKNOWN FOUNDATIONS

The policies implemented by the FHWA regarding reduction of unknown foundation bridges has prompted state DOTs to explore various methods to determine the foundations for these bridges, either directly through field testing or indirectly by other methods. Additionally, risk-

based approaches have been implemented by several states to prioritize their investigations based on the results of National Cooperative Highway Research Program (NCHRP) Project 24-25. In this study, Stein and Sedmera (2006) presented a broad strategy to identify which unknown foundation bridges were most critical based on anticipated risk and cost of failure. Recommendations included field reconnaissance to evaluate foundations for high priority bridges and for other critical bridges that did not meet a minimum performance level. A cost-benefit analysis should be performed for low-risk bridges to determine if scour countermeasures or automated monitoring systems are warranted. McLemore et al. (2010) summarized the experience of the Florida Department of Transportation (FDOT) with this risk-based method and demonstrated how it could be modified to incorporate the unique database of bridges for a particular state.

1.3.1 Experimental Approaches

Previous risk-based studies demonstrated that some percentage of unknown foundation bridges will possibly qualify for aggressive management plans, which typically involve determination of foundation properties to assess scour vulnerability or to properly design scour countermeasure systems. Experimental approaches which rely on field reconnaissance are the most common methods by which unknown foundation properties are determined. Excavation to expose a full-depth portion of a bridge foundation is the most direct and accurate method of these experimental approaches. However, excavation procedures are cost-prohibitive, typically require access to barges, can be hazardous to the workers, and can possibly undermine the foundation under investigation (Olson et al. 1998). Other conventional testing methods (e.g. coring, probing, etc.) suffer similar limitations and are typically avoided for most unknown foundation evaluations (Table 1-1). As a result of these issues, positive discovery of unknown bridge foundations has traditionally been accomplished by non-destructive testing techniques.

1.3.1.1 The Role of Non-Destructive Testing (NDT) For Transportation Infrastructure

Non-Destructive Testing (NDT) or Non-Destructive Evaluation (NDE) techniques are a broad category of methods that indirectly measure properties of a physical system without causing damage to it. Evaluation of the system properties is based on the measured response of the physical system to some stimulus (e.g. stress waves, electromagnetic radiation, etc.). NDT methods are routinely utilized across multiple measurement scales in fields ranging from

medicine (e.g. medical ultrasound) and manufacturing (e.g. testing of welds) to the geo-sciences (e.g. geophysical exploration of the Earth's composition). NDT techniques are often utilized in civil engineering for the assessment of transportation infrastructure. Example applications include: integrity testing of known pile and drilled shaft foundations (e.g. GI Deep Foundations Committee Task Force 2000); quality assurance (QA) of pavement construction (e.g. Von Quintus et al. 2009); assessment of cracks in structural concrete (e.g. ACI 1998); subsurface soil investigations (e.g. Wightman et al. 2003); and structural health monitoring (e.g. Hsieh et al. 2006).

1.3.1.2 The Role of Non-Destructive Testing (NDT) for Unknown Foundations

The policies implemented by the FHWA to consider unknown foundation bridges as "Scour Critical" prompted a resurgence of studies regarding NDT methods to address deficiencies in predictions of foundation characteristics. Many of these NDT methods originated from other fields or were adapted from other applications within civil engineering and transportation infrastructure inspection. The most comprehensive of NDT studies for unknown foundations was initiated by NCHRP Project 21-05 and summarized by Olson et al. (1998) and Olson and Aouad (2001). The initial study consisted of a summary of current and emerging NDT techniques and their applicability to unknown foundation inspection. Limited field testing and numerical modeling of these techniques were also performed. The focus was on determining the reliability of NDT to provide accurate evaluation of unknown foundation characteristics, including type, geometry, and depth. The field testing was performed at multiple bridges with known foundations in Colorado, Alabama, and Texas with all methods that were considered state-of-practice at the time. The study also augmented these results using case histories from consulting projects at bridges in the state of Connecticut with unknown foundations. The advantages and limitations of each method were discussed in the context of providing information regarding unknown foundations. The second phase focused on the methods that had proven more robust and reliable based on the field results of the first phase. This second study consisted of multiple "blind" field tests at 21 bridge sites in North Carolina, Minnesota, New Jersey, Michigan, Oregon, Massachusetts and Colorado. General recommendations were provided to bridge owners regarding suitability of NDT methods based on anticipated foundation type, subsurface soils, and site conditions. Since NCHRP Project 21-05, several other projects have been completed that have advanced the state-of-practice for unknown foundation NDT methods and

have added to the body of knowledge through case histories. The results of NDT studies to address the issue of unknown foundations are summarized in the following sections along with a description of the various NDT techniques utilized.

1.3.1.3 Surface NDT Methods

Surface NDT methods are applied at or near the ground surface from an accessible area of the foundation element (Wightman et al. 2003). They are typically the most robust from a site access standpoint since the only major requirement is the ability to locate instruments either on an exposed area of the foundation directly or on a member connected to the foundation (e.g. bridge pier). However, due to their placement at the ground surface, many surface NDT methods suffer from complications related to complex substructures (e.g. pile caps, grade beams, etc.). Surface NDT methods were some of the first to be implemented for unknown foundations as many were a logical extension of methods used for pile integrity testing and geophysical methods utilized in subsurface investigations. The following surface NDT methods for unknown foundations will be discussed: Sonic Echo/Impulse Response, Bending Waves, Ultraseismic, Spectral Analysis of Surface Waves, Ground Penetrating Radar, Dynamic Foundation Response, and Electrical Resistivity Imaging/Induced Polarization.

1.3.1.3.1 Sonic Echo/Impulse Response

The Sonic Echo/Impulse Response (SE/IR) method was adapted from similar testing for quality assurance of the condition and integrity of newly constructed piles and drilled shafts (e.g. Rausche et al. 1988, Finno and Gassman 1998, Olson et al. 1998, Briaud et. al 2002, ASTM D5882-07). The test is based on the principle that longitudinal stress (i.e. acoustic) waves will reflect at interfaces between materials with significant changes in acoustic impedance (a measurement of the stiffness of the material) (Fig. 1-6). It consists of impacting a deep foundation with a hammer and measuring the reflected waves from the bottom using a receiver (accelerometer or vertical geophone) attached to the top of the foundation (Figs. 1-7 – 1-8). If the top of the foundation is inaccessible, the side can be impacted and the reflection measured by two receivers at different elevations on the opposite side (to distinguish reflections from above or below the test location) (Fig. 1-9). An accurate estimate of the wave velocity of the foundation material is important to obtain quality predictions and can be accomplished through direct measurements with side-mounted receivers. The SE method interprets the resulting

reflection data in the time domain (Fig. 1-10). The foundation depth is determined based on the time separation between successive reflection events (e.g. first arrival and first multiple reflection, etc.). The IR method examines the reflection data in the frequency domain (Fig. 1-11). Multiple reflections from the foundation bottom are observed as evenly spaced frequency peaks in the plot of the mobility transfer function (i.e. wave velocity divided by impact force). Other names for the SE method include Seismic Test, Sonic Test, Pile Integrity Test, Echo Test, Impulse Echo, Impact Echo, and Pulse Echo. The IR method is also often referred to as Sonic Mobility, Transient Dynamic Response, Impulse Response Spectrum, and Impedance Method.

Multiple studies have explored the application of SE/IR to assess unknown foundations. Olson et al. (1998) discussed the application of SE/IR during NCHRP Project 21-05 where it was utilized at every bridge during the first phase study with mixed results (Table 1-2). Olson et al. (1998) noted that reflections could be affected by the presence of beams and columns in the bridge substructure and that damping of the signals in steel piles was considerable enough to prevent reflections from reaching the top of the piles. SE/IR fared worse during the second phase of NCHRP Project 21-05, where it proved inconclusive in 14 out of 15 bridges tested during blind studies (Olson and Aouad 2001) (Table 1-3). Hertlein and Walton (2000) and Hertlein and Walton (2007) discussed the application of IR to three case histories where old unknown foundations were evaluated for potential reuse in rehabilitated structures. In one project IR was utilized in conjunction with soil borings to make predictions about the anticipated capacity of concrete shaft foundations to be reused for a baseball stadium expansion. Another application involved the estimation of shaft length with IR to determine the bearing layer for old shaft foundations that would be reused for a newly developed high rise (Block 37, Chicago). Finally, IR was also utilized to estimate timber pile depth and capacity for rehabilitation efforts of shore protection structures along the southwest shore of Lake Michigan. In each case, IR was successful in evaluating unknown foundation lengths and provided significant project savings through foundation reuse. More recently, Yu et al. (2007) successfully utilized SE in conjunction with other methods to estimate the length of unknown Auger Cast-in-Place (ACIP) piles to determine their capacity and suitability for an expansion plan at St. Joseph Hospital in Savannah, GA. Robinson & Webster (2008) summarized their experiences using SE as consultants with the North Carolina Department of Transportation (NCDOT) for their unknown bridge foundation evaluations. They found that SE was generally successful for timber and concrete piles, but

proved inconclusive for a number of steel piles because they were often encased in concrete at and below the water line. Hossain et al. (2011) unsuccessfully utilized SE in conjunction with subsurface techniques to evaluate the depth of steel H-piles at a bridge in Texas as part of a blind study of NDT techniques for the Texas Department of Transportation (TxDOT).

As noted in the case histories, SE/IR has had an inconsistent success rate in accurately predicting foundation length. Contributing to this mixed record are several shortcomings which limit applicability of SE/IR to unknown foundations (Table 1-4). Chief among these is the inability to resolve reflection wave arrivals for complex substructures and soil profiles (Hertlein and Watson 2007). For example, pier crossbeams, splices in piles, and pile caps often dominate the reflection records and mask any reflected energy from foundation bottoms (McLemore et al. 2010, Olson and Aouad 2001). Also, soil stiffness plays a role in damping of the wave energy as it travels through the foundation. For piles with length to diameter ratios of approximately 20:1 or larger, very little, if any, reflection energy from the bottom will be read at the surface in stiff soil profiles due to damping of the acoustic waves (Olson and Aouad 2001). As noted in the case studies in Olson et al. (1998), Olson and Aouad (2001), and Hertlein and Walton (2007), the situation is even worse for steel piles that often have much larger surface areas for damping to occur.

Data acquisition for an SE/IR test can be performed quickly (e.g. 15 - 30 minutes for a 2-person crew) and it is also a relatively inexpensive method (e.g. $4,500 - $11,400 per test, see Table 1-5). A commercial SE/IR system can be assembled for approximately $10,000 to $20,000 (Olson and Aouad 2001) and training of DOT personnel with such a system is estimated to require anywhere from a few days to two weeks (costs not included in equipment total). Site access constraints (e.g. vegetation, steep slopes, location over waterways, etc.) present minimal challenges as limited equipment is necessary, and the equipment that is required has a small footprint and is portable. It is necessary however to have direct access to an exposed substructure surface to directly mount the receiver (e.g. Fig. 1-9) and background sources of acoustic wave energy (e.g. traffic noise) should be minimized.

1.3.1.3.2 Bending Waves

The Bending Waves (BW) method was originally developed to evaluate the length of unknown timber piles (Douglas and Holt 1994, Holt and Douglas 1994). The test setup is similar to the SE/IR method but uses flexural (i.e. bending) waves instead of longitudinal waves (Figs. 1-12 – 1-13). Instrumentation consists of two receivers mounted at a fixed gage length on the same side of a foundation. Identical equipment is often utilized for both the SE/IR and BW methods. The main difference between the SE/IR and BW methods lies in the highly dispersive nature (i.e. wave velocity is a function of wavelength) of flexural waves in long members such as piles (Olson and Aouad 2001). The flexural wave reflections are post-processed using the Short-Kernel Method (SKM) of analysis. Essentially, this method computes the cross-correlation (i.e. the similarity between two waveforms) of the received signals with respect to a "Kernel Seed" of 1-cycle period functions ranging in frequencies from approximately 500 Hz to 4000 Hz (Douglas and Holt 1994, Holt and Douglass 1994). The dispersive relationship between flexural wave velocity and wavelength is developed by computing the flexural wave velocity for each kernel seed frequency. The flexural wave velocities are then utilized to compute the distance to the pile bottom based on the amount of time it took the receivers to record the reflected signals.

A number of studies have demonstrated the applicability of the BW method to unknown foundations. Douglas and Holt (1994) and Holt and Douglas (1994) summarized the results from a large NCDOT study of timber piles in the mid 1990's. Forty timber piles ranging in length from 6 ft to 60 ft (1.8m to 18.3 m) were testing using BW. Of the forty piles tested, twenty six allowed an assessment of the BW length predictions based on pile records or after the piles were pulled from the ground. Douglas and Holt (1994) found that the accuracy of length predictions varied in the range of at approximately ±10%. Olson et al. (1998) explored the use of BW as part of the first phase NCHRP Project 21-05 study and attempted the method at one bridge site in Colorado. A single timber pile was tested and the resulting prediction using BW agreed well with SE/IR. During the second phase of NCHRP Project 21-05, the BW method was further examined in conjunction with multiple NDT methods. Olson and Aouad (2001) found that BW results were inconclusive during the blind field tests performed at 7 timber bridge sites (Table 1-3). Mercado and O'Neill (2000) also utilized the BW method in conjunction with subsurface methods on concrete piles of known length at one bridge site in the Houston, Texas area. For this case study, BW (denoted as Transient Forced Vibration Survey) over predicted the concrete pile length by approximately 8%, which was the worst of the predictions. Mercado and O'Neill (2000) also

noted that the BW method was one of the easiest methods to perform in the field, but required a high demand for data post-processing. Stegman and Holt (2000) summarized three case histories where BW and other NDT techniques were utilized to estimate foundation integrity and the capacity of piles after lengths were evaluated and compared to soil boring information. In the first case, BW was used to estimate the thickness of the abutments for an old railroad bridge foundation. The BW results confirmed the back abutment wall was vertical but that the concrete was deteriorated (i.e. numerous "early" reflections in BW results). In the second case, BW was used to evaluate the length of monotube piles for an existing water tank. In the final case, timber piles were tested with BW and later extracted from the ground to compare foundation length predictions. The project team was unaware of the foundation characteristics prior to BW testing which resulted in a true blind study. Comparison of the predicted lengths from BW to the actual pile lengths only showed an error of approximately 7% (Stegman and Holt 2000). Moreover, BW was able to predict the location of fractures in the piles as a result of the extraction process.

Based on the results reported in the literature, length predictions within approximately 10% of actual values have been attained with BW. However, the results have been mixed and most studies have primarily been applied on long, slender timber pile foundation elements. One of the main limitations of BW is the highly attenuative behavior of flexural waves in comparison to longitudinal waves. Theoretical studies in Olson et al. (1998) have shown that flexural waves will not reach receivers at the surface of a 12 meter long, 1 meter diameter concrete shaft if the shaft is embedded more than 5 m (16.4 ft). Stiff soil layers can result in a "false bottom" prediction (i.e. shorter pile length predictions) and reflections from the top surface of the foundation can make data interpretation more difficult. Finally, BW is unable to distinguish piles beneath pile caps much like SE/IR and other surface NDT methods (Table 1-4). The main advantages of the BW method are similar to the SE/IR method (i.e. fast, inexpensive, no borings necessary, etc.).

BW can be performed quickly (e.g. 15 - 30 minutes for a 2-person crew) and is a relatively inexpensive method (e.g. $4,500 - $11,400 per test, see Table 1-5). Since the BW and SE/IR tests share system components, it is conceivable that combined testing could be performed at only a slight increase in equipment rental expenses relative to individual tests. A custom test system

for BW is estimated on the order of $15,000 to $20,000 and field training with such a system is estimated to take anywhere from a few days to two weeks (Olson and Aouad 2001). As in SE/IR, site access constraints (e.g. lack of vegetation, steep slopes, location over waterways, etc.) present minimal challenges for BW since the required equipment is limited in footprint. Like SE/IR it is necessary to have direct access to an exposed substructure surface to directly mount the receivers (e.g. Figs. 1-12 – 1-13) and background acoustic noise should be minimized.

1.3.1.3.3 Ultraseismic

The Ultraseismic (US) method was developed as part of the NCHRP Project 21-05 study in response to the limitation of the SE/IR and BW methods to non-columnar substructures (Olson et al. 1998). US detects reflections of both longitudinal (vertical hammer impact) and flexural (horizontal hammer impact) wave energy from the bottoms of foundations much like SE/IR and BW. However, a larger number (3+) of multi-channel receivers are utilized (e.g. 3-component geophones, accelerometers) (Figs. 1-14 – 1-15). The US test setup is essentially a smaller scale geophysical seismic reflection survey which uses the bridge substructure as the medium for wave propagation (Wightman et al. 2003). US can be performed to obtain a vertical profile for a one-dimensional (1-D) image of the foundation depth or it can be performed in the horizontal direction for a two-dimensional (2-D) image. In vertical profiling, the geophones are placed at regular intervals in the downward direction on an exposed substructure surface (Fig. 1-16). Horizontal profiling places the geophones at regular intervals along the top fact of an exposed substructure surface (i.e. at the same elevation) (Fig. 1-17). This is more useful for massive abutment and wall-type substructures with longer top or side surfaces. The data is post-processed with techniques adapted from geophysical explorations (e.g. automatic gain control, signal stacking, migration, source deconvolution, etc.) due to the similarity in data acquisition techniques (Wightman et al. 2003).

Tables 1-3 and 1-6 summarize the results of US testing in NCHRP Project 21-05, in which the US method was originally developed (Olson et al. 1998, Olson and Aouad 2001). The results demonstrate that US has a higher success rate and is a more robust method compared to SE/IR and BW. Despite the potential of the US method, very little case history data can be found in the literature outside of NCHRP Project 21-05. However, many references to US are available in publications ranging from FHWA manuals to state DOT bridge inspection manuals (e.g.

Wightman et al. 2003, Indiana DOT 2010). Proceedings from the Unknown Foundations Summit in Lakewood, Colorado sponsored by the FHWA in 2005 also contain presentations with example US data from consulting projects. This signifies that state DOTs and bridge owners are exploring use of US for unknown bridge foundations. It is likely that case histories have not found their way to the literature at this point and this will occur as the engineering community acquires more experience with US testing.

As previously noted, US was developed to address the limitations of SE/IR and BW. The use of multiple receivers allows greater confidence when interpreting reflected waveforms from complex substructures. The additional data can minimize noise from attached substructure reflections and can distinguish waves traveling in the upward and downward directions (Wightman et al. 2003). However, there are limitations to US testing (Table 1-4). Despite its capabilities to resolve more complex substructures (e.g. abutment walls), US is still unable to detect piles beneath pile caps (Olson and Aouad 2001). Moreover, as US relies on the propagation of longitudinal and flexural waves through the foundation, wave damping effects of stiff soils still play a major role in the ability to receive signals from the foundation bottom. Finally, the US test requires access to a vertical face of approximately 4 ft or more to attach the multiple receivers.

The US test is similar in costs to SE/IR (e.g. $4,500 - $11,400 per test, see Table 1-5) and is only slightly slower to perform (i.e. 1 hour for a 2-person team). The increase in test time results from the multiple receivers that must be attached to the bridge substructure. Due to the similarity in equipment, combined testing could be performed with US, BW, and SE/IR at only a modest increase in equipment rental expenses relative to individual tests. Commercial systems exist that combine US, SE/IR, and BW and they range in cost from $30,000 to $35,000 (Olson and Aouad 2001). This range represents only a modest increase compared to a standalone US system (e.g. $20,000) and is more cost effective than purchasing separate standalone US, SE/IR, and BW systems. If a state DOT wishes to purchase their own hardware to perform testing, training will be necessary for their field engineers (up to 2 weeks with hands on exercises at suitable bridge sites). US has few constraints on site access (e.g. lack of vegetation, steep slopes, location over waterways, etc.) since the required equipment is portable. However, US requires direct access to an exposed substructure surface with a slightly larger footprint than the SE/IR

and BW methods due to the multiple receivers utilized during testing (i.e. compare Figs. 1-8, 1-13, and 1-15). As with SE/IR and BW, background acoustic noises should be minimized.

1.3.1.3.4 Spectral Analysis of Surface Waves

The Spectral Analysis of Surface Waves (SASW) method originated as a technique to determine the thickness and shear wave velocities of subsurface soils in response to limitations of traditional geophysical exploration methods such as seismic reflection or seismic refraction (Heisey et al. 1982, Stokoe et al. 1988, Stokoe et al. 1990). The test consists of a source of seismic waves (e.g. impact hammer, Vibroseis, etc.) and a pair of receivers (e.g. 3-component geophone) (Fig. 1-18). The receivers are spaced equidistant and the first receiver is located at the same distance from the source as the space between both receivers (Fig. 1-19). Rayleigh (i.e. surface) wave energy is imparted into the domain and recorded using a signal analyzer (e.g. seismograph). The process is repeated for multiple receiver spacings, which allows for calculation of a dispersion curve (i.e. wave velocity versus frequency) after post-processing of the data in the frequency domain. Computer algorithms are used to iteratively match a theoretical dispersion curve to the experimental results in a process known as forward modeling, which results in a soil velocity profile.

The majority of references to SASW testing discuss the evaluation of subsurface soil profiles for the purposes of seismic ground response analysis (e.g. Marosi and Hiltunen 2004, Comina et al. 2011). However, SASW has found other civil engineering applications such as analysis of pavement systems (e.g. Nazarian and Stokoe 1984) and characterization of municipal solid waste (Matasovie and Kavazanjian 1998). Olson and Aouad (2001) evaluated the applicability of SASW to characterizing unknown foundations as part of NCHRP 21-05. In the case of unknown foundations, the bottom depth is indicated by slower velocities of the surface waves in the underlying soils. However, only limited field studies were performed in NCHRP 21-05. The results showed good agreement for depth measurements of concrete abutments for two bridges in Connecticut but were inconclusive for a bridge in New Jersey and in Michigan. Olson and Aouad (2001) noted that SASW was suitable for more massive substructures that extend significantly in the lateral direction and have a ledge for testing access.

As previously discussed, the principal role of SASW in civil engineering is characterization of shear wave velocity profiles for subsurface soils. However, it shows some potential for evaluating massive substructures such as abutments. The primary limitation of SASW for unknown foundations is that a large flat surface is necessary to perform the testing (Table 1-4). As a result, bridge substructures with very deep dimensions relative to length may not allow the generation of the longer wavelengths necessary to reach the bottom of the foundation and resolve the velocity contrast with the underlying soils (Olson and Aouad 2001). Moreover, SASW is unable to resolve the depth and location of piles beneath pile caps.

SASW may take several hours to perform because the receivers must be repositioned after each seismic excitation to allow for a range of investigation depths. As a result it may only be possible to perform 1 - 2 tests at a given site per day. SASW costs are the same as other elastic wave methods (e.g. $4,500 - $11,400 per test, see Table 1-5), but again total number of tests are limited daily by the amount of set up time. A commercial SASW system is approximately $20,000 (Olson and Aouad 2001). However, SASW does share components with SE/IR, BW, and US, and a combined system could be assembled to perform all four tests. Such a combined field system would be less expensive (i.e. $35,000 to $40,000) to purchase compared to purchasing each individual system separately (Olson and Aouad 2001). SASW is applicable over a broad range of soil conditions and has been utilized on materials ranging from hot-mix asphalt (e.g. Nazarian and Stokoe) and municipal solid waste (e.g. Matasovie and Kavazanjian 1998) to extremely heterogeneous glacial till (Molnar et al. 2007). Site conditions can be a concern since it is necessary to have direct access to a large flat exposed substructure surface to directly mount the receivers. This may not be possible due to site easements, steep slopes, or presence of water. Limited studies have demonstrated the viability of the SASW method to characterize offshore sediments in remote deep waters (Luke and Stokoe 1998), though it remains to be seen how this application would transfer to characterizing unknown foundations.

1.3.1.3.5 Ground Penetrating Radar

Ground Penetrating Radar (GPR) is a method that has its roots in geophysical subsurface exploration, particularly with regards to detecting and mapping subsurface archaeological artifacts and stratigraphy. This method employs a surface antenna which radiates electromagnetic waves at very-high frequencies (VHF) to ultra-high frequencies (UHF) in the

microwave range (i.e. 30 MHz to 3000 MHz) (Fig. 1-20). Wave reflections are generated at the boundaries between materials with different dielectric constants, which allows the generation of images of the domain under investigation (Fig. 1-21). Different antennas provide the ability to adjust the frequency range of interest. Lower frequency antennas allow greater investigation depths at the cost of decreased resolution. Higher frequency antennas provide much better resolution but the electromagnetic waves do not penetrate as far and only allow limited investigation depths. GPR is the electromagnetic counterpart to stress-wave methods such as seismic reflection/refraction (and by extension SE/IR).

GPR has found numerous engineering applications including pavement assessment (Leng et al. 2009), monitoring of stream channel height for scour estimations (Haeni et al. 1992, Anderson et al. 2007), determination of subsurface soil water content (Huisman et al. 2003), location of buried shallow utilities (Wightman et al. 2003), integrity assessment of steel rebar in bridge decks (Parrillo et al. 2005), and mapping of karst topography (McLemore et al. 2010). As a tool for unknown foundation assessment, GPR has seen relatively little use primarily because it is unable to detect any information regarding the foundation element beneath pile caps. However, Olson and Aouad (2001) summarized GPR results as part of NCHRP Project 21-05 and observed that GPR was particularly useful when estimating the stem widths of bridge abutments. Stegman and Holt (2000) utilized GPR to confirm that an old railroad bridge abutment consisted of a tapered pedestal instead of a traditional footing. Thus GPR is useful as a means to detect whether a bridge pier is underlain by a cap/footing or by a single columnar foundation (e.g. drilled shaft). GPR was also used in Stegman and Holt (2000) to estimate the thickness of the abutments for the bridge in conjunction with BW.

There are many documented limitations with GPR (Table 1-4). As noted previously, it is unable to resolve any information beneath a pile cap or footing. Penetration of the electromagnetic signals is affected by the frequency of the signals as well as the electrical resistivity of the soils. Clayey soils and the presence of water (particularly salt or brackish water) can severely limit the depth of investigations to as little as a few centimeters (Wightman et al. 2003). Low frequency antennas are typically unshielded (i.e. electromagnetic energy radiates in all directions) and can result in reflections from power lines, other buildings, and even the bridge deck itself. These reflected signals may complicate data interpretation. Despite these issues, GPR can be a

convenient tool to make a preliminary assessment regarding the presence and geometry of a pile cap. For subsurface NDT methods, there are often limits placed on the proximity of the borehole to the foundation elements. GPR can be used to guide selection of borehole placement to avoid any potential pile caps and to maximize potential data quality from subsurface NDT methods.

The GPR test is slightly more expensive than other surface tests (e.g. $6,000 - $14,000 per test, see Table 1-5) primarily due to the higher costs of the specialized equipment. Depending on the desired antenna frequency, GPR systems can range in cost from $30,000 to as much as $80,000 (Olson and Aouad 2001). Estimated training time with a GPR system can approach one week. Depending on the dimensions of the investigation area, the rate of data collection can be somewhat slower than SE/IR, BW, and US, but typically faster than SASW (i.e. 1 - 2 hours for a 2-person team). There are few constraints on site access as GPR systems are portable and robust. They can be utilized on relatively steep slopes as long as the operator can propel the system and maintain good contact between the antenna and ground surface. GPR systems are also available for use over water. However, dense vegetation can diminish signal strength, frequency, and directivity if it causes the GPR antenna to uncouple from the ground surface (Shaari et al. 2003).

1.3.1.3.6 Dynamic Foundation Response

The Dynamic Foundation Response (DFR) Method was developed in reaction to the fact that at the time no surface NDT methods were capable of distinguishing between shallow spread footing foundations from deep foundations on pile caps (Olson et al. 1998). DFR relies on the concept that the dynamic response of a bridge substructure is affected by the characteristics of the underlying foundations. Shallow foundations should exhibit lower peak resonant frequency responses compared to deep foundations which are more rigid. These concepts have a sound theoretical connection to research in the area of soil dynamics and vibration analysis of foundations subjected to earthquake loading (e.g. Novak 1976, Novak and Aboul-Ella 1978). DFR relies on the excitation of the bridge substructure and measurements of the corresponding resonant frequencies using multiple accelerometers (Fig. 1-22). The excitation source can be as simple as a sledgehammer or a vehicle crossing the bridge to a large tunable truck-mounted geophysical vibrator (i.e. Vibroseis truck) (Fig. 1-23). The dynamic response of the substructure is compared to the input in order to develop transfer functions which illustrate the modal

response of the substructure and the corresponding resonant frequencies. This information is then used to infer foundation type (i.e. deep versus shallow).

Several studies have explored DFR as a means to assess foundation characteristics. In many ways, this application is similar to previous applications to assess the dynamic properties of a bridge and to evaluate potential damage to bridge components (e.g. Lee et al. 2011, Li et al. 2005, and Bolton et al. 2005). DFR focuses on the substructure as opposed to the bridge deck and other superstructure components. Olson et al. (1998) and Olson and Aouad (2001) explored DFR as part of NCHRP Project 21-05. A limited number of field tests were performed for bridges in the study with mixed results. Olson et al. (1998) reported that the resonant frequency of substructures exhibited sensitivity to foundation type but that the response was more complex in nature than the simple case of a single pile or spread footing (i.e. Novak 1976). Further testing would be necessary, particularly with dynamic sources capable of lower frequency excitations. Maser et al. (1998) and Maser et al. (2001) formulated closed form solutions for individual foundation stiffness in the vertical, horizontal, and rotational direction for foundations of varying dimensions. These solutions were verified via three-dimensional (3-D) finite element method (FEM) modeling and formed the basis for interpretation of field test results at six bridge foundations. The bridges were instrumented with strain gauges, tiltmeters, and linear variable differential transformer (LVDT) displacement transducers and the loading was applied by a loaded dump truck as it drove slowly across the bridge. The measured foundation rotation to horizontal stiffness ratio clearly distinguished the foundations on spread footings from those on piles (Maser et al. 2001, Maser et al. 1998). Olson (2005a) continued to investigate DFR as part of a separate FHWA sponsored project. Four bents on three bridges in east TX were subjected to dynamic modal vibration testing using the University of Texas Vibroseis (Fig. 1-23). The field tests examined whether the substructure response reflected any changes in damage state/condition and could provide insight about the type of foundation. The results were inconclusive and comparisons of modal transfer function data were unable to distinguish shallow versus deep bridge foundations. Olson (2005a) did explore other methods to post-process the data (i.e. Hilbert-Huang Transform), which resulted in more accurate assessments of damage states but not foundation type. More recently, Briaud et al. (2012) explored DFR (among other methods) to assess foundation lengths as a part of TxDOT funded research project. DFR was tested under laboratory conditions (concrete slabs buried at different depths in

the Haynes Coastal Engineering Laboratory), in the field (one bridge site w/ accelerometers directly on pile and on bridge bent), and through numerical simulations. The preliminary laboratory results showed promise, but field testing proved unsuccessful in identifying the dominant foundation frequency. The numerical modeling showed that pile length had limited effects on the dominant frequency of the substructure.

Based on the case studies, DFR has a mixed record regarding assessment of foundation type. Though it is intuitive that substructure dynamic response would differ between deep and shallow foundations, the differences are difficult to systematically identify in practice due to the complexities of bridge dynamic responses. Further research is necessary to ascertain the usefulness of DFR in the context of identification of unknown foundations.

The DFR test is similar in cost to other surface NDT methods (e.g. $4,500 - $11,500 per test, see Table 1-5). The costs to assemble a DFR system should compare reasonably well to commercial systems available for US (i.e. approximately $20,000). Moreover, a custom system could be developed that is capable of DFR testing as well as the other stress-wave based surface NDT methods (SE/IR, BW, US) due to their similarities in hardware requirements. Such a system would likely range in cost from $30,000 to $35,000 (Olson and Aouad 2001). The DFR source can be as simple as a large sledge hammer or a loaded dump truck (as in Maser et al. 1998). Larger dynamic sources (e.g. Vibroseis truck) would increase the expenses associated with field testing. Data collection in DFR is laborious primarily because several configurations of the accelerometers and source are necessary to properly excite the bridge substructure over sufficient mode shapes (e.g. 25 - 36 source-receiver combinations for a single bridge in Olson et al. 1998). As a result it is likely that only one bridge substructure could be tested per day (i.e. 6 - 8 hours for a 2-person team). Additionally, there may be considerable constraints on site access. Mobilization of traffic (MOT) may be necessary if the seismic source will be placed directly on the bridge deck and road surface. Stress waves induced by traffic on the bridge superstructure can affect the recorded data. Testing at off-peak hours or MOT could address traffic noise in recorded data. Steep slopes, presence of vegetation, and water flow would have minimal impacts on testing as long as field engineers have access to the small exposed surfaces on the bridge substructure (e.g. pier) to attach the accelerometers. Finally, DFR is applicable over a wide range of soil conditions. The influence of the soil stratigraphy at the site should be

incorporated into any numerical models to properly assess the dynamic response of the bridge substructure.

1.3.1.3.7 Electrical Resistivity Imaging/Induced Polarization

Electrical Resistivity Imaging (ERI) and Induced Polarization (IP) are common near-surface geophysical approaches that are utilized to image subsurface ground conditions (e.g. Loke and Lane 2004, Kim et al. 2002, Hiltunen and Roth 2003, Rinaldi et al. 2006, Meyer et al. 2007, Morse et al. 2012). Both methods rely on measuring the electrical response of the ground to induced currents. In the ERI method, a direct current is injected into the ground surface using a pair of electrodes (Fig. 1-24). The voltage potential of the ground in response to this direct current is then measured with another pair of electrodes. An average impedance value is computed based on the ratio of the measured voltage potential to the current. This impedance is converted into an apparent resistivity and the electrode configuration is changed to allow multiple measurements and the development of a pseudosection (Loke 2000) (Fig. 1-25). An image of the subsurface is developed from these pseudosections based on inversion techniques. ERI measures the response to a long-term applied direct current whereas IP relies on measuring the transient response between electrodes after the current is removed (Fig. 1-26). Non-polarizing electrodes must be used in IP to prevent long term charge accumulation at the impedance mismatch between the electrode surface and the soil pore-fluid electrolytes. For ERI/IP, configuration of the electrodes plays a major role in the resolution and sensitivity of the measurements (Samouëlian et al. 2005). Depth of investigation is largely controlled by the lateral extent of the electrodes (Fig. 1-27). A large spacing between electrodes increases the depth of investigation at the cost of a decrease in resolution (Fig. 1-27). Zonge (2005) summarizes the most common electrode configurations (e.g. dipole-dipole, Schlumberger, Wenner, etc.). Most modern systems consist of a large array of electrodes (100+) that can be automatically switched on to take measurements (Fig. 1-28). This avoids the complicated process of re-arranging electrode configurations to create pseudosections as previously mentioned.

Recent studies from Texas have demonstrated the potential for ERI/IP to evaluate the depth of unknown foundations. Hossain et al. (2011) utilized ERI to determine the length of three TxDOT Bridges in conjunction with SE and Parallel Seismic testing. Two of the bridges were founded on

steel H-pile groups with a pile cap and the other was supported by drilled shafts. The foundation characteristics were known to TxDOT but were initially withheld from the research team until data was acquired and predictions of foundation lengths were made. Hossain et al. (2011) found that ERI was able to accurately predict the length of the two H-pile foundations. However, site access constraints did not allow them to arrange their electrodes with sufficient lateral extent to allow deep investigations at the bridge with the drilled shaft. This resulted in an estimate that was much shallower than the true length of the drilled shafts. Briaud et al. (2012) investigated both ERI and IP as part of a multi-year project to examine experimental and inferential methods to evaluate unknown foundations. ERI studies took place at four bridge sites (two with unknown foundations), one field test site, and 1 laboratory test site. ERI was used on concrete slabs/footings, concrete pile foundations, and drilled shafts. IP field testing was performed at the National Geotechnical Experimentation Site (NGES) at the Riverside Campus of Texas A&M University (footings, concrete piles, drilled shafts, and H-piles) and at three bridges in the Brazos District of Texas (all concrete piles). In general Briaud et al. (2012) found good agreement between predicted foundation length and actual lengths for both the ERI and IP methods. However, it was noted that ERI did have some issues for slender foundation elements (< 1 m) when attempting to image depths greater than 5 m. Moreover, some predictions for IP were limited by investigation depth due to an inadequate number of non-polarizing electrodes available for the field testing.

As noted in the case histories, ERI and IP show promise as another useful surface NDT method to evaluate unknown foundations. One of the key advantages of ERI and IP is that they do not rely on the foundation as a medium through which measurements are made. This means that ERI and IP do not suffer from issues related to complex substructures that plague other surface methods such as SE/IR, BW, etc. In fact, ERI and IP can image below pile caps as noted in the results from Briaud et al. (2012) and Hossain et al. (2011). Another useful aspect is that ERI and IP are not negatively affected by clayey soils as is the case for GPR. However, ERI and IP rely on visualizing foundations as a result of resistivity contrasts in the subsurface. ERI and IP will have a hard time distinguishing deep foundation elements if the resistivity of the soils at a site are similar in magnitude to the intact concrete or steel in the element. Data can also be affected by grounded metal objects in the vicinity of the test location (Wightman et al. 2003). Also, the amount of space available for testing will have a big impact on the depth of the investigations as

longer dipole arrays will gather data from greater depth. Further research is necessary to continue developing ERI and IP for unknown foundation assessment.

The ERI and IP test are slightly higher in cost relative to other surface NDT methods and compares well with GPR (i.e. $6,000 - $14,000 per test), primarily because of the specialized equipment and software necessary to process the data. A standalone ERI/IP system can range in cost up to $80,000 or more depending on number of electrodes. It is relatively straightforward to develop a combined ERI and IP system by acquiring both polarizing and non-polarizing electrodes. Data collection in ERI and IP can become time-intensive if 3-D data is desired. Otherwise, testing time is similar to SASW (i.e. 1 - 2 tests at a given site per day). As noted in both Briaud et al. (2012) and Hossain et al. (2011), there are considerable constraints on site access. It is important to have a large test area to string out the multiple electrodes so that investigation depth is optimized (e.g. Fig. 1-28). This may not always be possible based on site topography, easements, and bridge geometry. Relatively steep slopes would not likely represent an issue provided the field engineering could maneuver and string out the electrodes. However, the presence of heavy vegetation may impact the ability to drive electrodes into the subsurface and locate them after doing so. Briaud et al. (2012) was able to perform some custom modifications to the ERI polarized electrodes to allow them to work over water. However, the inversion of the data becomes increasingly complex for IP recordings over water. It was necessary to perform multiple iterations of the inversion process to arrive at some of the results for known foundations in Briaud et al. (2012). The likelihood of performing that many iterations and arriving at an accurate prediction for an unknown bridge over water would be very low. Finally, ERI and IP are applicable over a wide range of soil conditions, wider in fact than GPR. However, issues are encountered in areas where the surface of the ground is hard because the electrodes must be embedded a shallow distance into the ground. Also, dry soil conditions near the surface may cause issues with the electrical contact between the electrode and ground (Wightman et al. 2003).

1.3.1.4 Subsurface NDT Methods

Subsurface NDT methods are applied by lowering measurement systems into boreholes alongside or within the bridge substructure (Wightman et al. 2003). They typically offer greater flexibility with regards to applicable foundation types (e.g. piles beneath a pile cap can be

distinguished from footings). However, they tend to be more expensive because a borehole must be drilled prior to testing, maintained during testing, and grouted after completion of testing. Also since drilling rigs must be present on site, access constraints cause more issues for subsurface testing programs. The following subsurface NDT methods for unknown foundations will be discussed: Parallel Seismic, Borehole Sonic, Borehole Radar, Cross-Hole Sonic Logging, Induction Field, and Borehole Magnetic.

1.3.1.4.1 Parallel Seismic

The Parallel Seismic (PS) method was originally developed for unknown foundations and has since become one of the most common NDT techniques to determine the length of bridge foundations (Olson and Aouad 2001). The test consists of measuring the arrival times of wave energy that is imparted to the foundation from a hammer blow at the side or top of the bridge substructure (similar to SE/IR, BW, US). The main difference between PS and surface NDT techniques is that the receiver (hydrophone or geophone) is lowered in a cased borehole alongside the foundation (Fig. 1-29). Data is typically acquired at approximately 1 - 2 ft intervals using a digital signal analyzer (Wightman et al. 2003). The foundation bottom is identified by a sudden break in the slope of the first wave arrival times versus depth (i.e. the waves travel more slowly in the soil beneath the bottom of the foundation) (Fig. 1-29). The borehole should be located in close proximity to the foundation (i.e. 3 - 5 ft) for optimum signal quality and it should extend approximately 10 ft below the foundation bottom to identify the slope change in first arrival times (Olson and Aouad 2001). To ensure good coupling between the borehole casing (typically PVC or metal) and borehole wall, cement-grouting or a sand backfill should be utilized. Hydrophone receivers require the borehole be filled with water prior to testing while geophone receivers can be clamped to the casing without the addition of water.

Several studies have been performed throughout the years that demonstrate the abilities of PS to evaluate unknown foundation characteristics. Often times, PS has been performed in conjunction with multiple methods, including surface methods. Olson and Aouad (2001) summarized the PS results from NCHRP Project 21-05. PS was utilized in a number of the bridges, typically with very good success (Tables 1-3 and 1-7). Olson and Aouad (2001) noted that PS had the widest range of application for determining the depth of different types of foundations. Mercado & O'Neill (2000) also utilized the PS method at the National Geotechnical

Experimentation Site (NGES) at the University of Houston to verify the length of a known drilled shaft foundation to within 6% accuracy. Multiple studies have also modeled the PS method numerically to verify the range of applicable conditions for the test and to demonstrate that PS could be utilized to evaluate foundation integrity as well as depth (e.g. Niederleithingher et al. 2006, Huang & Chen 2007). Hertlein and Walton (2007) and Yu et al. (2007) both utilized PS predictions for foundation length in conjunction with subsurface soil data to estimate the capacity of foundations for reuse in rehabilitated structures. Robinson and Webster (2008) summarized the favorable experiences of consultants working with NCDOT with various NDT methods, including PS. Niederleithinger and Fritsche (2010) utilized PS to evaluate the length of a steel sheet pile. Hossain et al. (2011) utilized PS testing in conjunction with RI to assess the length of known foundations in a blind study for TxDOT. Reasonable agreement was recorded between PS, RI, and the actual steel H-pile length at one bridge site. Recent references to PS have focused on improving the test apparatus or data interpretation. For example Sack and Olson (2009) discuss the use of a Seismic Cone Penetration Test cone (SCPT) apparatus that could double as the receiver for a PS test performed in conjunction with SCPT testing. Niederleithingher and Taffe (2006) discuss the development of a PS system that utilizes multiple receivers. Niederleithingher et al. (2013) is exploring new procedures for curve-fitting PS first-arrival data based on information regarding borehole distance, inclination, and soil properties.

Based on the summary of case histories, it should be clear that much interest has been shown and much work performed with PS. This is not surprising since PS is one of the most robust of the subsurface NDT methods (particularly when geophones are used) with a fairly long history and proven track record (Olson and Aouad 2001). The primary advantage of PS is its ability to distinguish characteristics among a wide range of substructure elements, including abutment walls and pile caps. Since a borehole is generated during PS testing, length estimates can often be used in conjunction with the subsurface boring data to estimate foundation capacity (e.g. Hertlein and Walton 2007). However, PS does have its limitations (Table 1-8). Adequate coupling of the access tube can sometimes be problematic in loose granular or rocky soils (Hertlein and Walton 2007). Hydrophones are particular sensitive to the tube wave that is generated by the impact at the surface (Wightman et al. 2003). Dry or granular soils can cause rapid attenuation of the wave energy traveling through the substructure element. The borehole must be located close to the foundation and background acoustic noise sources must be minimized to optimize

signal strength (Olson and Aouad 2001, Wightman et al. 2003). Finally, any discontinuities between pile cap/grade beams and the underlying foundation elements can completely block the generated waves (Hertlein and Walton 2007).

As a subsurface test, PS is generally more expensive than any other surface tests (i.e. $10,000 - $22,800 per test, see Table 1-5) primarily due to the costs associated with drilling operations. As a standalone system, PS equipment can range from $15,000 for hydrophone-based systems up to $25,000 for geophone-based systems (Olson and Aouad 2001). Many components between a PS and a SE/IR, BW, and US system are similar and it would be possible to develop a combined system that can perform all four tests (at a cost of roughly $50,000 according to Olson and Aouad 2001). Studies have demonstrated that PS can be performed successfully using the geophone in a SCPT system as a receiver (e.g. Sack and Olson 2009). Training time for DOT engineers with a PS system is estimated at 1 - 2 weeks. Data collection for PS typically takes longer than many surface methods because of the drilling operations. Typically 2 - 4 bridge substructure units may be tested on a given day depending on the depth of the boring (i.e. 2 - 4 hours for a 2-person team, not including drilling crew). There are a few constraints on site access since it will be necessary to mobilize a drill rig to the field. In areas with steep slopes or with high vegetation, this may necessitate a smaller all terrain rig which may limit drilling depths. For locations over waterways, use of drilling barges may be necessary, with a corresponding increase in drilling expenses. The receivers are typically designed to be submersible without harming any electronics.

1.3.1.4.2 Borehole Sonic

The Borehole Sonic (BHS) method is a more recently developed subsurface NDT technique. It relies on the propagation of longitudinal (i.e. acoustic P-waves) through soil from a source-receiver pair located within a cased borehole alongside a foundation (Fig. 1-30). The source generates longitudinal waves and the receiver picks up any reflected wave energy from interfaces of different stiffness (i.e. acoustic impedance). A plot of reflected wave energy versus depth allows an “image” to be created of any interfaces within the zone of influence of the system. The bottom of a foundation would be determined as the depth at which reflection signals are no longer obtained. The farthest distance through which the acoustic wave energy can be propagated before soil damping diminishes the signal strength is a function of the

material velocity and predominant wave frequency of the source-receiver pair (Lee and Santamarina 2005). Higher frequency waves allow greater resolution at the cost of higher attenuation in soils. Lower frequency waves will propagate farther but will have poorer resolution. BHS is essentially a SE-based test where the waves are travelling horizontally through soil as opposed to vertically through the foundation.

Only limited studies have demonstrated the potential applicability of BHS for foundation assessment. Olson et al. (1998) only considered proof-of-concept studies as part of the first phase of NCHRP Project 21-05 and Olson and Aouad (2001) did not document any additional field testing during phase two. Two separate BHS systems were utilized at two bridge sites during phase one of that study. One was a prototype mock-up designed at the University of Texas, and the other was a full commercial borehole sonic logging tool typically used in the oil exploration industry. Both systems proved unsuccessful in recording reflected energy from smaller drilled shafts (4 ft diameter) and concrete piles (14 in square), but the University of Texas system did record reflections from a massive 10 ft diameter caisson. Descour and Kabir (2010) utilized a modified BHS method (called Single Hole Reflector Tracing in their study) that consisted of a seismic source in between two geophones within a single borehole. The source was excited at three depths between the receiver geophone locations and the corresponding reflections from known foundation were recorded. The entire system would then be lowered by a few feet and data would be reacquired to generate a profile of the pre-drilled concrete piles. The BHS results in Descour and Kabir (2010) showed that the pile bottoms could be identified by changes in the reflected signal strength. However, there were issues with imaging individual piles as the reflections appeared to line up with the survey holes rather than the actual patterns of the piles. Also signal polarity changed in what appeared to be the same pattern as the location of the piles. This was likely related to wavelength of the signals relative to the size of the piles causing potential issues with dispersion. Coe and Brandenberg (2010) and Coe and Brandenberg (2012) demonstrated that P-wave reflections (i.e. the basis for the BHS method) were capable of generating images of complex laboratory soil models and cast-in-steel-shell concrete piles in the field. In this particular case, the BHS system actually operated at the ultrasonic frequency range (i.e. larger than approximately 20 kHz). The system developed as part of Coe and Brandenberg (2010) and Coe and Brandenberg (2012) will be utilized as part of this current study of NDT techniques for unknown bridges in the Commonwealth of Pennsylvania.

Thus BHS has shown some potential based on previous case histories, though the literature has proven sparse on the matter. BHS has the potential to provide better resolution than several of the subsurface methods, including PS. Moreover, with the seismic wave source inside the borehole, improper coupling between caps or grade beams and underlying foundation elements would not present any issues. The major potential limitations of BHS are similar to those discussed for PS (e.g. borehole tube coupling, etc.) (see Table 1-8). In particular, the fact that high frequency acoustic waves are attenuated very rapidly in soils presents a major challenge. The limits on distance between borehole and foundation element must be characterized in order to ensure the receiver can record reflections from the foundation interface. Additionally, improper orientation of the BHS system will limit the potential amount of reflected wave energy, especially for slender elements. Despite these limitations, the BHS shows promise as a tool to evaluate unknown foundations and it will be further evaluated as a part of this current study.

The costs for BHS compare favorably with the PS test (i.e. $10,500 - $23,000 per test, see Table 1-5). Commercial BHS systems are limited to those utilized in other applications (e.g. borehole sonic logging) so custom hardware is typically necessary. The system that will be utilized in this study was assembled for approximately $40,000 including data acquisition system, ultrasonic P-wave transducers, associated electronics, and custom machining. This overall cost would decrease for lower frequency P-wave transducers (with a corresponding decrease in signal resolution). Details of the system can be found in Coe and Brandenberg (2012). It may be possible to combine a PS with BHS system as they could share a common dynamic signal analyzer. However, the BHS requires a tunable seismic source that can fit inside the borehole. Data collection for BHS will typically take longer than many surface methods because of the drilling operations. Typically 2 - 4 bridge substructure units may be tested on a given day depending on the depth of the boring (i.e. 2 - 4 hours for a 2-person team, not including drilling crew). Training time for DOT engineering is similar to PS (i.e. 1 - 2 weeks). Since the PS and BHS test are so similar in layout, it should be expected that the two tests will share mutual constraints on site access. The site must accommodate the use of a drilling rig to create boreholes in which to lower the BHS system. In areas with steep slopes or with high vegetation, this may necessitate a smaller all-terrain rig which may limit drilling depths. For locations over

waterways, use of drilling rig barges may be necessary with a corresponding increase in drilling expenses. The source-receivers are typically designed to be submersible without harming any electronics.

1.3.1.4.3 Borehole Radar

The Borehole Radar (BHR) method is essentially the electromagnetic counterpart to the BHS method described in the previous section (Wightman et al. 2003). It utilizes the same principles as GPR discussed in Section 1.3.1.3.4, except the electromagnetic waves are now propagating in the horizontal direction as the radar antenna is lowered down a borehole alongside the foundation (Fig. 1-31). As before, antennas are manufactured with different dominant frequencies and selection of the proper antenna must consider resolution and lateral propagation requirements.

BHR has been previously used to detect tunnels (Farid et al. 2012), to image voids and fractures in bedrock (Haeni et al. 2002, Kim et al. 2004), and to determine the existence of reinforcing bars within buried foundation elements (Yang et al. 2010). However, very few studies of BHR can be found in the literature for direct evaluation of unknown foundations. Olson and Aouad (2001) summarized the experiences of NCHRP Project 21-05 with BHR. Multiple bridge foundations in the first phase of the study were tested using BHR with various degrees of success (Table 1-9). BHR generally provided accurate predictions for the depth of bridge abutment walls but not for stem and toe thicknesses. However, clay soil profiles, bentonite-grout mixtures at the borehole-casing interface, and buried transmission lines resulted in poor signal quality at a few sites. The ground water table was also discernible in the results at some sites.

BHR suffers from the same limitations regarding electromagnetic wave propagation as GPR (see Section 1.3.1.3.4. Clayey soils and the presence of salt water can severely attenuate the electromagnetic waves (Wightman et al. 2003). Transmission lines near the test site can result in unwanted noise in the recorded signals (Olson and Aouad 2001). Moreover, as a subsurface NDT borehole method, BHR suffers from limitations similar to the BHS test described in the previous section (e.g. borehole to foundation distance, alignment issues, etc.) (Table 1-8).

BHR costs more than BHS (i.e. $11,500 - $25,000 per test, see Table 1-5) primarily due to the cost premium on radar systems relative to stress-wave based systems. For example, the omnidirectional system utilized in NCHRP Project 21-05 sells for approximately $60,000 ($10,000 for the antenna, $50,000 for the two channel data acquisition system) and a directional BHR system may cost as much as $250,000 (Olson and Aouad 2001). Training times for BHR will compare with BHS and PS (i.e. 1 - 2 weeks). Data acquisition for BHR will be comparable to BHS (i.e. 2 - 4 bridge substructure units per day, 2 - 4 hours per substructure for a 2-person team, not including drilling crew). The depth of the desired borings will have an impact on the timeframe and overall cost of testing. BHR will have similar constraints on site access as BHS. The site must accommodate the use of a drilling rig to create boreholes. A smaller all-terrain rig may be necessary in areas with steep slopes or with high vegetation. This may impact the potential drilling capabilities and expenses. For locations over waterways, use of drilling rig barges may be necessary, which would correspond to an increase in drilling expenses. The receivers are typically designed to be submersible without harming any electronics.

1.3.1.4.4 Cross-Hole Sonic Logging

The Cross-Hole Sonic Logging (CSL) method has traditionally been utilized as an assessment tool for the integrity of drilled shaft foundations (e.g. Briaud et al. 2002, Likins et al. 2004, ASTM D6760-08) or as a geophysical subsurface exploration techniques to characterize soil shear wave velocity profiles (e.g. Stokoe and Woods 1972, ASTM D4428M-07). However, the test is finding some renewed interest from bridge owners interested in evaluating unknown foundations. The test layout is essentially the equivalent to two BHS tests, except the source and receiver are not located within the same borehole (Fig. 1-32). Testing occurs as a seismic wave source propagates waves from one case borehole to a receiver in another borehole on the opposite side of the foundation member. Reflection energy can be simply plotted and visually inspected to locate the presence of first arrivals on the receiver after the bottom of the foundation has been reached or more advanced tomographic inversion techniques can be used with data from a combination of multiple source-receiver depth locations (e.g. Fig. 1-33). Other names for CSL include Cross-Borehole Sonic, Cross-Hole Sonic, Cross-Hole Seismic, and Cross-Hole.

As noted previously, CSL has predominantly been utilized for drilled shaft integrity testing and measurements of shear wave velocity profiles of soils. However a limited number of case studies exist where CSL techniques are implemented to predict foundation dimensions. For example, Descour and Kabir (2010) applied CSL techniques to create tomographic inversions of the subsurface below bridge abutment foundations for a viaduct in Pittsburgh. The results revealed that the velocity tomogram tended to "fuse" the concrete piles and pile cap into one monolithic feature. However foundation bottoms were identified by noting where the tomographic velocity model predicted much slower velocities indicative of soils and not concrete.

CSL suffers from the same limitations as BHS since the nature of the system is practically identical (see Section 1.3.1.4.2). The main drawback relative to BHS is that CSL requires the construction of two boreholes on opposite sides of a foundation (Table 1-8). However, it is apparent in Fig. 1-34 that CSL techniques have the capability to provide much more detailed information (e.g. high resolution 2-D or 3-D tomograms) about the region of interest and may be suitable for high-risk unknown foundation evaluations.

CSL is generally one of the most expensive NDT methods (i.e. $12,700 - $28,000 per test, see Table 1-5) due to the additional borehole requirements. A custom CSL system can be developed at roughly the same cost as a BHS system (approximately $40,000 depending on frequency requirements). Very little actually differs between the general equipment requirements for CSL and BHS. Training time will be similar to BHS (i.e. 1 - 2 weeks). CSL testing rates on a daily basis will likely approach SASW due to the additional boreholes (i.e. 1 - 2 bridge substructure units per day, 4 - 8 hours per substructure for a 2-person team, not including drilling crew). Again, boring depths will have an impact on the timeframe and overall cost of testing. CSL will share similar site constraints with BHS. A drill rig must be able to access the test site to create boreholes. A smaller all-terrain rig may be necessary to accomplish this in areas with steep slopes or with high vegetation. This may impact the potential drilling capabilities and expenses. For locations over waterways, use of drilling barges may be necessary, which would correspond to an increase in drilling expenses. The receivers are typically designed to be submersible without harming any electronics.

1.3.1.4.5 Induction Field

The Induction Field (IF) method relies on the principle of electromagnetic induction which states that a voltage potential is produced in response to a changing magnetic field. Similar techniques have had a long history in geophysical borehole logging for the oil exploration field (e.g. Doll 1949). There has recently been a rise in the number of applications of this technology to unknown foundation evaluations since its development for this purpose in New Zealand (Wright 1979, Beattie 1982). In this context, IF is performed by inducing an alternating current (AC) into a conductive foundation element (i.e. steel rebar, steel pile). The AC field in the foundation element couples with the subsurface soils where it is picked up by a return electrode placed in the ground (e.g. piece of steel rebar, another steel foundation member, etc.). The resulting current flow induces a magnetic field in the foundation element that is measured using an induction coil lowered alongside in a cased borehole (Fig. 1-35). The foundation bottom is located by visually inspecting the plot of induced pile voltage versus induction coil depth to observe breaks in the slopes of the curve (Fig. 1-35). IF is essentially the electromagnetic analog to the PS method discussed in section 1.3.1.4.1 (Olson and Aouad 2001).

The amount of discussion regarding IF in the unknown foundation literature is sparse, but it appears to be gaining in popularity based on the results of recent studies. Olson et al. (1998) discussed two case studies in New Zealand where IF was first successful developed to determine the length of steel foundations. Olson and Aouad (2001) summarized their experiences with IF testing for NCHRP Project 21-05. During phase two, IF testing was performed on a bridge in Texas and in Colorado as part of the blind field studies. Olson and Aouad (2001) found good agreement between IF and PS for the bridge in Colorado but IF was less successful at a site in Texas. Jalinoos et al. (2006) utilized IF in conjunction with other electromagnetic NDT methods to determine the tip elevation of a steel sheet pile bulkhead for a channel dredging project at the Port of Long Beach in California. The IF results compared favorably with the other NDT methods and allowed confidence in the pile length estimates. Additionally, Jalinoos et al. (2006) demonstrated that the depths of the concrete pile caps were also identifiable in the field IF data. Robinson and Webster (2008) summarized the favorable experiences of consultants with various NDT methods, including IF. In one case, a NCDOT bridge with unknown foundation length was tested with IF. IF was selected because an insufficient length of the piles was available above grade for SE testing and the steel H-piles were embedded below a large pile cap. The results demonstrated that the piles extended into the weathered bedrock at the site.

Robinson and Webster (2008) also discussed the use of IF to assess foundations lengths for emergency repairs at the Birmingham Bridge outside of Pittsburgh, Pennsylvania (as documented in Splitstone et al. 2010). The IF results clearly indicated the depths of the steel H-piles at the critical bridge pier where settlement was concentrated and allowed an evaluation of appropriate emergency retrofit designs.

IF suffers from limitations similar to other subsurface borehole NDT techniques such as PS and BHS (Table 1-8). The additional drawback is the requirement for the foundation to contain a conductive material (i.e. steel) throughout its length. Thus unreinforced concrete piles/shafts and timber piles cannot be testing with IF. Though Jalinoos et al. (2006) demonstrated that pile cap depths are identifiable in IF results, it is necessary for the cap to be electronically connected with the foundation element being tested. Any breaks in the reinforcements between pile cap and underlying pile will render testing unsuccessful. Moreover, access to the reinforcing steel is necessary at the ground surface to establish the electronic AC connection. PVC must be utilized as the borehole casing as steel will mask the voltage signals from the foundation element. Similarly, the presence of metals or transmission lines beneath the surface can impact the test results. Finally, the induction coil is able to detect the magnetic field within a fairly narrow range, and the borehole must be located within a few feet of the foundation element to maximize signal strength.

IF compares favorably with the cost of other subsurface NDT methods (i.e. $10,000 - $22,500 per test, see Table 1-5). An IF system is estimated to cost approximately $20,000 (Olson and Aouad 2001). Training time for DOT engineers will be relatively short (i.e. approximately 2 days). Data acquisition for IF will be comparable to the BHS (i.e. 2 - 4 bridge substructure units per day, 2 - 4 hours per substructure for a 2-person team, not including drilling crew). The depth of the desired borings will have an impact on the timeframe and overall cost of testing. IF will have similar constraints on site access as other subsurface NDT methods (i.e. drill rig access). A smaller all-terrain rig may be necessary in areas with steep slopes or with high vegetation. This may impact the potential drilling capabilities and expenses. For locations over waterways, use of drilling barges may be necessary, which would correspond to an increase in drilling expenses. However, the induction coil is designed to be submersible for data collection underwater and in

fluid-filled boreholes. The presence of water may complicate data interpretation if it occurs at the same location as the foundation bottom.

1.3.1.4.6 Borehole Magnetic

The Borehole Magnetic (BM) method is very similar to the IF method discussed in the previous section (1.3.1.4.4). It too relies on the relationship between magnetic fields and voltage potentials and has its roots in borehole logging and geophysical surveying. However the BM method does not input AC electrical energy into the subsurface but instead uses a borehole magnetometer instrument to measure the secondary magnetic field produced by steel foundation elements in response to the Earth's magnetic field (Fig. 1-36). Beneath the toe of the steel element, the secondary field will rapidly diminish which allows an estimate of foundation length (Wightman et al. 2003). Unlike other subsurface NDT methods, no source mechanisms are necessary (e.g. voltage or current source, impact hammer, etc.). BM is a passive test which measures the inherent magnetism of the steel foundation element.

Like IF, the cases where the BM method has been documented are limited. Use of the BM method in the field of unknown foundations is a more recent development. For example, Olson and Aouad (2001) do not document the BM method in NCHRP Project 21-05. Jo et al. (1999) and Jo et al. (2003) described the successful implementation of the BM method for foundation length estimation. They found that errors in foundation length prediction were typically less than 1 ft and readings were observable from boreholes as far away as approximately 10 ft under favorable conditions. Yu et al. (2007) utilized BM testing in conjunction with PS and SE to determine the length of auger-cast piles for a redevelopment project at St. Joseph Hospital in Savannah, GA. Results from the BM method compared favorably to PS and SE. Additionally, the BM method was able to detect a change in the reinforcement design of the auger-cast piles.

The BM method suffers from the same limitations as the IF test due to the similarities in test layout and theory (Table 1-8). The chief issue again is the requirement for continuous steel throughout the entire length of the foundation system. However, access to the steel at the ground surface is unnecessary because no source of electricity is input into the foundation. The presence of metals or transmission lines beneath the surface can impact the test results and PVC must be utilized as the borehole casing.

BM compares favorably with the cost of other subsurface NDT methods (i.e. $9,800 - $22,500 per test, see Table 1-5). The cost to purchase a BM system will be comparable to an IF system (i.e. approximately $20,000). Engineers could be trained to perform BM testing in as little as two days. The amount of time in the field for testing will compare with IF (i.e. 2 - 4 bridge substructure units per day, 2 - 4 hours per substructure for a 2-person team, not including drilling crew). The depth of the desired borings will have an impact on the timeframe and overall cost of testing (i.e. deeper exploration will take longer and cost more for drilling). BM will have similar constraints on site access as other subsurface NDT methods (i.e. drill rig access). Sites with steep slopes or with high vegetation may require a smaller all-terrain rig, which can impact the potential drilling capabilities and expenses. For locations over waterways, use of drilling barges may be necessary, which would correspond to an increase in drilling expenses. However, the magnetometer is designed to be submersible for data collection underwater and in fluid-filled boreholes.

1.3.2 Inferential Approaches

In response to the significant costs associated with experimental techniques (both destructive and non-destructive), several methods have been developed to infer foundation information based on readily available information. Combined with a risk-based approach (e.g. Stein and Sedmera 2006) such methods may provide suitable evaluations from which to develop appropriate plans of action (POA) for low-risk bridges with unknown foundations.

The simplest approach to evaluate an unknown foundation is to infer an embedment depth and foundation type based on known nearby foundations, regional and historical foundation construction practices, date of bridge construction, and any subsurface information and construction records that may be available. Stein and Sedmera (2006) noted the following observations based on a thorough literature review and responses to surveys by state DOT representatives: older structures (built before 1960) are usually built on timber piling; depth of piles can be assumed as at least 10 feet for bridges with unknown foundations; shallow foundations can be assumed to support bridges with unknown foundations if bedrock is found near the surface; the tops and bottoms of a typical spread footing can be assumed to be 3 feet and 7 feet below the soil surface, respectively. Stein and Sedmera (2006) also stressed that

every effort be exhausted to locate any original plans or construction records and that bridge owners quantify the risk associated with failure for bridges with unknown foundations.

Another approach to estimate the depth of unknown foundations is reverse engineering. In reverse engineering, structural loads for the bridge are calculated based on structural analysis to derive a design load for the foundation. Embedment of the foundation is then predicted based on knowledge of the subsurface soil conditions (e.g. bearing capacity curve). McLemore et al. (2010) documented the development of reverse engineering techniques as part of FDOT's efforts to evaluate unknown foundations across the state. In general, reverse engineering tended to under-predict the design pile load which would lead to conservative estimates for pile embedment length for scour analysis. Sayed et al. (2012) summarized the development of a static/back-calculation approach where minimum pile embedment is calculated based on soil profile structural load information. In this process a 3-D nonlinear FEM model of the foundation system is developed and a deterministic iterative process is performed using multiple trial embedment values until a stable condition is reached which satisfies static equilibrium. Sayed et al. (2012) found better agreement using this method to predict pile length at three bridges in Florida compared to predictions from SE testing.

Recently, a growing number of studies have explored the use of Artificial Neural Networks (ANN) to predict foundation lengths of unknown foundations. ANN methods consist of a mathematical model with capabilities similar to biological neural networks (e.g. central nervous system) (Pridy and Keller 2005). The model creates a series of interconnected nodes, each capable of processing information in parallel with the other nodes (Fig. 1-37). The network is provided data examples from which to "learn" the complex relationships relating the inputs and outputs of a system. Though ANN methods have their roots in biological and computer science fields, they have been applied to study a wide variety of complex problems. In recent years, ANN has been applied to many types of geotechnical problems including prediction of pile capacity, estimation of scour, soil modeling, site characterization, earth retaining structures, settlement of structures, slope stability, tunnel design, and liquefaction (e.g. Bateni et al. 2007, Lee et al. 2007, Shahin et al. 2008, Zounemat-Kermani et al. 2009, and Kaya 2010). McLemore et al. (2010) describes the development of ANN for utilization with FDOT bridges. Two ANNs were developed to predict the length of concrete and steel piles (CPILE, SPILE) based on input data such as year

of bridge construction, design pile load, pile size, pile type, and slopes of soil bearing capacity curves (as a proxy for soil strength). An ANN was also developed to predict design pile load (PLOAD) as an alternative to reverse engineering techniques when the design pile load is unknown. McLemore et al. (2010) found that the ANN accurately predicted pile lengths for the bridges in the study after being trained by a number of the bridges in the study database. Briaud et al. (2012) discusses a similar study to verify an ANN for evaluation of unknown foundations in Texas. Briaud et al. (2012) also explored the ability to utilize ANN to determine the length of pile foundations in a probabilistic sense. Both approaches were found to provide accurate estimates regarding foundation length for the selected bridges in the Bryan District of Texas.

1.3.3 Observations Regarding Unknown Foundation Research

As described in the previous section, many methods are available to evaluate unknown foundations. Some methods have been adapted from other applications (e.g. SASW, GPR, BHR, IF) and others were developed specifically to address the problem of unknown foundations (e.g. US, PS). A number of methods have fallen out of favor with the engineering community while others have enjoyed renewed emphasis. The following summarizes some observations regarding NDT methods for unknown foundations:

- It is not uncommon to note the use of multiple methods when evaluating unknown foundations based on the number of case histories where a multi-test approach was undertaken (e.g. Hossain et al. 2011, Olson et al. 1998, Olson and Aouad 2001, Yu et al. 2007, etc.). This is not surprising given that surface tests are often limited in scope and cannot image below pile caps. Many bridge owners may therefore elect to perform a subsurface test. The additional expenses of another subsurface or surface test at that point are comparably minimal, particularly if test equipment is shared among the selected methods and combined hardware packages are available for rental and/or purchase. Parallel seismic in conjunction with a stress-wave form of subsurface test (e.g. SE/IR, US) appears to be one such common multi-test approach (as recommended in Olson and Aouad 2001).

- PS has proven to be one of the most versatile and accurate methods for evaluation of unknown foundations. For this reason it is probably one of the most common subsurface NDT methods employed in field studies. More unknown foundation case studies were

located in the literature for this method compared to any other method (see Section 1.3.1.4.1). Recent studies with PS have attempted to improve data interpretation techniques (e.g. Niederleithingher et al. 2013) and expand PS testing capabilities with multiple receivers (e.g. Niederleithinger and Taffe 2006) or by combining PS with CPT (e.g. Sack and Olson 2009).

- An increasing number of studies are focusing on electromagnetic methods adapted from geophysics and oil exploration (e.g. Jo et al. 2003, Jalinoos et al. 2006, Yu et al. 2007, Jo et al. Hossain et al. 2011, and Briaud et al. 2012). These methods avoid some issues with traditional stress-wave methods (though at the expense of new limitations related to electromagnetism). For example, it appears that ERI as a surface method has some potential to detect foundation lengths beneath caps to distinguish embedded footings from complex deep foundations.

- There is a growing trend towards use of inferential approaches, particularly in conjunction with regional-specific modeling and risk-based assessments of bridge scour. This allows state DOTs with significant numbers of unknown foundation bridges to address high-risk structures in a timely manner and to prioritize potential field NDT investigations for their most critical bridges (e.g. principal arterials) where NDT methods are often still warranted.

- It must be emphasized that selection of an appropriate method to evaluate unknown foundations is influenced by many factors. Care must be exercised in both selection of an appropriate method and interpretation of test results.

Figure 1-1: Scour at a coastal bridge pier (Douglass and Krolak 2008).

Figure 1-2: Scour in sandstone supporting bridge abutment (Arneson et al. 2012).

Figure 1-3: Local scour in Pensacola, FL during Hurricane Ivan.

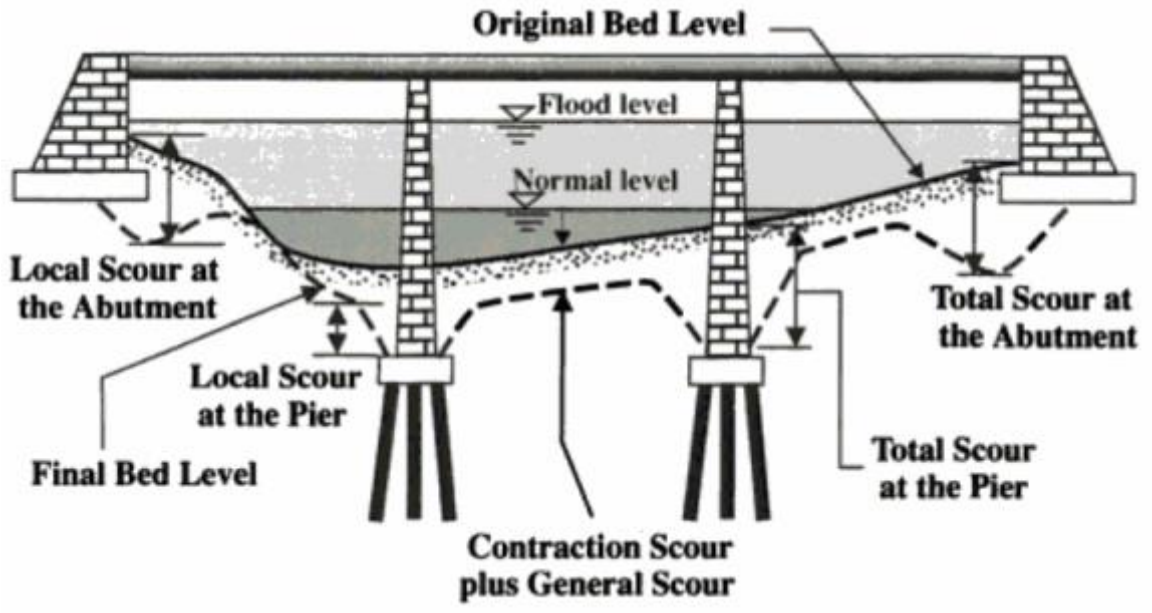

Figure 1-4: Types of scour (Melville & Coleman 2000).

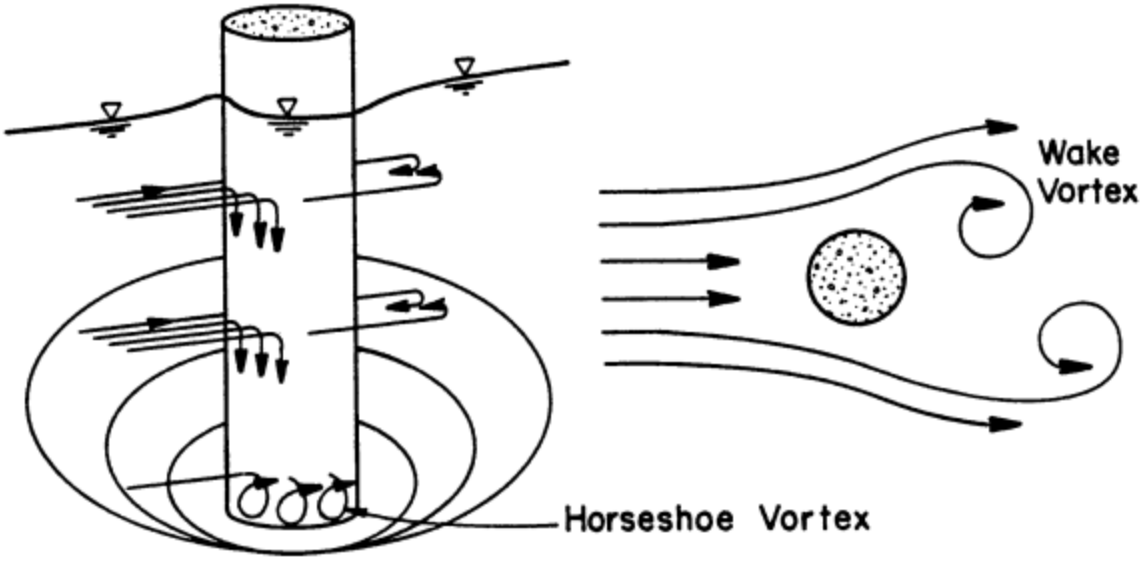

Figure 1-5: Schematic representation of vortices that cause local scour at a cylindrical pier (Arneson et al. 2012).

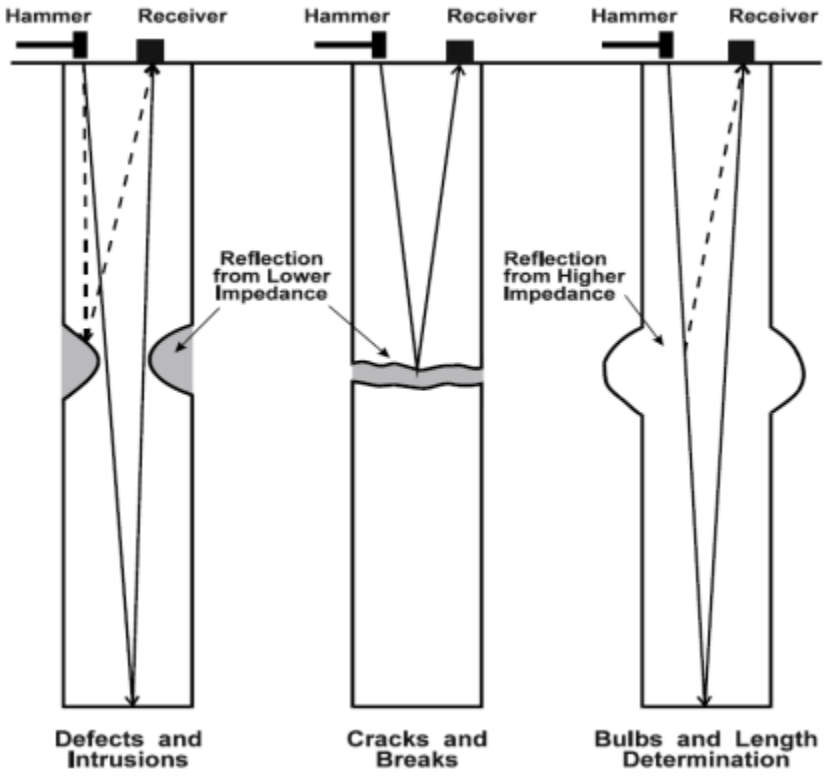

Figure 1-6: Effects of changes in acoustic impedance (i.e. stiffness) on stress waves during SE/IR (adapted from Stein and Sedmera 2006).

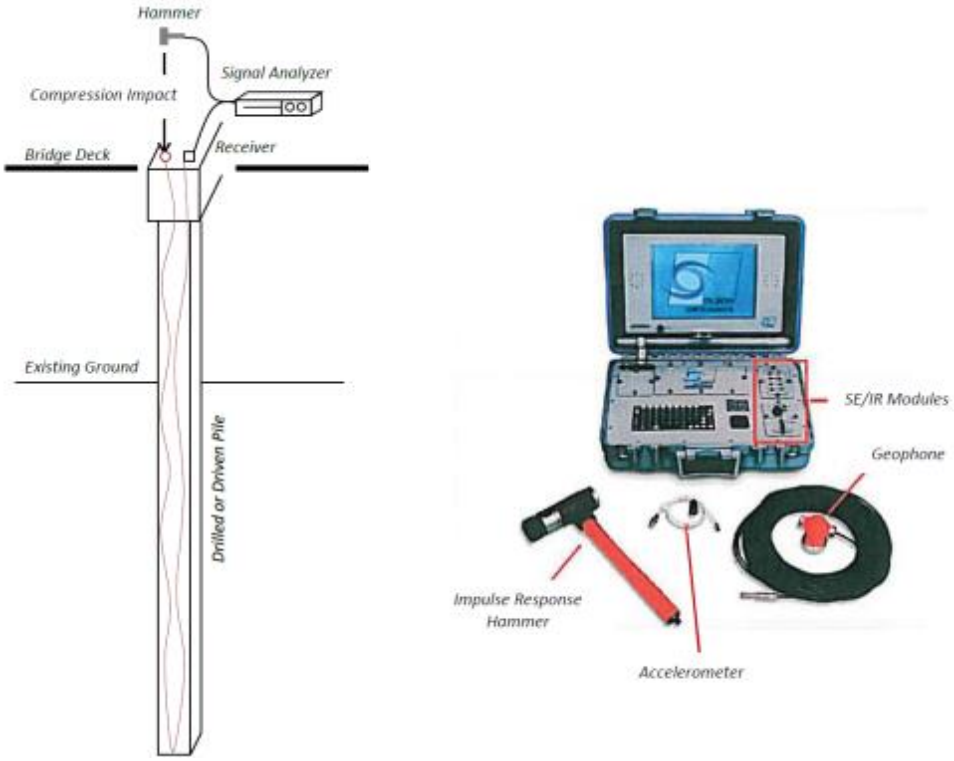

Figure 1-7: Sonic Echo/Impulse Response (SE/IR) test layout and field equipment (adapted from McLemore et al. 2010).

Figure 1-8: SE field testing (Beard 2005).

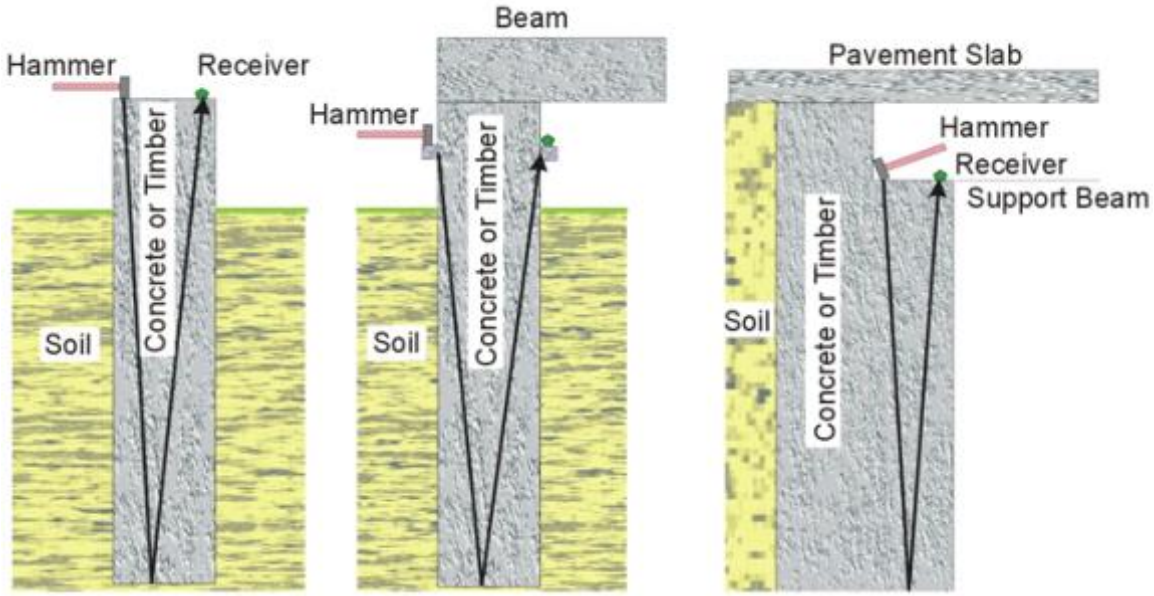

(a) (b) (c)

Figure 1-9: SE/IR test layout: (a) Access to Top of Foundation (b) Access to Side of Foundation (c) Access to top of wall structure (e.g. Bridge Abutment) (adapted from Wightman et al. 2003).

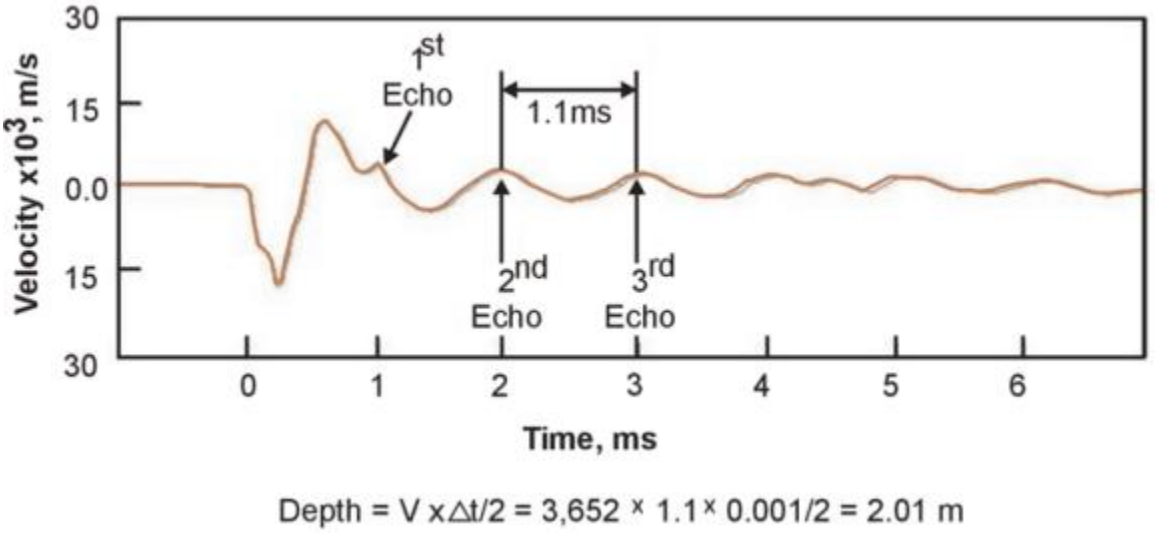

Depth = V x△t/2 = 3,652 ˣ 1.1 ˣ 0.001/2 = 2.01 m

Figure 1-10: Example SE test results and interpretation (Wightman et al. 2003).

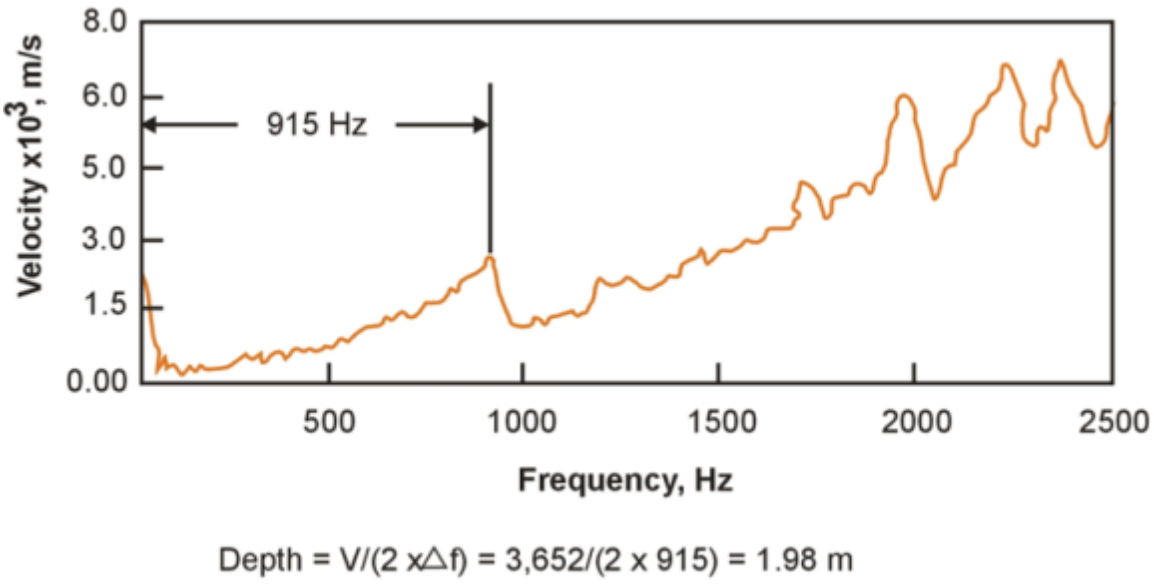

Figure 1-11: Example IR test results and interpretation (Wightman et al. 2003).

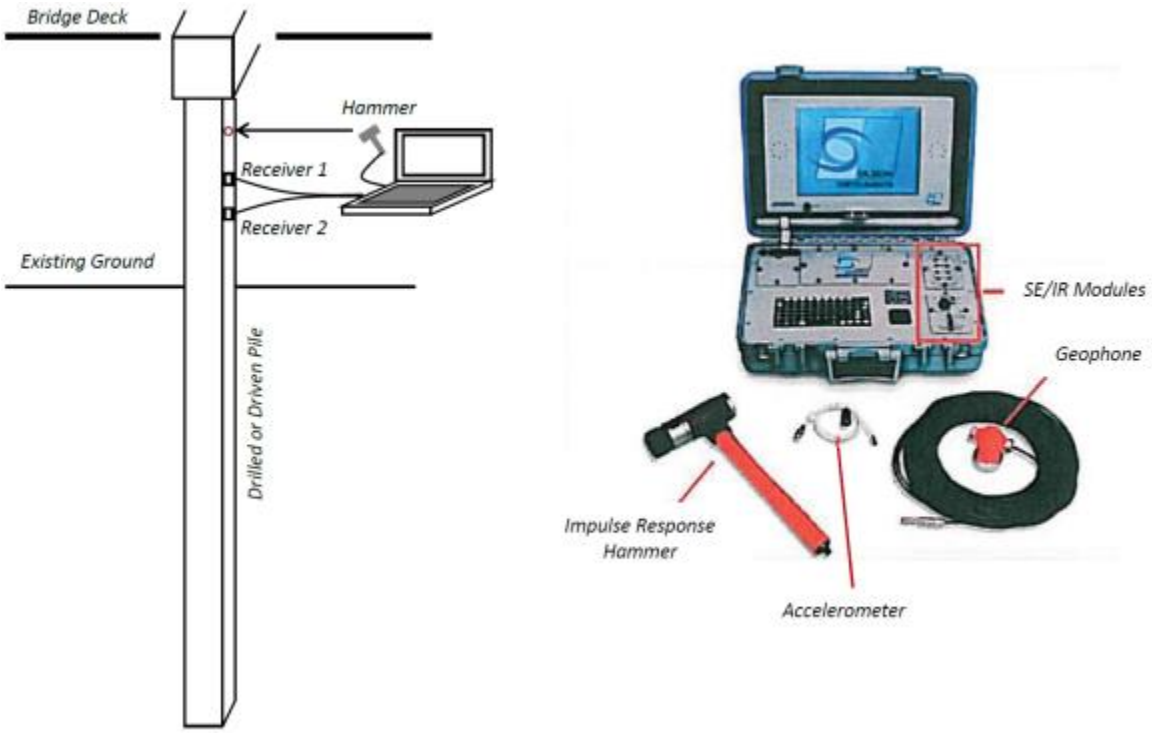

Figure 1-12: BW test layout and field equipment (adapted from McLemore et al. 2010).

Figure 1-13: BW field testing (Olson 2005b).

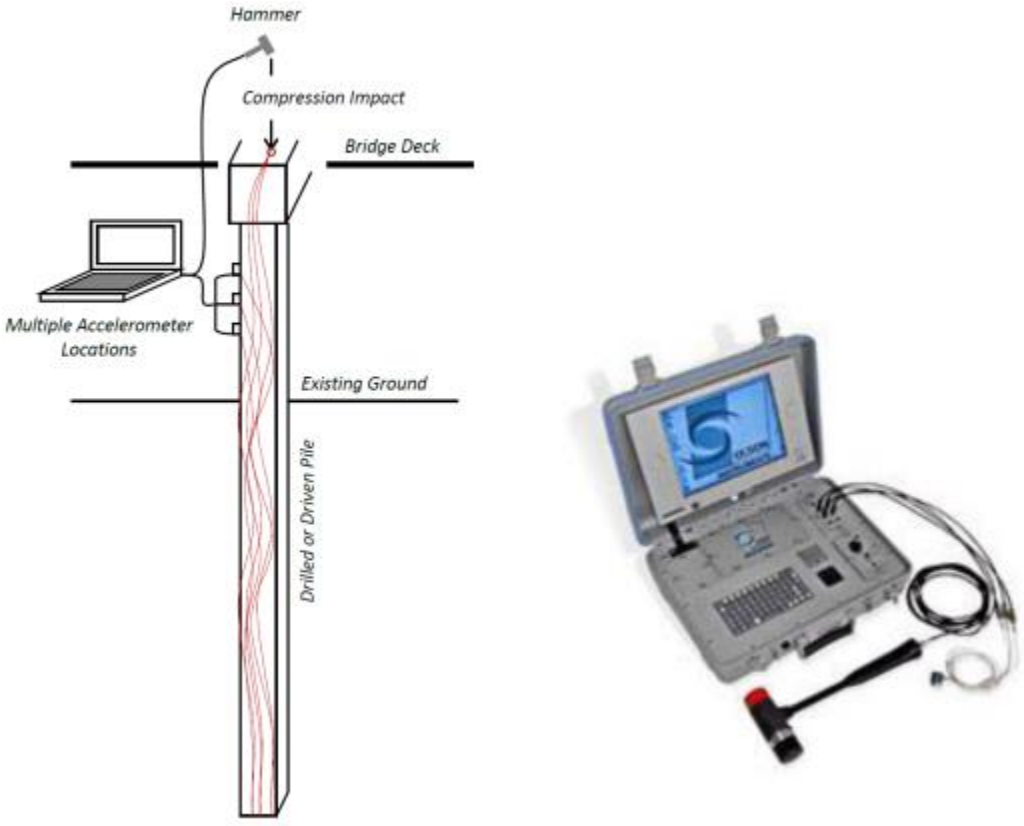

Figure 1-14: US test layout and equipment (adapted from McClemore et al. 2010).

Figure 1-15: US field testing (Holt and Hardy 2005).

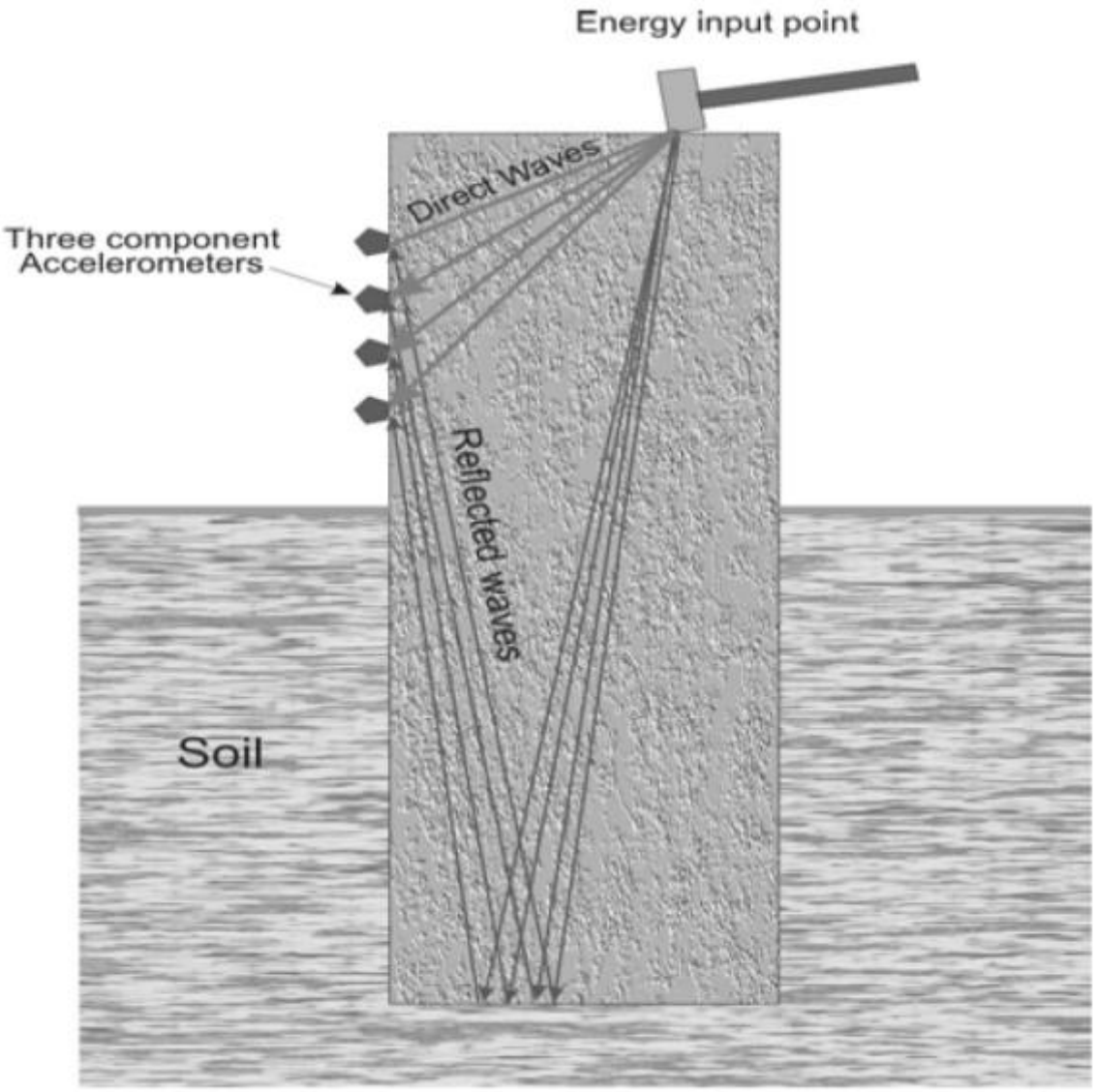

Figure 1-16: US vertical profiling (Wightman et al. 2003).

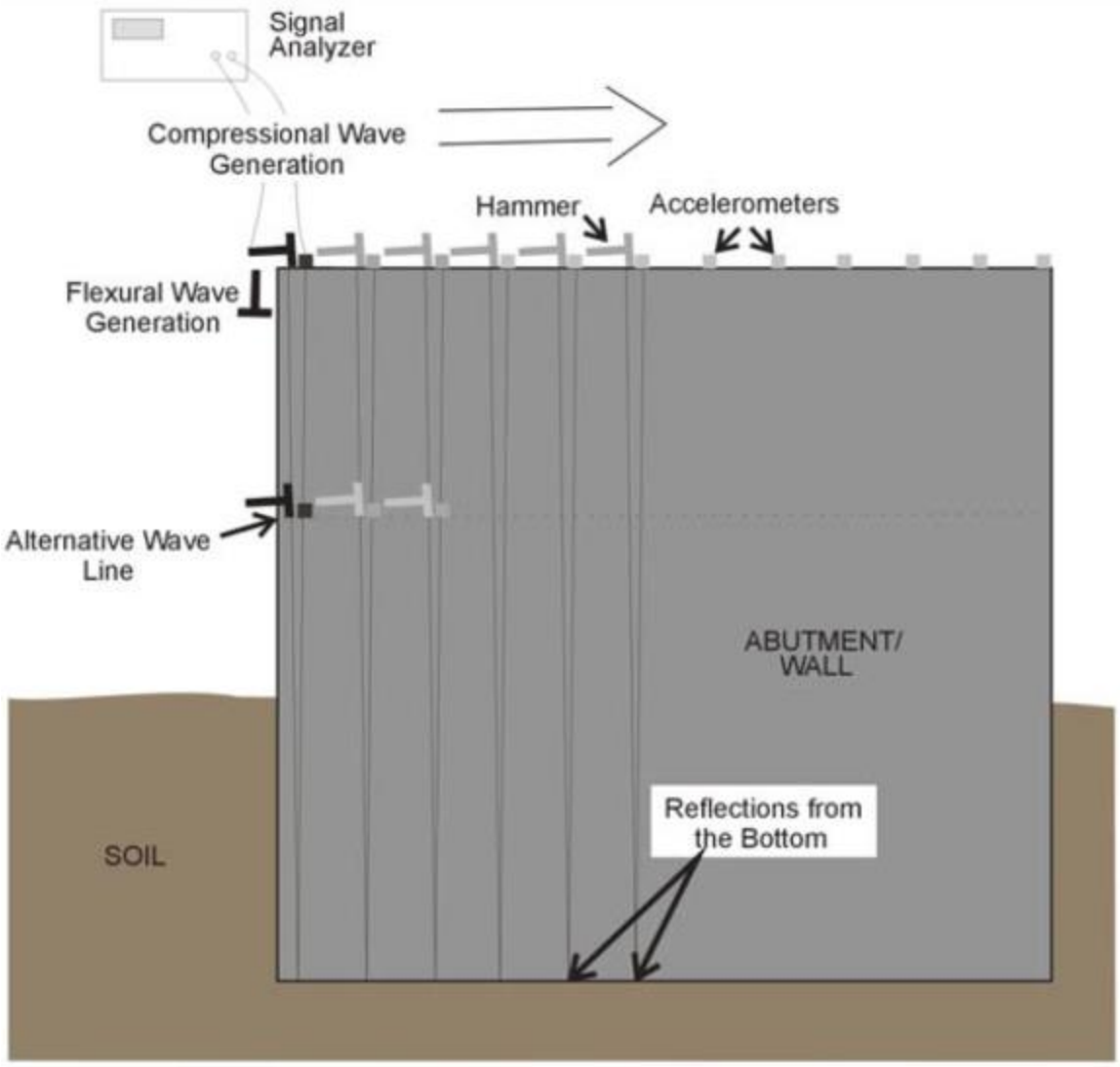

Figure 1-17: US horizontal profiling (Wightman et al. 2003).

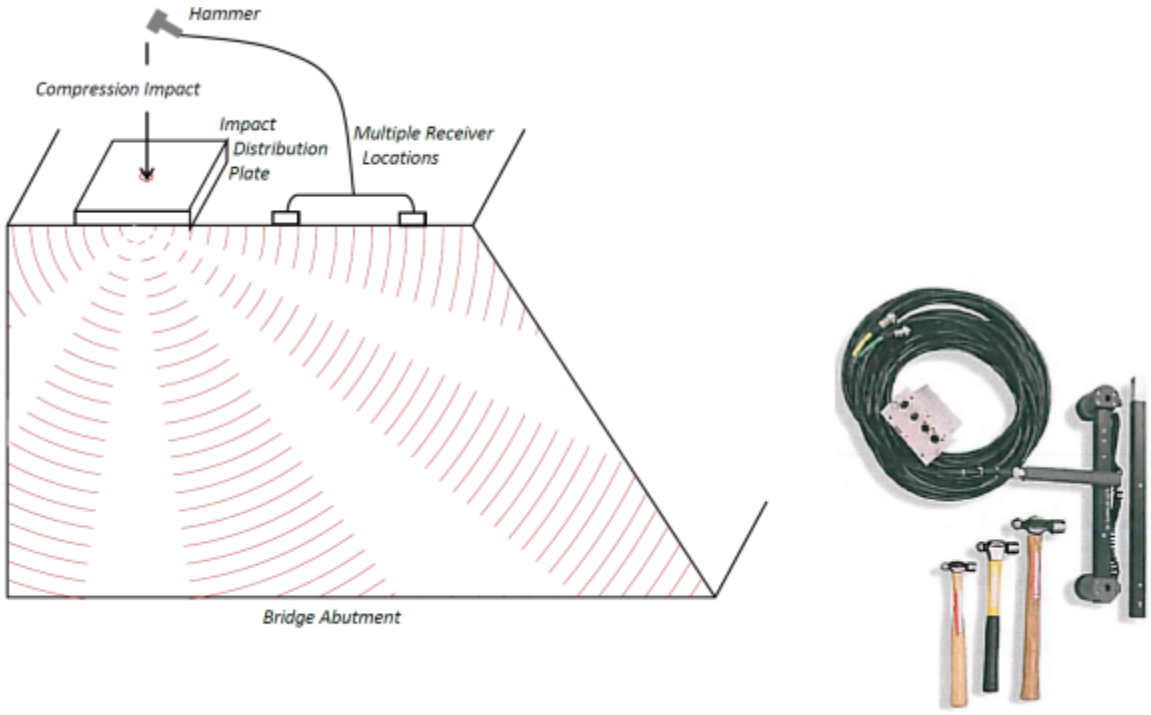

Figure 1-18: SASW test layout and field equipment (adapted from McClemore et al. 2010).

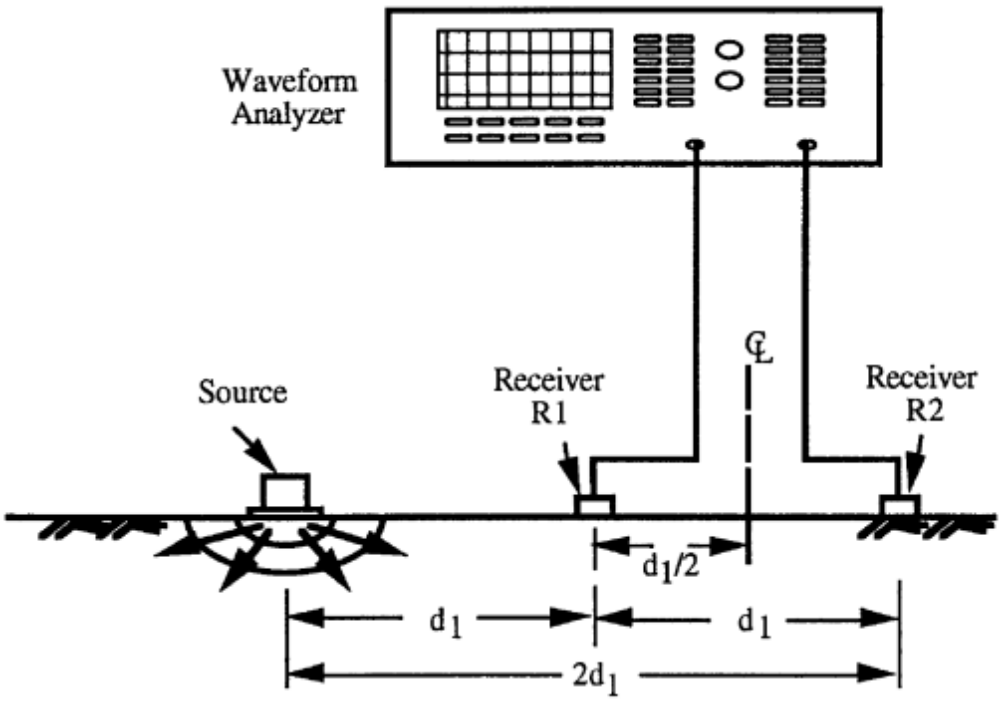

Figure 1-19: SASW source and receiver test layout (Olson et al. 1998).

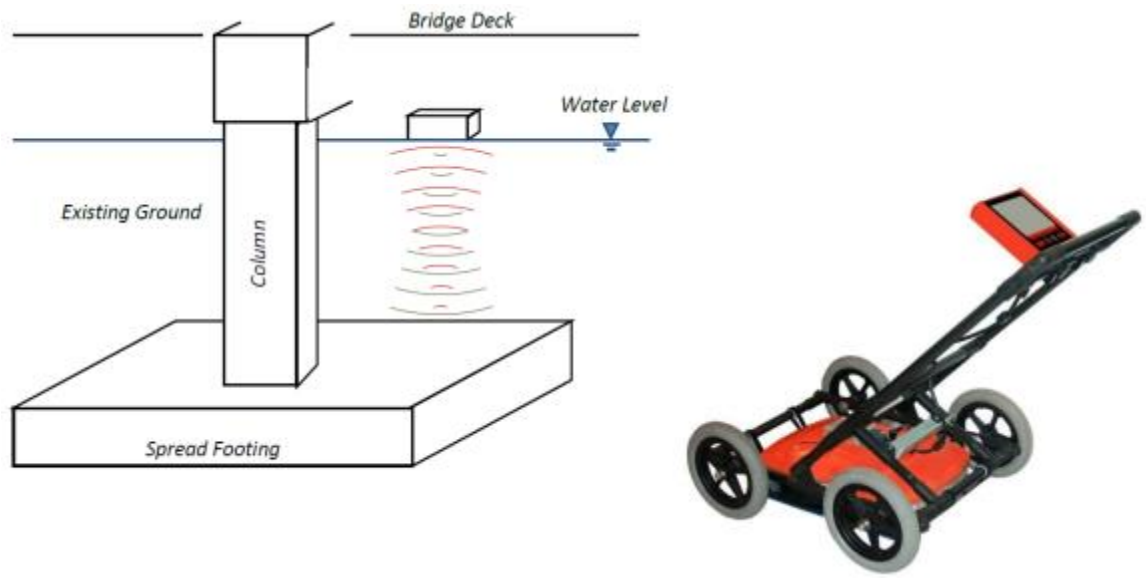

Figure 1-20: GPR test layout and field equipment (adapted from McLemore et al. 2010).

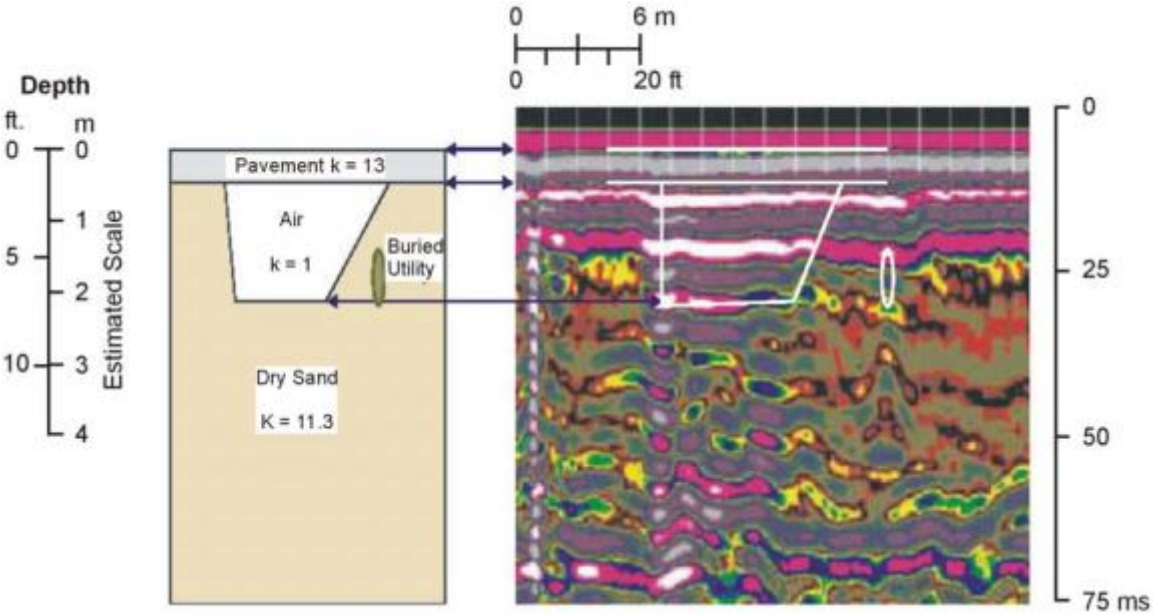

Figure 1-21: Example GPR test data and interpretation (Wightman et al. 2003).

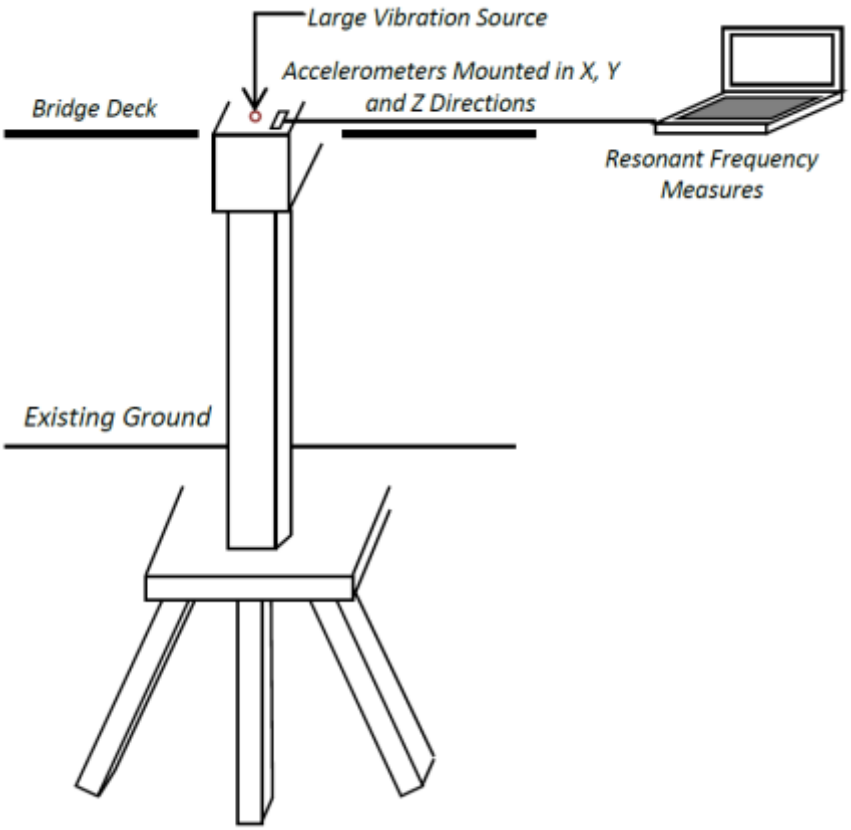

Figure 1-22: DFR test layout (adapted from McLemore et al. 2010).

Figure 1-23: Vibroseis truck for use during DFR method (Olson 2005b).

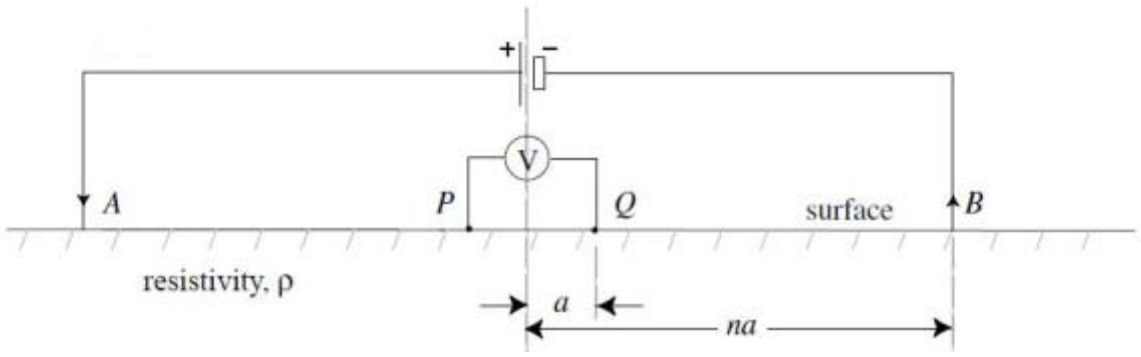

Figure 1-24: ERI concept (Briaud et al. 2012).

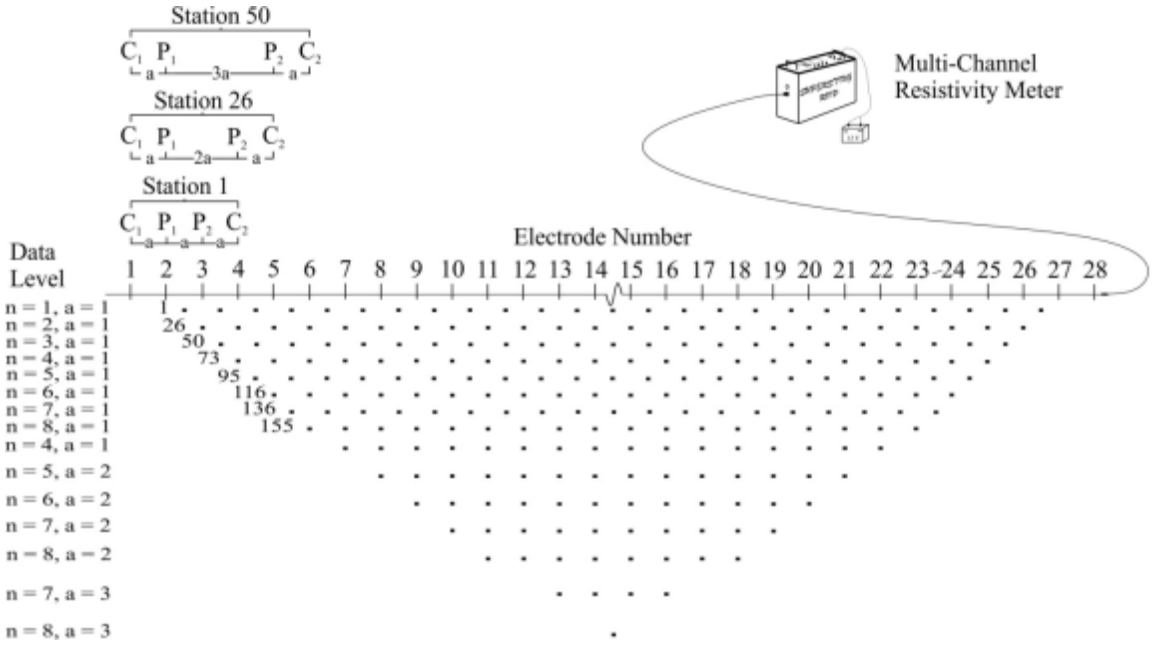

Figure 1-25: Arrangement of electrodes for a 2-D survey and sequence of measurements to create a pseudosection (after Loke 2000).

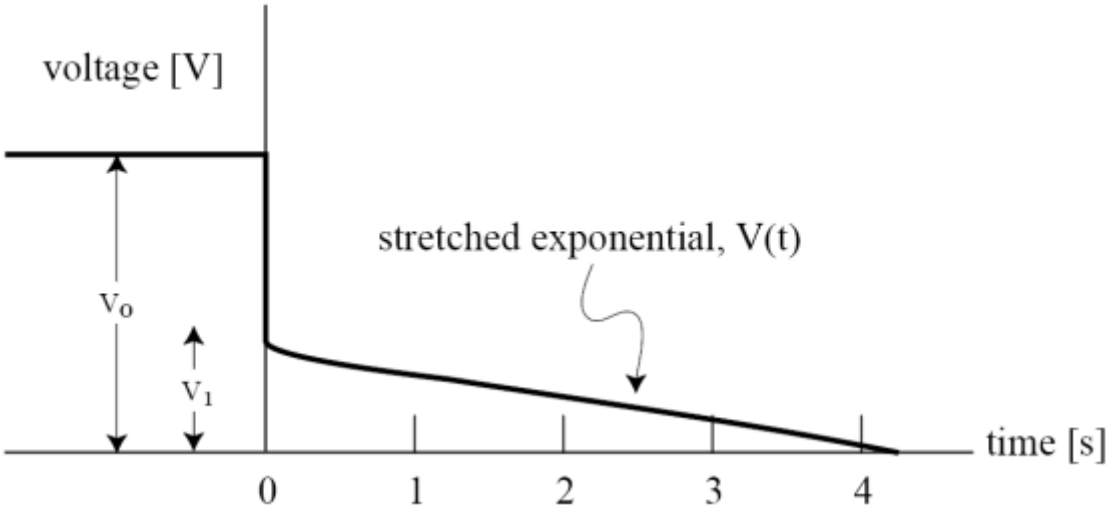

Figure 1-26: Induced polarization decay curve (Briaud et al. 2012).

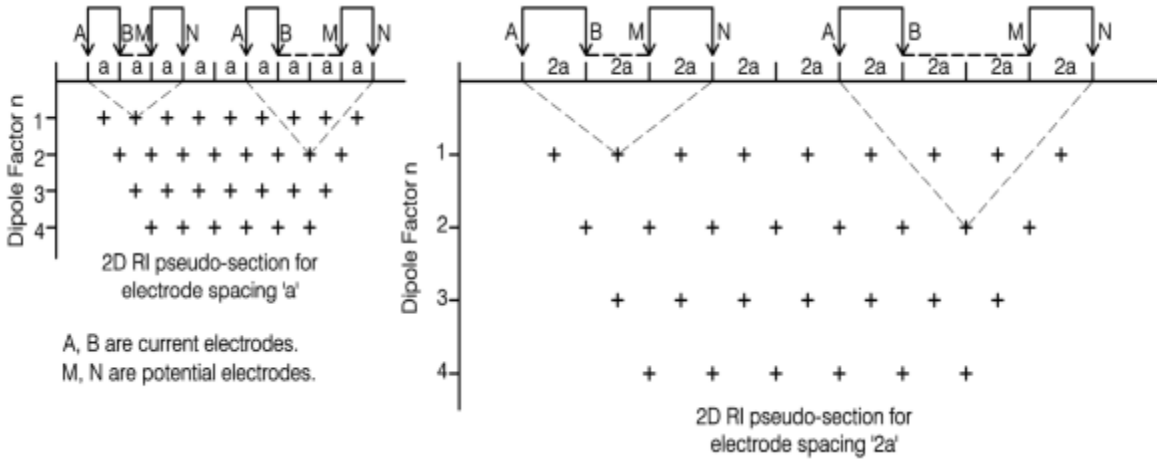

Figure 1-27: Depth of penetration versus resolution in the ERI method (Khan et al. 2012).

Figure 1-28: Multi-Electrode system for ERI testing (Briaud et al. 2012).

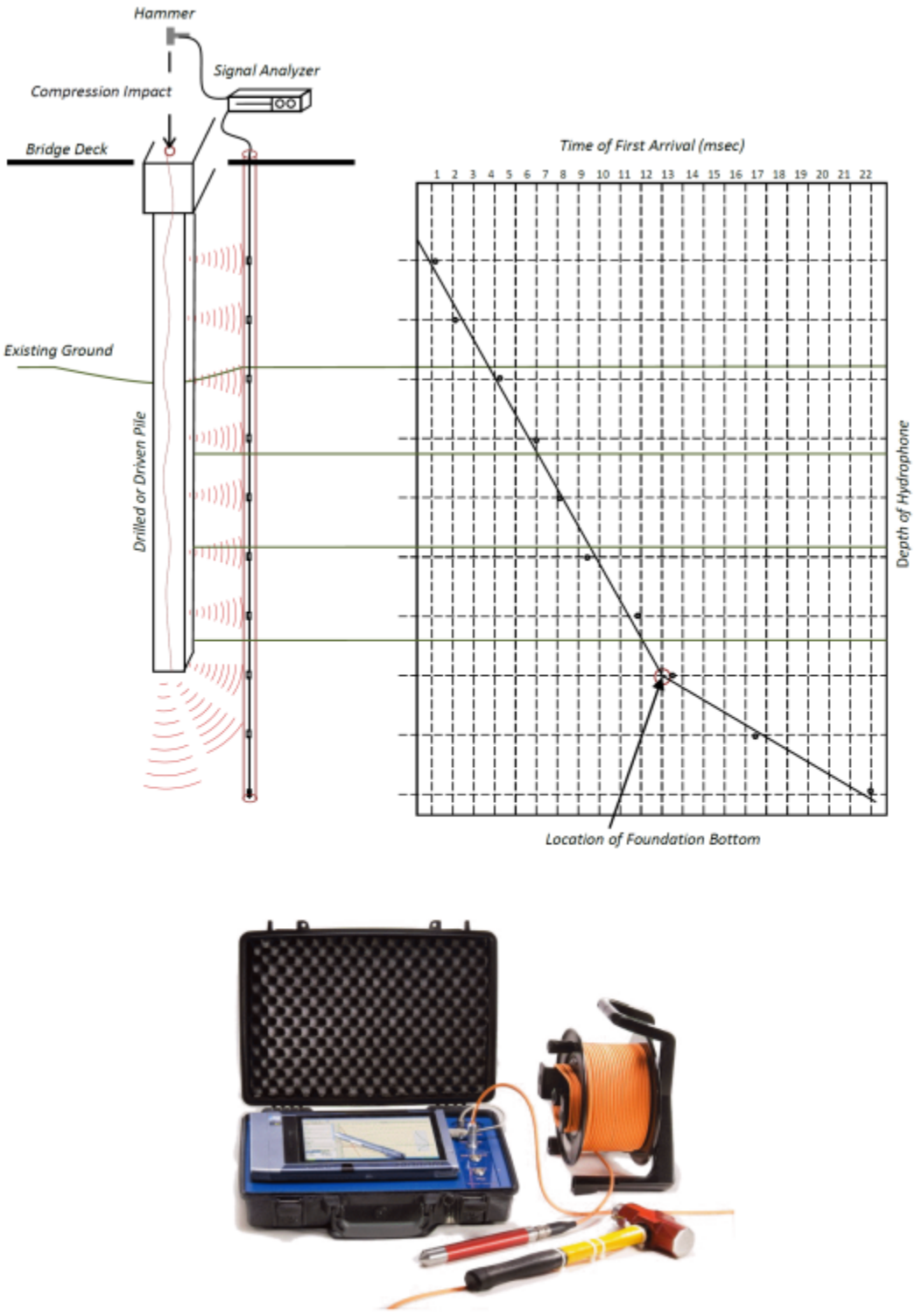

Figure 1-29: PS test layout, field equipment, and example of data interpretation (adapted from McLemore et al. 2010).

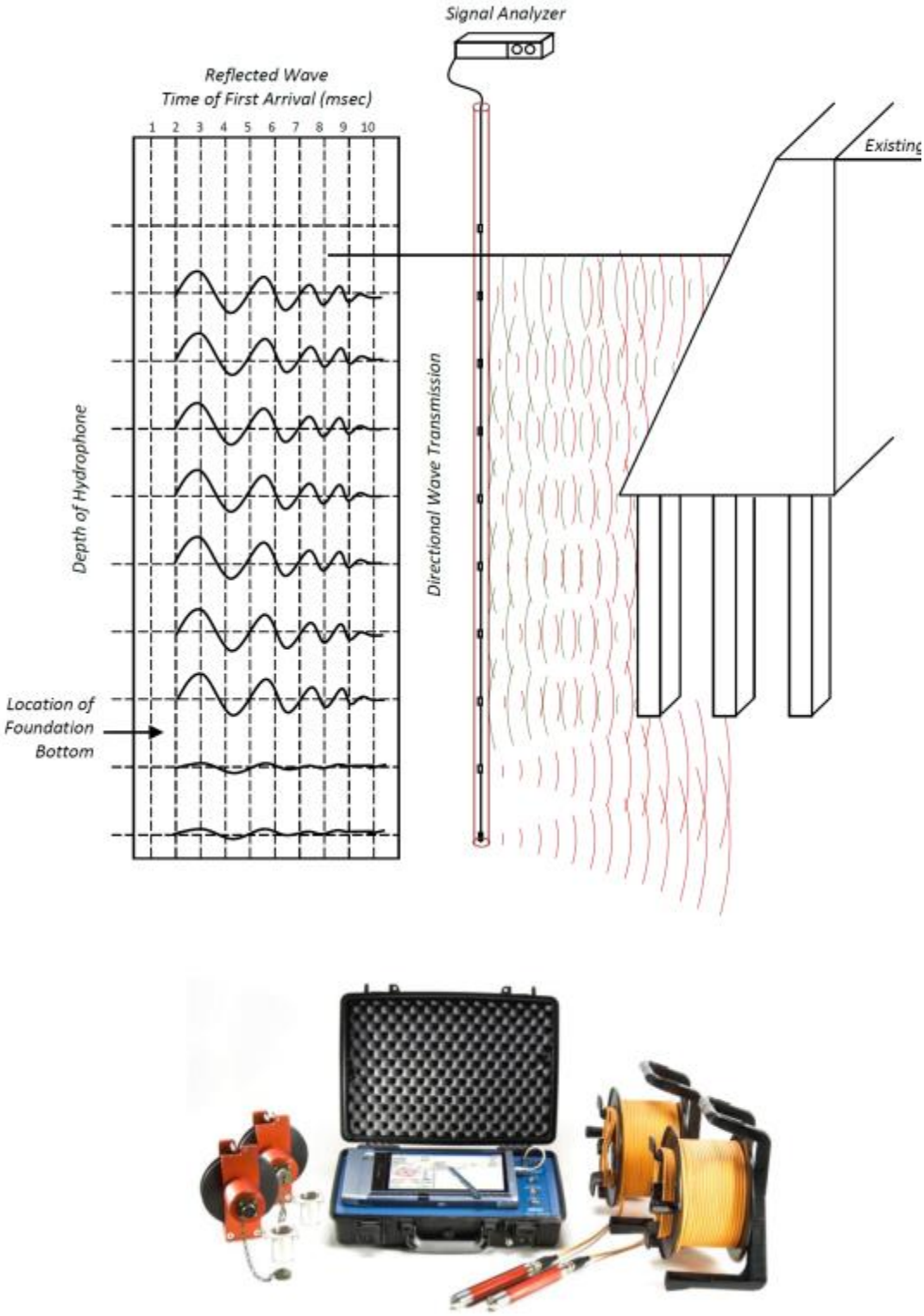

Figure 1-30: BHS test layout, field equipment, and example of data interpretation (adapted from McLemore et al. 2010).

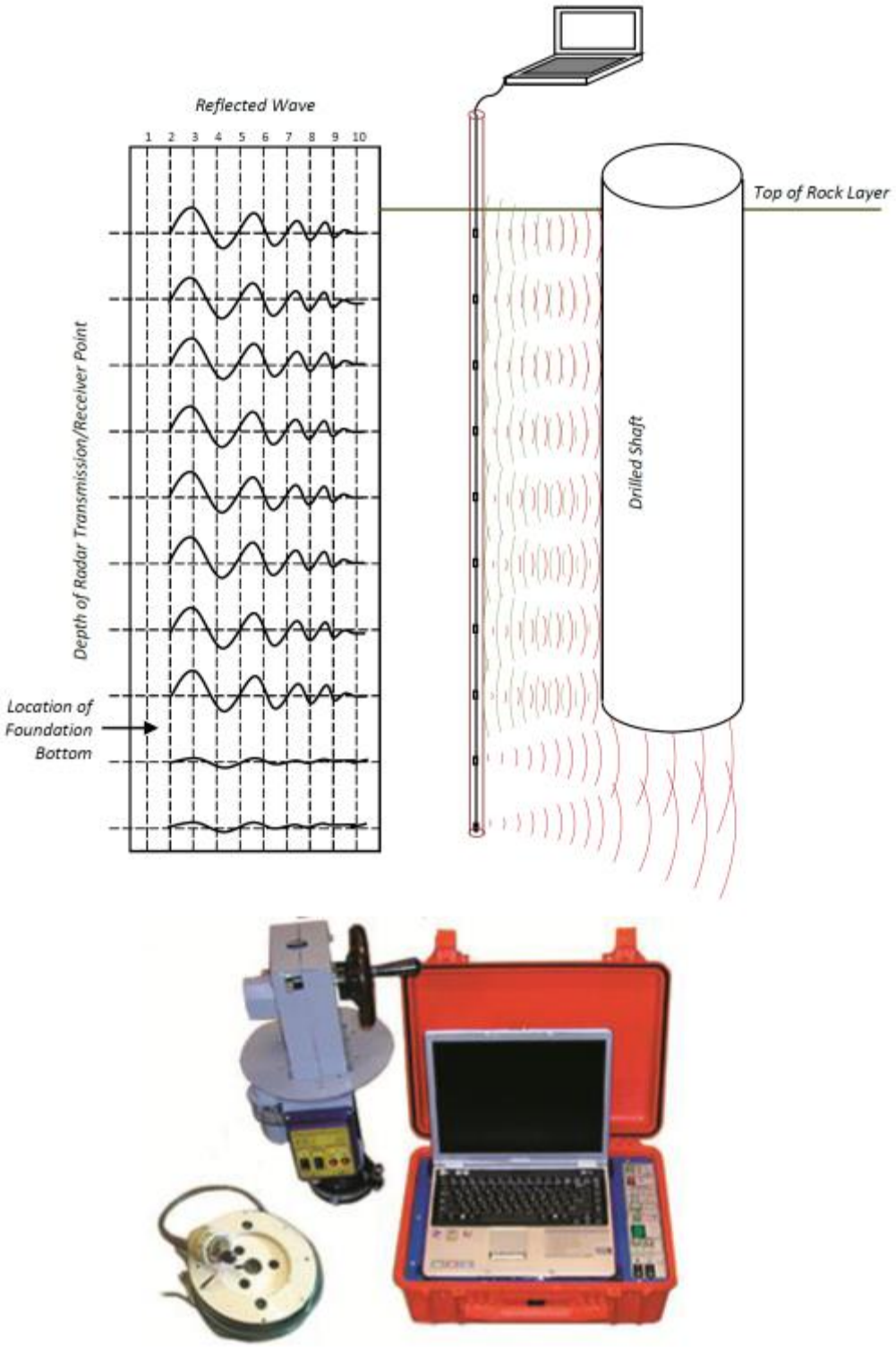

Figure 1-31: BHR test layout, field equipment, and example of data interpretation (adapted from McLemore et al. 2010).

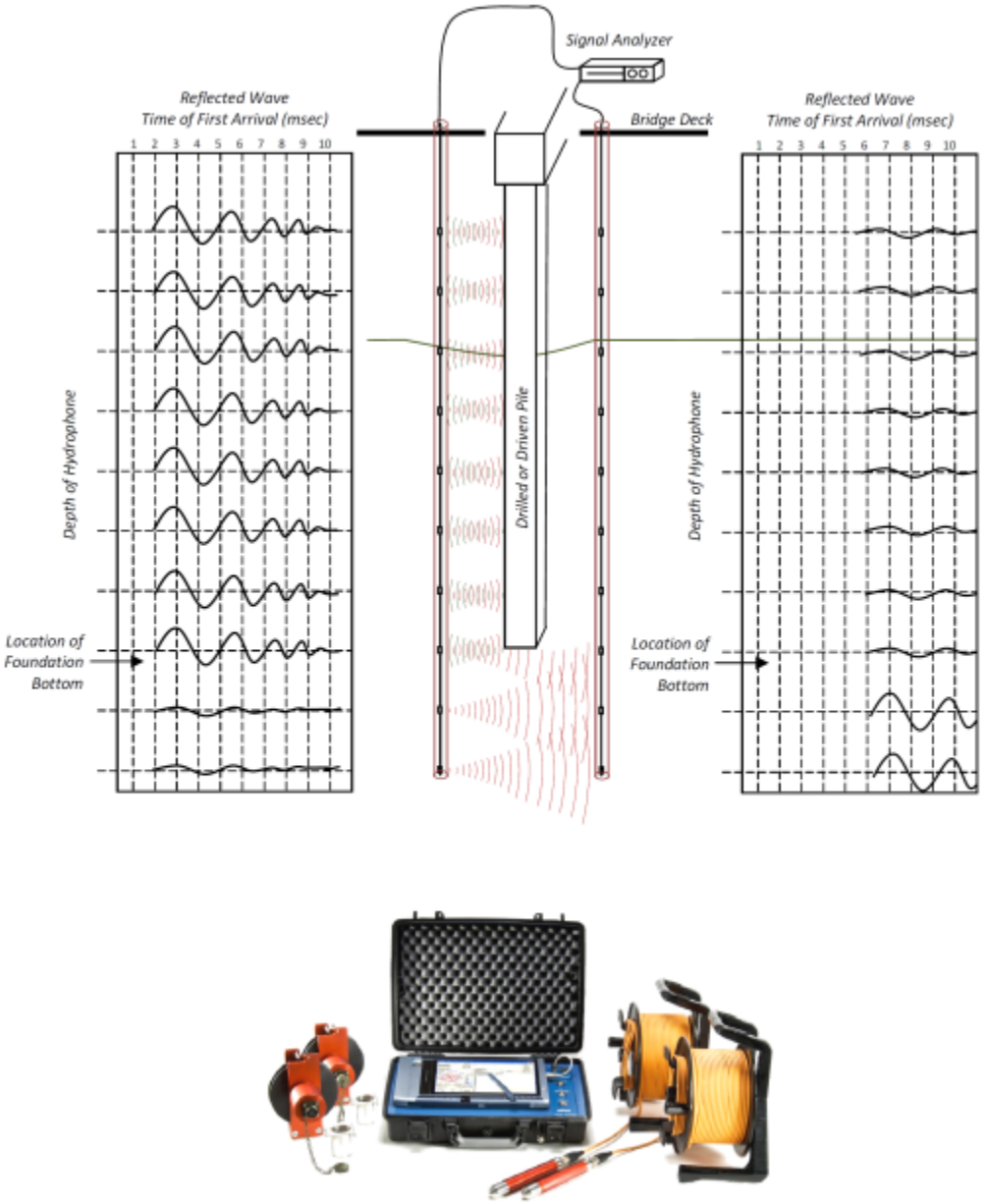

Figure 1-32: CSL test layout, field equipment, and example of data interpretation (adapted from McLemore et al. 2010).

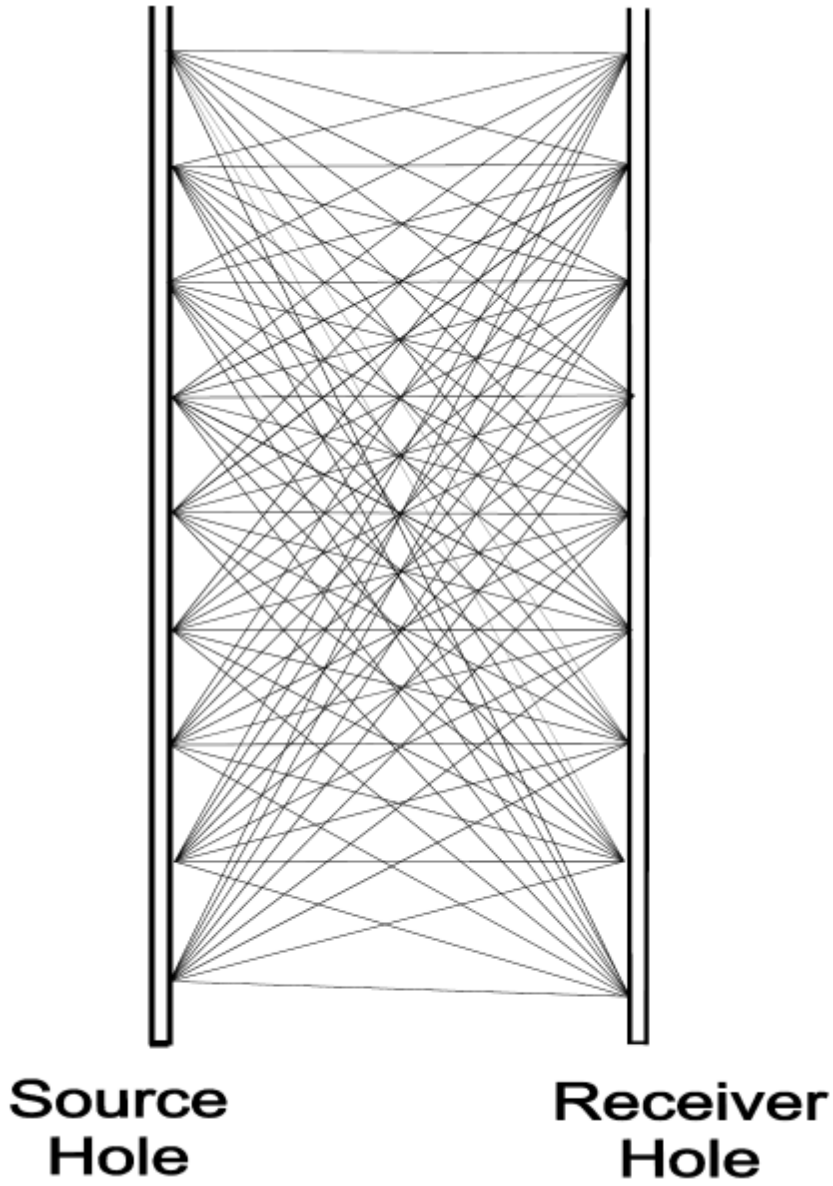

Figure 1-33: Combination of source-receiver depth locations for CSL tomographic survey design (Wightman et al. 2003).

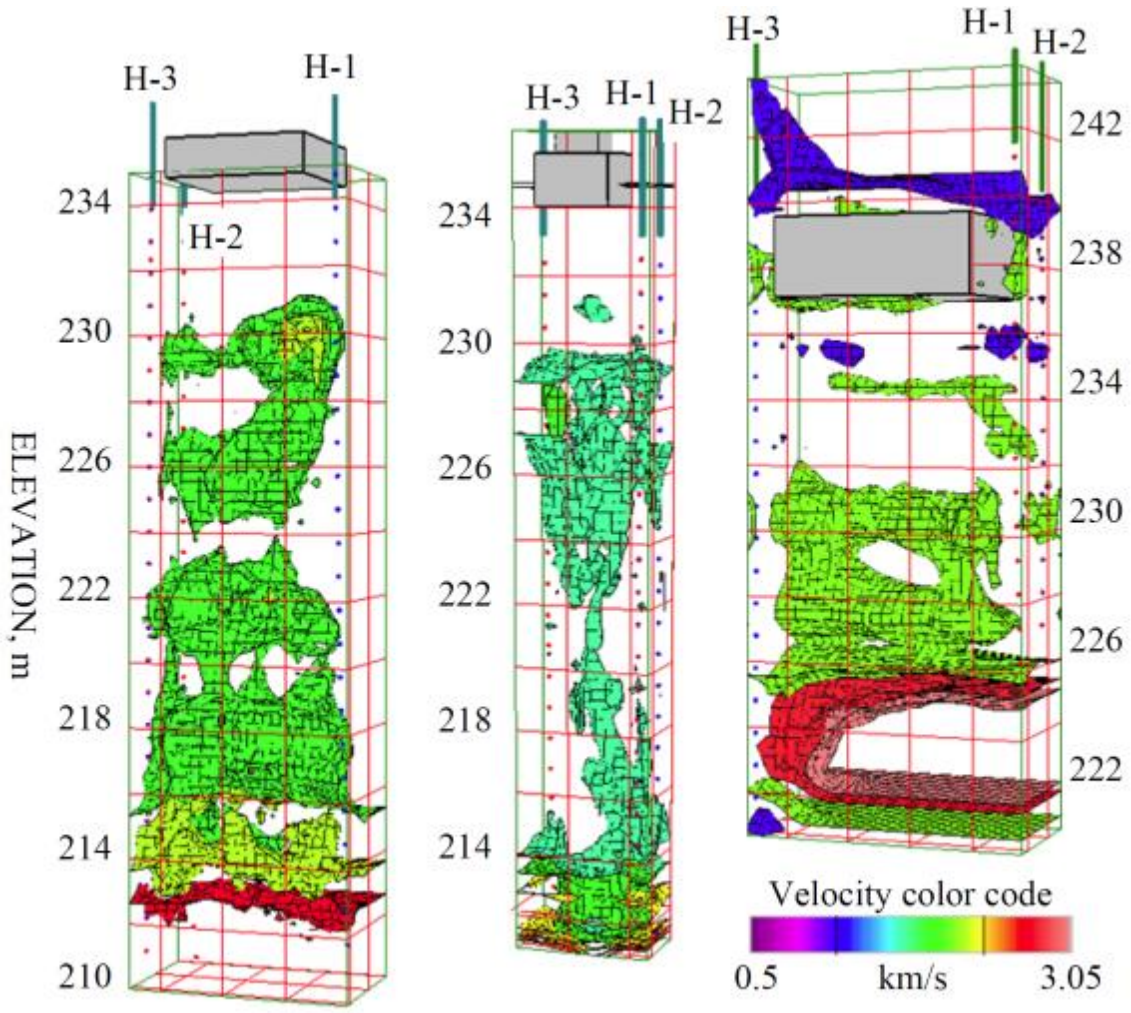

Figure 1-34: Example 3D tomogram of seismic velocity beneath foundations acquired by CSL method (Descour and Kabir 2010).

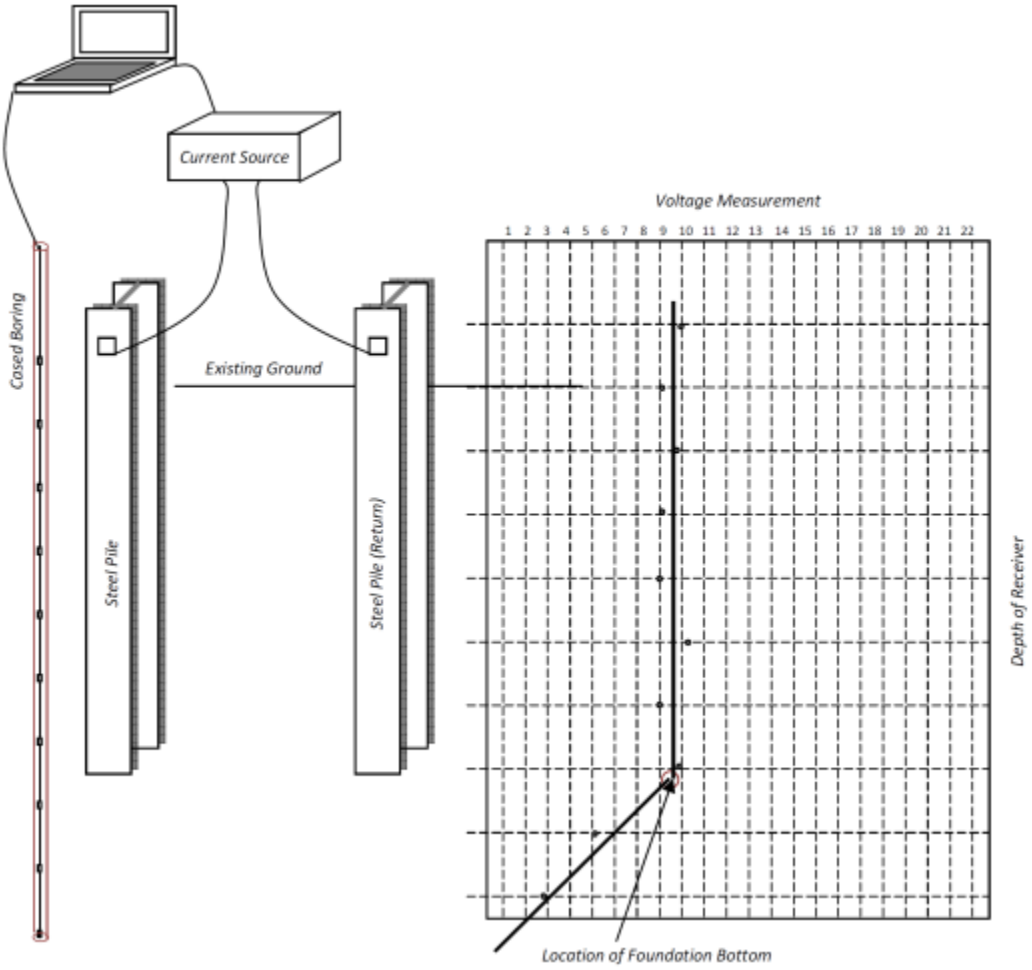

Figure 1-35: IF test layout and example of data interpretation (adapted from McLemore et al. 2010).

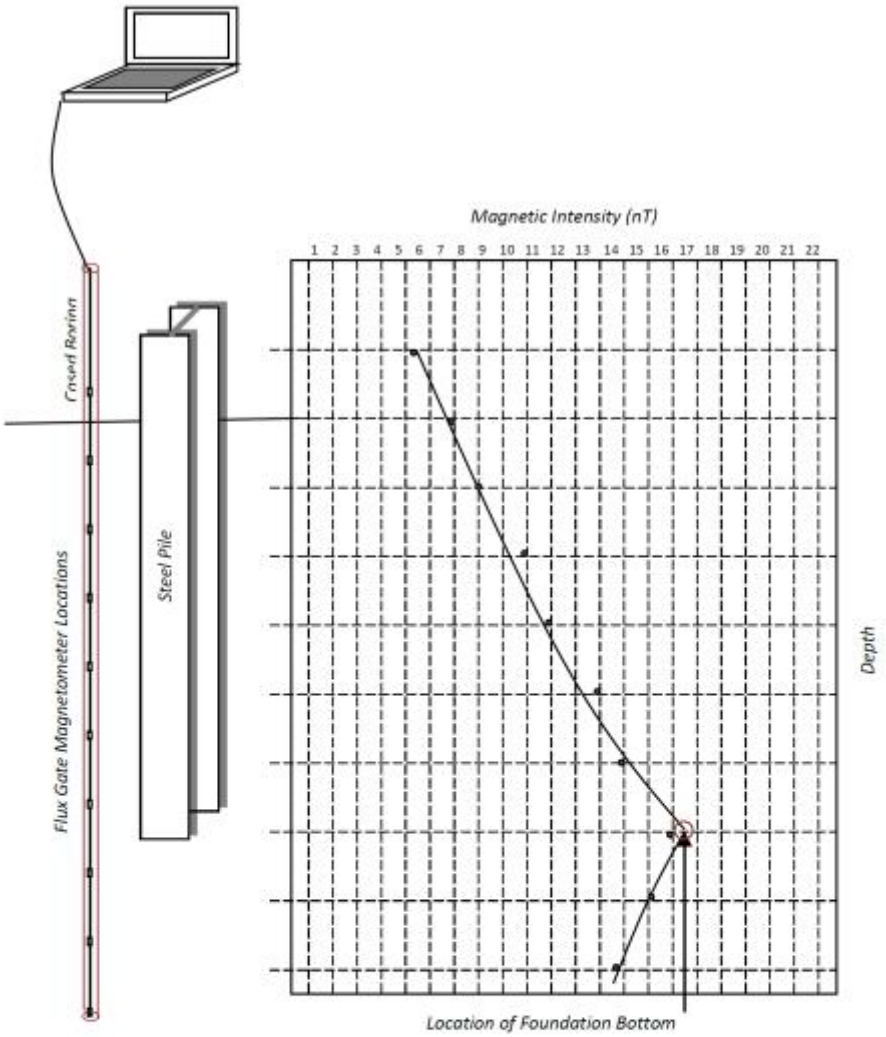

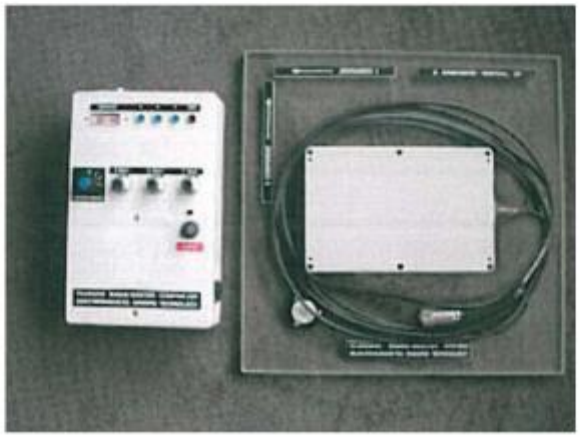

Figure 1-36: BM test layout, field equipment, and example of data interpretation (adapted from McLemore et al. 2010).

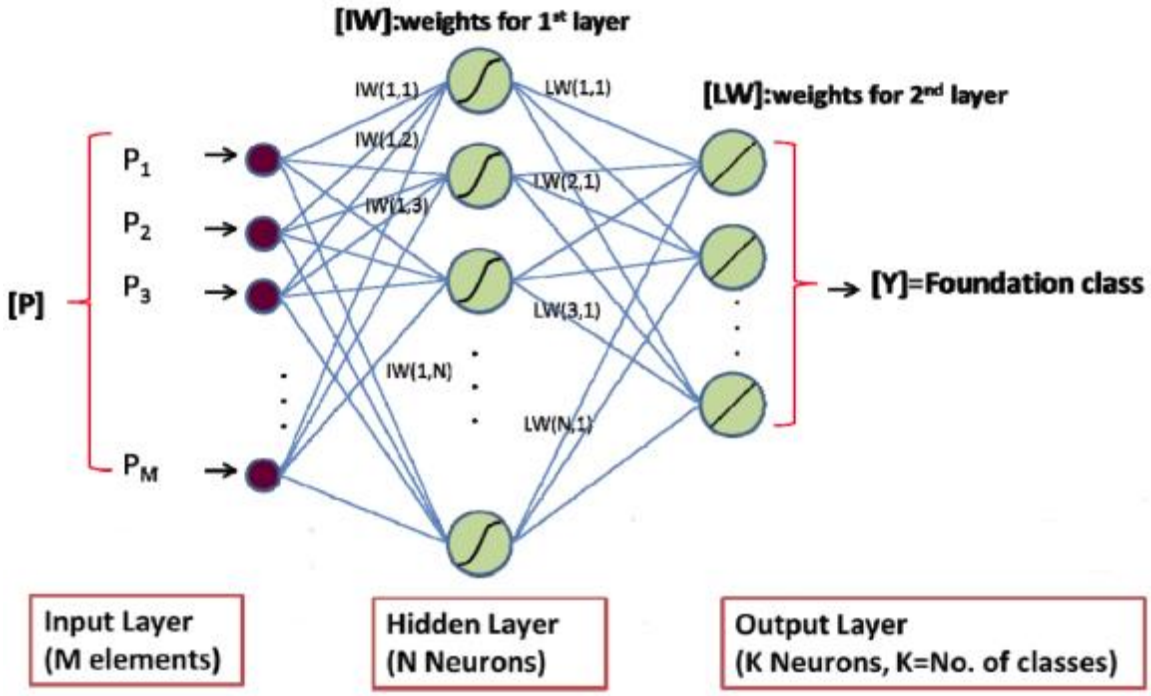

Figure 1-37: ANN model structure (adapted from Briaud et al. 2012).

METHOD	REMARKS
Excavation	• Positive identification of foundation • Expensive • Difficult
Probing	• Fast • Inexpensive • No positive identification of foundation (only negative information obtained) • Limited depth capacities • Possible false indications of foundation depth in rip-rap, rock and gravelly soils, and boulders
Drilling/ Coring	• Fast • Reliance placed on penetration rate and examination of cuttings • No pile depth information • More positive that probing • More expensive • Traffic is impeded • Safety of workers is a concern • Damage to the element must be repaired • Unlikely that piles below the pier or abutment will be encountered by a single borehole
Remote Subsurface Exploration	• Expensive • Time consuming • May require barge • Multiple angled drill holes needed to confirm pile location and type • No pile depth information

Table 1-1: Conventional Investigation Methods (adapted from Olson et al. 1998).

Bridge	Tested Unit	Substructure Type	Actual Depth (ft)	Predicted Depth (ft)
Golden (Colorado)	North Pier	Concrete Columns on shallow footings, connecting breast wall	(42.8' from top of beam to bottom of footing), embedded depth of 14.8'	No Success
Coors (Colorado)	Pier 4	Concrete columns on shallow footings supported by steel piles	(31.1' from top of beam to bottom of footing), embedded depth of 28.8', steel piles are 25' long,	No Success
	Pier 2	Concrete columns on shallow footings	(26' from top of beam down column to bottom of footing), embedded depth of 4.5'	No Success
Franktown (Colorado)	Northeast Wing (Abutment)	Exposed timber piles	28' embedded depth of 21'	29.8' (SE Tests) 27.9' (IR Tests)
	Middle Pier	Cap on top of exposed timber piles	28' embedded depth of 25'	23.8' (SE Tests) 23.2' (IR Tests)
Weld (Colorado)	West Abutment	Massive concrete abutment supported by steel piles	(6.0' depth of abutment) Steel piles are 34.5 ' long (1 ft in pilecap), embedded depth of 34'	6.6' (SE Tests) 6.5' (IR Tests) No success for steel pile length
Alabama (Alabama)	Bent 4	Steel piles extending from top to bottom	(39' from ground surface to tip of pile)	No success
Old Bastrop (Texas)	Caisson	Two circular columns connected by a breast wall supported by a belled concrete footing on a rectangular concrete footing	(38' from top of columns to top of bell section, 18' thick bell section, 16' thick rectangular section), embedded depth of 35'	35.9' (upper columns, SE tests) no success for the bell and rectangular sections depth determinations
	Piles	Concrete columns supported by a pile cap of concrete piles	3' thick pile cap, 32' long concrete piles, embedded depth of 33.3'	No success
New Bastrop (Texas)	Drilled Shaft	Concrete columns supported by shafts	45' long shafts, embedded depth of 38'	38' (Depth below grade, SE tests)

Table 1-2: Summary of SE/IR test results from first phase of NCHRP Project 21-05 (Olson et al. 1998).

Test Method	Blind Predictions	Post-Processed Predictions
Parallel Seismic	Depths of 12 out of the 19 bridges tested were predicted to within ± 13% of the actual bottom of foundation depths. Bottom foundation depths of the other 6 bridges were incorrectly predicted	Depths of 16 out of the 19 bridges tested were predicted to within ± 13% of the actual depths. There was no indication in the PS test results to support the actual depths for the remaining three bridges
Ultraseismic	Results were inconclusive on 6 out of the 18 bridges tested. Depths of 8 out of the 18 bridges were predicted within ± 14% of the actual depths. Depths of the other 4 bridges were incorrectly predicted	Test results were inconclusive on 6 out of the 18 bridges tested. Depths of 11 out of the 18 bridges were predicted within ± 14% of the actual depths. There was no indication in the US data to support the actual depth reported for the Johnston County Bridge # 33.
Sonic Echo/Impulse Response	Results were inconclusive on 14 out of the 15 bridges tested. Only one bridge with timber piles foundation in North Carolina showed an echo which corresponded to the tip of the pile	Results were inconclusive on 14 out of the 15 bridges tested. Only one bridge with timber piles foundation in North Carolina showed an echo which corresponded to the tip of the pile
Bending Waves	Results were inconclusive on all 7 timber pile bridges tested with the BW method	Results were inconclusive on all 7 timber pile bridges tested with the BW method
Induction Field	Tests were performed on two bridges, one in Colorado and one in Texas. The IF results showed a drop in amplitude below the tip of the steel pile at the Colorado bridge with good agreement with the depth predicted from Parallel Seismic tests. The IF results at the steel-pile bridge in Texas were inconclusive	Tests were performed on two bridges, one in Colorado and one in Texas. The IF results showed a drop in amplitude below the tip of the steel pile at the Colorado bridge with good agreement with the depth predicted from Parallel Seismic tests. The IF results at the steel-pile bridge in Texas were inconclusive

Table 1-3: Summary of NDT test results from second phase of NCHRP Project 21-05 (Olson and Aouad 2001).

Testing Method	Confidence in Estimation*	Application	Advantages	Disadvantages
Sonic Echo	75%	Typically used for column type substructures. Best penetration achieved in loose soils. Used for determining the geometry and thickness of the foundation.	Low cost, very quick, no soil boring required, minimal maintenance of traffic (MOT) required, can be easily used in conjunction with subsurface NDT to ensure accuracy. Data collection can be automated.	Imperfections, splices, or stiff soils can cause inaccurate foundation depth estimations. Complex foundation elements, such as subsurface pile caps and underlying piles, will not be distinguishable.
Bending Waves	75%	Typically used for column type substructures. Best penetration achieved in loose soils.	Easily adapted to timber piles, low cost, very quick, no soil boring required, minimal MOT required, can be easily used in conjunction with subsurface NDT to ensure accuracy.	Imperfections, splices, or stiff soils can cause inaccurate foundation depth estimations. Complex foundation elements, such as subsurface pile caps, and underlying piles, will not be distinguishable. Data interpretation effected by superstructure impact.
Ultra-Seismic	85%	Used for determining the geometry and thickness of the foundation. Best penetration achieved in loose soils.	Adaptable to most driven piles, low cost, very quick, no soil boring required, minimal MOT required, can be easily used in conjunction with subsurface NDT to ensure accuracy.	Imperfections, splices, or stiff soils can cause inaccurate foundation depth estimations. Complex foundation elements, such as subsurface pile caps, and underlying piles, will not be distinguishable.
Surface Wave Spectral Analysis	75%	Used for determining the geometry and thickness of the foundation.	Accurate estimation of foundation depth at bridge abutments, low cost, very quick, no soil boring required, minimal MOT required, can be easily used in conjunction with subsurface NDT to ensure accuracy.	Requires a large flat surface which may eliminate most pile foundations from acceptable application.
Ground Penetrating Radar	N/A	Used to indicate the geometry of flat, tabular foundations and bedrock depths.	Accurate estimation of foundation depth at bridge abutments, low cost, very quick, no soil boring required, minimal MOT required, can be easily used in conjunction with subsurface NDT to ensure accuracy.	Primarily only useful for tabular foundations buried beneath accessible terrain. High initial cost of equipment. Signal can be complicated by adjacent substructures.
Dynamic Foundation Response	N/A	Typically used for column type substructures. Best penetration achieved in loose soils.	Test may be able to determine existence of a complex foundation and can be easily used in conjunction with subsurface NDT to ensure accuracy.	Not a means of accurately estimating foundation depth. Method will require a database compiling test results from existing bridge sites to determine existence of complex foundation.

* Confidence in estimation refers to the accuracy of the test relative to the known problematic variables associated with the test procedure.

Table 1-4: Summary of advantages and limitations of surface NDT methods (adapted from McLemore et al. 2010 & Abboud and Kaiser 2012).

Testing Method	Mobilization[2]	MOT[3]	Testing Equiptment[4]	Testing Personel[5]	Soil Boring / Probes[6]	Lab & Engineering[7]	Total Cost
			Surface NDT Methods[1]				
Sonic Echo	0.5 - 1.5	0 - 1.0	0.5 - 0.9	1.0 – 3.0	0	2.5 – 5.0	4.5 – 11.4
Bending Waves	0.5 - 1.5	0 - 1.0	0.5 - 0.9	1.0 – 3.0	0	2.5 – 5.0	4.5 – 11.4
Ultra-Seismic	0.5 - 1.5	0 - 1.0	0.6 - 1.1	1.0 – 3.0	0	2.5 – 5.0	4.6 – 11.6
Surface Wave Spectral Analysis	0.5 - 1.5	0 - 1.0	0.5 - 0.9	1.0 – 3.0	0	2.5 – 5.0	4.5 – 11.4
Ground Penetrating Radar	0.5 - 1.5	0 - 1.0	2.0 - 3.5	1.0 – 3.0	0	2.5 – 5.0	6.0 – 14.0
Dynamic Foundation Response	0.5 - 1.5	0 - 1.0	0.5 - 1.0	1.0 – 3.0	0	2.5 – 5.0	4.5 – 11.5
			Subsurface NDT Methods[1]				
Parallel Seismic Test	0.5 - 2.0	1.0 - 2.5	0.5 - 1.3	1.0 – 3.0	2.0 - 4.0	5.0 - 10.0	10.0 – 22.8
Borehole Radar	0.5 - 2.0	1.0 - 2.5	2.0 - 3.5	1.0 – 3.0	2.0 - 4.0	5.0 - 10.0	11.5 – 25.0
Borehole Sonic Test	0.5 - 2.0	1.0 - 2.5	1.0 - 1.5	1.0 – 3.0	2.0 - 4.0	5.0 - 10.0	10.5 – 23.0
Cross Hole Sonic Test	0.5 - 2.0	1.0 - 2.5	1.2 - 2.5	1.0 – 3.0	2.0 - 4.0	5.0 - 10.0	12.7 – 28.0
Induction Field	0.5 - 2.0	1.0 - 2.5	0.5 - 1.0	1.0 – 3.0	2.0 - 4.0	5.0 - 10.0	10.0 – 22.5
Borehole Magnetic	0.5 - 2.0	1.0 - 2.5	0.3 - 1.0	1.0 – 3.0	2.0 - 4.0	5.0 - 10.0	9.8 – 22.5

Notes:
1. All values are x $1,000
2. Mobilization costs include equipment and personnel.
3. MOT costs are from 0 to 9 hours.
4. Testing equipment costs are based on 5% of the average cost to purchase testing equipment.
5. Testing personnel costs are based on 4 to 9 hours of a field engineer and trained technician's time.
6. Soil boring and/or probes costs include drilling, casing, grouting, etc.
7. Laboratory and engineering estimates include data analysis, computations and report preparation with recommendations.

Table 1-5: Estimated costs of NDT methods (adapted from McLemore et al. 2010 & Abboud and Kaiser 2012).

Bridge Location	Tested Unit	Substructure Type	Actual Depth (ft)	Predicted Depth (ft)
Golden (Colorado)	North Pier	Concrete Columns on shallow footings, connecting breast wall	(42.8' from top of beam down column to bottom of footing), embedded depth of 14.8'	42.0' (P-Wave) 42.9' (Flexural Wave) (from top of beam)
Coors (Colorado)	Pier 4	Concrete columns on shallow footings supported by steel piles	(31.1' from top of beam down column to bottom of footing), Steel piles are 25' long, embedded, depth of 28.8'	31.1' (P-Wave) 29.7' (Flexural Wave) 33.9' (Frequency) (from top of beam)
	Pier 2	Concrete columns on shallow footings	(26' from top of beam down column to bottom of footing), embedded depth of 4.5'	25.9' (Flexural Wave) (from top of beam)
Franktown (Colorado)	Northeast Wing (Abutment)	Exposed timber piles	28' embedded depth of 21'	Not successful
	Middle Pier	Cap on top of exposed timber piles	28' embedded depth of 25'	23.0' (Compression) (from top of pile)
Weld (Colorado)	West Pier	Concrete wall on concrete footing supported by steel piles	(18.9' from top of wall to bottom of footing), Steel piles are 25' long, embedded depth of 34.6'	18' (from top of wall) (Flexural)
Alabama (Alabama)	Bent 4	Steel piles extending to the bottom of the superstructure	(39' from ground surface to tip of pile)	34'-35' (compression) 35' (flexural) (from ground surface)
Old Bastrop (Texas)	Caisson	Two circular columns connected by a breast wall supported by a bell shape concrete footing supported on a rectangular concrete footing	(38' from top of columns to top of bell section, 18' thick bell section, 16' thick rectangular section), embedded depth of 35 '	two depths: 37' (from top of bell section) and 18.6' (from top of bell section) Both depths are from flexural waves
New Bastrop (Texas)	Drilled Shaft	Concrete columns supported by shafts	45' long shafts, embedded depth of 38'	45'(from top of shaft) or 38' (from ground surface) Flexural

Table 1-6: Summary of US test results from first phase of NCHRP Project 21-05 (Olson et al. 1998).

Bridge Location	Tested Unit	Substructure Type	Actual Depth (from top of ground surface(ft))	Predicted Depth (ft)
Coors (Colorado)	Pier 4	Concrete columns on shallow footings supported by steel piles	28.8'	27' (Geophone) 29' (Hydrophone)
Alabama (Alabama)	Bent 4	Steel piles extending to the bottom of the superstructure	East Pile: 39' Middle Pile: 39'	East Pile: 30' (Geophone) Middle Pile: 31.6' (Geophone) 34.6' (Hydrophone)
Old Bastrop (Texas)	Caisson	Two circular columns connected by a breast wall supported by a bell shape concrete footing supported on a rectangular concrete footing	35'	Borehole 1: 35.3' (Geophone) 38.3' (Hydrophone) Borehole 6: 35' (Geophone)
	Piles	Concrete columns supported by a pile cap of concrete piles	33.3'	32' (Geophone) 33' (Hydrophone)
New Bastrop (Texas)	Drilled Shaft	Concrete columns supported by shafts	38'	35.3' (Geophone)) 38.3' (Hydrophone)

Table 1-7: Summary of PS test results from first phase of NCHRP Project 21-05 (Olson et al. 1998).

Testing Method	Confidence in Estimation*	Application	Advantages	Disadvantages
Parallel Seismic Test	90%	Used or determining the foundation depths for a large range of foundation types. Can possibly determine foundation orientation also.	Test may provide accurate foundation depth estimates for most foundation types. Also, allows for the collection of soil data when the borehole and casing are constructed.	Access for test may require significant MOT. Pavement core will typically be installed through the bridge deck.
Borehole Radar	80%	Used for determining the foundation parameters. The test is sensitive to steel members.	Test will provide accurate depth approximations in sandy soil conditions where there is no presence of salt water. Also, allows for the collection of soil data when the borehole and casing are constructed.	Not reliable in a brackish environment. Clayey soils may interfere with radar transmission. Access for test may require significant MOT. Pavement core will typically be installed through the bridge deck.
Borehole Sonic Test	85%	Used for determining the foundation parameters.	Test will accurately determine the depth of large bridge abutments. Also, allows for the collection of soil data when the borehole and casing are constructed.	Test may require a large reflective surface for the sonic wave (i.e. Large piles, drilled shafts, etc.). Requires soil boring.
Cross Hole Sonic Test	95%	Used as a highly accurate method for determining the foundation parameters.	Will provide data from two receiver locations for increased accuracy. Also, allows for the collection of soil data when the borehole and casing are constructed.	Two soil borings are required for test. Access for test may require significant MOT. Pavement core will typically be installed through the bridge deck.
Induction Field	80%	Used for determining the foundation parameters of a foundation containing steel elements.	Very accurate test for the estimation of steel pile depth. Reinforced concrete may also yield good results if there is significant access to steel reinforcing. Also, allows for the collection of soil data when the borehole and casing are constructed.	Requires access to conductive material. Access for test may require significant MOT. Pavement core will typically be installed through the bridge deck.
Borehole Magnetic	90%	Used for determining the foundation parameters of a foundation containing steel elements.	Test can be extremely accurate with the presence of a large amount of ferrous material. Also, allows for the collection of soil data when the borehole and casing are constructed.	Prestressed piles may not have enough ferrous material to yield accurate results. Further testing will be required.

* Confidence in estimation refers to the accuracy of the test relative to the known problematic variables associated with the test procedure.

Table 1-8: Summary of advantages and limitations of surface NDT methods (adapted from McLemore et al. 2010 & Abboud and Kaiser 2012).

Bridge Location	Tested Unit	Substructure Type	Actual Depth (from ground surface (ft))	Predicted Depth (ft)
Coors (Colorado)	Pier 4	Concrete columns on shallow footings supported by steel piles	28.8'	Not successful (man-made noise sources)
	Pier 2	Concrete columns on shallow footings	4.5'	Not successful (man-made noise sources)
Alabama (Alabama)	Bent 4	Steel piles extending to the bottom of the superstructure	East Pile: 39' Middle Pile: 39'	East borehole: 31' Middle Pile: 28.1'
Old Bastrop (Texas)	Caisson	Two circular columns connected by a breast wall supported by a bell shape concrete footing supported on a rectangular concrete footing	35'	Borehole 1: Not successful Borehole 6: Not successful (clayey site conditions)
	Piles	Concrete columns supported by a pile cap of concrete piles	33.3'	Not successful (clayey site conditions)
New Bastrop (Texas)	Drilled Shaft	Concrete columns supported by shafts	38'	Not successful (clayey site conditions)

Table 1-9: Summary of BHR test results from first phase of NCHRP Project 21-05 (Olson et al. 1998).

2. P-WAVE SYSTEM LABORATORY VERIFICATION

Inadequate knowledge of conditions within a domain is not a problem unique to civil engineering and bridge substructures. Fields such as medicine and geology have faced a similar challenge, which has led to the development of various noninvasive imaging methods (e.g. medical ultrasound, seismic reflection/refraction, etc.). As noted previously in the literature review, similar non-destructive testing (NDT) methods have been developed and are commonly used in civil engineering to assess the condition of various infrastructure components. A key aspect of a number of these NDT methods is the use of compressional waves (i.e. P-waves). One goal of this study is to continue the development of an innovative ultrasonic P-wave system as a promising field NDT tool to assess unknown foundations. A laboratory study was implemented to evaluate the effectiveness of this system in anticipation of mobilization in the field. The following sections describe important aspects related to P-wave propagation and summarize the results from the laboratory study.

2.1 FUNDAMENTALS OF P-WAVE PROPAGATION

The application of energy (e.g. hammer strike) during a typical non-destructive test causes a displacement in particle position from equilibrium. Assuming the applied energy does not stress the material above the elastic limit, the particles fluctuate about their equilibrium position due to electrostatic forces between atoms. The corresponding vibration propagates as a mechanical wave and the time-varying deformation can be measured to determine information about the material through which the wave propagates. As described in the following sections, several factors affect the manner in which the mechanical wave propagates through the tested material.

2.1.1 MODE OF PROPAGATION

In general, there are three principle modes by which a mechanical disturbance can propagate through a material: (1) Compression wave, (2) Shear wave, and (3) Surface waves (ACI 1998). Compression waves, also known as pressure, longitudinal, dilatational, and primary waves (i.e. P-waves), involve motion of the particles in the same direction of wave travel (Fig. 2-1). The motion is analogous to that of sound waves where the air particles experience compression and rarefication as the waves travel across a fixed location. P-waves are capable of propagating

through solids and liquids. Shear waves (i.e. S-waves), also known as secondary, flexural, and transverse waves, involve motion of the material particles in a direction perpendicular to wave travel (Fig. 2-1). This perpendicular direction can be separated into two polarizations (i.e. vertical plane and horizontal plane motion). Due to the inability of liquids to withstand shear, S-waves cannot propagate through liquids. P- and S-waves are categorized as body waves since they are the only types of wave that can possibly develop in an infinitely long body [e.g. see Kramer (1996) for a derivation of governing equations]. Surface waves result from interactions of body waves at the surficial boundary between the tested material and another interface (e.g. air). The most prominent types of surface waves are Rayleigh and Love waves (Fig. 2-2), of which the Rayleigh wave is more commonly observed in NDT techniques (ACI 1998). Though surface waves are important in geophysical exploration and seismology, the focus of typical NDT applications are body waves.

2.1.2 VELOCITY OF PROPAGATION

P-waves have been used extensively in non-destructive testing (e.g. McIntire 1991), medical ultrasound (e.g. Gomm and Mauseth 1999), and exploratory geophysics (e.g. Waters 1992; Sheriff and Geldart 1995) to explore domains of vastly different scales. P-waves can propagate through liquids and travel faster due to the stiffer compressional response of materials in relation to shear (Kramer 1996). In an infinite continuum the P-wave velocity of a material can be determined as follows:

$$\mathbf{V_p} = \sqrt{\frac{\mathbf{M}}{\boldsymbol{\rho}}} = \sqrt{\frac{\mathbf{B} + \frac{\mathbf{4}}{\mathbf{3}}\mathbf{G}}{\boldsymbol{\rho}}} \tag{1}$$

M, B, and G are the constraint, bulk, and shear moduli of the material through which the P-wave propagates (Lee and Santamarina 2005). Bulk modulus, B, is related to Young's modulus (i.e. Modulus of Elasticity), E, by the following expression:

$$\mathbf{B} = \frac{\mathbf{E}}{\mathbf{3}(\mathbf{1} - \mathbf{2}\boldsymbol{\nu})} \tag{2}$$

where ν is the Poisson's ratio of the material. Shear modulus, G, is related to Young's modulus, E, by the following expression:

$$\mathbf{G} = \frac{\mathbf{E}}{\mathbf{2(1+\nu)}} \tag{3}$$

Combining Eqs. (1) – (3) yields the following expression for P-wave velocity as a function of E and v (ACI 1998):

$$\mathbf{V_p} = \sqrt{\frac{\mathbf{E(1-\nu)}}{\boldsymbol{\rho}\mathbf{(1+\nu)(1-2\nu)}}} \tag{4}$$

As v approaches 0.5 (i.e. the material becomes incompressible) the P-wave velocity approaches infinity. Typical values of the P-wave velocity for a wide range of materials are provided in Table 2-1. As noted in Table 2-1, the P-wave velocity of saturated soil at typical confinement pressures is similar to the P-wave velocity of water.

2.1.3 Effects of Multiple Material Interfaces

The preceding discussion derived expression for P-wave velocity based on an assumption of an infinitely long homogeneous material (e.g. infinite half-space). Once boundaries exist between multiple materials (e.g. concrete and air interface as developed in a crack), the propagation of P-waves becomes increasingly complex. Some of the wave energy is transmitted through the boundary between materials, some is transformed into waves of different modes or polarizations (e.g. surface waves), and some is reflected away from the boundary (see Aki and Richards 1980 for a detailed analysis) (Fig. 2-3). The manner in which the wave is distributed between these three alternatives depends on the angle of incidence between the incoming wave and the boundary as well as on the specific impedance, Z, of the material, where Z is defined as the product of wave velocity and density (i.e. $Z = \rho V_p$). Typical values for the specific impedance are provided in Table 2-1 for a wide range of materials. When an incoming P-wave strikes the boundary between materials at angle normal to the interface (i.e. 90 degrees), only transmission and reflection occur. Assuming the impedance of the first material is Z_1 and the second material is Z_2, the transmission and reflection coefficients can be computed as:

$$\mathbf{T} = \frac{\mathbf{2Z_2}}{\mathbf{Z_2 + Z_1}} \tag{5}$$

$$\mathbf{R} = \frac{\mathbf{Z_2 - Z_1}}{\mathbf{Z_2 + Z_1}} \tag{6}$$

The transmission coefficient, T, is the ratio of the transmitted wave pressure amplitude to the incident wave pressure amplitude, and the reflection coefficient, R, is the ratio of the reflected wave pressure amplitude to the incident wave pressure amplitude. The summation of T and R must always equal to 1 since the amount of the transmitted and reflected energy must equal the total amount of incident energy. Large differences in material impedances (i.e. impedance mismatch) will result in a significant amount of reflected wave energy from the material interface and very little transmission of waves. This contributes to why NDT techniques have been so successful in locating defects in concrete as the impedance mismatch between concrete and air is very large (ACI 1998).

2.1.4 Frequency of Propagation

The frequency content of a P-wave is also an important parameter because it affects the ability of the wave to detect an anomaly in its wave path (i.e. spatial resolution). Generally, the axial resolution (i.e. in the direction of wave travel) is of the same order of magnitude as the wavelength of the P-wave (Lee and Santamarina 2005). The wavelength, λ, of a P-wave is related to its velocity, V_p, and frequency, f (i.e. $\lambda = V_p/f$). The lateral resolution corresponds to the ability to detect an anomaly in the transverse direction and is dependent on the frequency of the wave as well as the size and directivity pattern of the sensor(s) that input and receive the wave energy. In addition to resolution, the frequency of a P-wave affects the distance the wave cab be transmitted through the material. The wave amplitude decreases with distance of propagation due to geometric spreading and material damping. Higher frequencies are attenuated more rapidly than low frequencies (Santamarina et al. 2001). Thus selection of an appropriate frequency range for a given application must balance the competing needs of resolution and depth of transmission. For example, in reflection seismology the frequencies utilized for P-waves typically range from 1 – 200 Hz. The depth of wave propagation is extremely important in geophysical exploration since bedrock may be hundreds of meters below the ground surface. The low frequencies utilized allow for greater exploration depths at the expense of resolution. For medical diagnostics, ultrasonic waves are utilized, which signifies that the frequency of the wave propagation is larger than the upper limit of human hearing (i.e. approximately 20 kHz). Higher resolution results are generated with the ultrasonic waves relative to the results from geophysical exploration (e.g. see Fig. 2-4). NDT methods for civil engineering structural materials (i.e. concrete, metals) typically utilize P-waves at frequencies

comparable to medical ultrasonic. The scales of interest for geotechnical engineering straddle the intermediate range of frequencies between seismic exploration and medical ultrasonic methods.

2.1.5 Application of Ultrasound in Soils

The application of ultrasonic P-waves in soils presents several challenges, some of which are unique to the nature of soils as particulate materials. In general, there are four major considerations that will affect the ability to transmit ultrasonic waves in soils: (1) selection of frequency, (2) degree of saturation, (3) dispersion, and (4) coupling.

2.1.5.1 Selection of Frequency

As previously discussed, selection of frequency will affect the spatial resolution of any P-wave ultrasonic system. High frequencies in the ultrasonic range are desirable because they increase resolution. However, soils are highly attenuative and ultrasonic P-waves will not transmit large distances [i.e. 2+ m (6.5 + ft)]. Equation 7 describes the relationship between wave amplitude and distance:

$$\frac{\mathbf{A_2}}{\mathbf{A_1}} = \left(\frac{\mathbf{r_2}}{\mathbf{r_1}}\right)^{\zeta} \mathbf{e}^{(\omega \mathbf{D}/\mathbf{V_p})(\mathbf{r_2}-\mathbf{r_1})\mathbf{T}^{-1}} \tag{7}$$

where r_2 and r_1 are distances to the source; A_2 and A_1 are the wave amplitudes at r_2 and r_1, respectively; ζ is a geometrical damping term (0 for plane wave fronts, 0.5 for cylindrical wave fronts, and 1.0 for spherical wave fronts); ω is the angular frequency of the wave; D is the damping coefficient of the soil; V_p is the P-wave velocity of the soil; and T is an apparent attenuation factor that accounts for partial transmission, mode conversion, and other sources of heterogeneity (Santamarina et al. 2001). Several of the terms in Eq. (7) are difficult to compute analytically, particularly if the location of reflectors in the soil domain is unknown. Thus it is important to experimentally characterize the attenuation of a particular transducer system to ensure an appropriate selection of frequency for the desired application in soil.

2.1.5.2 Degree of Saturation

The transducers that are typically used to generate ultrasonic P-waves are impedance matched to particular media. Transmission of ultrasonic waves into the soil will suffer tremendously if the impedance of the soil is significantly different than the design impedance of the transducer.

Thus the degree of saturation will play a major role in ultrasonic wave transmission since the P-wave velocity (and by extension, the impedance) of a soil is highly dependent on degree of saturation. The Gassmann equation can be utilized to explore the effects of saturation on the P-wave velocity of a soil (Santamarina et al. 2001, Lee 2003, Lee and Santamarina 2005):

$$\mathbf{V_p} = \sqrt{\frac{\left(\mathbf{B_{sk}} + \frac{\mathbf{4}}{\mathbf{3}}\mathbf{G_{sk}}\right) + \left[\mathbf{n}\left(\frac{\mathbf{S}}{\mathbf{B_w}} + \frac{\mathbf{1-S}}{\mathbf{B_a}}\right) + \frac{\mathbf{1-n}}{\mathbf{B_g}}\right]^{-1}}{(\mathbf{1-n})\boldsymbol{\rho}_\mathbf{g} + \mathbf{nS}\boldsymbol{\rho}_\mathbf{w}}} \tag{8}$$

where B_{sk} is the bulk modulus of the soil skeleton; G_{sk} is the shear modulus of the soil skeleton; n is the porosity of the soil; S is the degree of saturation of the soil; B_w is the bulk modulus of water; B_a is the bulk modulus of air; B_g is the bulk modulus of the soil grains; ρ_g is the density of the soil solids; and ρ_w is the density of water. The Gassmann equation neglects inertial effects between the pore fluid and solid particles (Biot 1958 a, b; Qiu 2010). However, it is still a useful expression to illustrate the effects of saturation on P-wave velocity as noted in Fig. 2-5. The curves in Fig. 2-5 characterize the P-wave velocity as a function of saturation for input parameters representing a typical clay. A small reduction in saturation (i.e. S = 99%) results in a drastic reduction of the P-wave velocity. Consider a case where the transducer has a delay line comprised of polypropylene (ρ = 0.89 Mg/m^3, V_P = 2,700 m/s, and Z = 2,400 Mg/m^2/s) in contact with a clay (ρ = 1.60 Mg/m^3). Based on Fig. 2-5, it is possible that such a clay can have a P-wave velocity as low as 200 m/s (Z = 320 Mg/m^2/s) for an S = 99% and as high as 1600 m/s (Z = 2560 Mg/m^2/s) when S approaches 100%. Computing the transmission coefficient, T, as in Eq. (5) yields a value of approximately 0.2 for S = 99% and nearly 1 for S = 100%. So for this particular case it may be impossible to detect reflected ultrasonic P-waves through clay that is almost completely saturated (S = 99%) due to the low transmission ratio, while adequate signal recovery may still be possible when S = 100%. Hence, it is critical that the transducer matching layer have an impedance that is similar in magnitude to the impedance of the soil in contact. It may be necessary to utilize transducers with different matching layers or of different construction if saturated and unsaturated soil conditions are expected.

2.1.5.3 Dispersion of Ultrasonic Waves

It is possible that the wavelength of propagation may approach the internal scale of the particulate soil. In such cases, the soil no longer behaves as a continuum and waves can become scattered. Santamarina et al. (2001) showed that a particulate material can become dispersive

when the wavelength is shorter than approximately 20 times the internal scale of the material (i.e. mean grain size of soil). Thus a limiting grain size could be established based on the anticipated frequency of wave propagation and the P-wave velocity of the soil. Consider an ultrasonic wave of 100 kHz frequency and a soil from Fig. 2-5 with V_s = 200 m/s. For saturated conditions (S = 100%), V_p = 2000 m/s, and for unsaturated conditions (S = 99%), V_p = 400 m/s. Based on the relationship between wavelength, frequency, and velocity (i.e. $\lambda = V_p/f$), the corresponding wavelengths for saturated and unsaturated conditions would be 20 mm and 4 mm, respectively. If the mean grain size of the soil was approximately 1 mm, it would be possible that the 100 kHz waves would transmit through the saturated soil but would scatter under unsaturated conditions as the ratio of the wavelength to internal scale fell well below the recommended value of 20 by Santamarina et al. (2001). Thus it is critical that limits be placed on the internal scale of a soil for a given frequency.

2.1.5.4 Transducer Coupling

Adequate coupling of the transducer with the soil can become difficult under certain conditions, which can drastically reduce the amount of ultrasonic wave energy transmitted into the soil. Couplants are often introduced in other NDT applications to ensure good coupling between the transducer and the material being tested. For example, gels are often utilized in medical ultrasound and in concrete flaw detection to ensure any gaps of air which can diminish signal transmission are eliminated. Unfortunately, the effects of transducer coupling are much harder to analyze in a quantitative manner compared to the effects of frequency, saturation, and dispersion. Moreover, improper coupling is one of the most common causes of poor ultrasound performance (Thomas Eischeid, Ultran Group, personal communication). In general, soft soil conditions can improve coupling because the soil is capable of conforming to the shape of the transducer (Coe and Brandenberg 2012). Stiffer soils may crack as they come in direct contact with the transducers. The presence of water can improve coupling performance in those situations because gaps between the soil and transducer may be filled in by the pore fluid. Finally, as the confining pressure increases, the transducer comes into firmer contact with the soil, which can eliminate potential air gaps and improve transducer coupling.

2.2 PREVIOUS APPLICATIONS OF P-WAVES IN CIVIL ENGINEERING

As previously discussed in the literature review, P-waves have been used regularly in civil engineering, particularly for NDT purposes. The following sections summarize previous applications of p-waves across multiple frequency ranges in civil engineering.

2.2.1 NDT OF INFRASTRUCTURE MATERIALS

NDT techniques are often utilized in civil engineering for the assessment of transportation infrastructure. Example applications include: integrity testing of known pile and drilled shaft foundations (e.g. Likins et al. 2004, GI Deep Foundations Committee Task Force 2000, Finno and Gassman 1998, Rausche et al. 1988); quality assurance (QA) of pavement construction (e.g. Von Quintus et al. 2009); assessment of cracks in structural concrete (e.g. ACI 1998); and structural health monitoring (e.g. Lee et al. 2011, Hsieh et al. 2006, Li et al. 2005, Bolton et al. 2005). The applicable frequencies of interest range from very low (e.g. units of Hz) for pile integrity testing to very high (i.e. ultrasonic, > 20 kHz) for assessing cracks in concrete.

2.2.2 GEOPHYSICAL EXPLORATION

Despite a wide range of applications for infrastructure assessment, P-waves have seen little use at the geotechnical scales of interest, particularly at the ultrasonic range of frequencies. Most references to the application of P-waves in geotechnical engineering have been very shallow geophysical explorations. For example, Grandjean (2006) utilized a seismic "multi-approach" that identified contaminants in the field using a number of different types of waves, including P-waves. Kase and Ross (2004) used reflection imaging in advance of tunnel excavation to identify potentially difficult soil conditions. Nichols et al. (1987) located rebound fracture zones in Pierre shale using shallow seismic reflection imaging. Frequency content for these studies was typically less than a few hundred Hz.

2.2.3 UNKNOWN FOUNDATIONS

As noted in the review of NDT methods for evaluating unknown foundations, P-waves have been utilized in previous unknown foundation studies. Probably the most common application of P-waves for unknown foundations has been the Sonic Echo/Impulse Response (SE/IR) test (e.g. Hossain et al. 2011, Robinson & Webster 2008, Yu et al. 2007, Hertlein and Walton 2007, Olson and Aouad 2001, Hertlein and Walton 2000, and Olson et al. 1998). SE/IR has proven to be inconsistent in its ability to predict unknown foundation lengths, particularly for more complex

substructures (e.g. footing on piles). On the other hand, Parallel Seismic (PS), which also utilizes P-wave energy, has been more robust and successful in evaluating unknown foundation lengths (e.g. Hossain et al. 2011, Niederleithinger and Fritsche 2010, Robinson and Webster 2008, Hertlein and Walton 2007, Yu et al. 2007, Olson and Aouad 2001, and Mercado and O'Neill 2000). However, like other subsurface methods it requires a borehole drilled alongside the unknown foundation. Whereas SE/IR and PS generate the necessary P-waves by impacting the foundation at the ground surface, the Borehole Sonic (BHS) and Cross-Hole Sonic Logging (CSL) methods rely on sources lowered into the borehole alongside the receiving element. As a result, they are less impacted by the presence of complex foundations, improper coupling between caps or grade beams and underlying foundation elements, and strong impedance contrasts near the surface. Moreover, they can often generate an "image" of the foundation element and provide more information regarding its condition. Only a few studies exist where BHS was utilized to assess unknown foundations (i.e. Descour and Kabir 2010, and Olson et al. 1998). The results from these studies showed potential, but also a need to further develop such systems to perform over a wider range of conditions (as proposed in this study). CSL has primarily been utilized to assess the integrity of known drilled shafts (e.g. Briaud et al. 2002, Likins et al. 2004, ASTM D6760-08) or as a geophysical subsurface exploration techniques to characterize soil shear wave velocity profiles (e.g. Stokoe and Woods 1972, ASTM D4428M-07). However, a limited number of studies have utilized CSL techniques to assess unknown foundations (e.g. Descour and Kabir 2010). Again, such studies continue to demonstrate the potential of P-waves for unknown foundation evaluation and the need for continued development of test methods, instrumentation, and data interpretation.

2.2.4 Ultrasonic P-wave Reflection Imaging

Despite the extensive use of P-waves across a wide range of fields (including civil engineering) very little work has been performed to advance the state-of-practice at the scales of geotechnical interest. This is especially true of borehole P-wave methods to evaluate unknown foundations, despite the clear advantages of such methods over SE/IR and PS. Ultrasonic waves in such applications are in a position to generate a tremendous wealth of information at high resolution.

Only a handful of studies have examined the application of ultrasonic p-waves to image reflectors in soil domains at the field and laboratory scales. For example, Lee and Santamarina (2005) utilized 500 kHz transducers to conduct a series of laboratory tests to image soil layers and embedded objects in small-scale soil models and slurry surface position during sedimentation of kaolinite clay (Fig. 2-6). Coe and Brandenberg (2010) performed similar laboratory-scale experiments on soil models with 500 kHz transducers to examine the effects of complex geometries (e.g. multiple embedded anomalies, dipping and undulating reflectors, etc.) on reflection signals (Fig. 2-7). Three-dimensional images were obtained and data was compared with another set of transducers of lower operating frequency (100 kHz). In general, Coe and Brandenberg (2010) found that data post-processing using migration was necessary to render accurate locations for angled reflectors, signal-stacking was necessary to improve the low signal-to-noise ratio for the 500 kHz signals (e.g. see Brandenberg et al. 2008), and lateral spatial resolution was poorer than the axial resolution.

In terms of field applications, Coe and Brandenberg (2012) describe the results of field testing using a 100 kHz ultrasonic P-wave reflection imaging system. This system was designed to be pushed alongside an embedded structural element (i.e. foundation, jet grout, etc.) using the *nees@UCLA* CPT 20-ton CPT truck (Figs. 2-8 – 2-10). This ultrasound probe was able to image a cast-in-steel-shell (CISS) pile in very soft clayey soils beneath a bridge in northern California (Figs. 2-11 and 2-12). Thus this system has the potential to provide a very clear image of any unknown bridge foundation as a logical extension of the work performed in Coe and Brandenberg (2012). Such high resolution information can allow assessment of not just the length of an unknown foundation, but also potentially material type, integrity, and geometry. For example, Coe and Brandenberg (2012) deduced that the tested pile had undergone a small amount of drift during construction or was purposely driven at a slight batter based on the acquired reflection signals (Figs. 2-11 and 2-12). However, a few issues were noted that likely affected the ability of the system to successfully image the pile over a greater length. These issues included coupling between the transducers and soil, impedance mismatch due to unsaturated soils, and probe drift. Additionally, an experimental assessment of the P-wave transmission distances was not performed to evaluate the limits of the system. The uncertainty associated with these issues limits the application of this technology to a very narrow range of conditions. One goal of this study is to explore ways in which to address the current limitations

of the P-wave system utilized in Coe and Brandenberg (2012) so that it can be implemented as a robust tool to evaluate unknown bridge foundations.

2.3 LABORATORY STUDIES

This study will address issues related to coupling, impedance mismatch, and probe drift in the ultrasonic P-wave system developed by Coe and Brandenberg (2012). To accomplish this, during field testing the ultrasound probe will be lowered into a pre-drilled borehole that has been grouted and capped with PVC piping and filled with water (similar to the setup used in PS testing). The water in the borehole should ensure high transmission of wave energy into the surrounding soil (assuming the coupling of the PVC and grout to the borehole wall is suitable). Probe drift would be minimized as the probe would be lowered straight into an existing opening rather than pushed into the ground.

A series of laboratory tests was developed to evaluate the effects of this new approach prior to mobilization in the field. A key focus of the laboratory testing was to evaluate system performance in relation to wave amplitudes and transmission distances. The following sections provide an overview of the system components and a summary of the laboratory testing results.

2.3.1 ULTRASONIC P-WAVE SYSTEM COMPONENTS AND OPERATION

The primary system components for both the laboratory work and proposed field work in this study include the ultrasonic transducers (100 kHz), source pulser, miniature direct current/direct current (DC-to-DC) converter, receiver amplifier, receiver analog filter, terminal block (SCB-68), data acquisition cards mounted in a National Instruments PXIe chassis, and a personal computer (Figs. 2-13 and 2-14). The primary component of the ultrasonic transducers is the gas-matrix piezoelectric disc which distorts in response to voltage potentials and registers voltage potentials when distorted. Thus a set of these piezoelectric transducers can be used as a source-receiver pair, whereby one transducer inputs waves into the soil and the other measures any reflected energy. The high-speed source pulser provides a +150 V_{DC} input signal to drive the source transducer. Such high voltages are necessary to ensure transmission of sufficient wave energy into the soil. The source pulser was triggered by a +5 V_{DC} step wave function from an arbitrary waveform generator. The DC-to-DC converter allows the source pulser to be powered by a conventional desktop power supply (i.e. +12 to +15 V_{DC}) while still providing the necessary

high voltage signal to the source transducer. The receiver amplifier minimizes the loss of charge in the cable for the transducer (which is capacitive in behavior). The amplified signal is filtered using a low-pass antialiasing analog filter with a corner frequency of 2.5 MHz. The terminal block and National Instruments PXI chassis and data acquisitions cards allow control of the data acquisition for the system via a personal computer. Command chain flow and data acquisition flow were illustrated in Fig. 2-10 for the case of the field work performed in Coe and Brandenberg (2012). More details about the specifications of each system component are provided in Coe and Brandenberg (2012), Coe and Brandenberg (2010), and Coe (2010).

2.3.2 Laboratory Testing And Results

The following sections summarize the laboratory tests utilized in this study to characterize the performance of the ultrasound probe. Initially, tests were performed using water models to simplify data interpretation and verify system performance. The results from these water models guided the development of an appropriate soil model to establish the limits of the ultrasound probe system for field application.

2.3.2.1 Laboratory Tests Without Soil

Test setups primarily composed of water afford a level of simplicity that is desirable when studying fundamental characteristics of the P-wave system. As the transducers in this study are impedance matched to be in contact with water, a maximum amount of wave transmission into the model is ensured. Additionally, it is unnecessary to apply vacuum to ensure adequate saturation levels as there are no small void spaces in which air particles can be trapped. Finally, construction of a soil model can take several days and it is critical to verify fundamental system behavior before investing such a significant period of time. It is for these reasons that testing proceeded with simple setups without significant amounts of soil present at the onset of this project.

2.3.2.1.1 Tests With PVC/Grout

Figure 2-15 highlights the first test that was performed as part of this laboratory study. This setup was developed to examine the effects of PVC and grout on wave transmission and signal amplitudes. Though both PVC and grout have specific impedances that are similar to water and saturated soil, it was still a concern that such an interface may appreciably diminish signal

quality. So as a proof of concept, the transducers were stacked as illustrated in Fig. 2-15 with a PVC sheet of approximately 6.4 mm (0.25 in) thickness and a fragment of grout sandwiched in the middle. The grout was mixed using a ratio of 450 g (1 lb) of bentonite, 450 g (1 lb) of portland cement, 2.80 kg (6.25 lbs) of water as recommended in ASTM D4428M-07. Figure 2-16 presents the resulting transmitted signals across the PVC/grout interface for two thickness of the grout. To ensure adequate coupling, a small amount of water was introduced at each of the interfaces between transducer, PVC, and grout. As expected, the amplitude of the received signals clearly demonstrates that the presence of a PVC/grout interface diminishes the amount of signal transmission (Figs. 2-16 – 2-18). Based on Eq. (5) only approximately 60% of the input signal would reach the receiver based on computing the transmission coefficient at each of the interfaces in this test setup (i.e. transducer-PVC, PVC-grout, grout-transducer). However, Eq. (5) does not take into account the effects of attenuation of the waves through the material nor was there an attempt to model the potential effects of improper coupling. Figure 2-18 shows that the signal transmitted through PVC and grout can be as low as 20% of the signal transmitted when the transducers are in direct contact. However, the signal-to-noise ratio of the signal transmitted through the PVC and grout is still sufficiently high and these tests were performed without the benefits of an amplifier and without performing signal stacking. In signal stacking, multiple input signals are transmitted in succession into the domain and the resulting reflections are added to increase the signal-to-noise ratio (e.g. see Brandenberg et al. 2008). Thus the results of this test show that while signal quality decreases due to the PVC/grout interface, it is not so excessive as to abandon the proposed borehole setup for field testing. However, further testing was warranted to continue evaluating the impacts of the PVC/grout interface when the transducer source and receiver are farther apart and the signals in Figs. 2-16 – 2-18 are further reduced due to attenuation.

2.3.2.1.2 Acrylic Chamber Tests

Figures 2-19 and 2-20 highlight the first major water model that was developed as part of this laboratory study. This model was developed to further examine the attenuation behavior of the ultrasonic transducers and explore the effects of PVC (and other plastics) on wave transmission and signal amplitudes in water. Steel plates of approximately 22.2 mm (7/8 in) thickness were arranged in a descending staircase pattern in the direction of transducer travel (Fig. 2-19). The

transducers were placed on top of the chamber and were dragged across the cross section from right to left at an approximately constant rate to develop an image of the domain.

Figure 2-21 presents the resulting reflection signals from the acrylic chamber model. Clearly visible are the reflections from the steel plates and the effects of propagation distance on signal amplitude. Since the reflectors are all the same material, the amplitudes of the reflected signals should be approximately the same. However, the steel plates closest to the transducers produce reflected signals of higher overall amplitude since the waves do not travel as far and are therefore less affected by geometric spreading and material losses. In order to magnify the appearance of weak reflections from deeper elements, a depth-dependent gain factor may be utilized to offset the diminishing effects of attenuation (Fig. 2-22). Figure 2-23 presents an image of the acrylic chamber model that applies a depth-dependent gain function to the data presented in Fig. 2-21. The resulting image has similar signal amplitudes for the reflectors at each depth of interest. However, the depth-dependent gain function also increases noise and the amplitude of multiple reflections.

The variation in signal amplitude with depth can be utilized to approximate the functional relationship between distance and attenuation. As noted in Eq. (7), the relationship between distance and attenuation can be difficult to compute analytically, particularly if the location of reflectors in the soil domain is unknown. Thus it is important to experimentally characterize the attenuation of a particular transducer system to ensure an appropriate selection of frequency for the desired application in soil. In this case, the data from Fig. 2-21 was utilized to develop a best fit trend line relationship between distance and attenuation as illustrated in Fig. 2-24. This expression can be utilized to predict signal amplitude at various distances for this water model. Care should be exercised in attempting to utilize this expression for any other model as the functional form is specific to the domain tested.

Figures 2-25 presents the resulting signals from the acrylic chamber model when a PVC interface is placed at 31.8 mm (1.25 in) from the transducer face. Likewise, Figs. 2-26 and 2-27 present the same results for the case of a Low-Density-Polyethylene (LDPE) interface at 31.8 mm (1.25 in), and a Polypropylene interface at 31.8 mm (1.25 in), respectively. Each material is approximately 6.4 mm (0.25 in) in thickness. The different plastics were chosen to represent a

range of impedance values (1.8, 2.4, and 3.3 $Mg/m^2/s$ for LDPE, Polypropylene, and PVC, respectively). The motivation was that if PVC proved to significantly diminish signal quality, another less stiff plastic would be more suitable to line the borehole in the proposed field setup. Comparing Fig. 2-23 to Figs. 2-25, 2-26, and 2-27 confirm that reflections at the plastic interface can obscure the domain of interest. The effects are greater in this test setup compared to the PVC/grout tests previously discussed because the signals must now travel a farther distance through attenuative material between the source and receiver transducers. Note that these results were obtained using signal stacking. The signal quality degraded significantly for the case of PVC and LDPE, though Polypropylene fared better. It was necessary to significantly increase the depth-dependent gain factor as well as the overall amplification for these acquired signals to allow proper interpretation of the acrylic chamber domain. Comparing the unadjusted amplitudes of the reflected signals from the bottom-most steel plate for all cases demonstrates that PVC cuts the most signal amplitude, followed by LDPE and polypropylene. This decrease in amplitude is expected and supported by estimates of the overall transmission coefficient, T, of a P-wave that enters and passes through these plastics twice in its path from source transducer to receiver through the water in the model (i.e. 9%, 38%, and 20% for PVC, LDPE, and polypropylene, respectively). Interestingly, LDPE fared worse with the recorded signals than the theoretical calculations would estimate. This issue of transmission could prove to be a major concern since field application will likely proceed with a PVC cased borehole. However, the increased density of soils may improve the situation, as will be tested in a soil model. The specific impedance of a typical soil is closer in magnitude to that of the tested plastics, which in theory will tend to increase the amount of wave energy transmitted [by as much as 20 – 30% based on use of Eq. (5)].

2.3.2.1.3 Gravel and Aluminum Water Model

Another aspect to consider regarding system performance with the 100 kHz transducers is the potential for wave scattering effects due to the particulate nature of soils. As previously discussed, wave scattering can occur when the internal scale of the propagation material (i.e. soil) approaches the same order of magnitude as the wavelength of the propagating wave. Santamarina et al. (2001) showed that soil may no longer behave as a continuum when the wavelength is shorter than approximately 20 times the mean grain size of the soil. For the case of the 100 kHz transducers, utilizing a P-wave velocity of water of approximately 1500 m/s and

the expression $\lambda = V_p/f$ results in a wavelength of approximately 15 mm (i.e. 0.6 in). Thus a soil with an internal length scale of approximately 0.75 mm (0.03 in) or larger may start to exhibit dispersive behavior. An effective grain size of approximately 0.75 mm or larger corresponds to typical coarse sands and gravels.

To verify the wave scattering effect and assess system performance, a water model was developed where a small layer of gravel was suspended in a #40 sieve above an aluminum plate (see Fig. 2-28). The majority of the gravel used to create the model is retained on the #4 sieve (i.e. 4.75 mm nominal opening). A series of P-wave signals (i.e. 100 stacks) was introduced into the domain at the center of the cross section and the corresponding reflections were measured using the ultrasonic transducers. This process was repeated at the same location a total of five times and the resulting signals were plotted side-by-side to aid in data interpretation (Fig. 2-29). As noted in Fig. 2-29, reflections were generated at approximately 31 mm and 212 mm, which likely correspond to the water-gravel and water-aluminum interface, respectively. Another major reflection is noted at approximately 152 mm. This reflection along with the "ringy" nature of the signal between 75 mm and 152 mm may be the result of multiple reflections as waves are scattered within the gravel. Interpretation of such a signal is undoubtedly more complicated due to the wave scattering effect, though it appears some wave energy is transmitted through the gravel and reaches the bottom of the model. This is likely possible due to the complex interparticle contacts between grains and the fact that the gravel contains solid, liquid, and gaseous phases, which may present a path for the ultrasonic waves to propagate around scattering interfaces. Nevertheless, it will be useful to avoid soil profiles with a significant amount of coarse sands and gravels during the selection of potential field sites as their presence will likely increase the difficulty of data interpretation.

2.3.2.2 Laboratory Tests in a Soil Model

Laboratory tests with water models allowed a fundamental understanding of some of the potential short-comings of the ultrasound probe as configured for field testing in this project (i.e. lowered into a PVC-cased borehole). However, it was necessary to perform tests in soils in order to further explore some of these issues and to verify system performance. For that purpose, a series of four cross sections were developed and constructed within a cylindrical soil container of approximately 610 mm (24 in) outer diameter and 914 mm (36 in) height (Fig. 2-

30). The cylinder was constructed from stainless steel and was placed under high vacuum to fully saturate the soil model. The soil model was constructed using poorly graded silica-based sand (Fig. 2-31) that was air-pluviated through a #20 sieve with a drop height of approximately 460 mm (18 in). Figures 2-32 – 2-36 present schematics of the four cross sections developed for testing purposes in the soil model. The cross sections were built vertically to mimic potential conditions that may exist in the field where the geometry will be horizontal. This was necessary to simplify construction of the soil model and to allow testing through a greater distance of soil based on the geometry of the container. The major goals of this suite of tests were to further explore limits on signal transmission through soils, effects of wave scattering from gravels, identification of embedded materials based on received signals, and the effects of the PVC/grout interface.

2.3.2.2.1 Limits of Signal Transmission in Soil Model

Figures 2-37 – 2-40 present the results from a series of two-dimensional scans across the soil model along the centerline of cross sections AA', BB', CC', and DD'. The received signals are plotted side-by-side at their respective locations as measured from the origin of the cross section (i.e. inside cylinder wall at A, B, C, and D). When plotted in this manner an "image" emerges of the soil model with reflection signals lining up at reflector locations. Note that the raw voltage signals can be mapped into 8-bit pixel values to form a grey-scale image of the domain as in Coe and Brandenberg (2012), Coe and Brandenberg (2010), and Coe (2010). However, due to the ringy nature of the signals, the resulting grey-scale images were actually more difficult to interpret and were deemed unnecessary to complete the analysis for this study. Likewise, migration was not utilized since the model interfaces for materials were made purposely flat (i.e. very little to no angle from horizontal). Migration is important to accurately resolve the location of reflectors with angled interfaces and circular cross sections (Coe and Brandenberg 2010). The increase in noise that results from post-processing using migration was not justifiable in this case due to the small effect it would have on the location of flat reflectors. Finally, note that it was not possible to completely isolate each of the cross sections from each other due to the directivity pattern of the transducers. As the transducers were scanned across a given cross section, reflections would be received from nearby reflectors embedded in other cross sections. For example, note the reflection signal at 195 mm in cross section BB' (Fig. 2-38) corresponding to steel plate located near A'. This proved to be only a minor inconvenience as

interpretation of the signals was relatively unaffected by the presence of reflections from other cross sections.

Besides the extent with which the reflectors were imaged at their correct locations, a major item of interest when examining Figs. 2-37 – 2-40 is the ability of the ultrasonic waves to transmit significant distances in the soil. This is important in order to place limits on the proximity of the probe to any foundation elements. Due to the high attenuation of ultrasound frequency P-waves in soils, it is necessary to better understand just how far the waves can propagate prior to the field component of this study (e.g. see sections 2.1.4 and 2.2.4 for further discussion). Previous studies (i.e. Coe and Brandenberg 2012, Coe and Brandenberg 2010) established lower-bound estimates for the two-way travel path capabilities of 100 kHz P-waves in soils (i.e. 0.6 – 0.8 m). Based on the results shown in Fig. 2-40, reflections from the bottom of the container are clearly visible at approximately 865 mm depth. This indicates that the lower-bound estimate for two way travel path can now be increased to approximately 1.7 m, which is more than a 100% increase from previous studies. By examining the time records of the signals, it was possible to distinguish a multiple reflection from the bottom (i.e. a wave that is reflected from the bottom after traveling twice through the entire depth of the container). Thus it seems possible for the 100 kHz wave to travel up to twice the previously cited distance (i.e. 3.4 m) in soils, though care must be exercised in inferring distances from multiple reflections as the data interpretation becomes increasingly complex. Thus, as long as the unknown foundation element is located within a range of 0.8 – 1.7 m two-way travel distance from the transducers, it will be possible to locate reflection signals in the recorded data as the probe is lowered in the borehole. At a two-way travel path of 1.7 – 3.4 m it still may be possible to record reflections, though confidence in this ability is lower than at 0.8 – 1.7 m.

2.3.2.2.2 Effects of Wave Scattering

As previously noted in section 2.3.2.1.3, wave scattering may become significant for soils with mean grain sizes of approximately 0.75 mm or larger for the 100 kHz P-waves used in this study. As the sand used to create the model is primarily made up of grains smaller than 0.75 mm (Fig. 2-31), a small amount of gravel was incorporated into the soil model at cross section DD'. Figure 2-40 presents the received signals across cross section DD'. The bottom of the container is clearly visible at approximately 865 mm in depth at the D end of the cross section where LDPE is

embedded approximately 75 mm below the soil surface. However, on the other side (D') where gravel is embedded at the same depth as LDPE, reflection signals from the container bottom are no longer visible. Also, note that the reflection from the LDPE is of higher amplitude than the reflection from the gravel despite an identical depth of embedment. These two observations imply that the gravel layer scattered the waves as opposed to providing clean reflection signals like LDPE. The lack of transmission of signals across gravels signifies that for waves of such high frequency, gravelly soil profiles should be avoided when using the probe to evaluate unknown foundations. If significant gravel content is noted at the site, it may be worthwhile to decrease the frequency of the waves to increase the wavelength and allow the gravel to behave as a continuum. Of course, this would come with a penalty of decreased axial resolution for the system. Though adjustment of the operating frequency is not possible with the current system in this study, tunable transducers are manufactured which would allow this capability for future studies.

2.3.2.2.3 Identification of Embedded Materials

An interesting aspect that was briefly explored using the results from the soil model was the ability of the ultrasound system to identify the materials embedded in the soil based on the reflection signal. Based on the mechanics of wave travel, different materials will impart a unique characteristic to a wave that strikes the material and is reflected away. Though this was not systematically studied, it is noteworthy to examine the subtle differences in the reflections recorded from the steel plate, timber, and concrete objects in the soil model across cross section CC' (Fig. 2-39). Since all three objects were placed at the same depth of embedment and had similar wavelength to thickness ratios (Steel = 2.6, Timber = 2.1, Concrete = 1.1), the differences in signal amplitude and frequency content are primarily due to the materials themselves. The steel plate had the highest reflection amplitude, followed by the concrete and wood. A systematic consideration of these effects would have to be undertaken to create a database of reflection signals based on material type, thickness of reflector, and medium of wave propagation. This type of investigation is time intensive and would necessitate the construction of several soil models and/or a suite of field tests across multiple known foundations with fairly uniform soil conditions, which is why it was not explored fully in this study. However, such a methodical investigation warrants future consideration if the goal is to allow prediction of unknown foundation material from the character of the reflection signals.

2.3.2.2.4 Effects of PVC/Grout Interface

As previously discussed in sections 2.3.2.1.1 and 2.3.2.1.2, signal quality during field testing will be negatively impacted by the presence of a PVC/grout lining on the borehole wall. To characterize how much the PVC/grout will prevent the acquisition of reflection signals from the unknown foundation, a couple of the cross sections (i.e. BB' and DD') contained small plastic sheets at a shallow embedment within the soil. All the sheets utilized in this testing consisted of either PVC, LDPE, or Polypropylene and they were all approximately 6.4 mm (0.25 in) in thickness (i.e. typical Schedule 40 pipe wall thickness) as utilized in testing with the acrylic chamber water model. Based on the results from cross section BB' and DD', LDPE allows the most amount of wave transmission to the bottom of the soil container followed by PVC and polypropylene. The bottom reflection is faintly visible below the PVC at approximately 865 mm, but is indistinguishable beneath the polypropylene. To further explore this, cross section AA' was scanned multiple times with various combinations of the plastic sheets and grout placed on the surface of the soil near A' (Fig. 2-41). Figures 2-42 – 2-44 present the results for the case where only the plastic sheets were placed on the surface near A'. The major difference with this setup compared to cross section BB' and DD' is that one side of the plastic sheet is now in direct contact with water (which has slightly lower impedance relative to saturated soil). The results demonstrate that all three plastic sheets allow transmission of enough wave energy to image the steel plate located at approximately 490 mm. Additionally, faint reflections are noted at approximately 865 mm for all three conditions. This signifies that if the transducers are lowered into a water-filled borehole with a PVC, LDPE, or polypropylene pipe lining the exterior wall, it may be possible to transmit a 100 kHz P-wave as far as a 1.6 m two-way travel distance.

For the remaining tests a small fragment of thin grout [approximately 12.7 mm (0.5 in)] was placed between the plastic sheet and the soil surface to mimic a plastic-lined and grout-filled borehole. Once the grout was introduced, the reflection signals were no longer acquired in those locations (Figs. 2-45 – 2-47). It made no difference whether the plastic was PVC, LDPE, or polypropylene. This signifies that the main culprit in signal transmission through a plastic-lined and grout-filled borehole is the grout. However, it should be noted that it was difficult to ensure adequate coupling between each of the interfaces (plastic-grout and grout-soil) when plastic and grout were used together. Though water will have filled in any voids that developed

between these interfaces, the resulting additional plastic-water-grout and/or grout-water-soil interfaces would undoubtedly introduce the potential for decreases in the overall transmission coefficient. Moreover, it was difficult to ensure that no air bubbles were trapped when placing the plastic on top of the grout or the grout on top of the soil. Air bubbles would manifest themselves by scattering waves and preventing wave transmission into the soil. Field installation of the plastic lining and grout within the borehole should ensure more adequate coupling between the plastic-grout-soil interfaces due to the lateral pressures that will exist within the borehole from the surrounding soils.

2.4 IMPLICATIONS TO FUTURE FIELD TESTING

Based on the results from the laboratory testing, several implications are noted for the future field testing proposed for this study. These observations are intended to aid in selection of an appropriate field site and foundation location as well as to guide field operations with the ultrasound probe.

- Ultrasonic P-waves were transmitted as far as 1.7 m (5.6 ft) based on a two-way travel distance. The potential two-way travel distance may have been as far as 3.4 m (11.2 ft), though there is less confidence in that assessment since this distance is inferred from a reflection multiple and not a direct reflection. If the foundations are located within approximately 0.85 m (2.8 ft) of the centerline of the borehole, it should be possible to record reflection signals of adequate signal-to-noise ratio and therefore make predictions about foundation length assuming the borehole extends slightly deeper than the foundation.

- The proposed method of casing the borehole with PVC and injecting grout to fill the void between PVC and borehole wall will prove to be problematic. Signal transmission was essentially reduced to nothing when a plastic/grout interface was introduced at the soil surface in the model during lab testing. This was not the case when only a plastic sheet was used, which mimics the situation where the borehole would be cased simply with a PVC pipe. A dialogue should be initiated with the drilling vendor to consider constructing the borehole with only a PVC casing. This method of construction will likely have some effects on signal quality for the other borehole tests proposed in the field study (i.e. parallel

seismic, borehole radar, borehole magnetometer), though the overall effect is hard to predict in advance. In some cases these effects will likely be fairly. For example, Olson (2001) noted that grouting the borehole in not essential if hydrophones will be used below the water table (which is the likely configuration for the field testing proposed in this study) (Olson 2001). Ultimately, the method of borehole construction will be largely dictated by the capabilities of the subsurface drilling vendor and the soil profile at the site (e.g. caving sands, etc.). It may be worthwhile to consider constructing a small test borehole to test signal quality with all the different field equipment prior to committing to a specific borehole construction method for the entire length of the foundation element.

- Gravels and soils with significant gravel content should be avoided for the purposes of this field study. As configured, the current field system has fixed frequency transducers that have a very short wavelength. At that wavelength scale, gravels cease to behave as a continuum for the purposes of wave propagation. The resulting wave scattering effect will prevent the acquisition of reflection signals from the foundation element.

- Though not systematically studied, it is clear that different foundation materials will reflect P-wave signals differently. For the purposes of the proposed field study, steel foundation elements are recommended because they always provided the highest reflection signal amplitudes in all the laboratory tests performed. Thus a steel foundation element will increase the likelihood of recording reflection signals across the variable conditions likely to be encountered in the field (e.g. soil types, distance of borehole from foundation element, etc.).

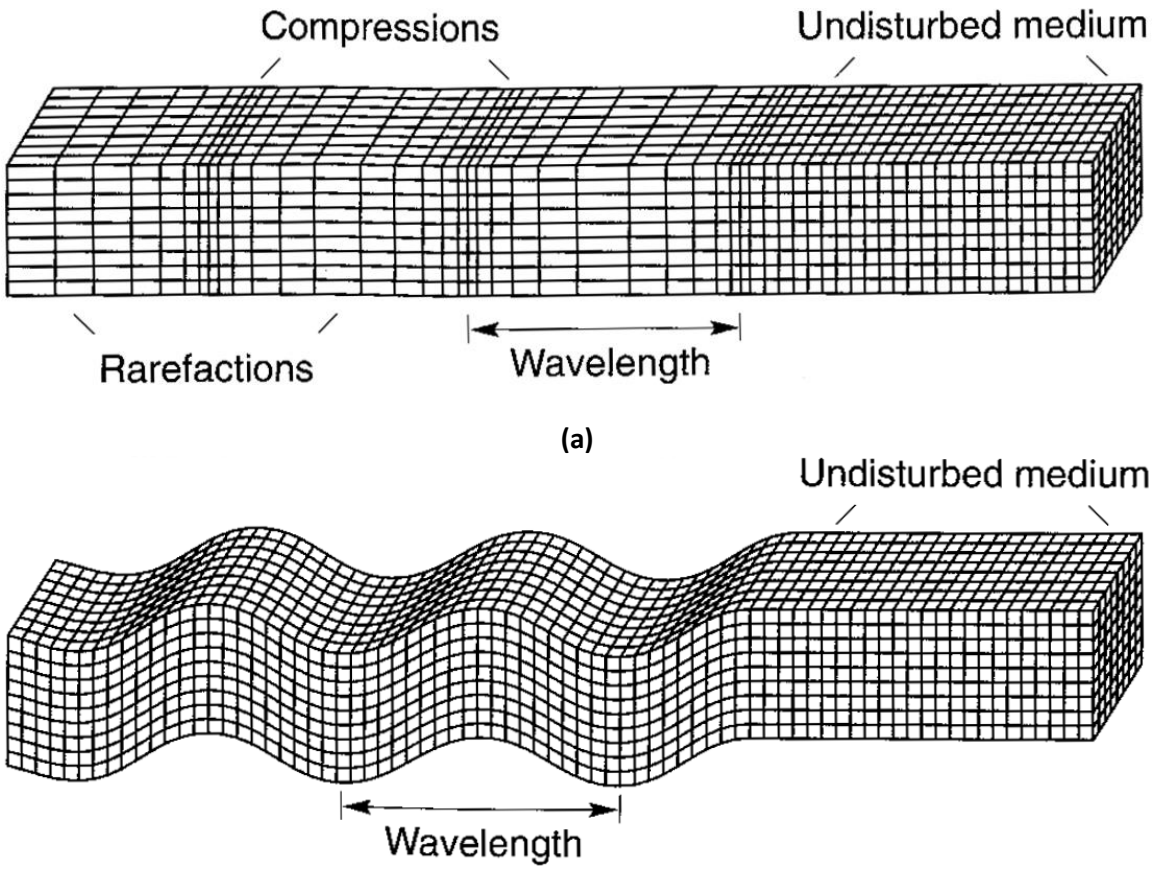

Figure 2-2: Deformations caused by: (a) Compression wave (i.e. P-wave), and (b) Shear wave (i.e. S-wave) (adapted from Bolt 2002).

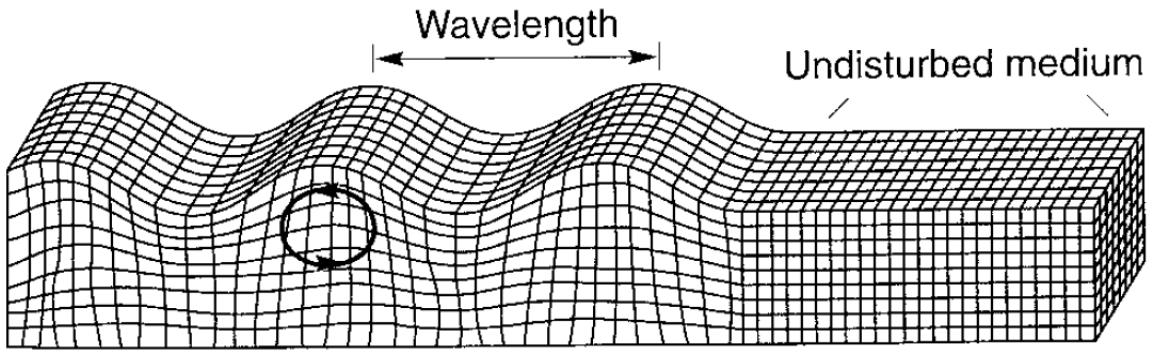

(a)

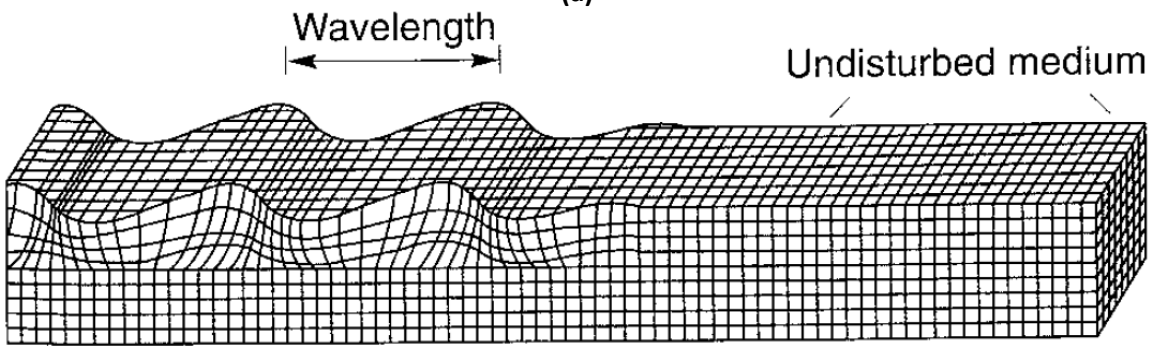

(b)

Figure 2-2: Deformations caused by body waves: (a) Rayleigh wave, and (b) Love wave (adapted from Bolt 2002).

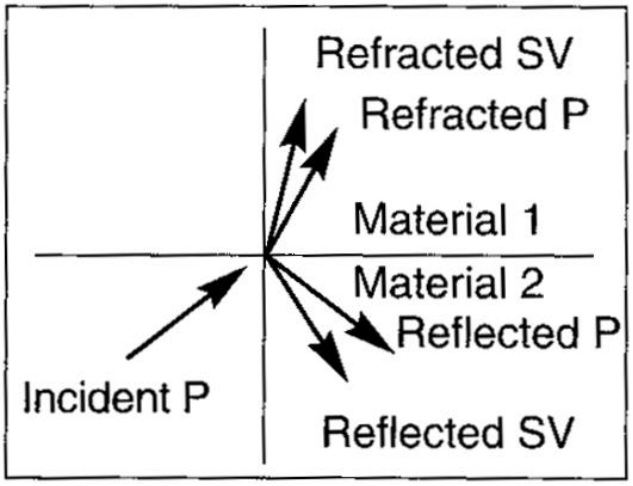

Figure 2-3: Reflection, transmission, and mode conversion of an incoming P-wave at the interface between two materials (adapted from Kramer 1996).

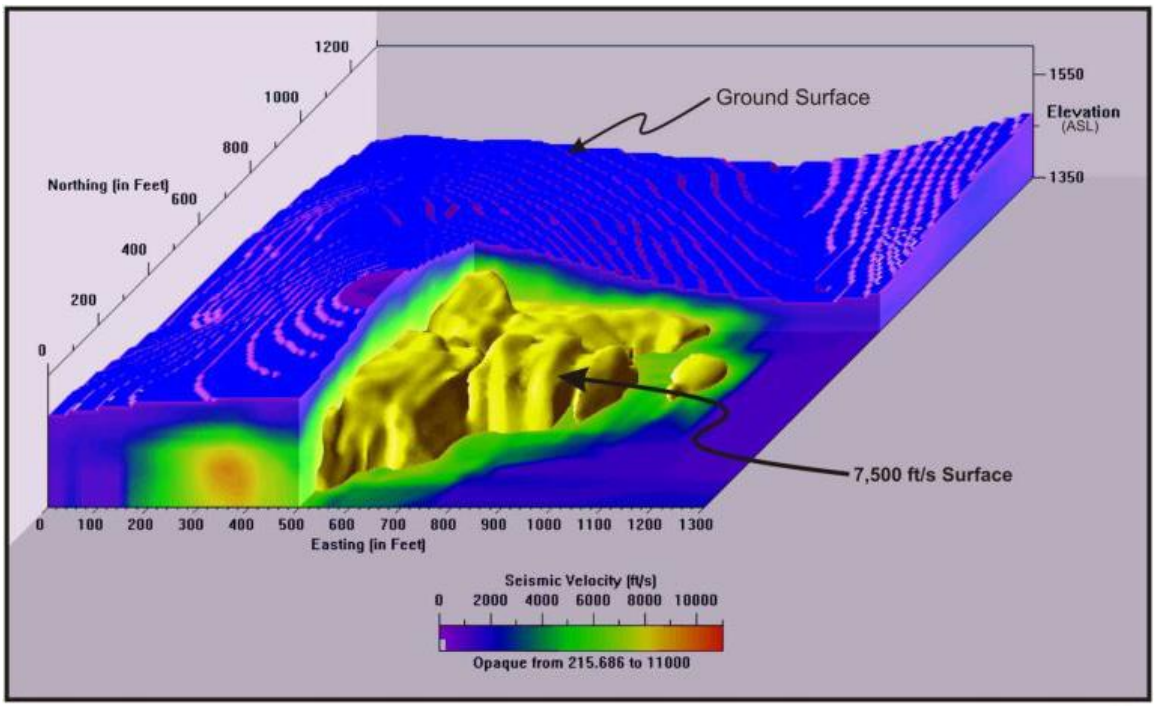

(a)

(b)

Figure 2-4: Comparison of resolution and exploration depth of (a) seismic refraction survey, and (b) medical ultrasound.

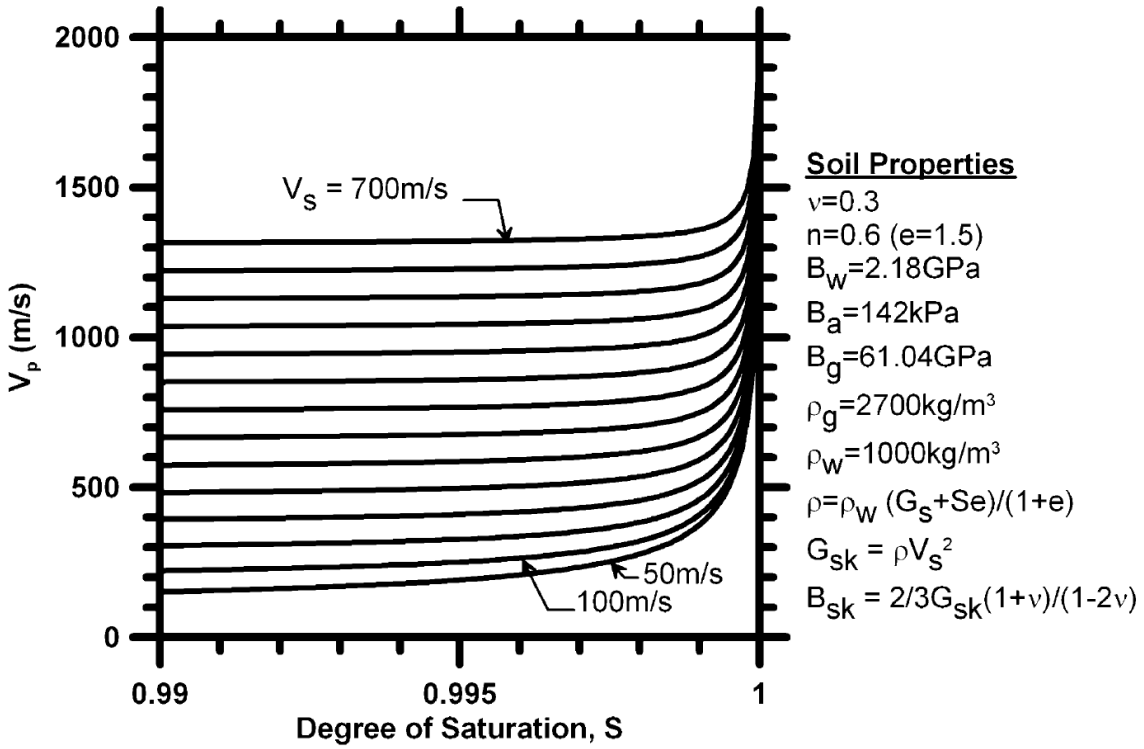

Figure 2-5: P-wave velocity as a function of saturation based on the Gassmann equation (Coe and Brandenberg 2012).

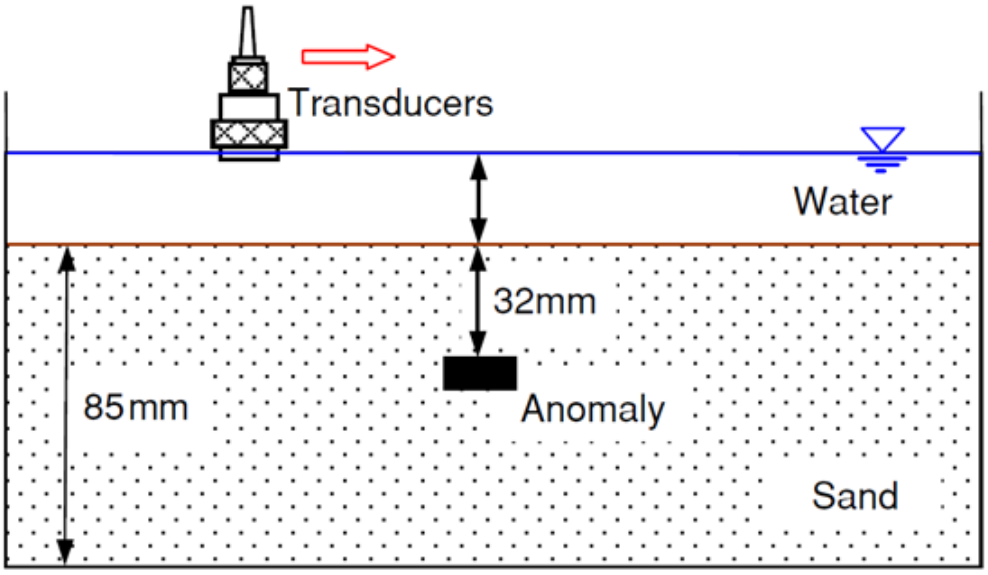

(a)

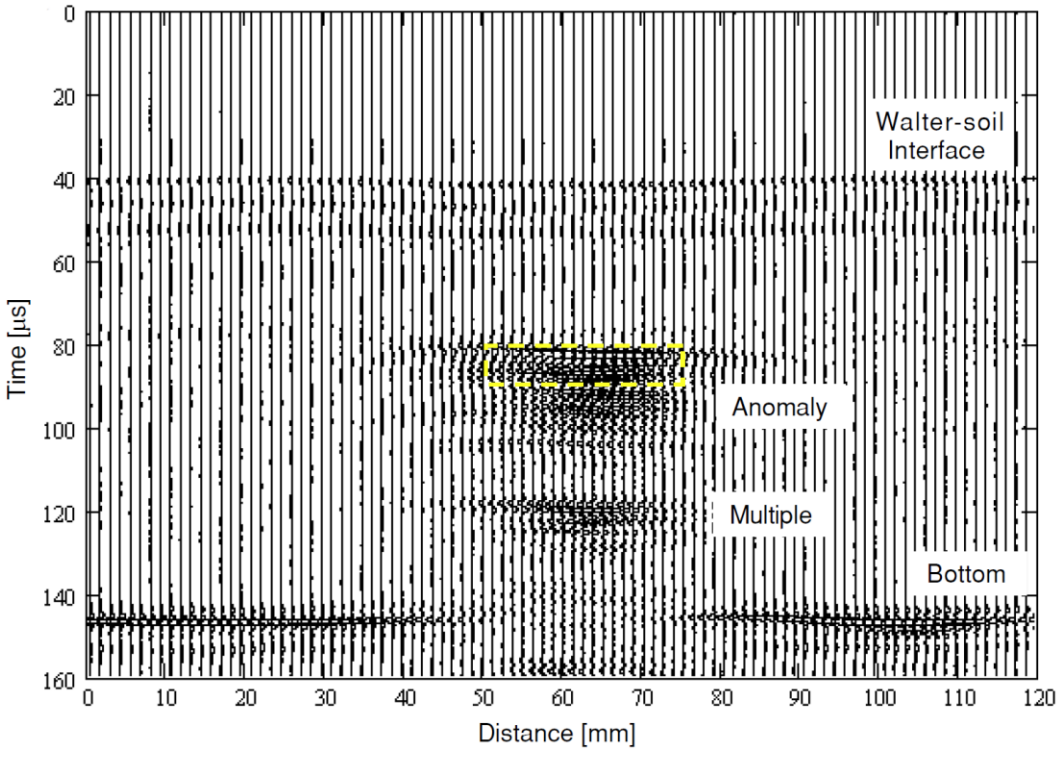

(b)

Figure 2-6: Detection of embedded anomalies in laboratory scale models from Lee and Santamarina (2005): (a) Schematic, and (b) Two-dimensional image.

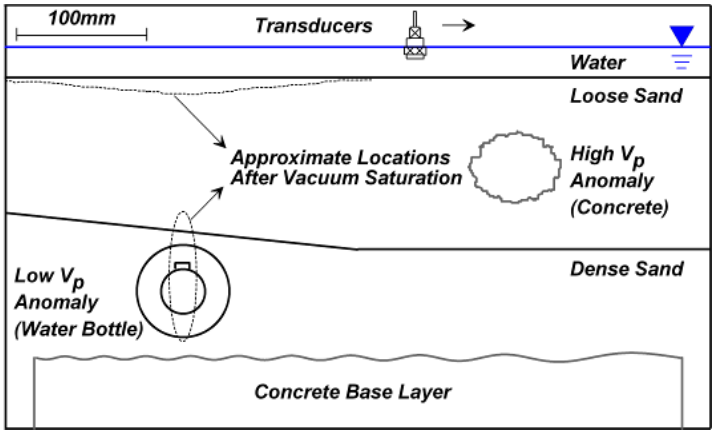

(a)

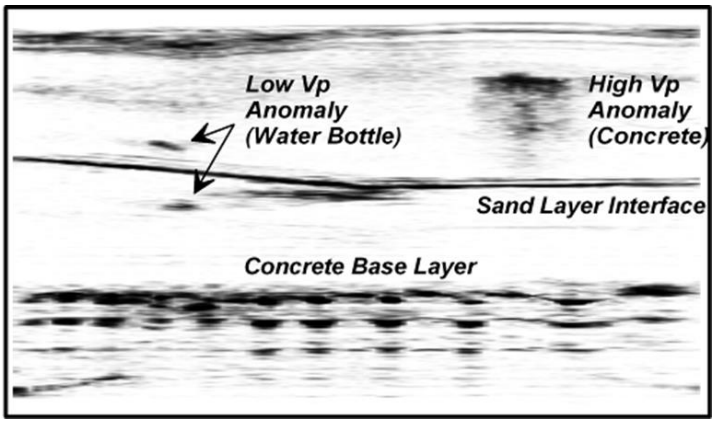

(b)

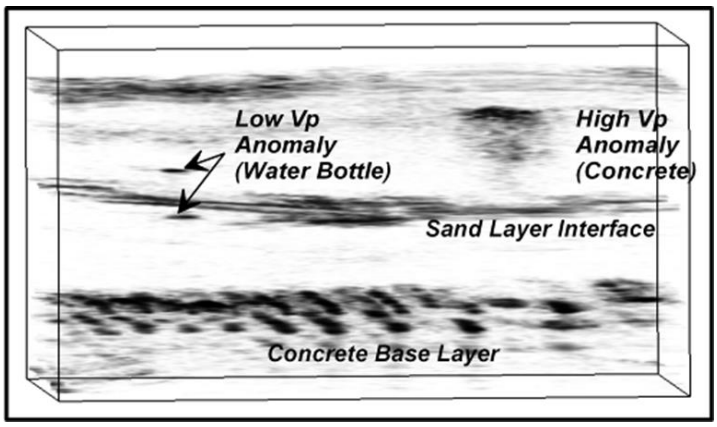

(c)

Figure 2-7: P-wave reflection imaging of soil models from Coe and Brandenberg (2010): (a) Schematic, (b) Two-dimensional cross section, and (c) Three-dimensional image.

Figure 2-8: Ultrasound probe utilized in Coe and Brandenberg (2012).

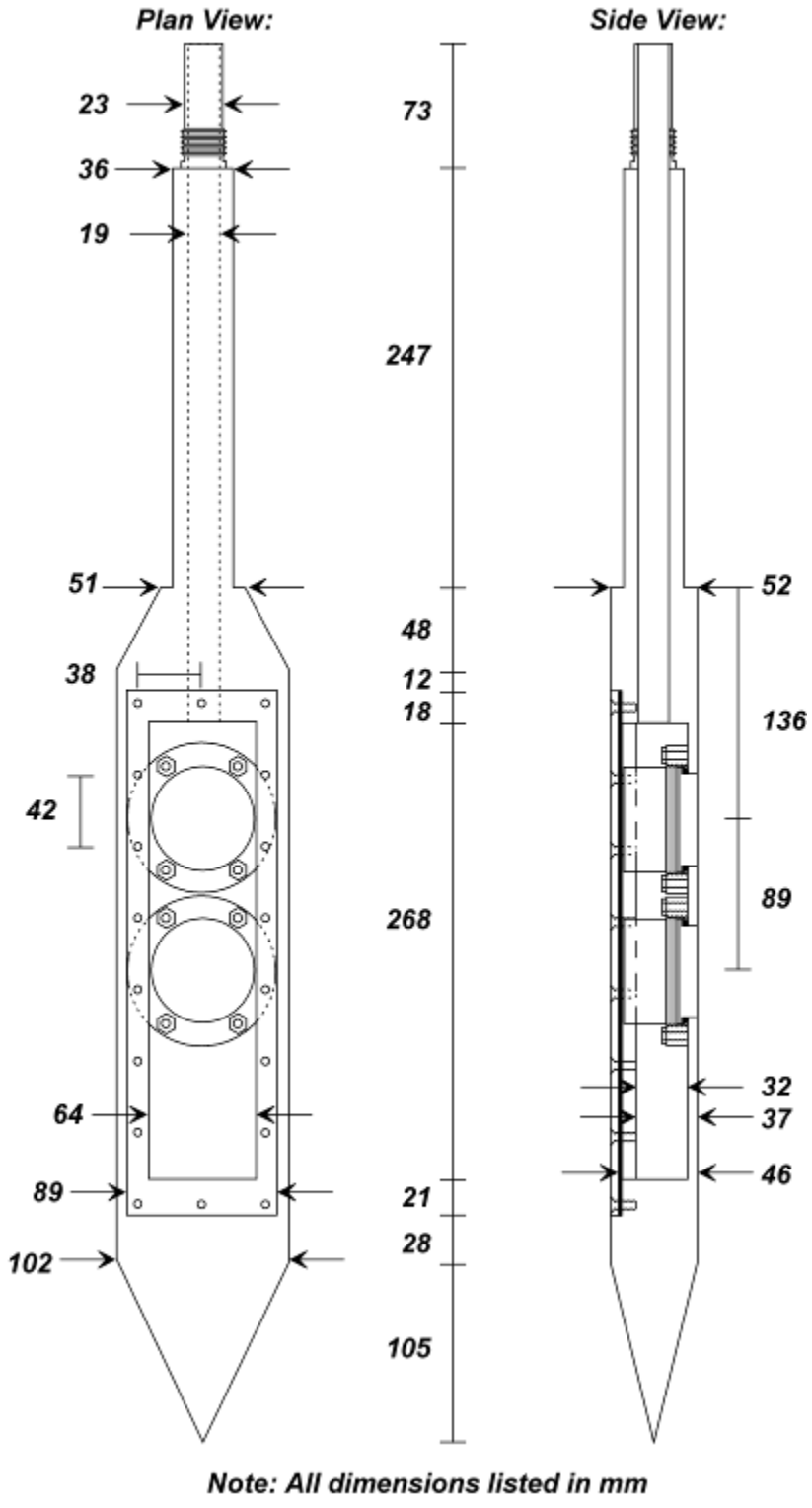

Figure 2-9: Schematic of ultrasound probe utilized in Coe and Brandenberg (2012).

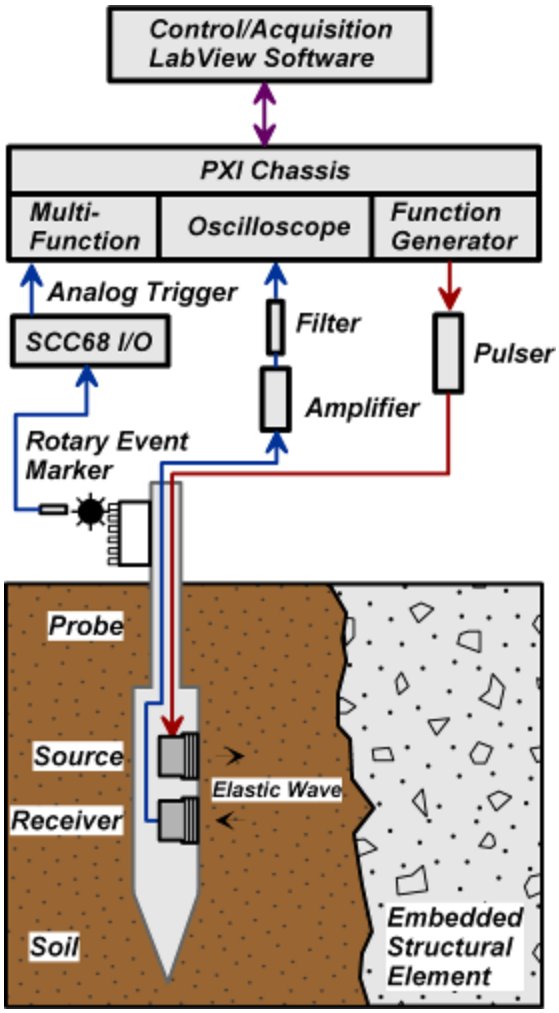

Figure 2-10: Schematic of ultrasound probe command chain flow and data acquisition as used in Coe and Brandenberg (2012).

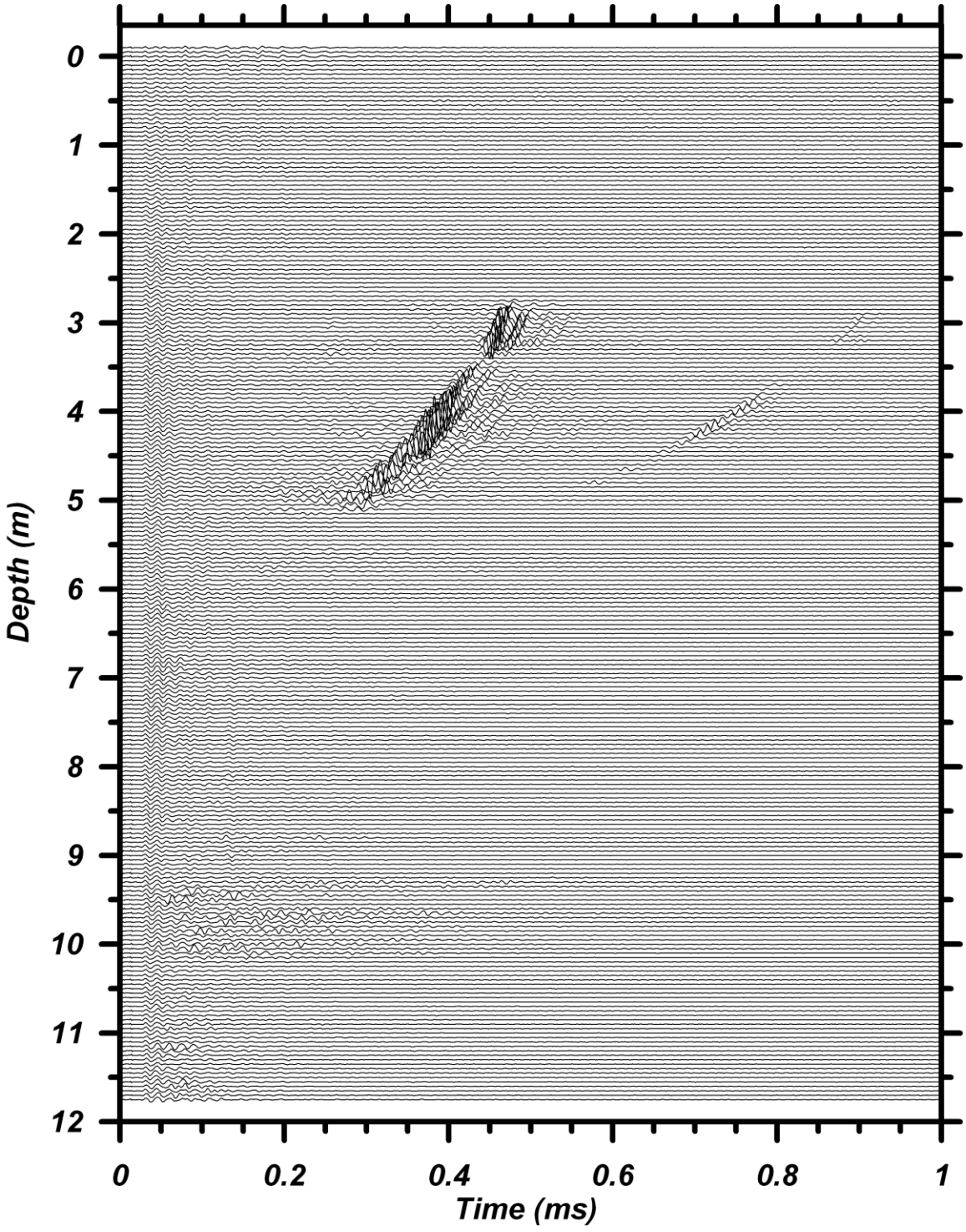

Figure 2-11: Recorded voltage signals from P-wave reflections at the Carquinez Bridge field test site in Coe and Brandenberg (2012) and Coe (2010).

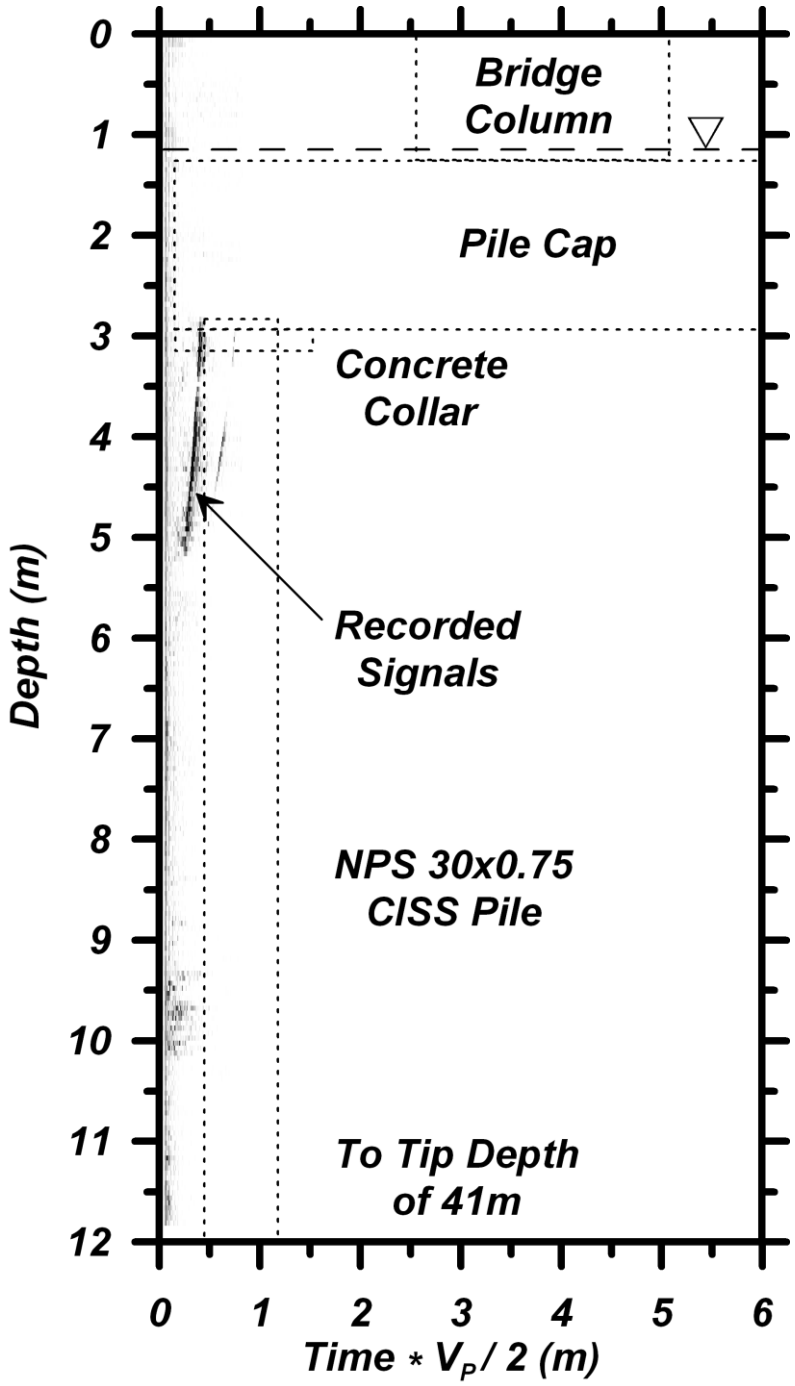

Figure 2-12: Ultrasonic image of Carquinez Bridge test site superposed on sketch of site geometry (Coe and Brandenberg 2012, and Coe 2010).

Figure 2-13: 100 kHz transducers utilized in this study (Coe 2010).

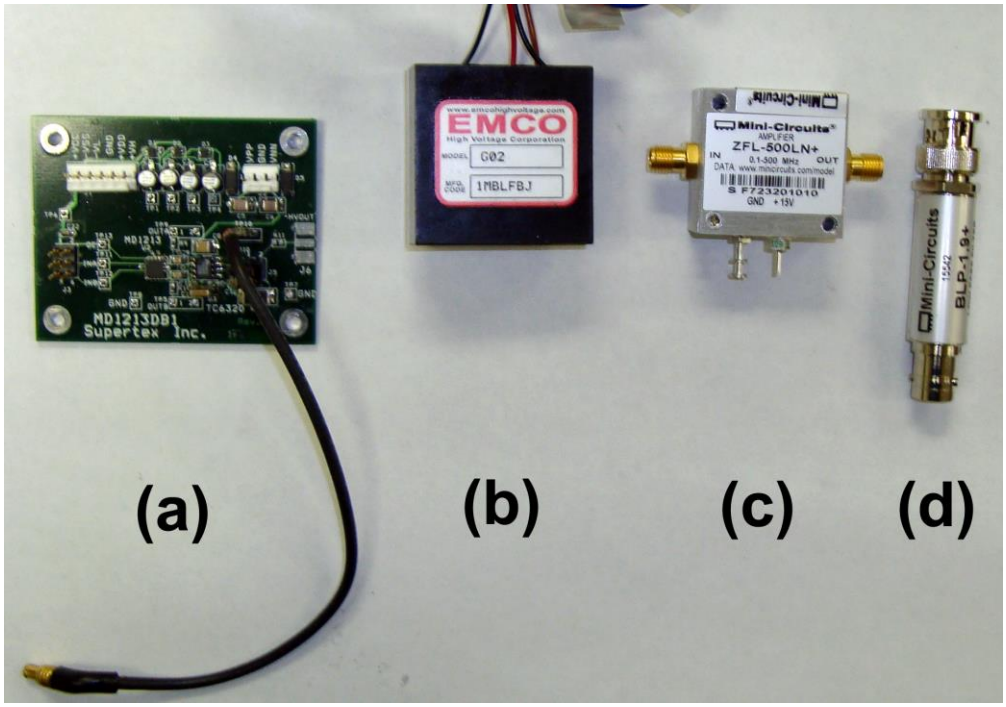

Figure 2-14: Ultrasound device components: (a) source pulser, (b) DC-to-DC converter, (c) receiver amplifier, and (d) receiver filter (Coe 2010).

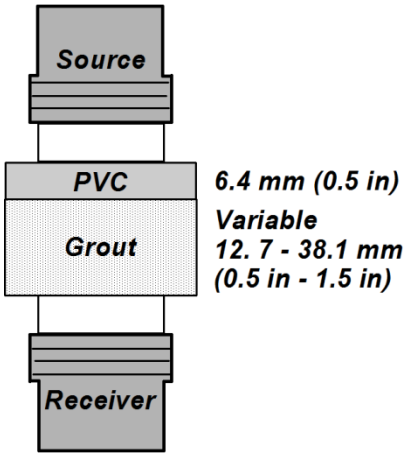

Figure 2-15: PVC/Grout test setup.

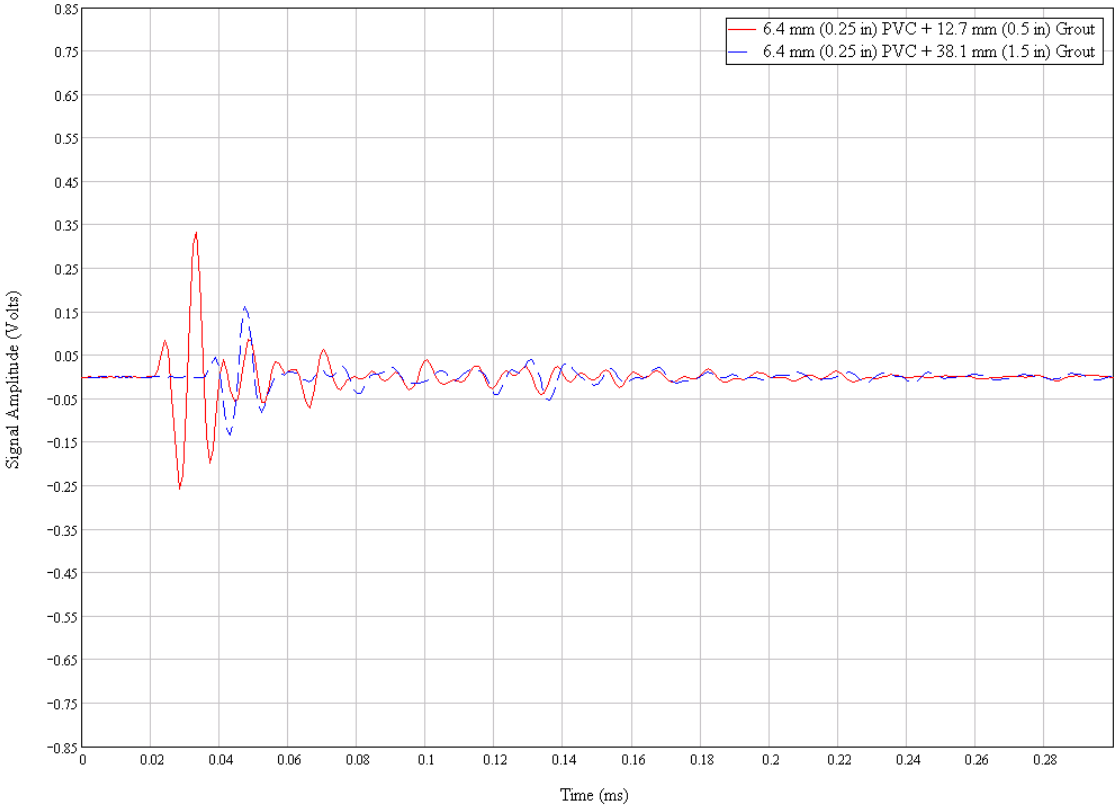

Figure 2-16: Results from PVC/Grout testing for two different grout thicknesses.

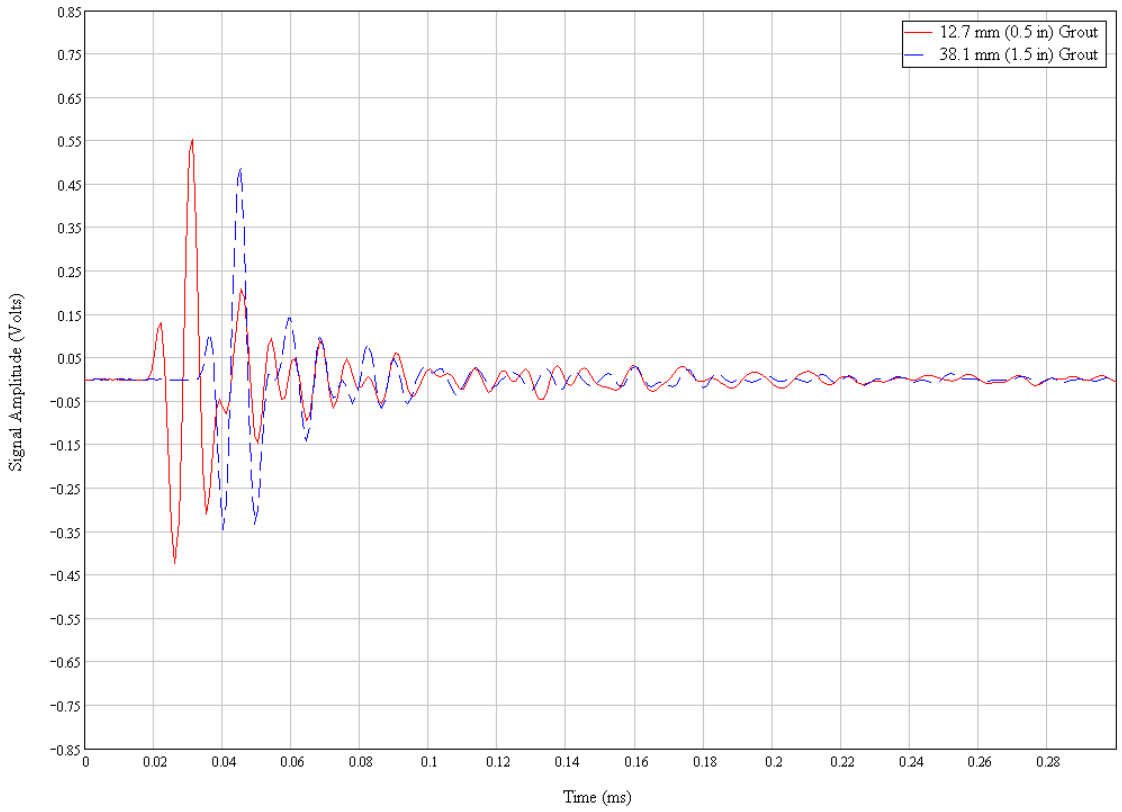

Figure 2-17: Results from grout testing with two different thicknesses of grout.

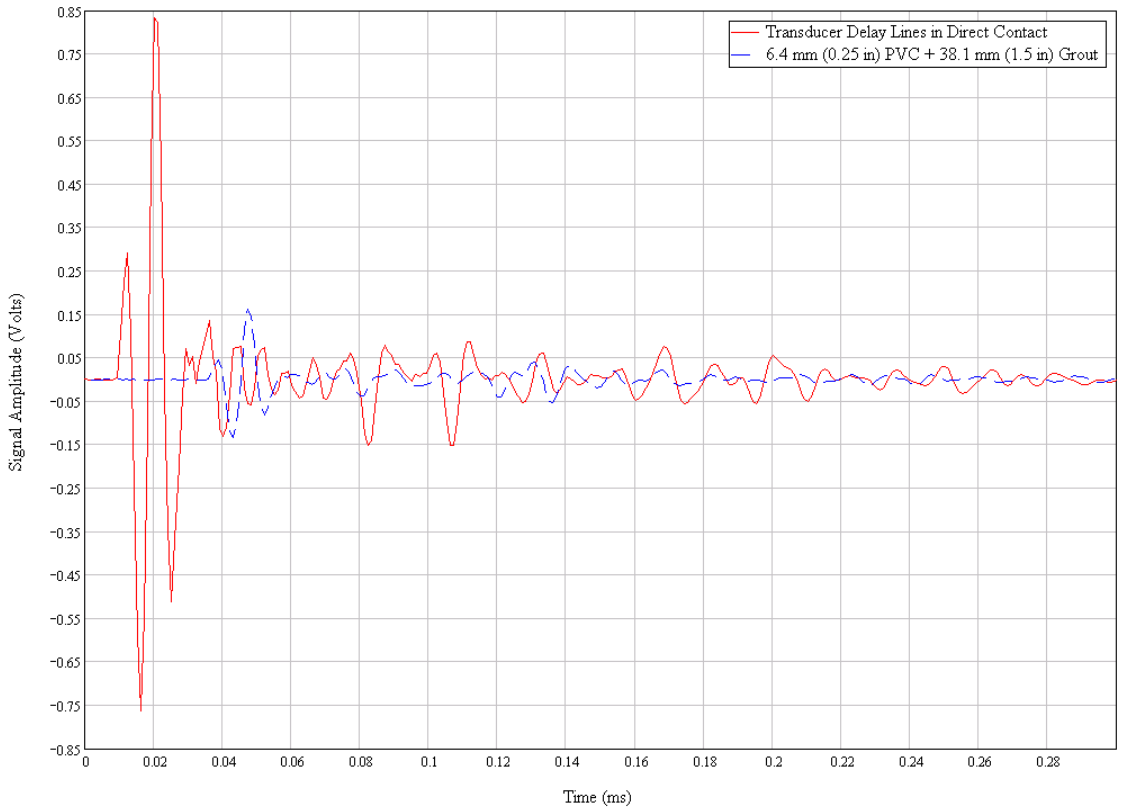

Figure 2-18: Results from PVC/Grout testing that compares direct signal through transducer delay lines to the signal received with PVC/grout interface.

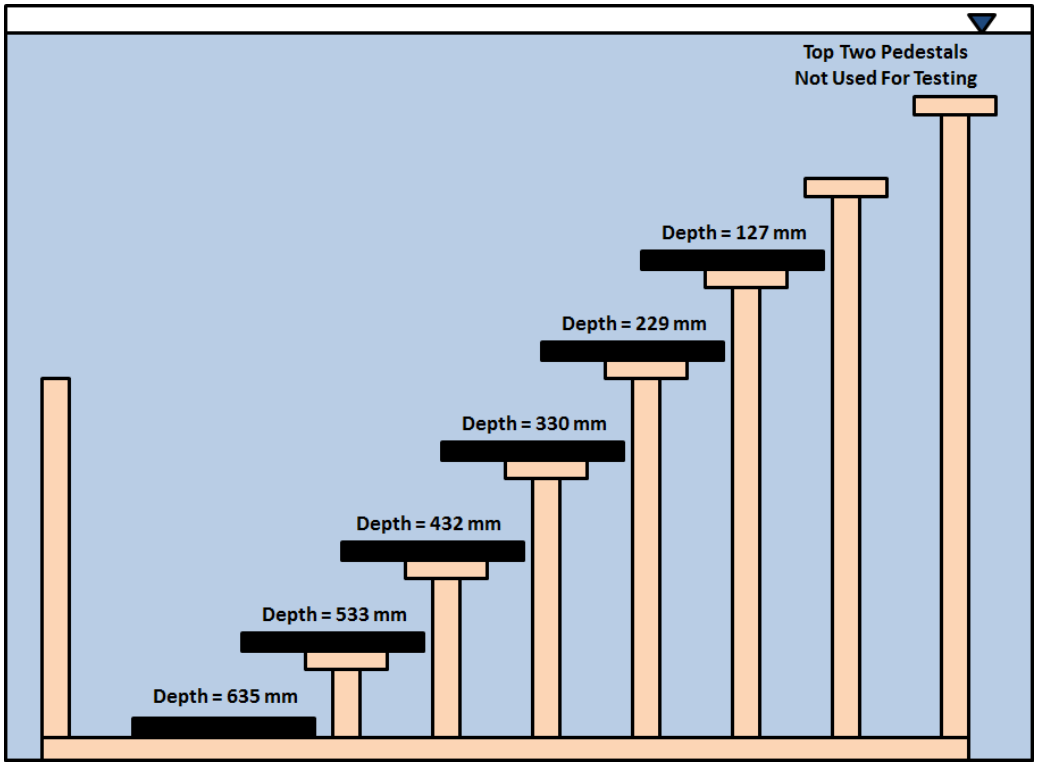

Figure 2-19: Schematic of acrylic chamber water model. Note: Data was obtained from scanning the model right to left.

Figure 2-20: Picture of acrylic chamber water model.

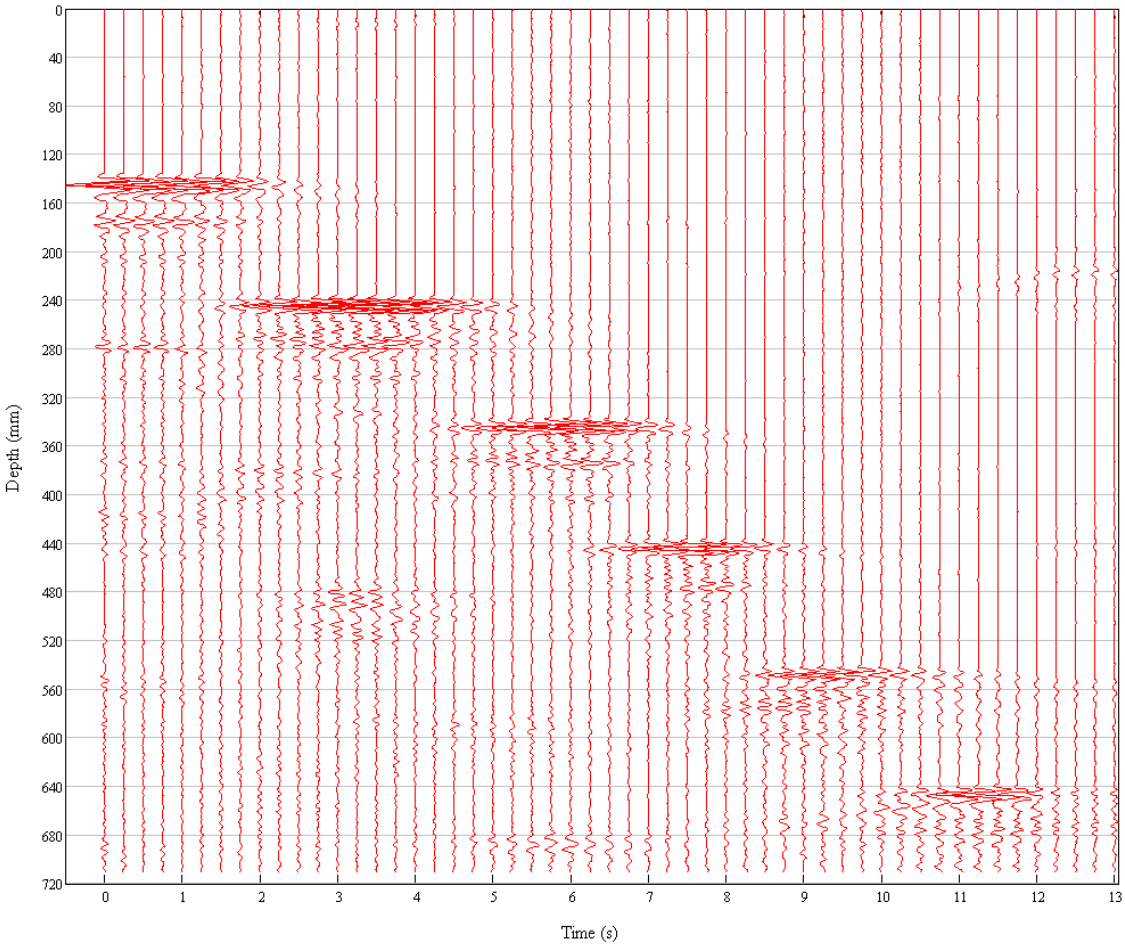

Figure 2-21: Data from acrylic chamber water model (no depth dependent gain factor applied to recorded voltages). Note: Data was obtained from scanning the model right to left.

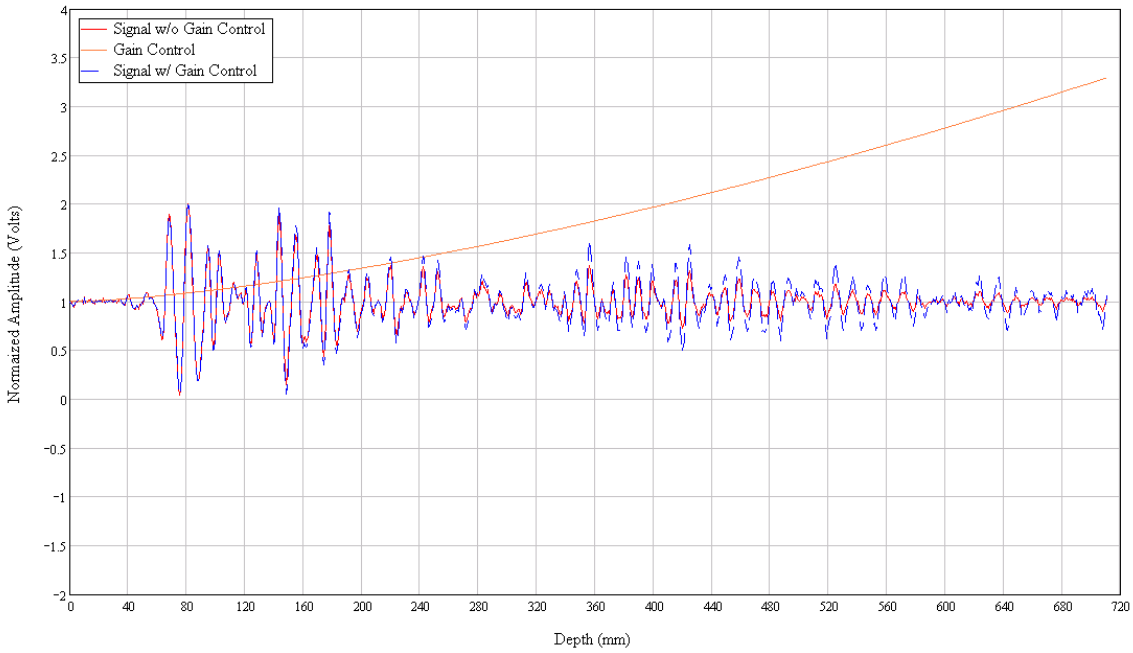

Figure 2-22: Example of depth dependent gain factor and its effects on amplitude for a signal from the acrylic chamber water model.

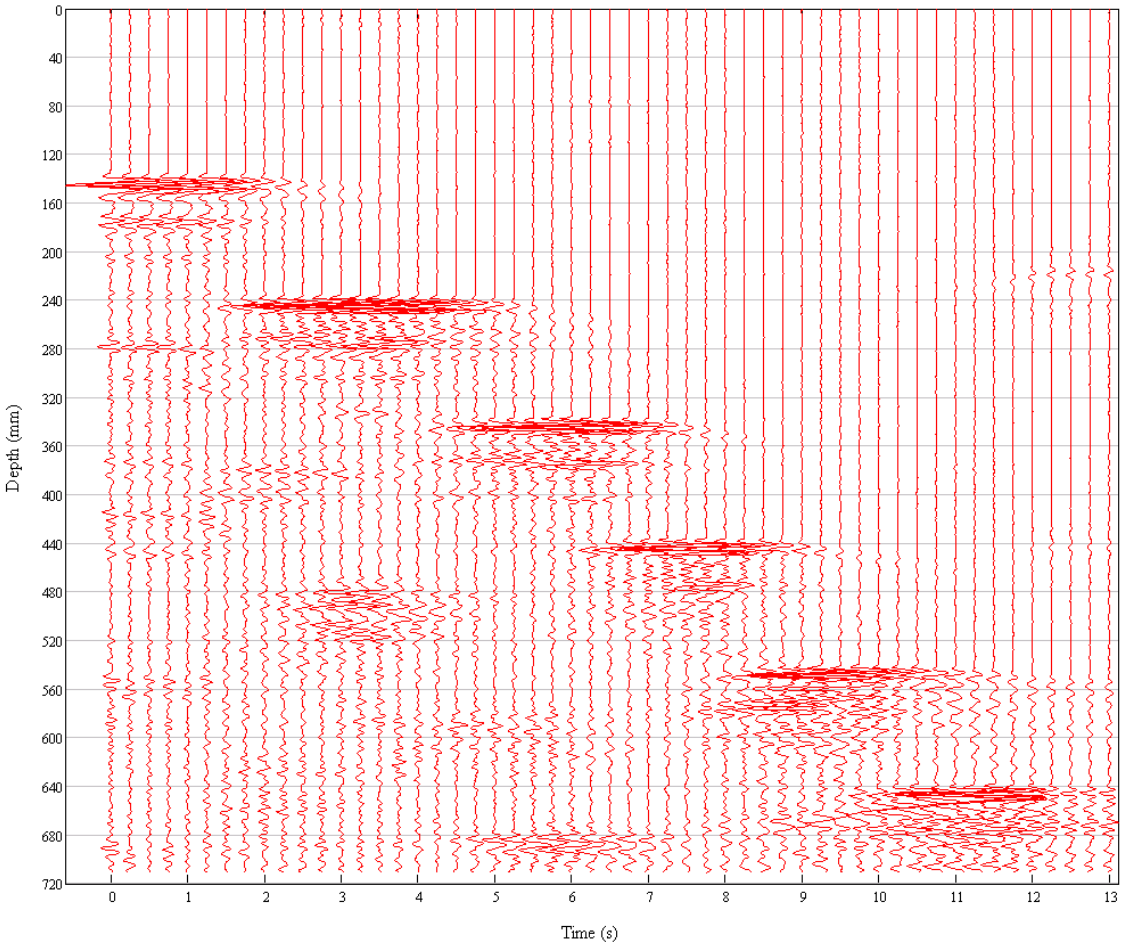

Figure 2-23: Data from acrylic chamber water model (with depth dependent gain factor applied to recorded voltages). Note: Data was obtained from scanning the model right to left.

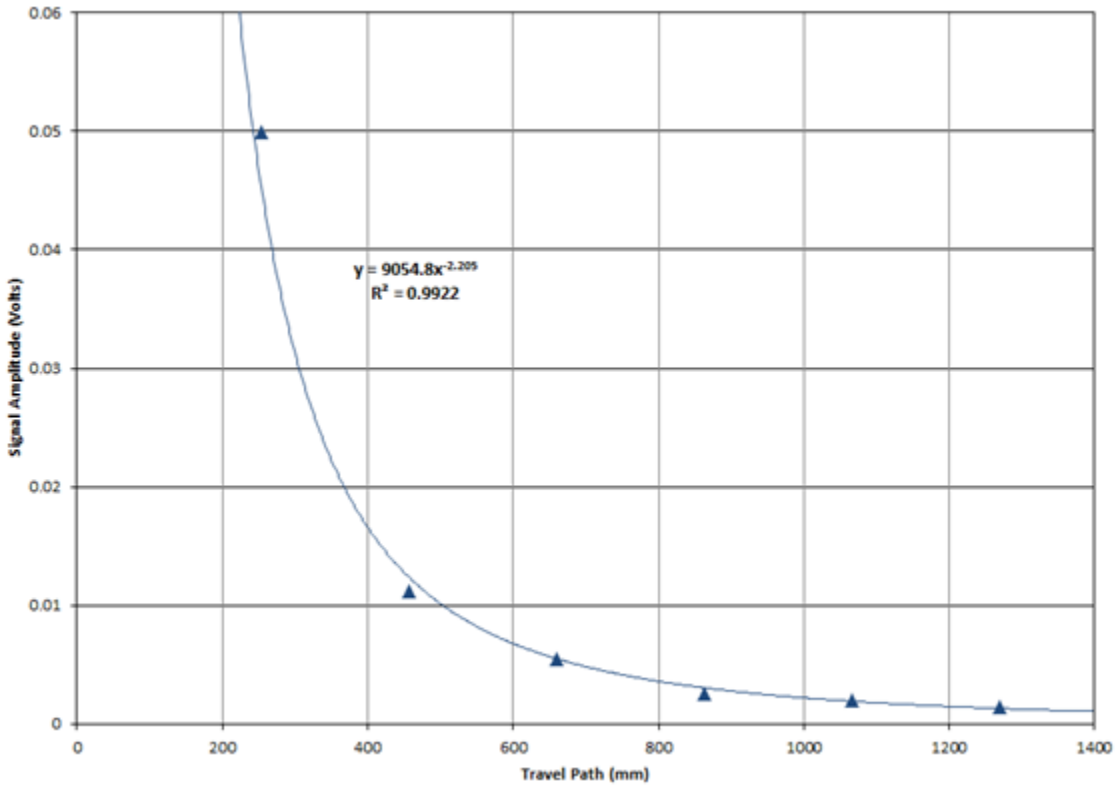

Figure 2-24: Signal attenuation for recordings from acrylic chamber water model.

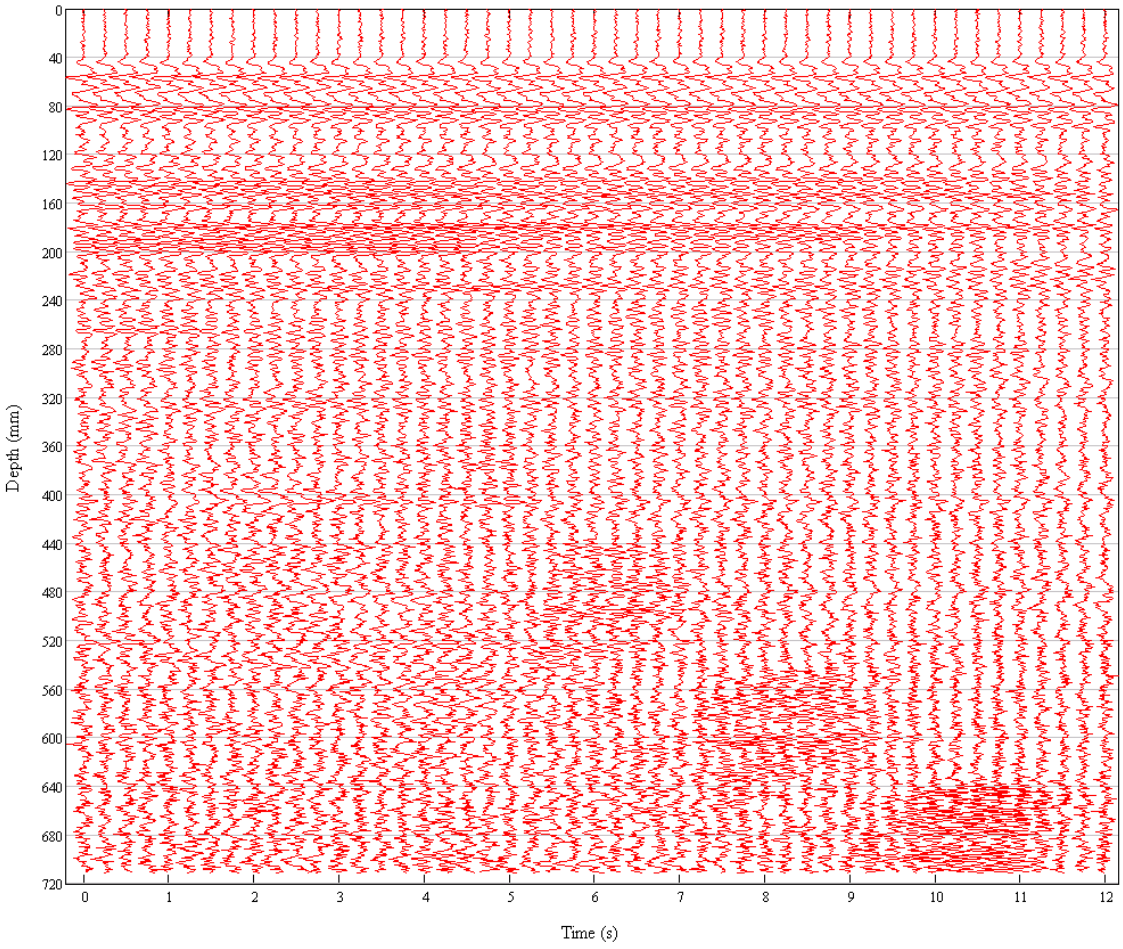

Figure 2-25: Data from acrylic chamber water model with PVC interface at 31.8 mm (1.25 in) (with depth dependent gain factor applied to recorded voltages). Note: Data was obtained from scanning the model right to left.

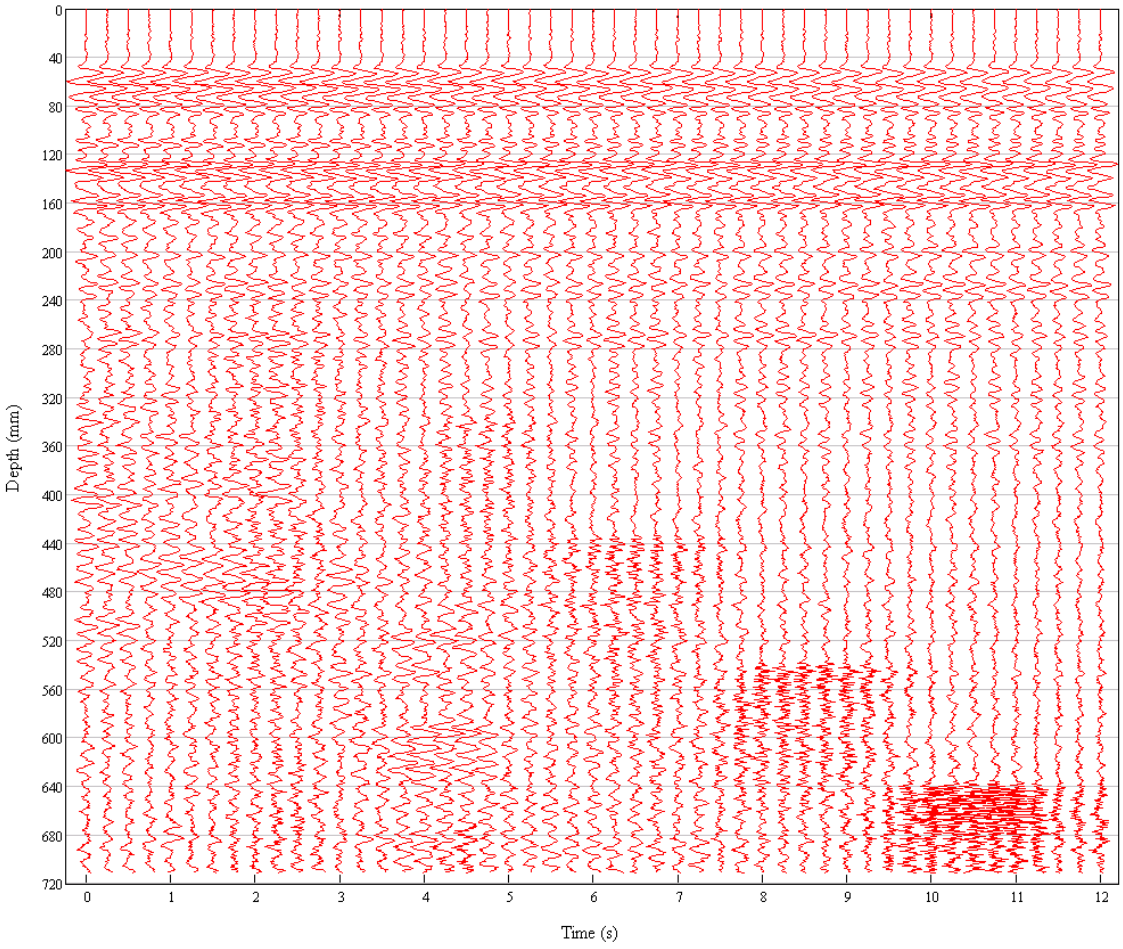

Figure 2-26: Data from acrylic chamber water model with LDPE interface at 31.8 mm (1.25 in) (with depth dependent gain factor applied to recorded voltages). Note: Data was obtained from scanning the model right to left.

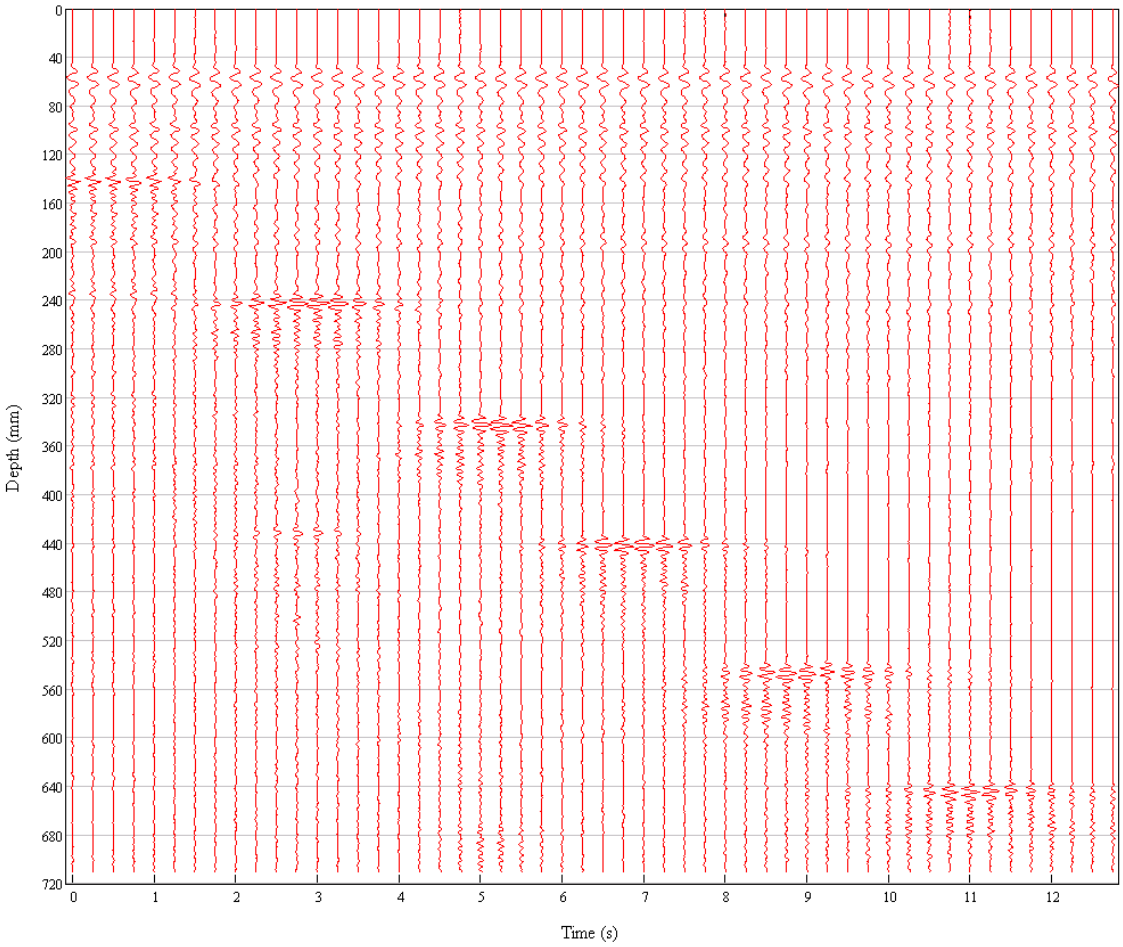

Figure 2-27: Data from acrylic chamber water model with polypropylene interface at 31.8 mm (1.25 in) (with depth dependent gain factor applied to recorded voltages). Note: Data was obtained from scanning the model right to left.

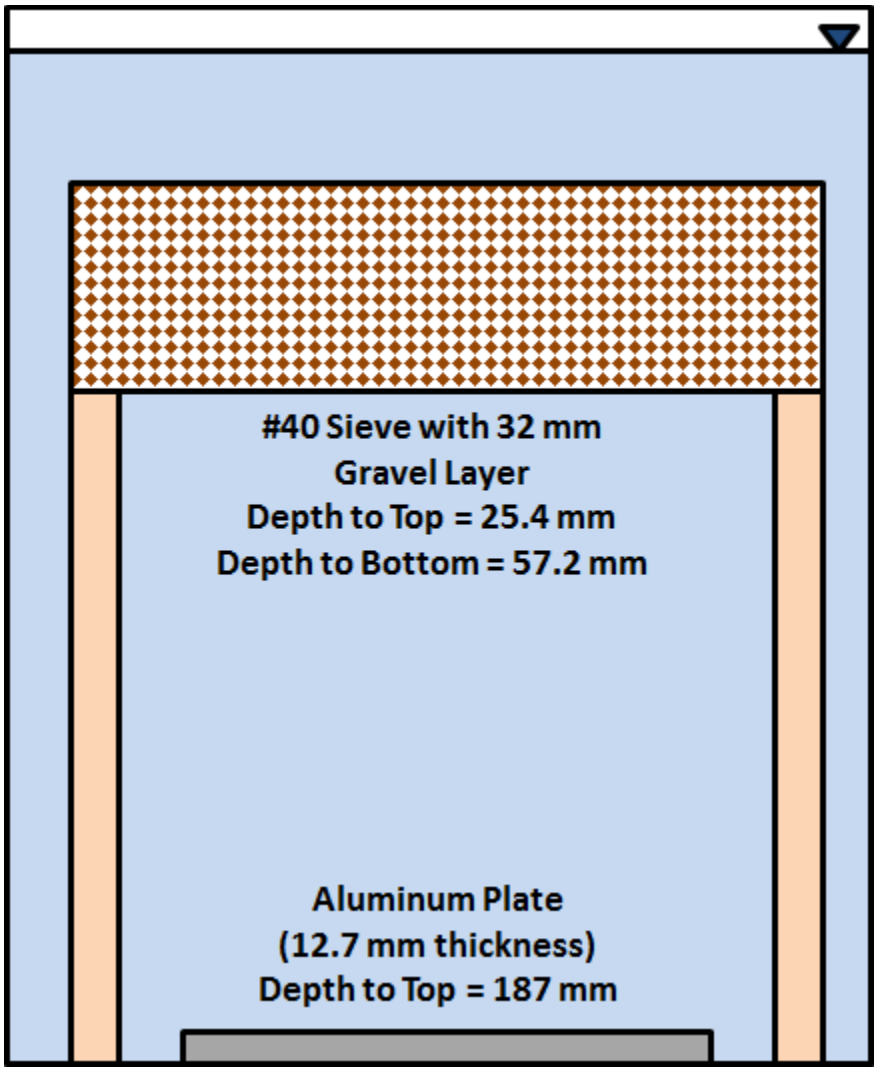

Figure 2-28: Gravel and aluminum water model schematic.

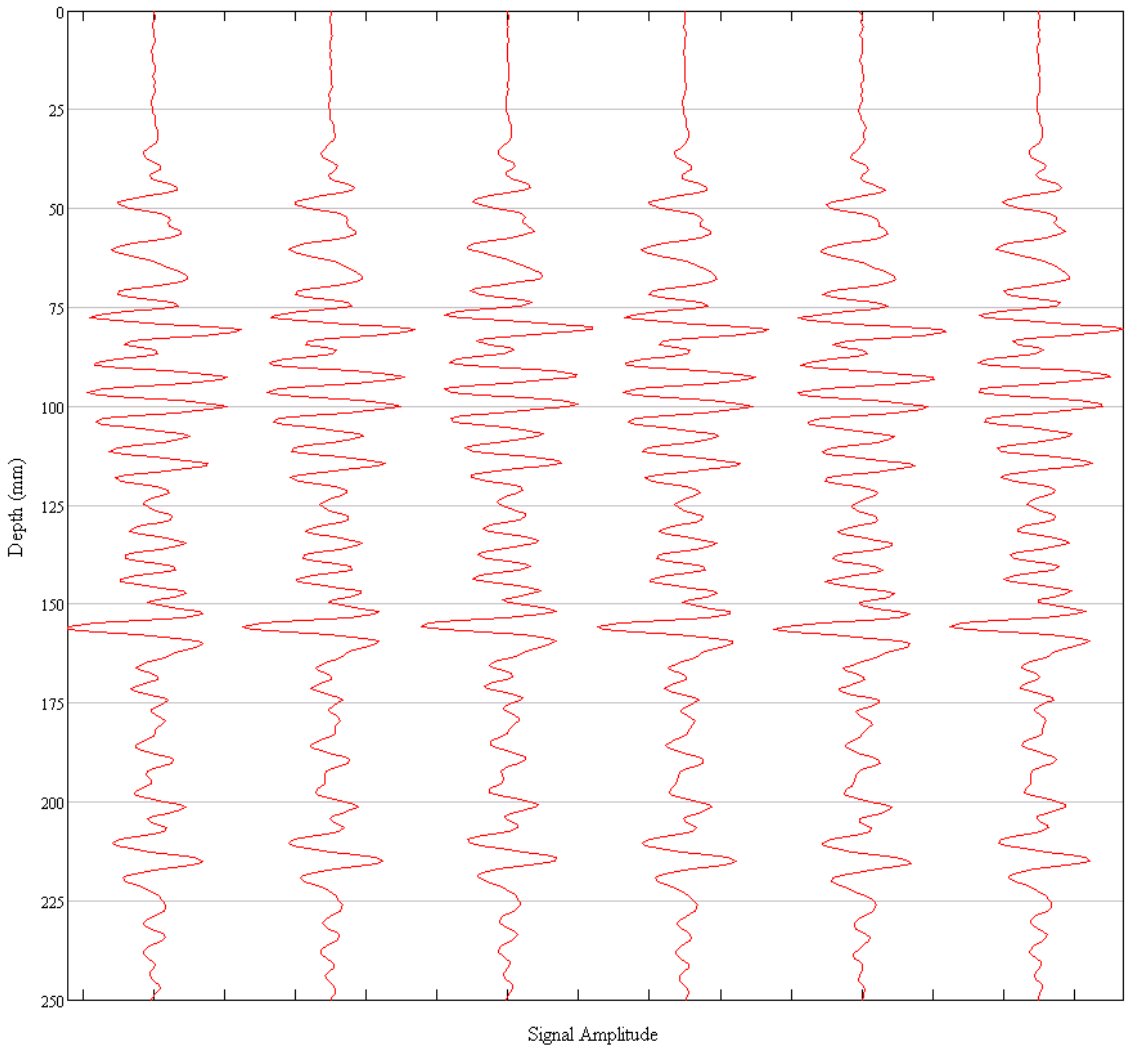

Figure 2-29: Reflection signals from gravel and aluminum water model.

Figure 2-30: Stainless steel vacuum chamber used to construct soil model.

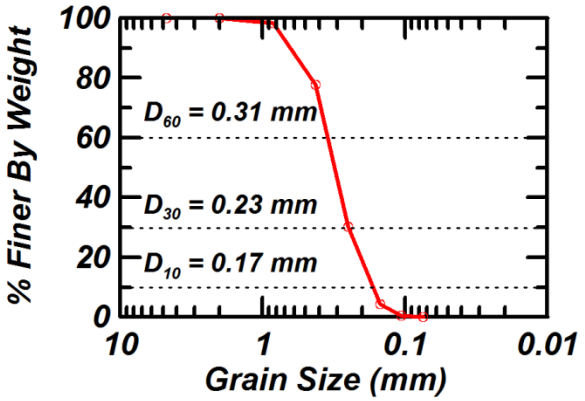

Figure 2-31: Grain size distribution for silica sand used to construct soil model.

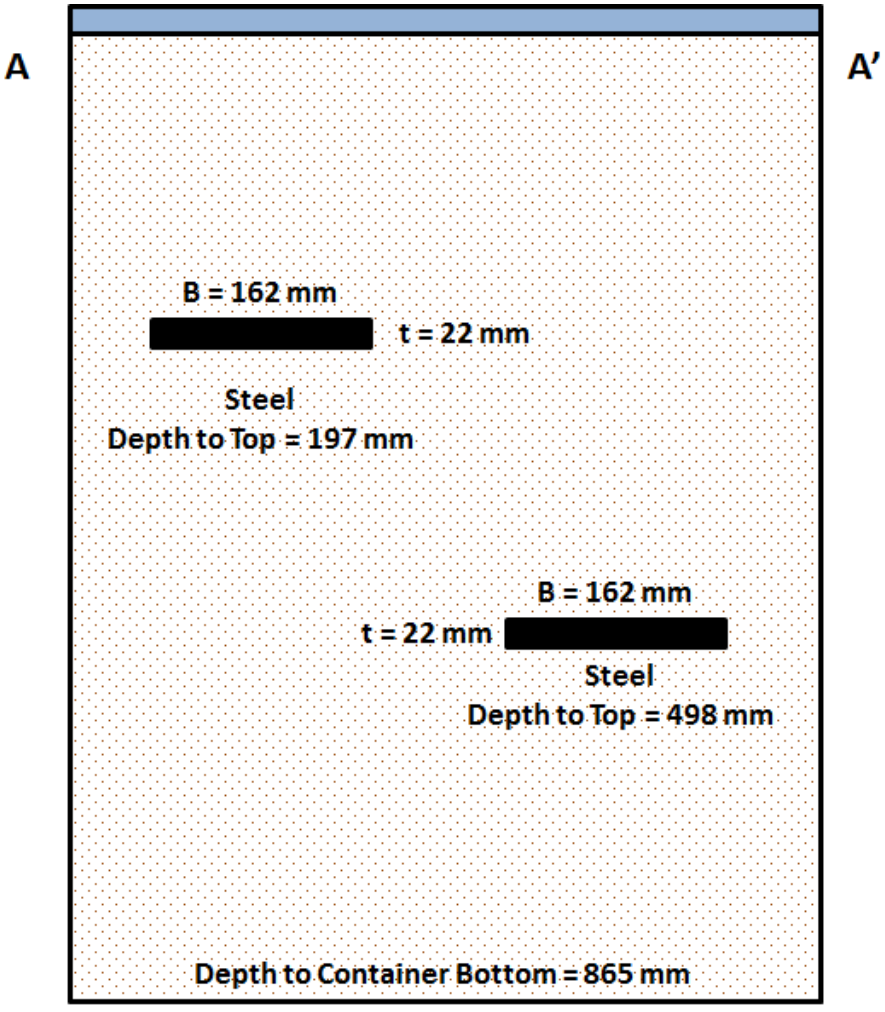

Figure 2-32: Schematic of cross section AA' for soil model. Note: Distances along cross section noted in Fig. 36.

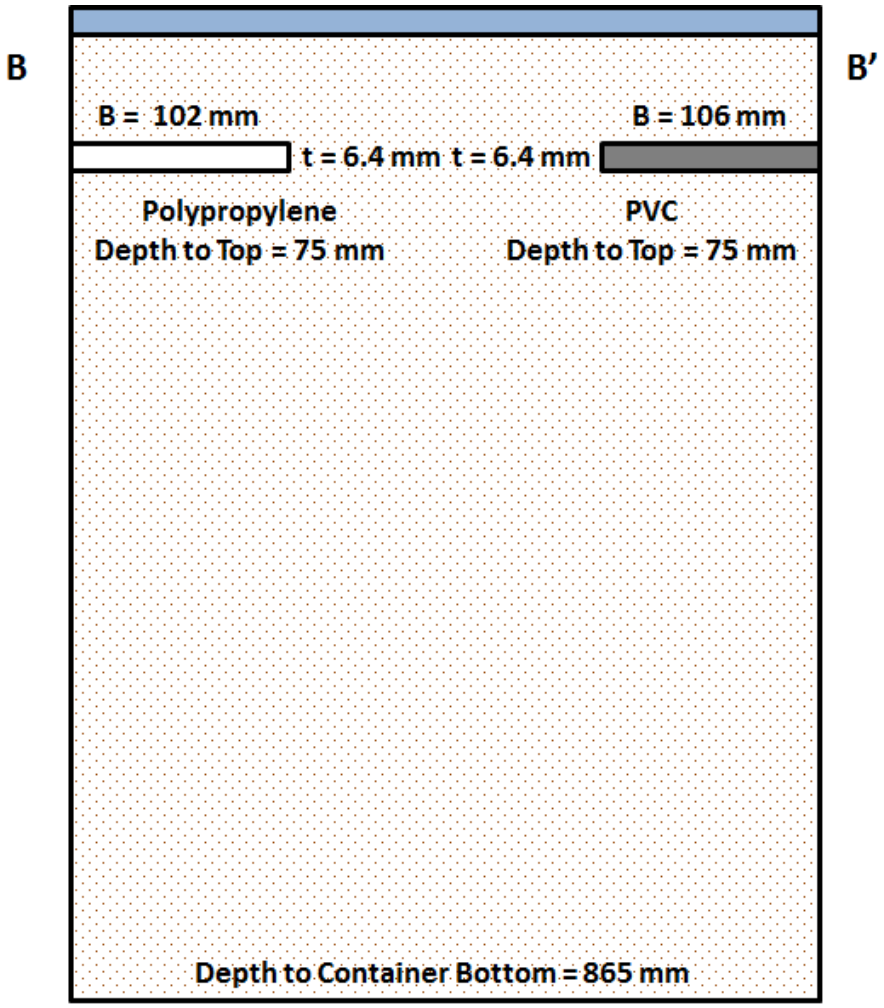

Figure 2-33: Schematic of cross section BB' for soil model. Note: Distances along cross section noted in Fig. 36.

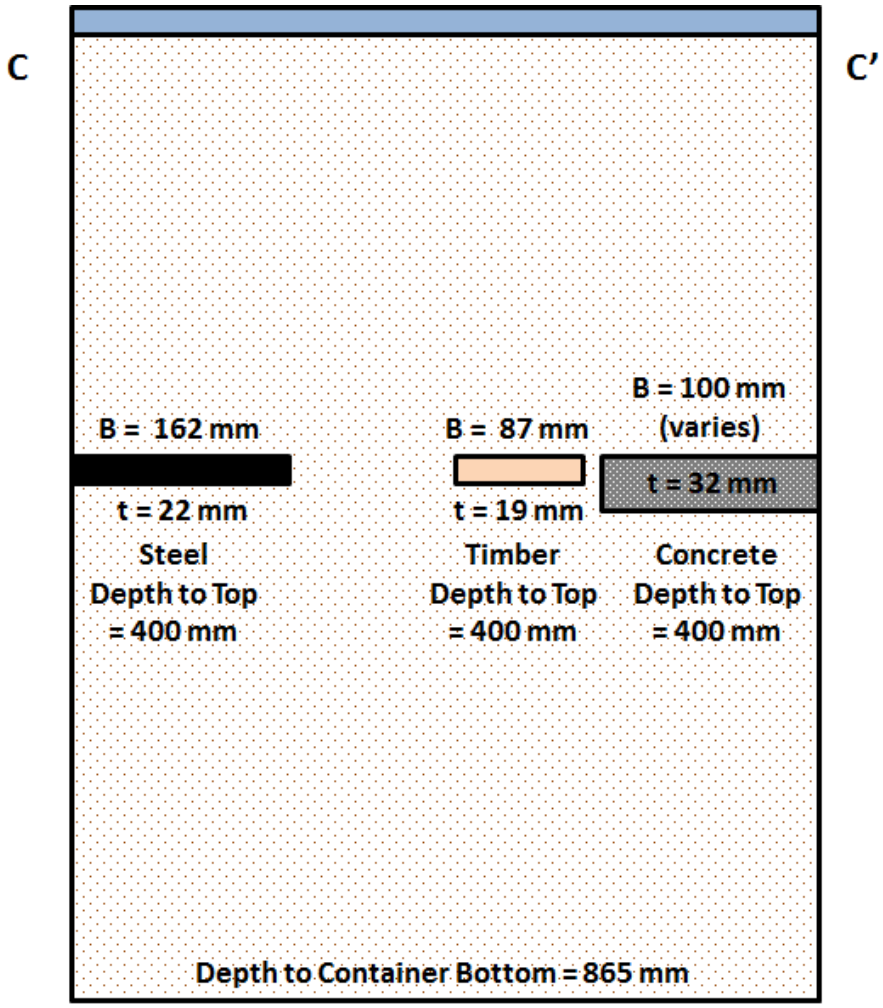

Figure 2-34: Schematic of cross section CC' for soil model. Note: Distances along cross section noted in Fig. 36.

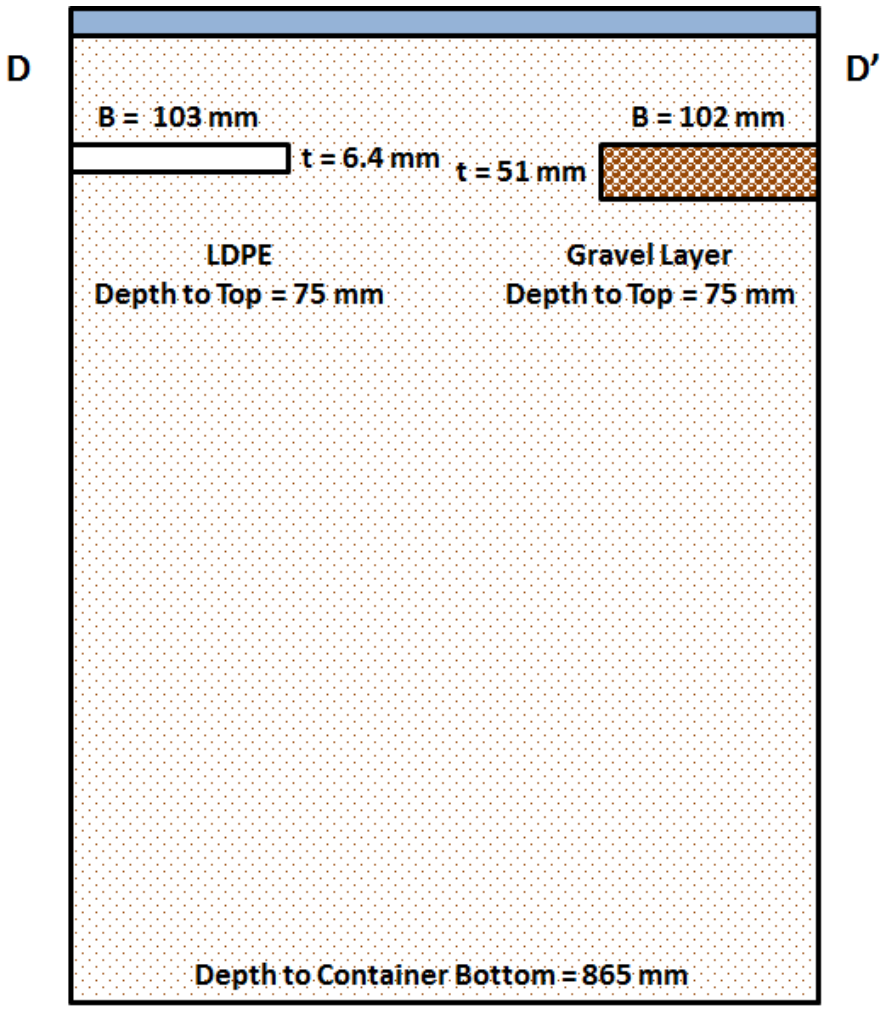

Figure 2-35: Schematic of cross section DD' for soil model. Note: Distances along cross section noted in Fig. 36.

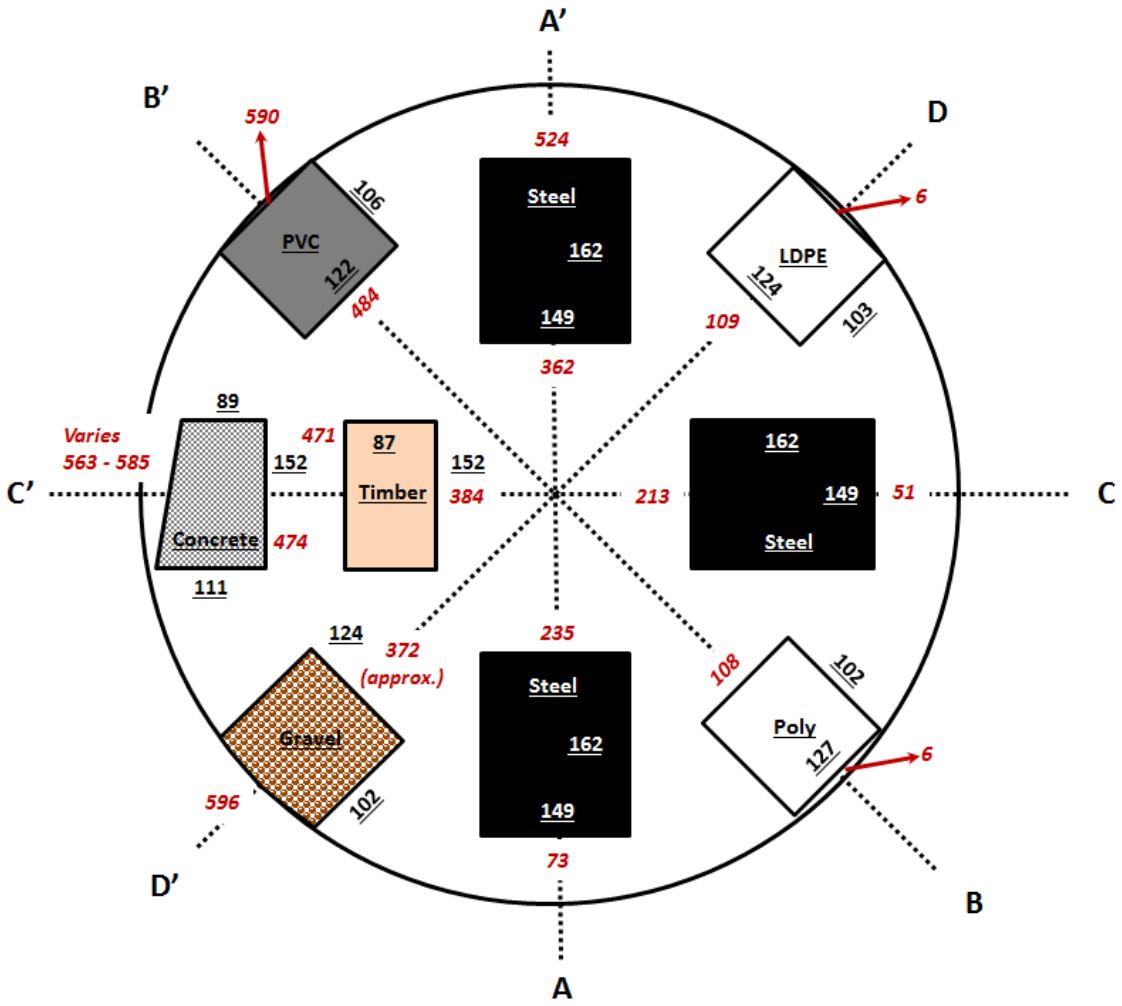

Figure 2-36: Overhead schematic of cross sections in soil model. Note: All dimension in mm; Red = Distance along centerline of cross section; Underline = Object dimension.

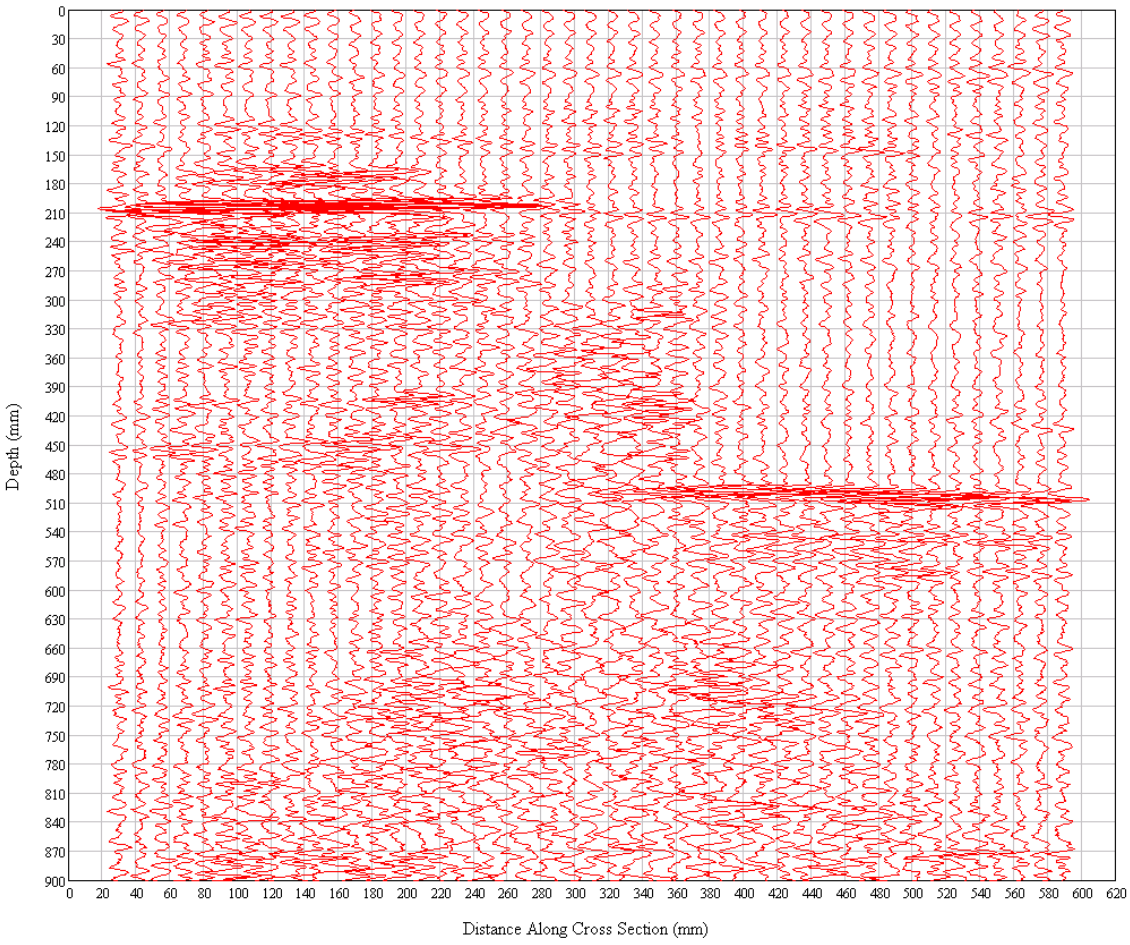

Figure 2-37: Results along cross section AA' in soil model.

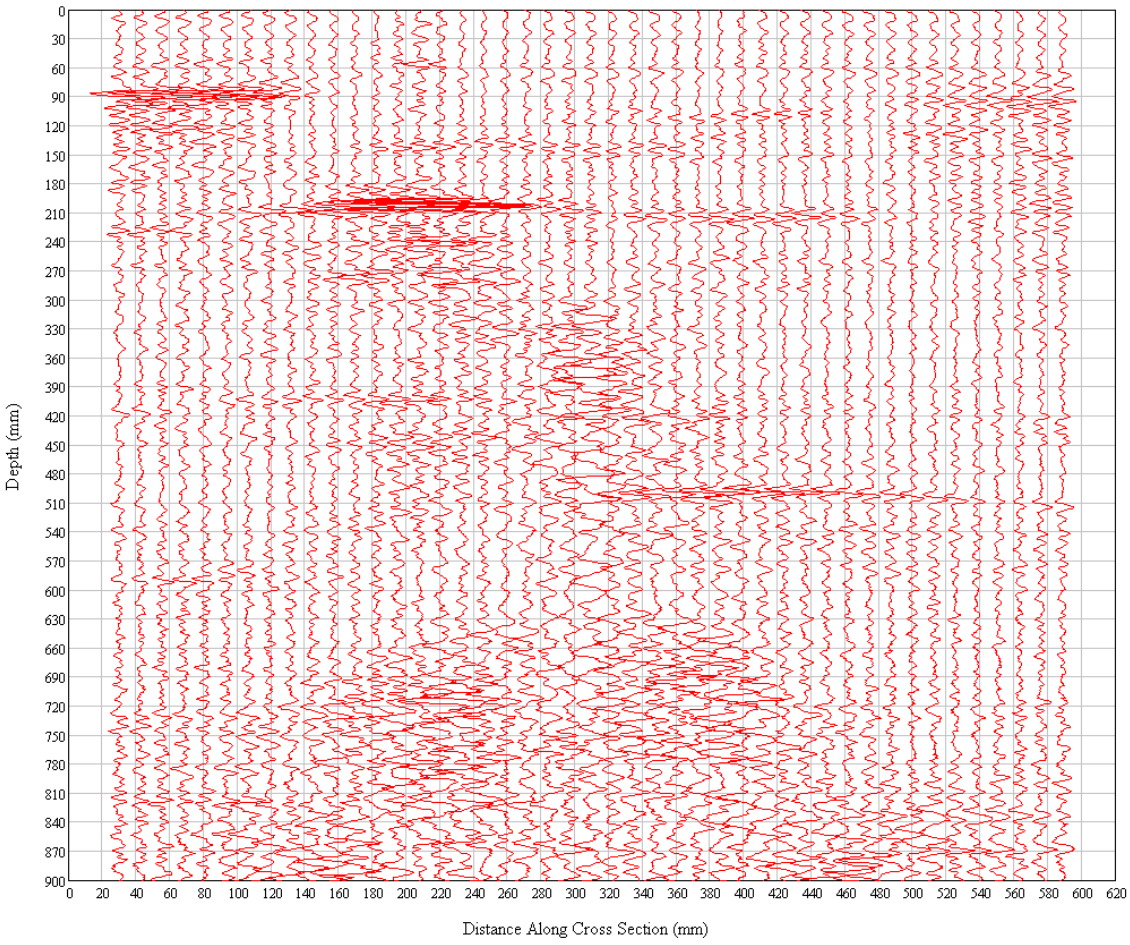

Figure 2-38: Results along cross section BB' in soil model.

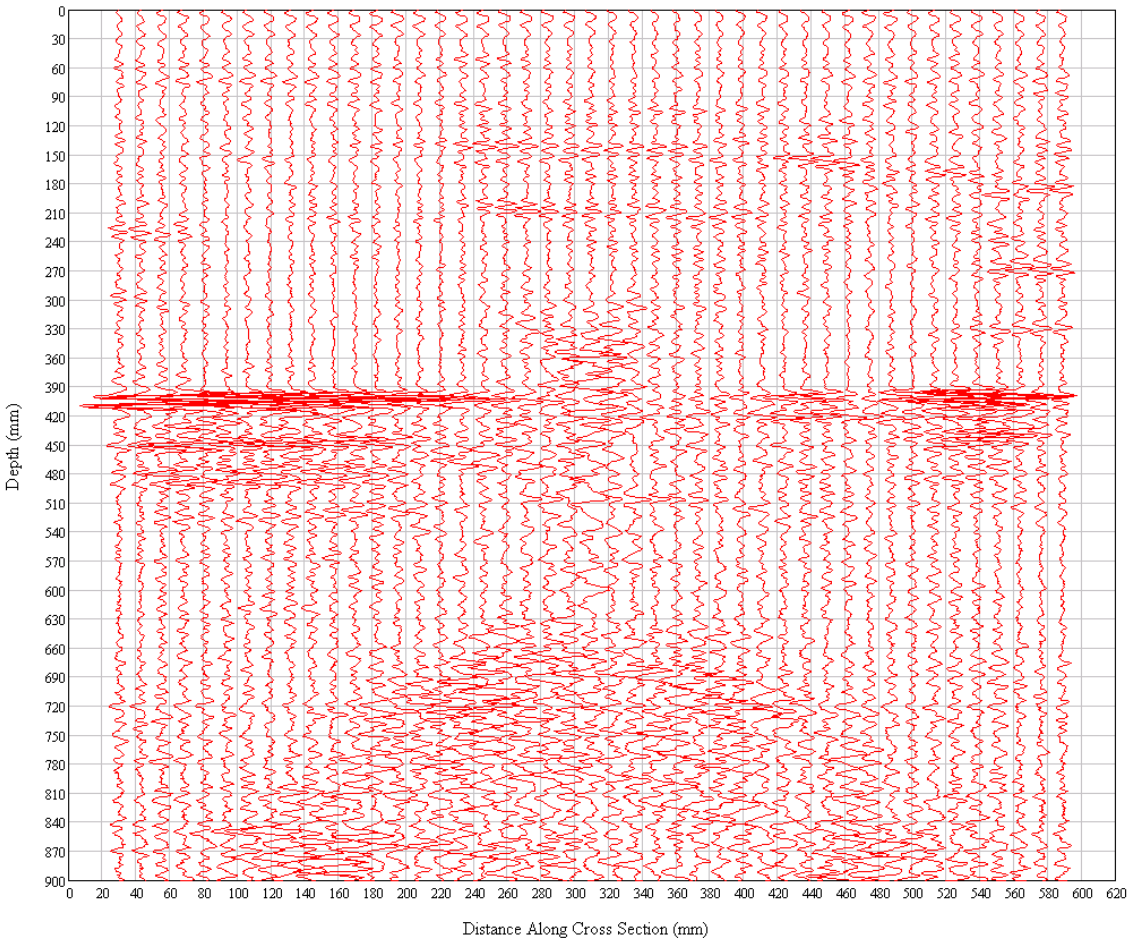

Figure 2-39: Results along cross section CC' in soil model.

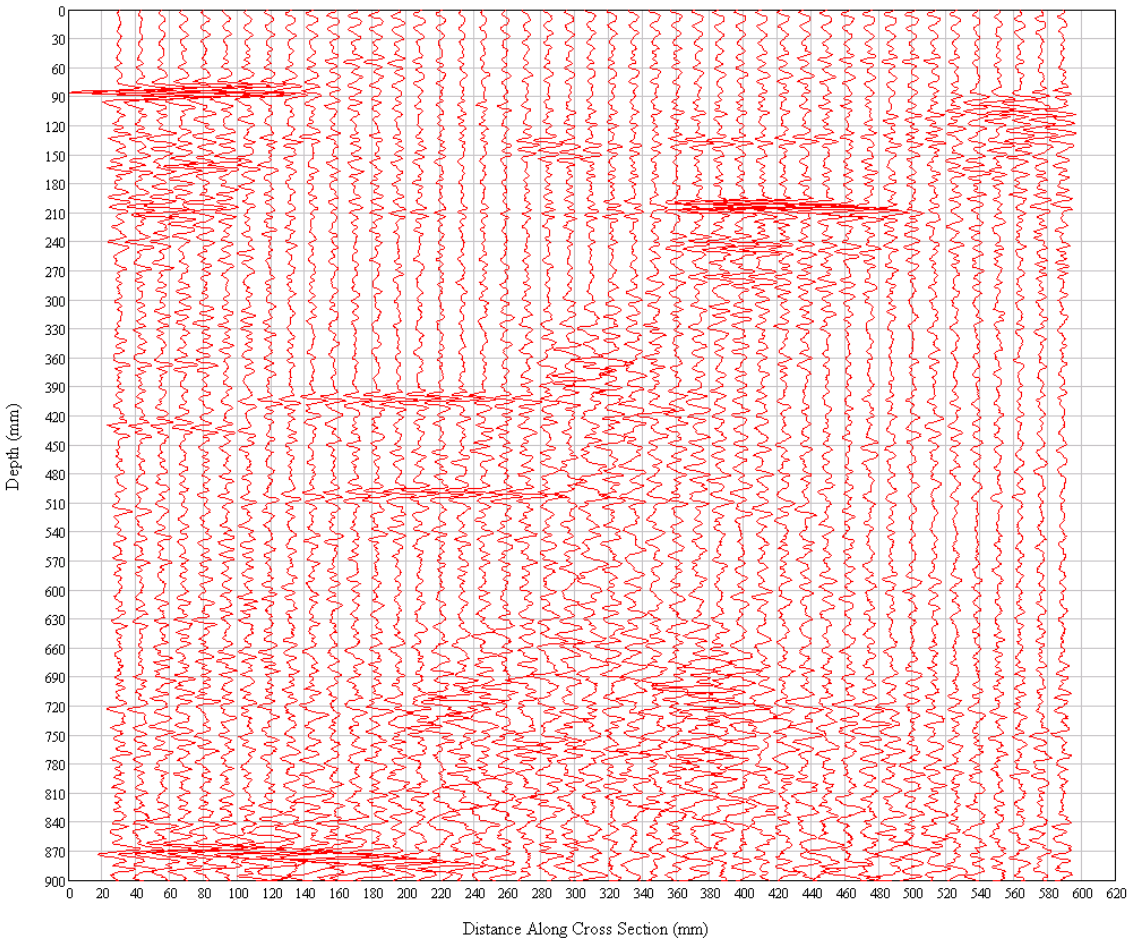

Figure 2-40: Results along cross section DD' in soil model.

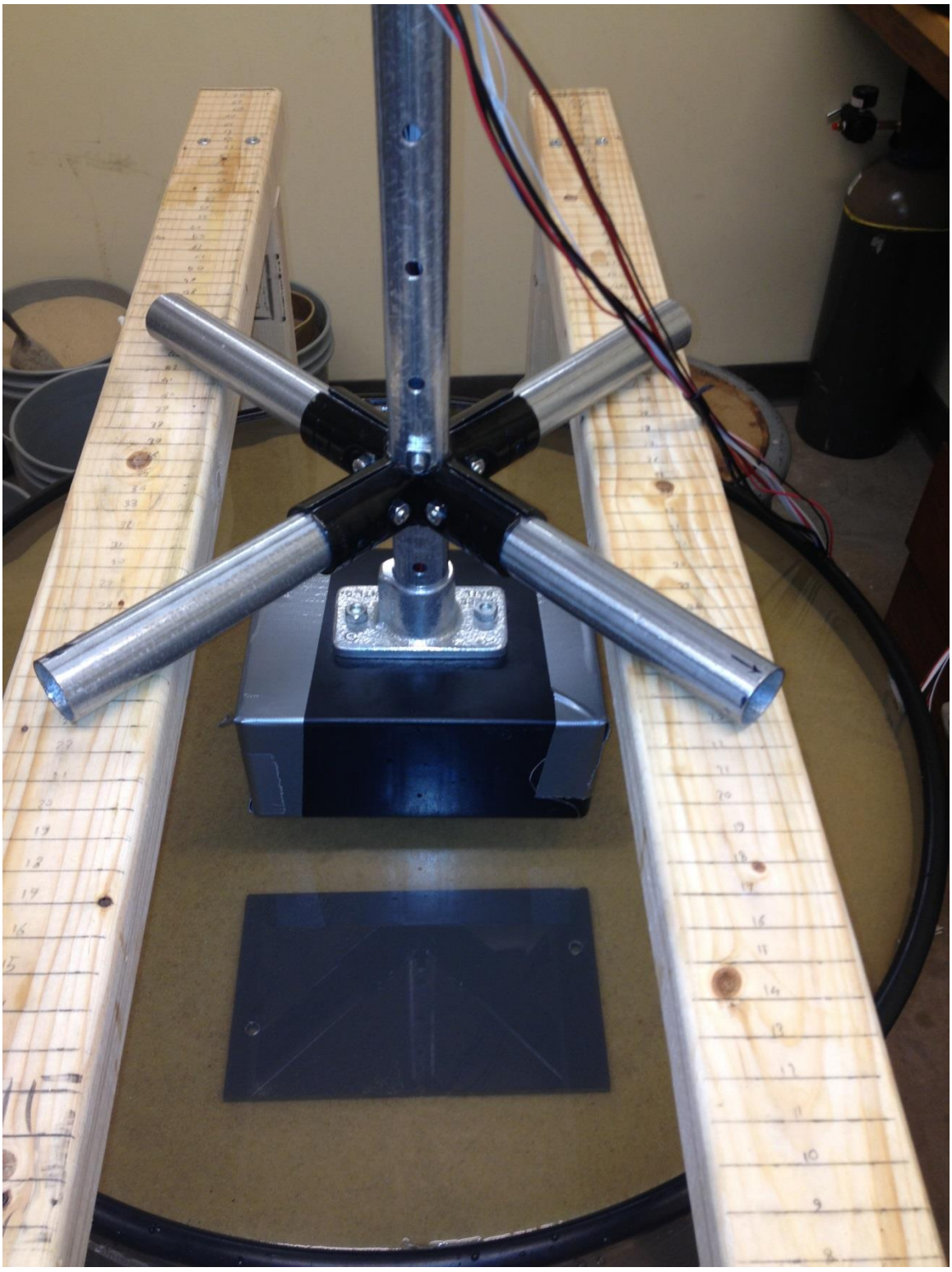

Figure 2-41: Scanning cross section AA' with PVC interface at surface of soil.

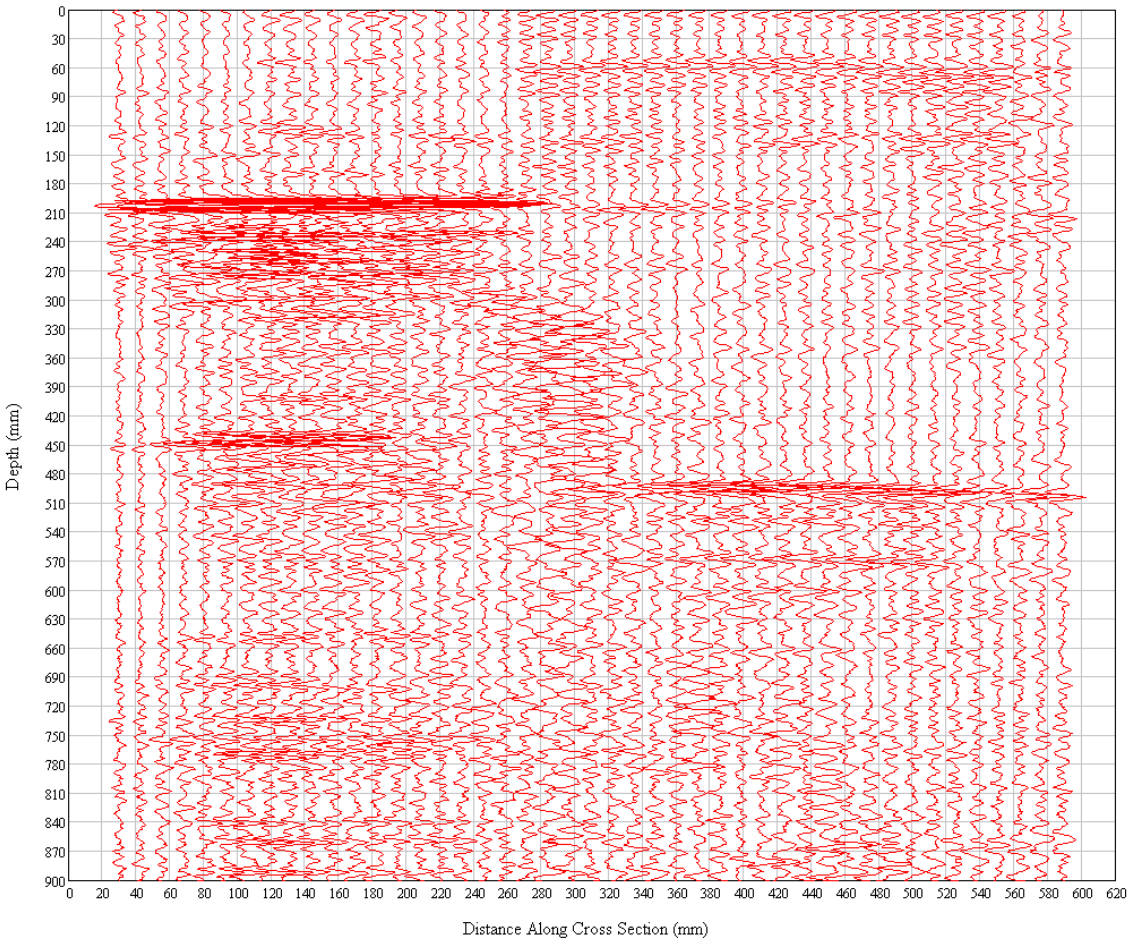

Figure 2-42: Results from cross section AA' with PVC sheet near A'.

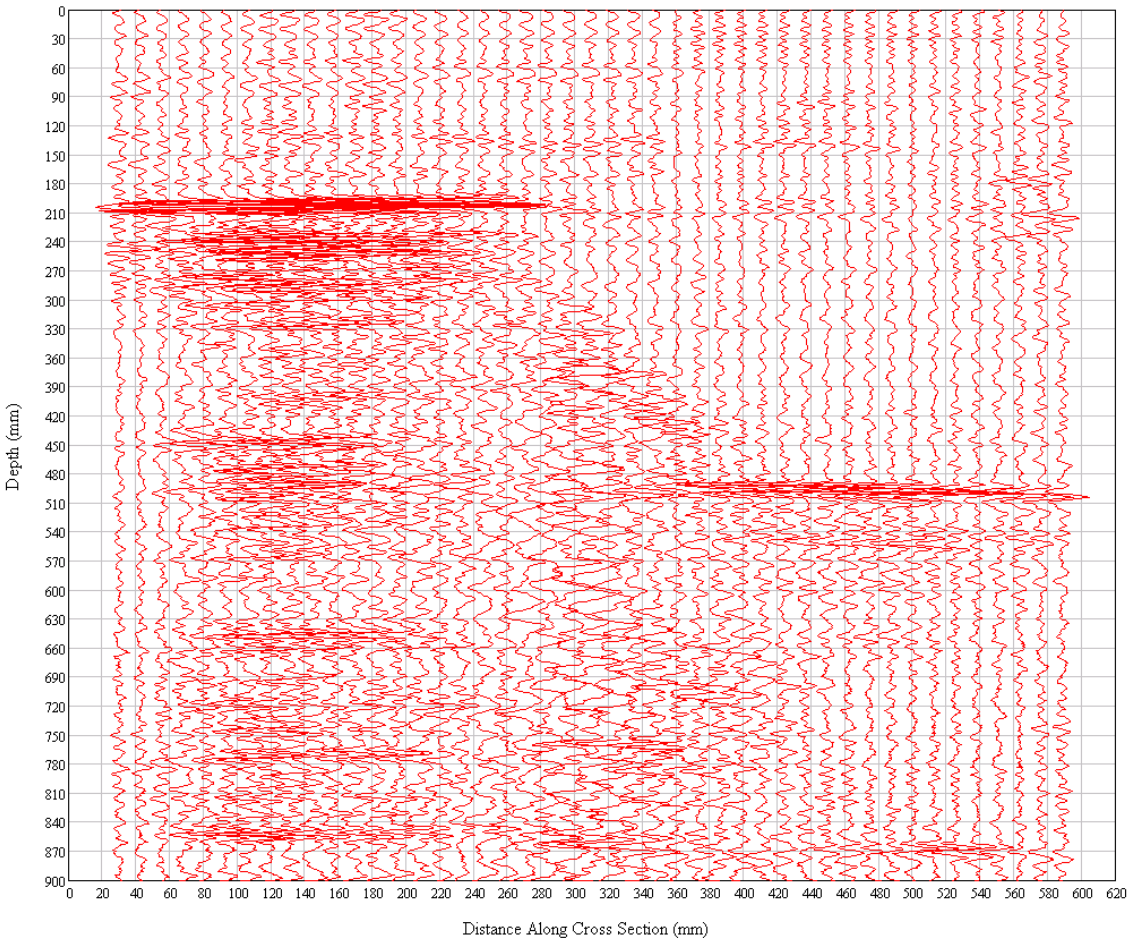

Figure 2-43: Results from cross section AA' with polypropylene sheet near A'.

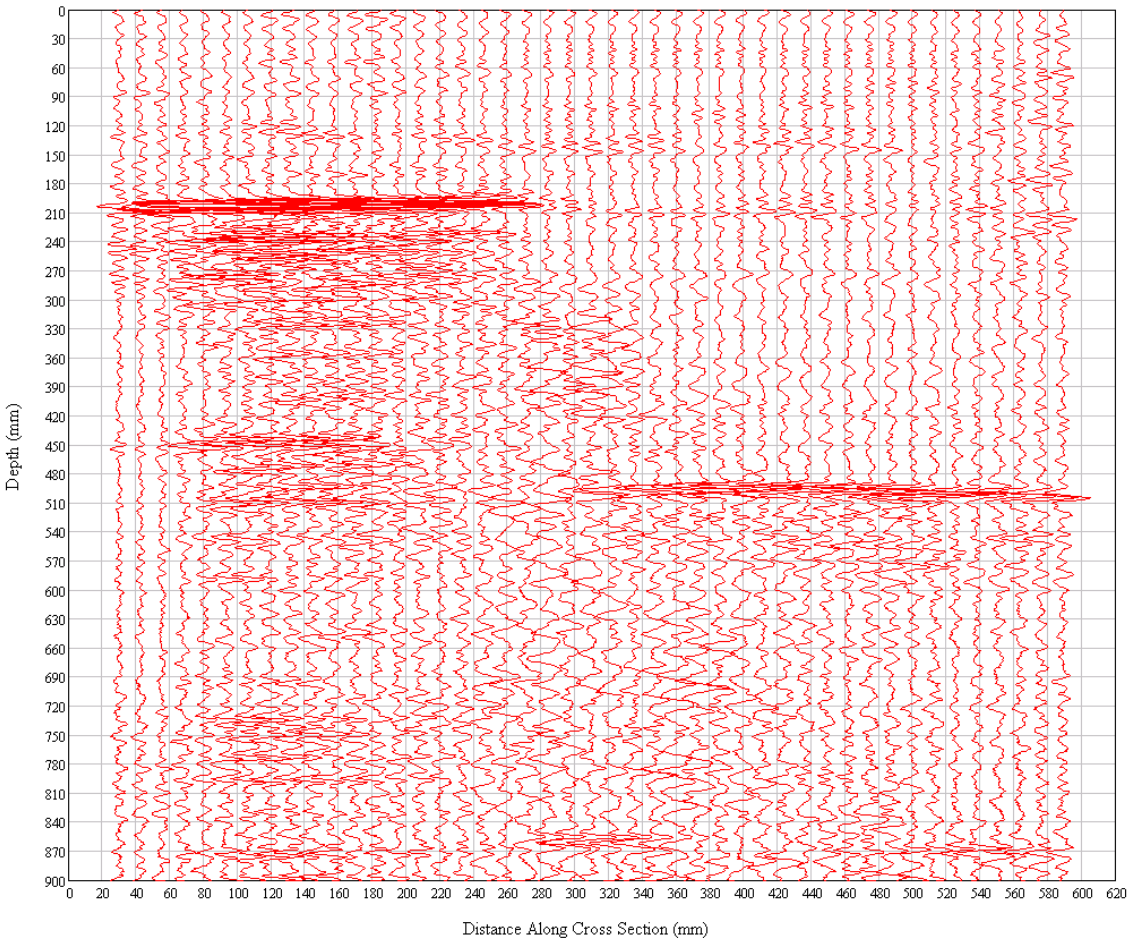

Figure 2-44: Results from cross section AA' with LDPE sheet near A'.

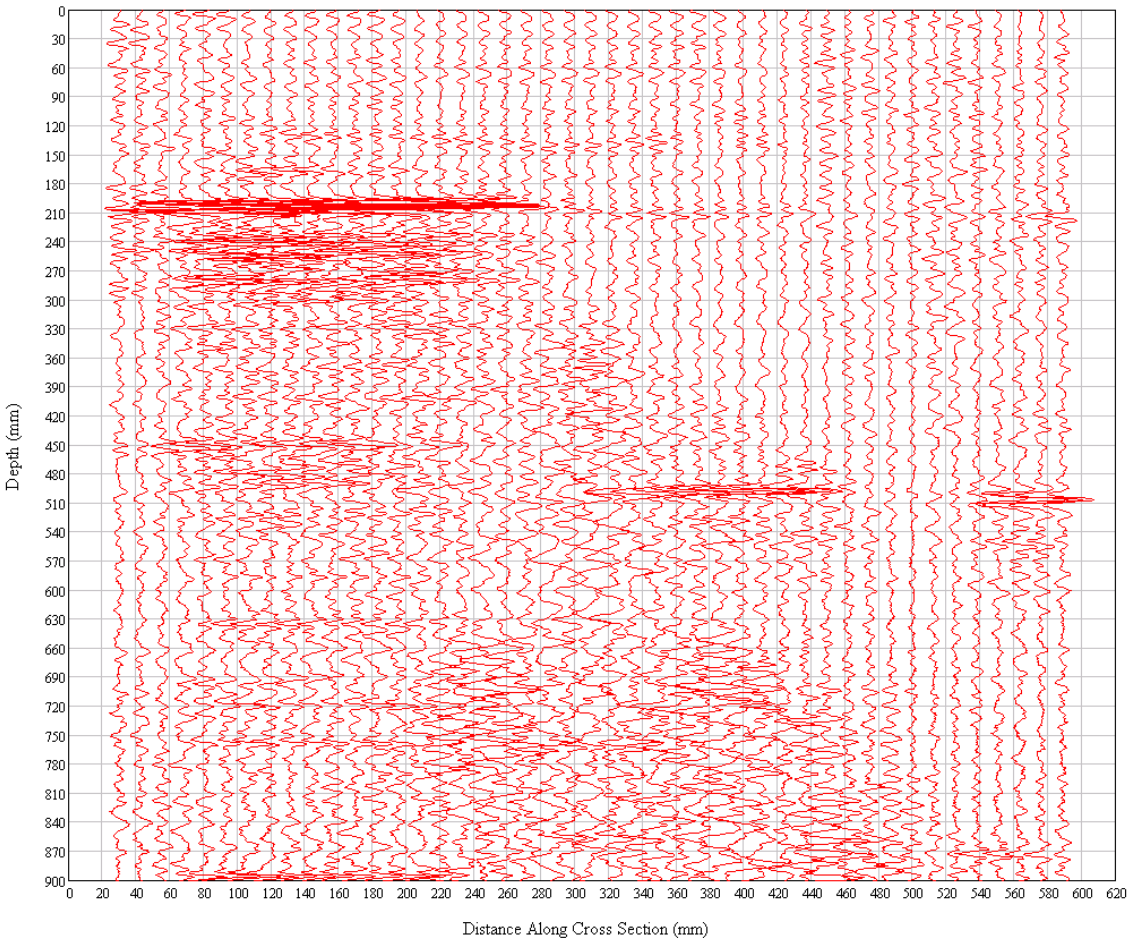

Figure 2-45: Results from cross section AA' with PVC sheet and 12.7 mm thick grout fragment near A'.

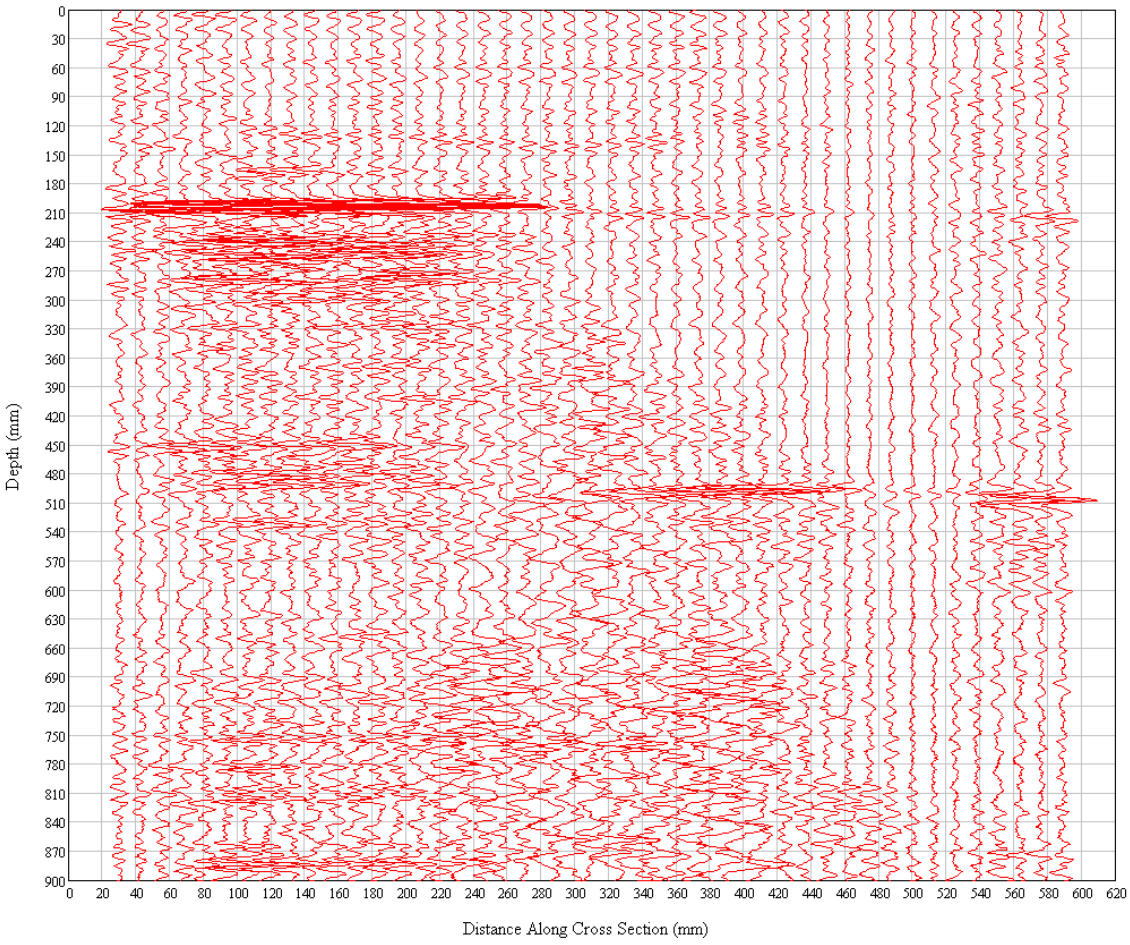

Figure 2-46: Results from cross section AA' with polypropylene sheet and 12.7 mm thick grout fragment near A'.

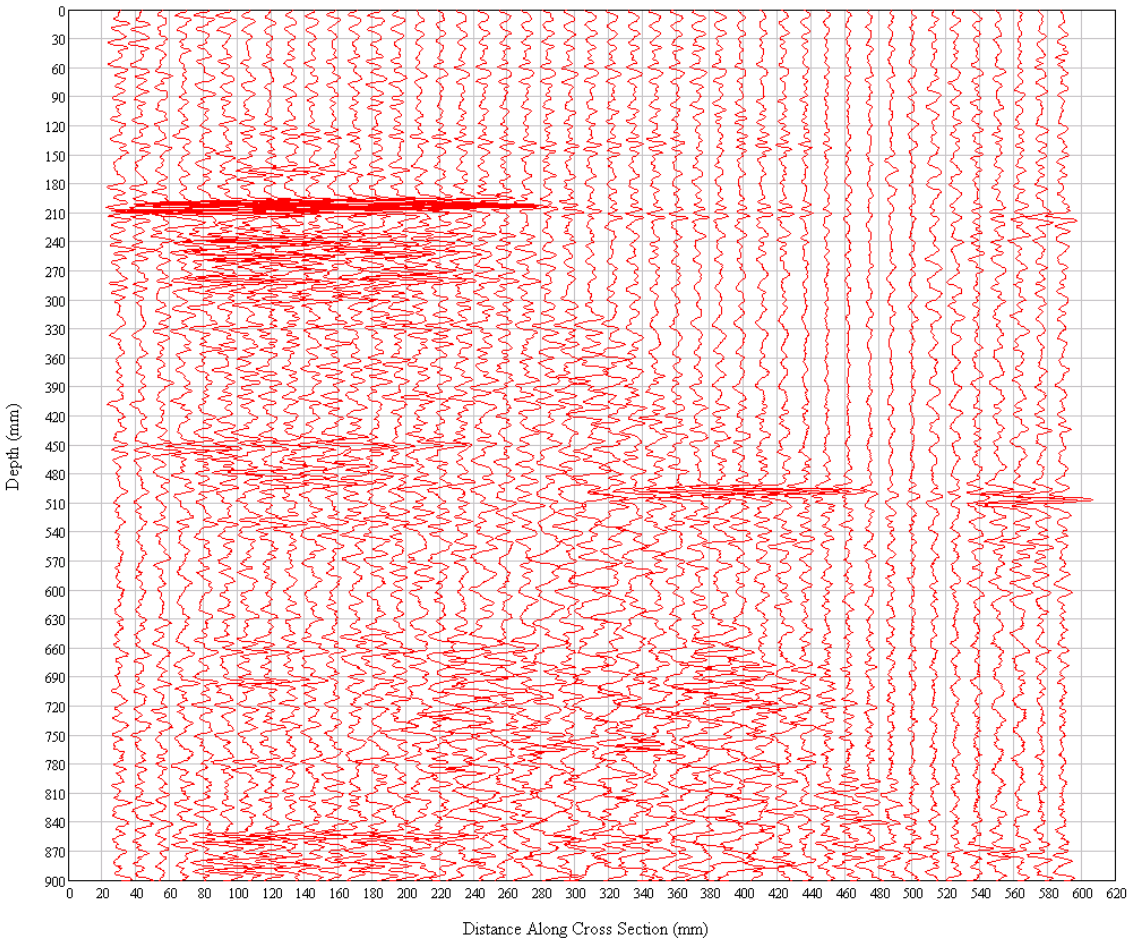

Figure 2-47: Results from cross section AA' with LDPE sheet and 12.7 mm thick grout fragment near A'.

	P-wave Velocity V_P [m/s]	Density ρ [kg/m^3]	Impedance = ρV_P [kg/m^{2}s] 10^6
Air (20°C, 1 atm)	343	1.204	0.0004
Deionized water	1480	998	1.5
Seawater	1531	1025	1.6
Sand (dry)*	150	1700	0.26
Clay (saturated)*	1500	1200	1.8
Ice	3500	917	3.2
Wood	4100	800	3.3
Plexiglass	2700	1200	3.2
Piezoceramic (PZT)	4000	7500	30
Aluminum	6400	2700	17.3
Lead	1900	11400	22
Copper	5000	8930	45
Steel	5900	7900	47
Nickel	5500	8850	49

*** Note: Wave Velocity and Density of soils correspond to ~100 kPa confinement**

Table 2-1: Nominal P-wave velocity, density, and acoustic impedance of several materials (adapted from Lee and Santamarina 2005).

3. SELECTION OF PENNDOT BRIDGE FOUNDATION SITES FOR FIELD TESTING

In addition to the laboratory testing to verify performance of the ultrasonic P-wave system, there was a significant field testing component that evaluated the usefulness of the ultrasonic system to evaluate unknown bridge foundations. During this field testing, the ultrasound probe used in laboratory testing was used to collect reflection signals from foundation elements at two Pennsylvania Department of Transportation (PennDOT) bridge locations. Data was also collected using various methods that span the range from state-of-practice to state-of-the-art (e.g. Parallel Seismic, Borehole Radar, Borehole Magnetometer, Ground Penetrating Radar, and Electrical Resistivity Imaging). Testing at both locations simulated unknown foundation conditions as the final foundation depths were not provided to the research team. As the ultrasonic P-wave system is still in an experimental stage and a suite of tests with very different equipment was planned, it was important to select an appropriate site or multiple sites. The following sections discuss the efforts by the research team, in collaboration with PennDOT, to locate suitable locations for field testing.

3.1 TIMELINE OF SITE SELECTION

On Tuesday, January 15, during the monthly conference call meeting for Month #2 of TEM 002, the PI of the this project, Dr. Joseph Coe, first discussed some preliminary matters related to site selection with Peter Berg (PennDOT District 6-0 Bridge Design Manager and Technical Advisor to TEM 002). The following items were discussed based on the meeting minutes:

- Foundation Type: A driven steel pile group (pipe or H-pile) with pile cap would likely be the most general condition for verification of field system performance of the NDT methods.
- Soil Profile: Should be well characterized by boreholes, at least at initial test for verification of field system performance. More homogeneous conditions would be desirable. Fine or silty sands would be the soil types that would likely allow best performance for p-wave and radar-based methods. Softer soils such as clays would be easier to drill and offer more contrast between soil and foundation.
- Water Table: No standing water at site due to issues with permitting and equipment. However, water table close to surface with a submerged foundation would be ideal. Minimal salt/brackish water.

- Access: Relatively flat site with generous clearance for typical truck-mounted drilling rig. Ideally, the site would allow access without encroaching right-of-way, disrupting traffic, or coordinating access during construction operations.

During the monthly conference call meeting for Month #3, the dialogue continued regarding site selection between Dr. Coe and Peter Berg. On this occasion, Sarah McInnes (PennDOT District 6-0 Geotechnical Engineer and co-Technical Advisor on TEM 002) participated to provide some feedback regarding typical soil conditions across District 6-0 bridges. Dr. Coe noted that probably the most important aspect related to selection of the bridge site would be site access (i.e. drill rig access, space for equipment, etc.). A pile group foundation on a pile cap would be the most general condition and would be preferable since the pile cap can mimic a shallow footing for the purposes of extrapolating the research findings to shallow foundations. Steel piles would likely allow greater signal strength for both electromagnetic and stress wave methods. The ideal scenario would be that the research team would have direct access to a bridge pier which is connected to a pile cap with an underlying steel pile group. Peter Berg expressed concern over the large database of potential bridge sites across the district and it was agreed that Dr. Coe would develop some preliminary site criteria to reduce the database to a more manageable size. He also noted that it would be very difficult to find a site that addressed every single concern in an adequate manner and that the criteria should list items in order of prioritization. A meeting was schedule at the District 6 office for Friday, March 8th to discuss selection of bridge test sites based on the preliminary criteria established by Dr. Coe.

Prior to the bridge site selection meeting on Friday, March 8th, Dr. Coe provided the preliminary site criteria via email to Peter Berg and Sarah McInnes. The following guidelines were noted in roughly the order of importance:

- Reinforced concrete pile cap with pile group foundation beneath single bridge pier/bent
- Steel Piles (H or Pipe)
- 1 ft + Pile Diameter
- Pile Cap close to surface (i.e. < 10 feet, ideally within 5 ft)
- Piles embedded less than 50 ft beneath surface
- Vertical clearance for drill rig (approximately 30ft + from ground surface to bridge deck)

- Horizontal clearance for field equipment (approximately 100 ft on either side of foundation to be tested) (e.g. Fig 1-28)
- Predominantly sand profile (i.e. as little clays as possible)
- Fine sands are preferable to coarser sands and gravels
- Water table close to surface (i.e. < 10 feet, ideally within 5 ft)

Based on these criteria and after discussions in the preliminary site selection meeting between Dr. Coe, Peter Berg, and Sarah McInnes, it was established that recent bridge construction project along the Delaware Expressway [Interstate 95 (I-95)] would likely meet several of the criteria for the field testing in this study. A meeting was planned for Wednesday, March 20, for Dr. Coe to review boring logs to ensure appropriate soil conditions for field testing.

During review of the boring logs, a number of sites were examined based on preliminary feedback from Sarah McInnes about the general soil conditions and these sites and the construction plans/timeframe. The review of boring logs centered primarily around three PennDOT District 6-0 I-95 improvement projects (Section GRI = Girard Avenue Interchange, Section BRI = Betsy Ross Bridge Interchange, and Section CPR = Cottman Avenue/Princeton Avenue). Dr. Coe continued reviewing boring logs after the meeting to narrow down specific foundation locations along these three I-95 construction project locations. Progress on this matter was discussed during the Month #3 conference call meeting. It was determined that GRI and BRI sites were most suitable based on the criteria discussed previously. In particular, both areas contained primarily sandy subsurface profiles (a little more gravels and clays in the BRI sections). The water table was closer to the surface at GRI. Both areas had foundation locations that were footings on steel-H piles of dimensions larger than 1 ft (305 mm) (among other foundation types). Depth to bedrock varied along the various cross sections at both sections, though generally GRI sections had shallower depths to bedrock. Both areas were not in tidal waterways and contained standing water, where the permitting process would be time-prohibitive. Finally, site access at multiple locations along GRI and BRI would allow relatively easy access to drill rigs, mobilization of field test equipment, and minimal travel distances. In general the CPR sections were rejected primarily based on these final factors. Site conditions and easements in those sections were pretty compact, which would likely impact the ability to adequately deploy some of the equipment without some form of maintenance and protection of traffic.

After a series of email conversations between Dr. Coe, Peter Berg, and Sarah McInnes in the two weeks after the Month #3 conference call meeting, Dr. Coe schedule a date and time to personally visit the final two potential field sites (GRI and BRI). Dr. Nyquist, the co-PI and geophysicist on this project, accompanied Dr. Coe to provide feedback regarding potential foundation locations based on his background with Electrical Resistivity Imaging (ERI) and Ground Penetrating Radar (GPR) investigations. Based on the site visits, three specific foundation locations were selected in the GRI and BRI sections of I-95. These locations will be discussed in more detail in the following sections.

3.2 SELECTED SITES

As described in section 3.1, final selection of potential field sites was narrowed down to GRI and BRI after careful review of boring logs. Based on reconnaissance at these sections, foundation locations were initially selected. The discussion in the following sections describes these locations. Chapter 5 describes the final location of the test foundations selected for this study after more detailed information was obtained regarding each of the selected sites.

3.2.1 BETSY ROSS INTERCHANGE (BRI) S.R. 0095-BR0 - RAMP B (S-10295)

The first selected site is located at section BR0 of the Betsy Ross Interchange improvement project. Two potential foundation locations were selected. The first foundation location is located on structure S-10295 at approximate station number 39. It consisted of a single reinforced-concrete (RC) bridge pier with an RC pile cap founded on steel H-piles. Figure 3-1 provides an overhead view of the site using Google Maps® with the locations of the two foundation locations highlighted. Figure 3-2 provides the location of the foundations on a section of the BRI master boring location plan. Finally, Fig. 3-3 is a picture taken at the site location during field reconnaissance. The primary reason why this foundation location was selected compared to other locations at BRI was the horizontal clearance necessary for electrical resistivity surveys. A general rule of thumb is that the horizontal layout of the resistivity probes must be approximately 3 – 5 times the desired depth of testing (Butler 2005). Many of the sites on the western side of I-95 at BRI had tremendous horizontal clearance. However, these locations were not on PennDOT property and required crossing rail lines. The permitting process for this would be time prohibitive, so the focus was on the eastern side of I-95 near the area

where the PennDOT maintenance office was located. Of the eastern side foundation locations, the selected location at S-10295 proved to have the most horizontal clearance. However, at the time of selection it was uncertain just how much the fencing along the outer perimeter of the site and any subsurface utilities in the area would affect the resistivity surveys. Unfortunately, this limitation of electrical resistivity is often difficult to overcome in high-traffic and densely populated areas. Moreover, the soil conditions at BRI were acceptable, though clays, organics, and gravels were more prevalent relative to GRI. It was understood that this may have implications for the radar and P-wave systems as the presence of clays and organics reduce radar signals and it was shown during the laboratory testing of this study that gravels scattered 100 kHz P-waves. Vertical clearance was generous at this location and construction was currently not underway which made scheduling the field testing easier.

The second selected site at BRI was actually located on the same structure (S-10295). More specifically, it was located at approximate bridge Station number 36 on Ramp B and it consisted of an RC column connected to an integral steel pier cap (Figs. 3-1, 3-2, and 3-4). As it was on the same structure as the first foundation location at this site, it was also founded on a steel H-pile foundation. The main reason this site was not selected for initial testing was that the horizontal clearance was limited compared to the first location, particularly due to the nearby fence that surrounds the area. Otherwise, vertical clearance, soil profiles, and ground water locations were similar to the first location. This second site served as an alternate for unknown foundation testing in case unexpected difficulties were encountered at the GRI site location. Additionally, since this location was located on the same structure as the first location, it was unlikely that there were significant differences between the foundations. Thus it was preferable to test at another site despite the logical difficulties presented by such an undertaking and the relative ease that a single site provided for field testing.

3.2.2 GIRARD AVENUE INTERCHANGE (GRI) S.R. 0095-GR3 (S-27043)

The second selected site is located at the Girard Avenue Interchange along I-95 just south of the Girard Avenue and Aramingo Avenue ramps at structure S-27043 (Fig. 3-5). More specifically, the site is accessed near the corner of Berks Street and Delaware Avenue and consists of a viaduct structure with a sequence of RC multi-column bents with individual steel H-pile footings. Figure 3-6 illustrates the foundation location on a section of the GR3 overall boring location

plan. This foundation location was selected compared to other locations at GRI due to the larger overall horizontal clearance (particularly in the direction parallel to I-95). Many of the other sites along BRI had subpar horizontal clearance and were currently undergoing construction operations. However, this selected location is still close to a perimeter fence and at the time of selection it remained uncertain just how much this would affect resistivity surveys. Likewise, it was likely that utilities in the area would cause anomalies in the resistivity data. Again, this limitation of electrical resistivity is present in any high-traffic and densely populated areas and often cannot be discovered until testing is underway. At the time of site selection, it was noted that vertical clearance would likely be an issue and mobilization of a track-mounted drill rig would be necessary. However, despite these limitations, this site actually had more promising soil conditions than the BRI locations based on a review of the boring logs. In particular, ground water location seemed to be shallower, there appeared to be less presence of clays and organics, and gravels were also kept to a minimum. This location would serve as the primary choice for the second set of field tests to evaluate an unknown foundation. Therefore, detailed foundation structural plans with final pile depths would not be shared with the research team until testing was complete and predictions were made regarding foundation type and location. The alternate site at BRI would be an option if any unexpected difficulties were encountered at GRI.

3.3 CONCLUDING REMARKS

The test sites described above were selected because they represented promising field conditions. At the time of selection it was believed that despite the issues that may be present with the ERI method, all the other methods planned for field testing stood a strong chance of acquiring some relevant data. Site access constraints and clearance issues had been minimized, which would allow a more timely completion of field testing. Finally, the distances to the site were convenient to the Temple University campus and research team. This would prove very useful given the large amount of field testing planned since multiple excursions to the site was often necessary on an on-going basis. Selection of such suitable sites could not have been accomplished without the diligent assistance offered by Peter Berg and Sarah McInnes. Their support and patience during the site selection process is gratefully acknowledged.

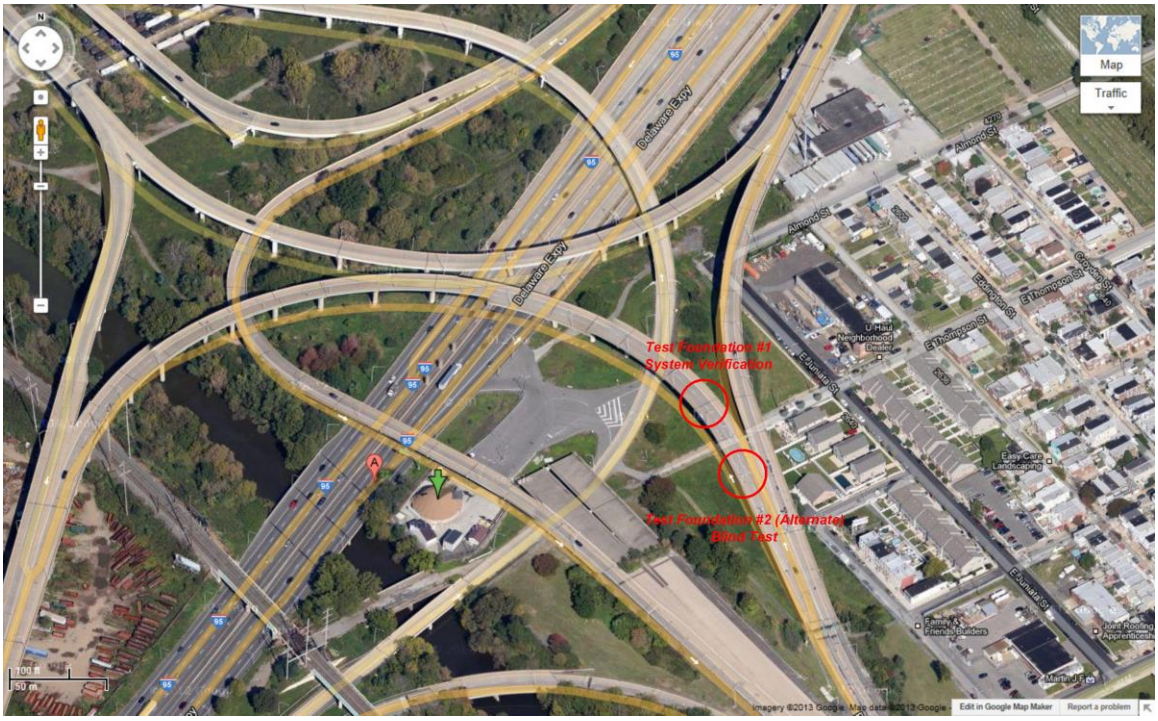

Figure 3-3: Overhead view of BR0 foundation locations (courtesy of Google Maps ®).

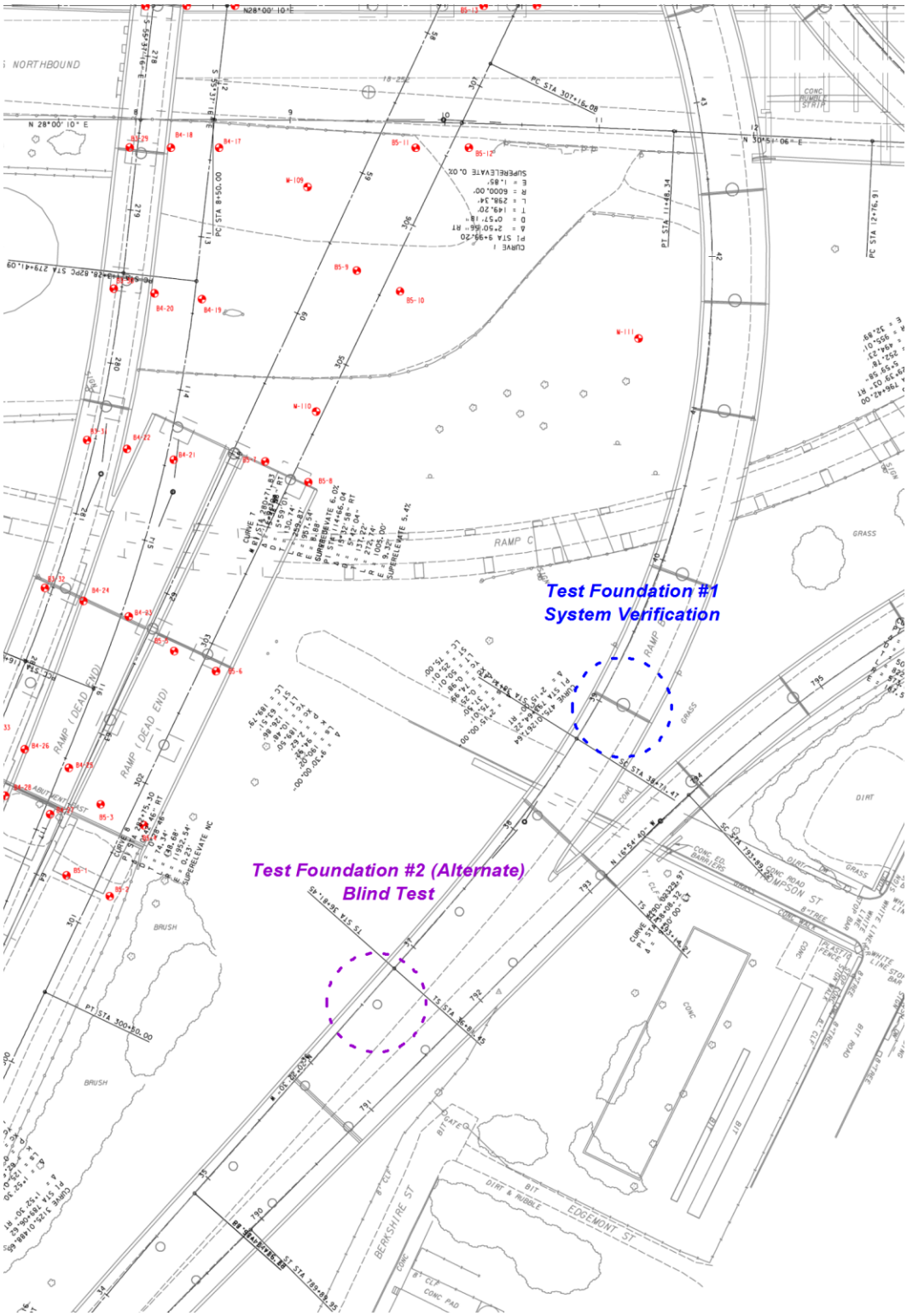

Figure 3-2: Location of BR0 foundation locations on section from master boring location plan.

Figure 3-3: Picture of first foundation location at BR0 taken during initial site reconnaissance.

Figure 3-4: Picture of second foundation location at BR0 taken during initial site reconnaissance.

Figure 3-5: Overhead and street view of GR3 foundation location (courtesy of Google Maps ®).

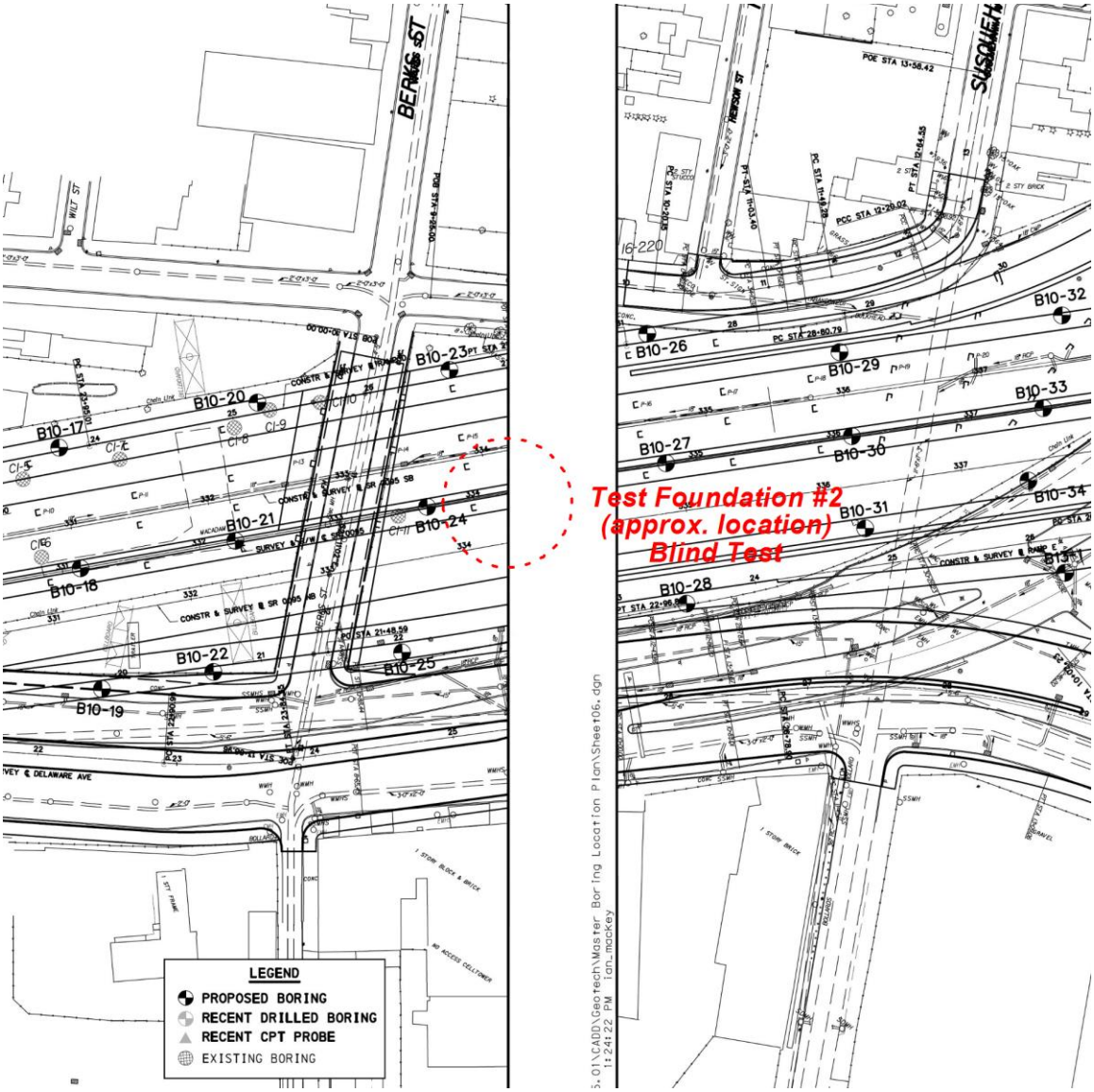

Figure 3-6: Location of GR3 foundation location on section from master boring location plan.

4. DEVELOPMENT OF FIELD TESTING PROCEDURES

During field testing as part of TEM 002, data was collected at two Pennsylvania Department of Transportation (PennDOT) bridge foundation locations using the P-wave ultrasound probe from laboratory testing and other Non-Destructive Testing (NDT) methods that span the range from state-of-practice to state-of-the-art. Testing at both bridge locations simulated unknown foundation conditions as the foundation lengths were not known with absolute certainty. Due to the considerable scope of proposed testing, it was necessary for the research team to develop a set of procedures to ensure efficiency in data collection and quality of test results. The following sections discuss the efforts by the research team to develop such procedures in anticipation of field testing.

4.1 SELECTION OF NDT FIELD METHODS

As noted in the Chapter 1 literature review, there are a number of different NDT techniques that have been developed to evaluate unknown foundations. Each method has advantages and disadvantages relative to site conditions, soil profiles, foundation geometry, and various other factors. The primary goal of this research is to verify the effectiveness of an ultrasonic P-wave system to evaluate the length of unknown foundations and to compare the results to other NDT methods. The following NDT methods were selected for field testing and comparison to the ultrasonic P-wave system:

- Parallel Seismic (PS)
- Borehole Radar (BHR)
- Borehole Magnetic (BM)
- Ground Penetrating Radar (GPR)
- Electrical Resistivity Imaging (ERI)

The rationale for selection of these methods is provided in the following sections.

4.1.1 PARALLEL SEISMIC (PS) METHOD

The PS method was selected because it is considered one of the most robust of the subsurface NDT methods (particularly when geophones are used) with a fairly long history and proven track record (Olson and Aouad 2001). As such, it allows a direct comparison between an approach that is still under development (i.e. P-wave ultrasonic) and one that is mature and well-developed (i.e. PS). Moreover, there are some issues that are addressed with a P-wave ultrasonic approach that are present in the PS method. For example, PS has issues if there are any discontinuities between the pile cap/grade beams and the underlying foundation elements (Hertlein and Walton 2007). Since the source and receiver are located inside the borehole, an ultrasonic P-wave system does not have these issues. Additionally, based on the results from laboratory testing and from previous studies (e.g. Coe and Brandenberg 2012, Coe and Brandenberg 2010, Lee and Santamarina 2005), the ultrasonic P-wave system can provide a high resolution image of the foundation element, which aids in interpreting foundation integrity. PS allows interpretation of the foundation bottom but does not provide an "image" of the foundation element.

4.1.2 Borehole Radar (BHR) Method

BHR was selected because it is the electromagnetic counterpart to the ultrasonic P-wave imaging system that was utilized in the field studies. The two methods have an identical test setup, except that BHR utilizes radar antennas to input electromagnetic waves and record reflections from materials with different dielectric constants. The ultrasonic P-wave system records reflection of ultrasonic (i.e. mechanical/stress) waves from materials with different stiffness. Thus, the utilization of BHR allowed an evaluation of the importance of wave type (i.e. electromagnetic versus mechanical/stress) in determining unknown foundation lengths at sites with relatively different soil profiles.

4.1.3 Borehole Magnetic (BM) Method

The BM method was selected due to the steel pile elements (cast-in-place concrete piles and H-piles) that are present at both foundation locations selected for field testing. As noted in the Chapter 1 literature review, BM has proven to be highly successful in the case studies where significant amounts of steel were present in the pile elements investigated (e.g. Jo et al. 1999, Jo et al. 2003, and Yu et al. 2007). Since the ultrasonic P-wave system is still under development and the foundation elements at both sites are embedded beneath a subsurface pile cap, there

was some uncertainty regarding the quality of data that could be obtained from the ultrasound probe and from a PS system. Thus, BM was selected because it would likely provide the estimate of foundation length with the highest level of confidence.

4.1.4 GROUND PENETRATING RADAR (GPR) METHOD

GPR was chosen primarily as a supporting method to obtain more detailed information of the foundation geometry. As a surface method, it was exceedingly unlikely that GPR would be capable of determining the length of the foundation elements because they were obscured by the pile cap. Thus, no direct comparison was made between GPR results and those from ultrasonic P-wave imaging. However, GPR was used to determine the horizontal extent of the pile cap for comparison with the foundation geometry available in plans provided by PennDOT. The purpose of this comparison was to evaluate the effectiveness of GPR as a tool to aid in selecting borehole locations in close proximity to the pile cap and underlying foundation elements for future studies.

4.1.5 ELECTRICAL RESISTIVITY IMAGING (ERI) METHOD

The ERI method provided an opportunity to compare the predictions from subsurface methods (i.e. ultrasonic P-wave, PS, BHR, BM) to one of the few surface methods that shows promise in evaluating complex foundations (i.e. footings on pile groups). As noted in recent case studies (i.e. Briaud et al. 2012 and Hossain et al. 2011), ERI has proven successful in imaging below pile caps. It was useful to compare the accuracy with which ERI was capable of determining the foundation lengths at both sites relative to the subsurface methods.

4.2 FIELD TESTING GUIDELINES

As previously noted, it was beneficial to develop a scheme to be followed for the field testing performed in this study. Such a plan allowed efficient collection of quality data in the limited timeframe allocated for field testing. The following sections describe the initial set of guidelines developed in anticipation of field testing. These guidelines are provided to fully document the manner in which this project proceeded, both during development of the field testing plan and after implementation. Several of these items were modified heavily as the field testing progressed due to changes in site condition, equipment and personnel availability, and on-going

analysis of field data. The final sequence and procedures followed for field testing are provided in Chapter 5.

For the NDT methods selected for this study, the following sequence was initially proposed:

1. Electrical Resistivity Imaging (ERI)
2. Borehole Magnetic (BM)
3. Parallel Seismic (PS)
4. Borehole Radar (BHR)
5. Ultrasonic P-wave System
6. Ground Penetrating Radar (GPR)

This sequence was developed to maximize the efficiency with which testing would proceed and to address equipment and drilling personnel availability. Whenever possible, surface methods were scheduled first to prevent any influence from the drilling operations on the acquired data. The exception to this was GPR which was scheduled after all subsurface methods due to issues with equipment availability. Subsurface methods were scheduled in approximate order of decreasing likelihood of superior data. The initial approach was to obtain data at both test sites with a given method before moving on to the next method in the sequence above. This would ensure consistent application of a given method since little time would elapse between subsequent field deployments with the same equipment and personnel. A discussion regarding initial plans for borehole construction and the development of testing guidelines for each method is provided in the following sections.

4.2.1 BOREHOLE CONSTRUCTION

At each foundation site, the initial plan was to construct a single borehole alongside the foundation to allow for evaluation of the foundation lengths using subsurface NDT methods. Several aspects affected the construction of the borehole at each of the two foundation sites. For example, the location of the borehole was selected to allow the subsurface methods to detect the presence of the closest pile element based on any provided foundation plans. Ideally, this pile element would be located on the outer row of piles. However, since one of the sites contained battered piles on the outermost piles, it was necessary to plan on targeting an inside

pile located one row from the outer edge of the pile cap. It was also imperative that the borehole be located as close as possible to whichever foundation element was tested so that high quality data was collected with sufficient signal-to-noise ratio. The strategy to accomplish this was to use hand measurements as collected from the foundation plans and to construct trial boreholes using hand augers. The initial plan was to utilize GPR to locate the horizontal extent of the pile caps. However, due to equipment issues the GPR system was not available for testing until after the boreholes were drilled. The initial goal was for drilling to proceed until the borehole extended 3 m (10 ft) into bedrock at each site to ensure that all NDT measurements obtained data beneath the bottom of the foundation elements. The borehole would be cased with 5 in Schedule 40 PVC piping, filled with water, and any gaps between the casing and borehole wall backfilled with sand. This would ensure adequate coupling between the NDT sensors and the surrounding geo-materials as well as between the borehole walls and the casing.

4.2.2 ELECTRICAL RESISTIVITY IMAGING (ERI) METHOD

ERI was to be performed prior to any of the subsurface methods so that the borehole did not affect any of the results. An Advanced Geosciences Incorporated (AGI) SuperSting R8 multi-electrode imaging system would be used to collect the resistivity data (Fig. 4-1). This system is connected to 28 resistivity electrodes which would be hammered into the ground to an approximate depth of 15 cm (6 in). Water would be poured in the regions immediately surrounding the electrodes to ensure adequate coupling between the electrode and ground surface. The electrodes were to be arranged as a linear array perpendicular to the underlying pile cap (Fig. 4-2). However, site constraints (e.g. fences, utilities, etc.) affected this arrangement since the linear array needed to extend in the horizontal direction about 3 - 5 times the desired vertical depth to be tested. Initial plans called for the direction of the linear array relative to the overlying bridge deck to range from parallel to perpendicular given site constraints (Fig. 4-2). Data was to be acquired using traditional four-electrode configurations illustrated in Fig. 4-3. For each four-electrode configuration type, the SuperSting R8 automatically cycles over the various electrode combinations inherent in a system with 28 electrodes. For a given linear array of electrodes, the three measurement configurations in Fig. 4-3 result in the generation of three depth profiles at each field site. These three depth profiles provide complementary information about the tested areas in the field sites.

4.2.3 Borehole Magnetic (BM) Method

The initial idea was to complete ERI testing and then initiate subsurface NDT methods with BHR method. A Schonstedt Borehole Gradiometer (MG230/235) (Fig. 4-4) was to be lowered into the borehole at a 0.3 m (1 ft) interval to measure the secondary magnetic field produced by the steel foundation elements in response to the Earth's magnetic field. Accurate depth intervals were to be ensured by pre-marking the magnetometer cable prior to lowering the borehole magnetometer. Due to the omnidirectional nature of the sensor, it was deemed unnecessary to exercise caution in keeping the magnetometer pointing in the same direction. Measurements were to be conducted as the magnetometer was lowered into and raised up from the borehole to duplicate results and ensure data repeatability.

4.2.4 Parallel Seismic (PS) Method

For PS testing an OYO Geospace MP-25 hydrophone string was to be utilized (Fig. 4-5). The MP-25-250 sidewinder hydrophone set cable contains twelve 10 Hz hydrophones at 1 m (3.3 ft) spacing. Thus, the original plan was to lower the hydrophones into the water-filled cased borehole at 12 meter intervals and therefore obtain data spaced at 1 m (3.3 ft) intervals. Elastic stress waves would be induced on the nearby foundation elements by impacting the bridge pier with a 12 pound sledgehammer. An impact plate would be used to spread the impact over a longer time interval to improve energy transfer and eliminate the potential for any damage to the pier. These stress waves would travel down the length of the foundation element and be detected by the nearby hydrophones. The initial plan was to strike the pile cap directly if the amount of energy transferred to the foundation elements was found to be very low and data quality was poor. Also, in such a case a hand auger could be used to expose a small section [e.g. approximately 50 mm (2 in) diameter] of the pile cap for direct impact with the sledgehammer. Initial plans called for the hydrophone string to be connected to a Geometrics ES-3000 twelve channel seismograph (Fig. 4-6) which would record the wave signals. The seismograph would begin recording hydrophone signals after receiving a trigger signal from a GISCO G-ST-01 piezoelectric hammer switch mounted on the sledgehammer (Fig. 4-7). The voltage output from this hammer switch can be used to sense when an impact force has been applied to the sledgehammer. This would ensure the signals from the hydrophones are synchronized and account for the increase in travel time between adjacent hydrophones. The hydrophones

respond to all around pressure changes and are not polarized with regards to direction. As such, it was deemed unnecessary to ensure that they were consistently pointing in the same lateral direction. As with the BM method, initial plans called for measurements to be conducted as the hydrophone string was lowered and raised within the borehole to duplicate results and ensure data repeatability.

4.2.5 BOREHOLE RADAR (BHR) METHOD

BHR was to proceed with a MALA Geoscience borehole radar system (Fig. 4-8). The system is based on a MALA ProEx control unit and can be configured to utilize 100 MHz and 200 MHz source/receiver radar antennas. Initial plans were for both sets of antennas to be utilized for this study using the reflection mode where the source and receiver antennas are located within the same borehole (similar to operation of the ultrasonic P-wave system described below). The source/receiver antenna pair would be connected to each other and lowered down the borehole using a MALA Tripod (Fig. 4-8) with digital depth encoder. The ProEx unit was to be configured to send a radar wave from the source antenna and record any reflections at the receiver antenna from the adjacent pile element using a 0.3 m (1 ft) interval based on the digital encoder signal. As borehole radar antennas are omnidirectional, it was not necessary to ensure the antennas faced the same direction as they were lowered within the borehole. As with the other subsurface methods, measurements were to be recorded on the way down and back up the borehole to ensure data repeatability.

4.2.6 ULTRASONIC P-WAVE METHOD

The ultrasound probe utilized in this field study (Fig. 4-9) would require a drilling rig to perform the testing (see Coe and Brandenberg 2012 for more detail on the probe dimensions). Due to the weight of the custom housing and the steel rods used to lower it into the borehole, it would be impossible to manually operate the system. This is one of the reasons this test was initially scheduled to be performed as the final subsurface test, since the drilling rig would already be onsite and could be used to seal the borehole after completion of this testing. The initial plan was to lower the source/receiver transducer pair and associated electronics into the borehole inside the custom housing and use a Unimeasure JX-series linear string potentiometer to measure the depth. The string potentiometer would therefore need to be affixed to the drilling rig so that the travel of the rod clamping mechanism could be recorded. The software was to be

programed to compute the distance based on the travel of the rod clamping mechanism and the number of rods that have been added to the system. Based on readings from the linear string potentiometer, an ultrasonic P-wave would be generated by the source transducer and any reflections from the nearby foundation element would be recorded at the receiver transducer at a 0.3 m (1 ft) interval. Care must be exercised to ensure the source/receiver transducer pair point in the same direction throughout the entire borehole depth. The plan to accomplish this was to mark the rods that were attached to lower the probe. As with the other subsurface methods, data acquisition would take place in the downward and upward direction within the borehole.

4.2.7 GROUND PENETRATING RADAR (GPR) METHOD

For GPR testing a MALA GPR ProEx system was proposed as the equipment (Fig. 4-11). Ideally, GPR testing would take place prior to construction of the boreholes for the subsurface NDT methods previously described. However, an issue with the electronics of the MALA GPR surface antennas meant that the GPR system was unavailable until after subsurface testing. Despite this shortcoming, it would still be possible to evaluate the effectiveness of GPR as a method to locate pile caps for drilling boreholes in collaboration with subsurface NDT methods. In terms of field testing guidelines, the initial plan called for a series of lines to be arranged in a grid pattern as illustrated in Fig. 4-12. The idea was to arrange these GPR survey lines at 0.3 m (1 ft) apart and for their locations to be determined via hand measurements relative to the bridge pier. The MALA GPR system would be rolled along these survey lines and a distance measuring wheel attached to the GPR cart would determine the horizontal location along a given survey line. Data acquisition was initially proposed to take place at a 0.3 m (1 ft) interval along a given survey line. Also, the lines would extend at least 1.5 m (5 ft) past the anticipated location of the pile cap so that the edges of the cap can be determined from the GPR data. After acquiring data using survey lines along one direction (e.g. blue lines in Fig. 4-12), the resulting two-dimensional (2D) data was to be analyzed to determine whether the 2D slices provided adequate prediction of the pile cap dimensions. Since pile caps are relatively flat, a true three-dimensional (3D) image would not appreciably improve predictions of the pile cap dimensions and the increase in time for additional survey lines would likely be unnecessary. The shielded GPR antennas for this system vary in frequency from 100, 250, 500, to 800 MHz. In the initial plan developed prior to field deployment, it was proposed to begin GPR testing with the lowest frequency antenna

available and repeat with each available antenna until data quality was poor and the pile cap dimensions could not be interpreted. Thus depending on the difference in soil profiles and depths of the pile caps, data would be acquired with different antennas at the two selected foundation sites.

4.3 CONCLUDING REMARKS

The preceding sections highlighted the major concerns relating to field testing with each of the NDT methods proposed for field testing in this project. Selection of each method was also discussed. The guidelines developed represent an attempt by the research team to anticipate and counteract any issues that may be present during field testing. However, due to the unpredictable nature of field testing, it was anticipated that many of these guidelines would require on-site modification to complete the field testing in a timely manner and to acquire high-quality data. Any modifications to the methods selected, testing procedures utilized, and amount of data acquired are discussed in more detail in Chapter 5.

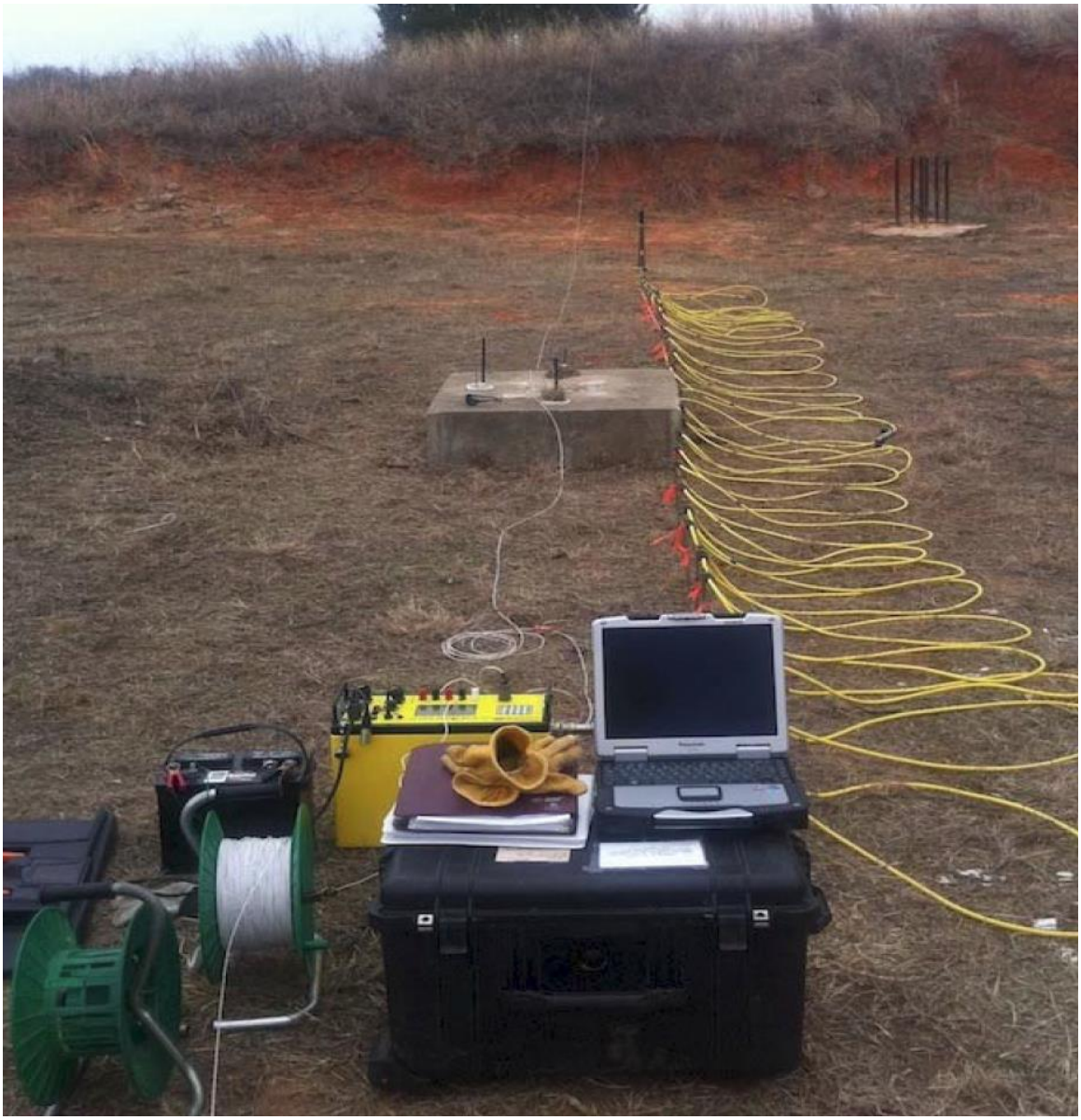

Figure 4-4: AGI SuperSting R8 system (from Briaud et al. 2012).

(a)

(b)

Figure 4-2: Placement of ERI linear electrode array (a) perpendicular, and (b) parallel to overlying bridge deck.

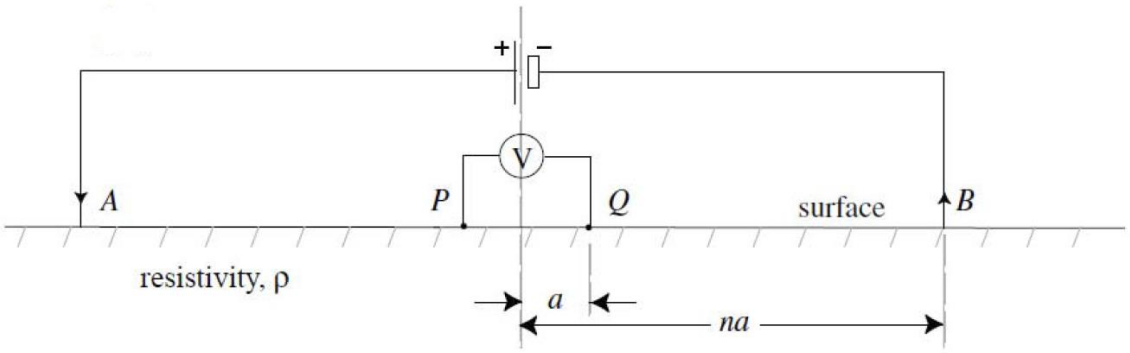

(a)

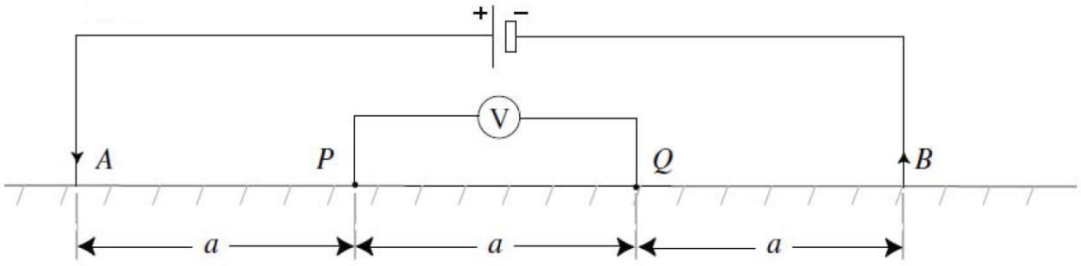

(b)

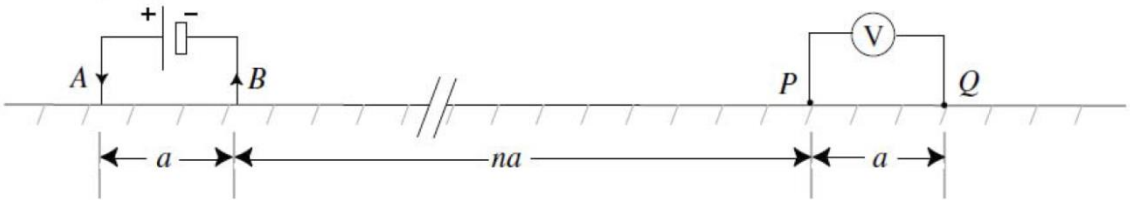

(c)

Figure 4-3: Traditional Four-Electrode Configurations: (a) Schlumberger; (b) Wenner; and (c) Dipole-Dipole (adapted from Briaud et al. 2012).

Figure 4-4: Schonstedt Borehole Gradiometer MG230/235 (Exploration Instruments, www.expins.com).

Figure 4-5: OYO Geospace MP-25 Hydrophone string (Exploration Instruments, www.expins.com).

Figure 4-6: Geometrics ES-3000 12-channel seismograph (Exploration Instruments, www.expins.com).

Figure 4-7: GISCO G-ST-01 piezoelectric hammer switch (www.giscogeo.com).

Figure 4-8: MALA Geoscience borehole radar system (www.malags.com).

Figure 4-9: Ultrasound probe utilized in field study (from Coe and Brandenberg 2012).

Figure 4-10: Unimeasure linear string potentiometer (JX series) used to trigger ultrasound probe (www.unimeasure.com).

Figure 4-11: MALA ProEx GPR system (www.malags.com).

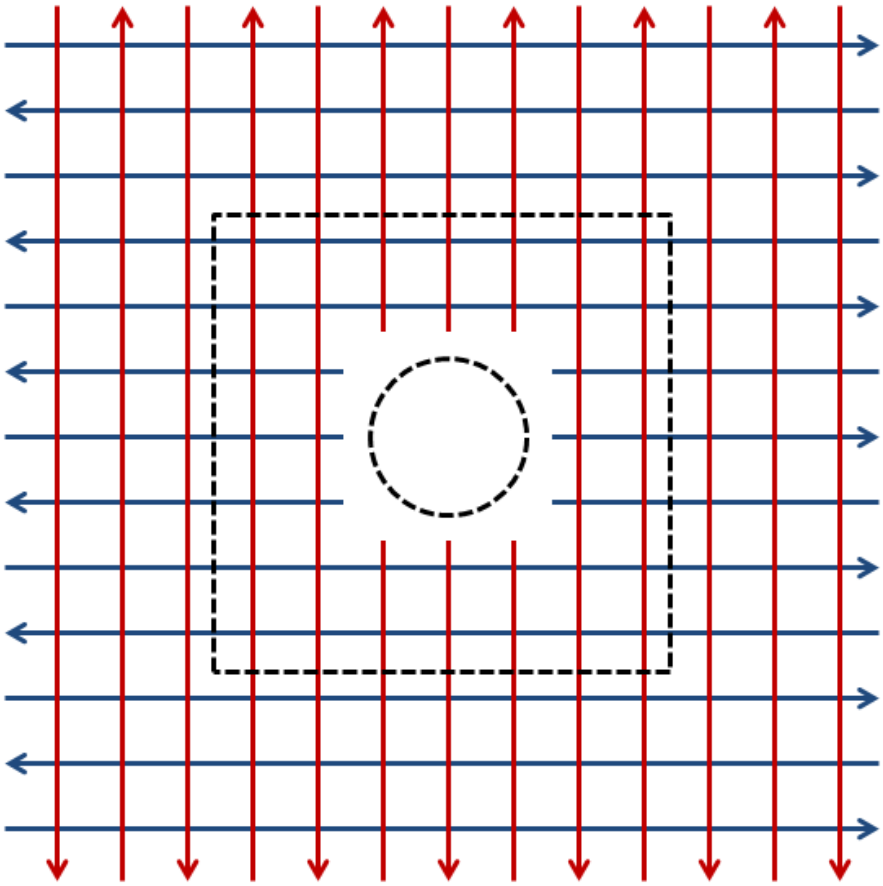

Figure 4-12: Typical GPR survey grid pattern (dashed black lines represent pile cap and bridge pier, colored arrows represent direction of GPR data acquisition).

5. FIELD TESTING

As part of TEM 002, field testing was performed at two Pennsylvania Department of Transportation (PennDOT) bridge foundation locations using a P-wave ultrasound probe and other Non-Destructive Testing (NDT) methods. At each site, a borehole was constructed alongside one of the bridge pier foundations for the subsurface NDT methods (e.g. Borehole Magnetic, Parallel Seismic, etc.) and locations were selected to perform surface NDT methods (e.g. Electrical Resistivity Imaging, Ground Penetrating Radar). The following sections discuss the efforts by the research team during drilling operations and deployment of the field testing NDT equipment. Discussion of the data collected and analysis performed are summarized in Chapter 6.

5.1 FIELD TESTING LOCATIONS

As discussed in Chapter 3, two locations were selected to perform the field testing in TEM002. In addition, a test site was chosen on the Temple University Ambler campus to verify NDT equipment system performance prior to and/or after deployment at the PennDOT bridge locations.

5.1.1 TEMPLE UNIVERSITY AMBLER CAMPUS TEST SITE (AMB)

The AMB test site is located on the Temple University Ambler campus near the intersection of East Butler Pike and Woods Driver (Fig. 5-1). It consists of a series of borehole test wells that were installed by the Temple University Earth and Environmental Science Department on the north-western end of the sports fields at the Ambler campus along Meetinghouse Road (Fig. 5-1). Presently, the wells are located in the area immediately adjacent to the soccer fields. They were installed in October of 1999 to perform research on sampling groundwater and mapping rock fractures. The wells have been subjected to significant geophysical logging over the last several years. The primary well that was used in this project is cased in 15.2 cm (6 in) diameter steel for approximately 15 m and thereafter remains uncased in bedrock until the bottom is reached (at approximately 27.5 m). It is located on the south-eastern end of the soccer fields (Fig. 5-1). This test well was used to verify equipment performance for Parallel Seismic, Borehole Magnetic, and Borehole Radar. The adjacent soccer field also served as an initial test location for Electrical Resistivity testing.

5.1.2 BETSY ROSS INTERSTATE 95 INTERCHANGE TEST SITE (BR0)

The BR0 test site is located along the Interstate 95 corridor in northeastern Philadelphia near the intersection of Juniata and Thompson Streets (Fig. 5-2). The substructure of interest is Pier 7 of Ramp B (S-10295) for State Road 90 (Betsy Ross Bridge), which carries traffic entering Pennsylvania from New Jersey and routes it to Interstate 95 in the southbound direction. The pier structure consists of a reinforced concrete circular column with integral steel pier cap (Fig. 5-3). The pier rests on a reinforced concrete pile cap which is supported on a group of 35 cast-in-place concrete piles at 1.06 m (3.5 ft) and 1.22 m (4 ft) spacings (Fig. 5-3). The outer row of piles is driven at a 2½ : 12 batter. The area in the immediate vicinity of the site is a major junction point for several off- and on-ramps as well as freight rail lines and utilities. Prior to development of the interchange, the area was largely residential and Thompson Street extended through the site as evidenced by the old curbs that are still present. Several utility lines run underneath this access road and are located within 10 m (33 ft) of Pier 7.

5.1.3 GIRARD AVENUE INTERSTATE 95 INTERCHANGE TEST SITE (GR3)

The BR0 test site is located along the Interstate 95 corridor in northeastern Philadelphia near the intersection of Delaware Avenue and Berks Street (Fig. 5-4). The substructure of interest is Pier 18 of the viaduct for Interstate 95 northbound near the Girard Avenue interchange. The substructure consists of a series of reinforced concrete multi-column bents (Fig. 5-5). Each bent rests on a reinforced concrete pile cap which is supported on a group of 9 steel H piles at 1.22 m (4 ft) and 1.37 m (4.5 ft) spacings (Fig. 5-5). The outer row of east-west facing piles is driven at a likely 2½ : 12 batter. The area in the immediate vicinity of the site has a long history as a residential area and archaeological investigations have been continuously performed the URS Corporation at the site for a long period of time as major construction project have been initiated at the Girard Avenue interchange.

5.2 BOREHOLE CONSTRUCTION

A single borehole was constructed alongside the selected bridge pier foundation at each of the PennDOT test sites. These boreholes were cased with PVC and remained open throughout the entire field testing operations. The following sections discuss the details related to borehole

construction at each of the sites, including final borehole locations, drilling procedures and techniques, and subsurface soil profiles.

5.2.1 BR0 TEST SITE

Drilling operations were initiated at the BR0 test site on Thursday, May 16, and completed on Friday, May 17. Figure 5-6 illustrates a typical subsurface soil profile near Pier 7 based on the original borings performed when the interchange was constructed in the 1970's. The borehole was drilled alongside the foundation using an Acker XLS track-mounted drill rig to advance a 150 mm (6 in) outer-diameter steel casing attached to a hollow coring bit (Fig. 5-7). Each flight of steel casing was 1.5 m (5 ft) in length. Drilling fluid was flushed inside the hollow center of the casing to flush away the running sands located at the site. At depths where difficult drilling conditions were encountered prior to bedrock, a 140 mm (5.5 in) roller-cone bit was lowered inside the casing to create a pilot hole (Fig. 5-8). Unfortunately, due to the size of the ultrasound probe, augers could not be utilized as they would result in either a hole that was too small for the necessary 140 mm (5.5 in) Schedule 40 PVC casing or a hole that required excessive backfill for the space between the pipe and borehole wall.

Drilling operations were to be terminated only after approximately 3 m (10 ft) of bedrock was cored at the borehole location. This would ensure the foundation bottoms would be visible in all proposed field tests. However, at BR0 drilling was terminated at approximately 12.2 m (40 ft) and coring of bedrock did not take place. The final depth was well short of the anticipated foundation bottom at 18.3 m – 21.3 m (60 ft – 70 ft) based on estimated depths to bedrock from previous borings at the site. Between the first and second day of drilling operations the subsurface sands caved and made advancing the casing extremely difficult. Due to the limited timeframe associated with drilling and field testing, it was decided to terminate borehole construction early and utilize BR0 as a test bed site for equipment debugging and data validation purposes. All testing would be performed at BR0 with the explicit understanding that the foundation bottoms would not be discernible. Schedule 40 PVC piping of 140 mm (5.5 in) outer diameter was lowered in the space between the steel casing and filled with water (Fig. 5-9). An expansion cap with metal bolt was used to ensure a water-tight seal (Fig. 5-9). After the PVC was in place, the steel casing was reattached to the drilling head on the rig and rotated up out of the borehole. The sandy drilling spoils in the immediate vicinity of the borehole were used to

backfill the gap between borehole wall and PVC pipe. The final location of the borehole was approximately 0.5 m (1.75 ft) away from the pile cap in between two of the battered outer piles (Fig. 5-10). The target pile was located approximately 2.0 m (6.5 ft) away from the final borehole location at BR0 (Fig. 5-10). The increase in target distance was necessary since it was very impractical to attempt to image the outer row of battered piles. Drilling costs and effort would be significantly increased with any attempts to drill the borehole at the same pile batter angle. Drilling a vertical borehole to image a battered pile would have the added difficulty of properly placing the borehole using tight tolerances to avoid damage to the pile from drilling. Additionally, the vertical borehole would mean any sensors lowered in the hole would naturally move closer to the pile, which can complicated data interpretation. Therefore to ensure a vertical target pile the row inward from the outer-most row of piles was utilized and target distance was increased.

5.2.2 GR3 TEST SITE

At the second site near the Girard Avenue Interchange (GR3), drilling operations were initiated on Monday, May 20, and completed on Tuesday, May 21. Figure 5-11 is a copy of the boring log near Pier 17 NB from recently completed site investigations for the Girard Interchange project. Drilling of the PVC-cased borehole proceeded in the same manner as previously described for BR0. Due to the difficult drilling conditions encountered, a 50 mm (2 in) split-spoon sampler was used to obtain a sample of the soils at an approximate depth of 7.6 m (25 ft). Based on the sample recovered, it is apparent that the site has areas with decomposed granitic rock material as well as artificial fill material (e.g. brick) (Fig. 5-12). At approximately 12.2 m (40 ft), an extremely hard layer believed to be the biotite schist bedrock was encountered and drilling operations switched to advancing a 140 mm (5.5 in) rock coring barrel inside the 150 mm (6 in) steel casing. After only approximately 1.5 m (5 ft) of coring, the barrel was retrieved as it was overheating and encountering increasingly higher resistance to drilling. It was discovered that the check valve which directs drilling fluid to lubricate the core barrel was no longer functional. The excessive heat caused the rock sample to fuse into the core barrel and it was impossible to disassemble the barrel to inspect the rock sample. Figure 5-13 shows the bedrock material inside the core barrel. Since the core barrel was no longer functional, drilling continued for another few feet (less than 1 m) using a 140 mm (5.5 in) roller-cone bit inside the steel casing. Borehole construction was terminated at a similar depth to BR0 [14.5 m (47.5 ft)]. The PVC

piping was lowered into the hole and filled with water. A screw cap with O-ring was used to ensure a water-tight seal (Fig. 5-14). Since the depth to bedrock was shallower at GR3 [12.2 m – 15.2 m (40 ft – 50 ft)] it was assumed that the cased borehole extended a reasonable depth below the anticipated foundation bottom. The final location of the borehole was approximately 0.6 m (2 ft) away from the pile cap in line with the outer pile on the pier column centerline (Fig. 5-15). The target pile was located approximately 0.9 m (3 ft) away from the final borehole location at GR3 (Fig. 5-15).

5.3 FIELD TESTING OPERATIONS

In order to increase the efficiency of data acquisition in the field, testing procedures were developed prior to deploying equipment in the field. These testing procedures were summarized in Chapter 4. After these guidelines were established, deployment with test equipment would typically occur at either the AMB or BR0 test site to ensure proper operation of all necessary equipment. These initial experiences at the first test site would occasionally lead to discovery of new essential procedures or replacement of procedures previously established. Moreover, to accommodate issues with equipment availability, personnel availability, and inclement weather, it was sometimes necessary to deviate from the original testing order and field procedures. For example, multiple methods were performed during concurrent time periods on the field testing calendar depending on research needs. Initial field testing was initiated as early as Wednesday, May 1, and testing was not complete with all methods until Friday, June 28. The following sections describe the manner in which testing was performed for a given method, including the general layout of sensors for data acquisition, issues with equipment, and any deviations from the originally proposed procedures.

5.3.1 BOREHOLE MAGNETIC (BM) METHOD

Initially, subsurface methods such as BM were scheduled to be performed after all surface methods (i.e. Electrical Resistivity Imaging, Ground Penetrating Radar) were completed. This was to ensure that any changes to the area around the borehole after drilling operations would not affect the results for surface testing. However, due to equipment and personnel availability, the surface methods were postponed and BM was performed first. BM testing was initiated on Thursday, May 23 and completed at BR0 and GR3 by Saturday, May 25. A test was also performed at AMB for data verification purposes on Monday, May 27.

Data acquisition was performed by lowering a SubSurface Instruments Borehole Gradiometer (BHG-1) (Fig. 5-16) into the borehole at a 1 ft (0.3 m) interval using a survey wheel and tripod (Fig. -17). The gradiometer measured the secondary magnetic field produced by the steel foundation elements in response to the Earth's magnetic field. The BHG-1 was utilized instead of the Schonstedt MG230/235 originally mentioned in Chapter 4. It was likely that the MG230/235 was already rented and the geophysical equipment rental company substituted an equivalent system from their rental pool. Initially, the cable included with the equipment was found to be faulty during a trial run at the AMB site. Flexing the cable while the gradiometer sat on the ground surface caused an excessive fluctuation in the instrument readings. This was remediated after the equipment rental company sent a new cable. The gradiometer cable was pre-marked at the appropriate interval to ensure accurate depth measurements. The magnetic flux density data was recorded by hand in milligauss (mG) after reading the output from the BHG-1 display. Readings were recorded as the sensor was lowered into and raised up from the borehole to duplicate results and ensure data repeatability. Testing was performed within the steel-cased borehole at the AMB test site to aid in interpreting the data acquired at the BR0 and GR3 test sites.

5.3.2 Electrical Resistivity Imaging (ERI) Method

ERI was initiated once the equipment became available and co-PI Dr. Nyquist was able to instruct the research team how to acquire data with the system. Since the process was very time-consuming, it was desirable to perform this testing early in the process in case any issues presented themselves that would affect the timeline of the project. Thus, ERI was performed during roughly the same time period as Borehole Magnetometer and Parallel Seismic. An initial ERI test for data verification and personnel training purposes was performed at AMB on Monday, May 13. At BR0 testing was completed on Saturday, May 25 and Tuesday, June 4. ERI field testing at GR3 took place on Wednesday, May 29 and Wednesday, June 5.

Resistivity data was acquired using an Advanced Geosciences Incorporated (AGI) SuperSting R8/IP 8 channel memory earth resistivity and induced polarization meter owned by the Temple University Department of Earth and Environmental Science (Fig. 5-18). A series of 28 electrodes were hammered into the ground surface at a constant interval to form a line for a single ERI

survey. The electrodes were hammered to a depth of approximately 15 cm (6 in). Two survey lines were set up at BR0 and GR3 to obtain subsurface information in two perpendicular directions (see Figs. 5-19 and 5-20). The first line was typically shorter in overall length and perpendicular to the direction of travel on the road directly overhead from the foundation (i.e. line was parallel to the pier cap). The second line was longer and was set up roughly parallel with the road overhead (i.e. line was perpendicular to the pier cap). Only a single line on the soccer field was set up at the AMB site. To ensure adequate electrical coupling between the electrodes and the ground surface, salt water was poured on the ground surface immediately surrounding the electrode (Fig. 5-21). The SuperSting was programed to acquire data along each survey line using three traditional four-electrode configurations (i.e. Schlumberger, Wenner, and Dipole-Dipole) (Fig. 5-22). Approximately 20 – 30 minutes was necessary for data acquisition for a given configuration (i.e. 1 hour to 1.5 hours total time for all data acquisition per survey line). For each method, the SuperSting R8 automatically cycled over the various electrode combinations inherent in a system with 28 electrodes. The result was the generation of three data files for each survey line at each site. The corresponding depth profiles provided complementary information about the field sites. For example, the Wenner configuration works well for resolving vertical changes in resistivity (i.e. horizontal structures, soil layers, etc.), while the Dipole-Dipole configuration is better suited for horizontal changes in resistivity (i.e. vertical structures, dykes, cavities, etc.) (Loke 2010). The data files were combined via processing software to enhance the quality of the results when necessary.

5.3.3 PARALLEL SEISMIC (PS) METHOD

Equipment to perform PS testing was rented from the same company that provided the BM system. Since both sets of equipment had a daily rental rate, it was desirable to perform testing in an efficient manner and return both sets as soon as testing was complete. Thus, PS was often performed concurrently with BM on the same day at a given site. An initial PS test to ensure equipment was functioning properly was performed at AMB on Wednesday, May 22. At BR0 testing was completed on Thursday, May 30. PS field testing took place at GR3 on multiple dates including Friday, May 24, Wednesday, May 29 and Thursday, May 30. The reason for the multiple test dates at GR3 was an attempt at improving the quality of the data collected since it was possible to directly strike the pile cap at GR3.

The PS equipment consisted of an OYO Geospace MP-25 hydrophone string with twelve 10 Hz hydrophones at 1 m spacing (Fig. 5-23). The hydrophone string was connected to a Geometrics ES-3000 twelve channel seismograph and a laptop computer which processed the seismic trace data and stored it to file (Fig. 5-23). Elastic stress waves were induced on the nearby foundation elements with a 12 pound sledgehammer connected to a GISCO G-ST-01 piezoelectric hammer switch. At BR0 the impacts were made to pier column while at GR3 it was possible to impact the pile cap directly over the target pile after hand augering (Fig. 5-24). During initial testing at AMB, the steel casing surrounding the borehole was impacted directly to send a tube wave down the length of the casing. This was also performed on the PVC casing at BR0 and GR3 as a means of verifying system behavior and ensuring appropriate data collection parameters (Fig. 5-25). A thick aluminum impact plate was used to spread the impact over a longer time interval to improve energy transfer and eliminate potential damage to the foundation. The hydrophone string was simply lowered in each PVC-cased borehole until the last hydrophone was just shy of resting on the casing bottom. This provided adequate data coverage throughout the length of borehole. In fact, at BR0 this often meant a few of the hydrophone were no longer submerged below the water level of the PVC casing. During initial testing at the AMB test site, the depth of the hydrophone string was often varied to study the effects of the steel casing on the recorded tube wave. Prior to testing, any visible gaps at the ground surface between the PVC and borehole wall was backfilled with sand and water (Fig. 5-26).

5.3.4 Ultrasonic P-wave Method

After the first group of test methods were complete (i.e. BM, ERI, and PS), the attention shifted to the ultrasonic P-wave method. Part of the reason for this was also due to the fact that the ultrasound probe would need to be mechanically lowered with equipment such as a drilling rig or winch system. As more rods are added to lower the probe down the borehole, the entire system will be excessively heavy for manipulation by hand. Since the research team did not initially have such equipment, the timeline was affected by the availability of a drilling crew to perform testing with the research team. Initial P-wave testing took place at the GR3 site since the target pile at that site was much closer to the borehole. P-wave testing at GR3 took place on Wednesday, June 12. However, it was determined that the data acquisition parameters employed on that attempt were not optimal and so testing was attempted again on Wednesday June 19. At BR0 P-wave testing was not completed until Wednesday, June 26.

The individual components of the P-wave system were previously summarized in Chapter 2. The source/receiver transducer pair and associated electronics were lowered into the borehole via the custom stainless steel housing. A truck-mounted motorized winch system was used to raise and lower the probe via a steel wire rope and pulley system affixed to an aluminum tripod (Fig. 5-27). A cable with water-resistant LEMO connector was threaded through all the rods to connect the electronics to the data acquisition system at the ground surface. A Unimeasure JX-series linear string potentiometer was initially used to measure the depth of the probe as it was lowered into the borehole by the winch. However, after reviewing the results from initial testing, it was determined that more signal stacking would be necessary and the probe would have to remain fixed at a given depth for a longer period of time. The increase in data acquisition time meant that data could no longer be recorded as the probe was brought up to the surface. The increase in time at each depth also meant that the string potentiometer was no longer necessary. All testing after the initial field day at GR3 was performed by marking the rods at a fixed 0.3 m (1 ft) interval. The rods were also marked with a vertical line to keep the operator oriented with where the transducers pointed. This line was used as a reference to keep the transducers facing the target pile. At GR3 the rods were purposely rotated away from this line to examine for any potential improvements in the data acquired. No improvements were readily apparent in the resulting data.

Great care was exercised to keep the electronics sealed from water. O-rings and a rubber gasket were used internally within the probe and all external seams were sealed with clear 100% Silicone RTV caulk (Fig. 5-28). An adhesive sealant was applied to the adaptor between the probe housing and the drill rods. The entire area was also covered in vacuum grease and wrapped with electrical and duct tape (Fig. 5-28). However, despite all the attention to water-proofing the system at the probe end, the rods used to lower the probe proved to be the weak point for water ingress despite a generous coating of grease on the threads. During initial testing the rods were submerged in water only for a period of a few hours since less signal stacking was performed. In this case no water leaked into the inside of the rods. However, during the remaining tests where the rods stayed submerged for a greater part of the day, water pooled near the connection (Fig. 5-29). However, it did not appear that water entered into the transducer housing since the electronics were still functional after testing.

5.3.5 GROUND PENETRATING RADAR (GPR) METHOD

In between test dates with the P-wave system, GPR was also performed. Ideally, this method would have been performed prior to any drilling at the site in order to locate the physical limits of the reinforced concrete pile cap. However, the GPR system was waiting on a necessary replacement part and was then utilized in another project by a faculty member within the Department of Earth and Environmental Science (who own the equipment). Once the equipment was available again, field testing for this project was commenced immediately. GPR testing was initiated at BR0 on Friday, June 21 and Monday, June 24, and was finally completed on Friday, June 28. The timeframe was similar at GR3 where testing started on Monday, June 24, and was completed on Friday, June 28.

The GPR equipment consisted of an MALA Geoscience ProEx System with shielded 250 MHz and 500 MHz antennas (Fig. 5-30). The higher frequency antenna provides high resolution information regarding the subsurface at the expense of signal penetration. Based on the anticipated depth to the pile cap at each site, the 250 MHz antenna was utilized at both sites and the 500 MHz was only attempted at GR3 where the pile cap was shallower [i.e. less than 0.5 m (1.6 ft)]. The antennas were in direct contact with the ground as they were pulled behind by the person acquiring data. A wheel with an attached rotary encoder was used to measure the distance travelled by the antenna. The test area included a square zone that was delineated using mason twine rope (Fig. 5-31). The overall dimensions of the square were approximately twice as large as the anticipated pile cap dimensions based on design plans provided by PennDOT. Within the test square a series of lines parallel with the pier cap (i.e. perpendicular to the direction of travel on the overhead road) were spaced at a 0.3 m (1 ft) interval within the test square (Fig. 5-32). The antennas were dragged consistently in the same direction from one end of a given survey line to the other. This resulted in a series of 2D slices of data with some slices actually completely outside the anticipated dimensions of the pile cap. The data acquisition interval was set at 3 cm (1.2 in) along a given survey line. This series of 2D slices was a compromise approach to acquire 3D information. A series of 2D slices can be arranged into a 3D reflectogram picture, though data will be interpolated in the areas between scans where no real data is present. A true 3D data set would also include a series of scan lines in the perpendicular direction. However, the increase in data acquisition time is justified when

attempting to visualize very steeply dipping reflectors. Since the pile cap is a fairly flat target, a series of 2D scans typically contain sufficient information to deduce the pile cap dimensions. In fact, the simplest approach to acquire information about the lateral extent of the pile cap is to just perform a single scan along two perpendicular directions, preferably crossing close to the pier column and center of the cap. This set of two perpendicular scans was also performed at both test sites. One final item to note, inclement weather during GPR work at GR3 forced testing to be performed under better cover at Pier 19 NB Column B instead of Pier 18 NB Column A. A large amount of water collects in the immediate vicinity of the Pier 18 NB and SB columns during storms, which is a problem for land-based GPR antennas. However, according to the design plans Piers 18 NB and 19 NB should have identical geometry.

5.3.6 BOREHOLE RADAR (BHR) METHOD

The final sequence of testing focused on BHR. Initial testing with BHR took place as early as Thursday, May 9 at the AMB test site. However, this initial test revealed that the MALA borehole antenna (100 MHz) borrowed by the research team were not functional. A new cable and another set of antennas (250 MHz) were provided by MALA Geoscience. Equipment verification tests were continued at the AMB test site in between other scheduled field dates (including May 9 and 27) with limited success. After each field visit, MALA was contacted to discuss potential causes for equipment issues and to ship back various pieces of equipment for inspection or replacement. Finally, after much correspondence, on Thursday, June 20, it was determined that both sets of antennas were the primary reason for unsuccessful operation of the system and would have to be shipped back to MALA's corporate offices in Sweden for repair or replacement. Based on this feedback, another supplier was located to rent a borehole antenna, which was rather difficult on short notice. New rental equipment was acquired on Tuesday, June 25 and was deployed to BR0 immediately for system performance verification. BHR was then completed on Wednesday, June 26 and Friday, June 28 at both BR0 and GR3.

The BHR equipment that was used to acquire data at BR0 and GR3 consisted of a Geophysical Survey Systems Incorporated (GSSI) 120 MHz borehole radar antenna and SIR-3000 controller unit (Fig. 5-33). The antenna was lowered using a survey wheel and tripod system at a constant 0.15 m (0.5 ft) interval and data was recorded by manual triggers via the SIR-3000 controller. Typically, data was acquired as the antenna was lowered into and raised out of the borehole to

ensure data repeatability. In many ways, BHR data acquisition was similar to BM in terms of peripheral equipment needs (e.g. surveying tripod) and ease of operation.

5.4 CONCLUDING REMARKS

Although the field testing procedures were well-planned and discussed in Chapter 4, it was necessary to modify procedures and timelines in response to variable conditions (e.g. equipment availability, etc.) and to items beyond control of the research team (e.g. faulty equipment, inclement weather, etc.). Despite the number of issues that presented themselves with drilling and with the equipment, all the testing proposed for TEM002 was completed and a large amount of high quality data was generated that will allow comparison of the effectiveness of each of the NDT methods. Analysis of this data and foundation predictions are provided in the subsequent chapters of this report.

(a)

(b)

(c)

Figure 5-5: Location of (a) AMB Test Site, (b) test well used in this project, and (c) photo of test well (courtesy of Google Maps®).

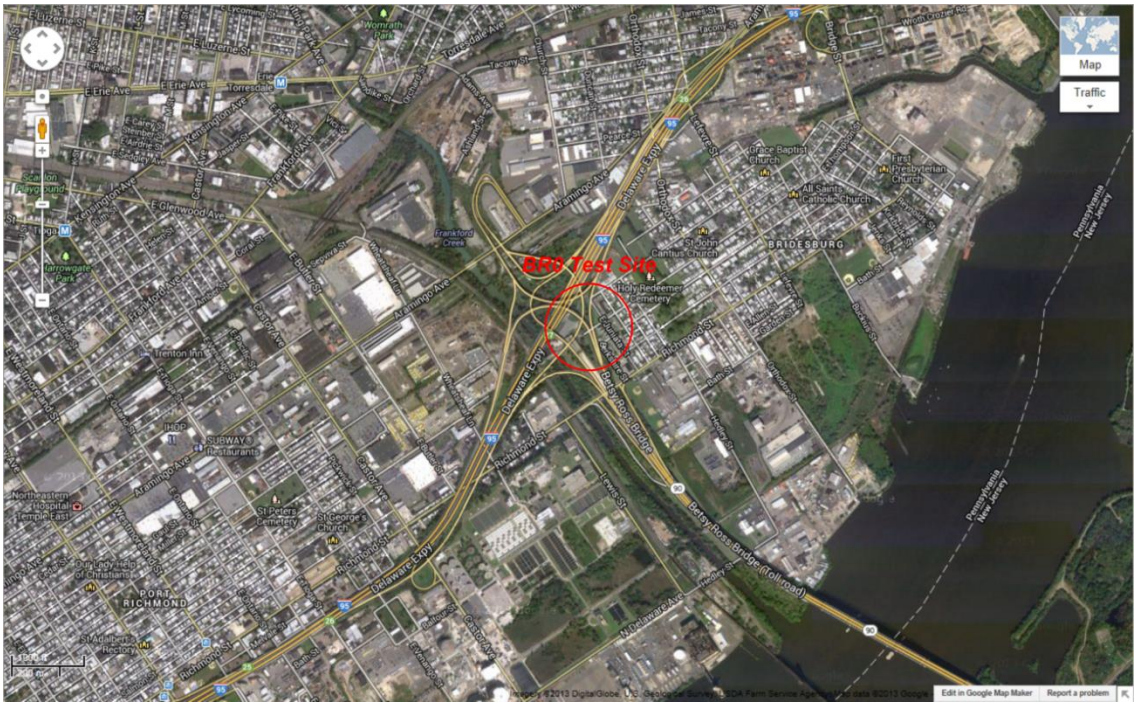

(a)

(b)

Figure 5-2: Location of (a) BR0 Test Site, and (b) Pier 7 used for field testing in this project (courtesy of Google Maps®).

(a)

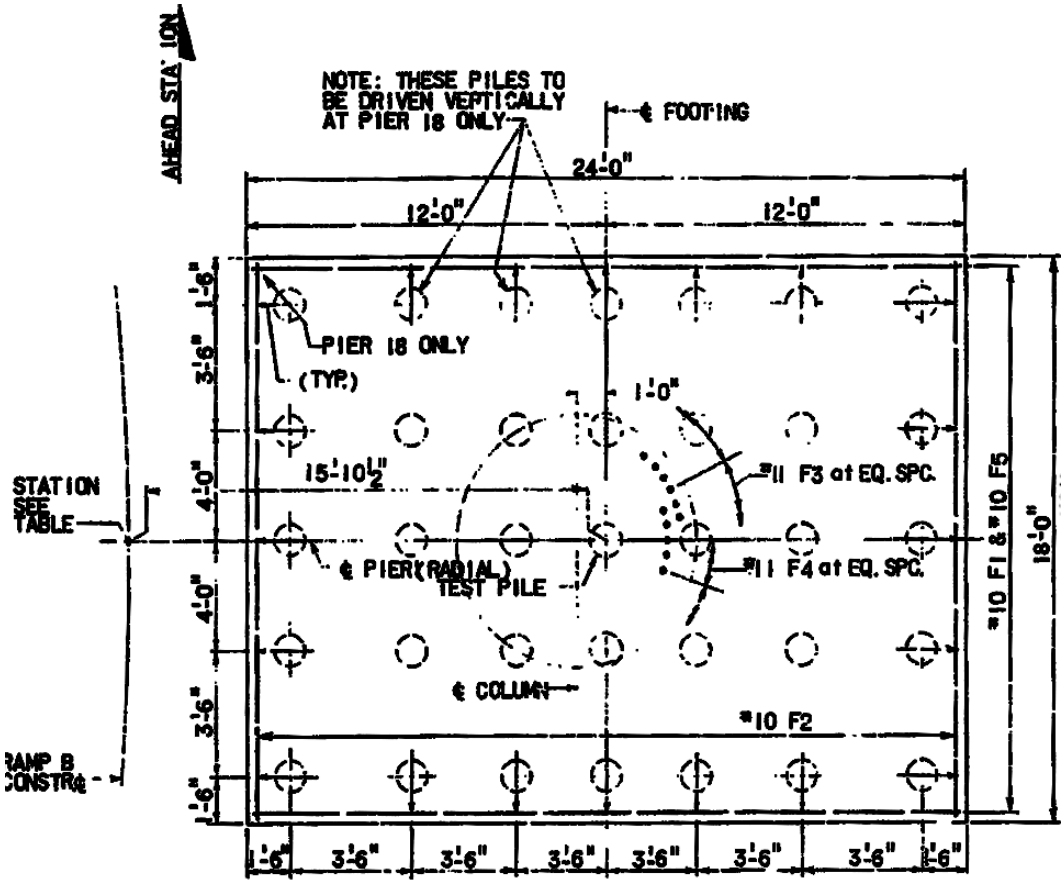

(b)

Figure 5-3: BR0 Test Site: (a) Photo of Ramp B Pier 7; and (b) Pier 7 Foundation Plans.

(a)

(b)

Figure 5-4: Location of (a) GR3 Test Site, and (b) Pier 18 NB used for field testing in this project (courtesy of Google Maps®).

(a)

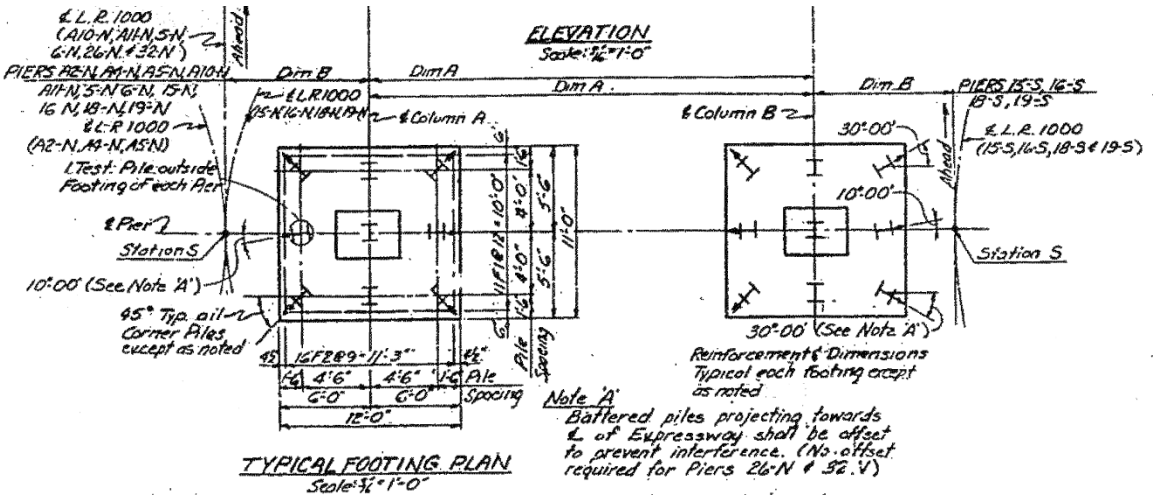

(b)

Figure 5-5: GR3 Test Site: (a) Photo of Pier 18 NB; and (b) Pier 18 NB Column A Foundation Plans.

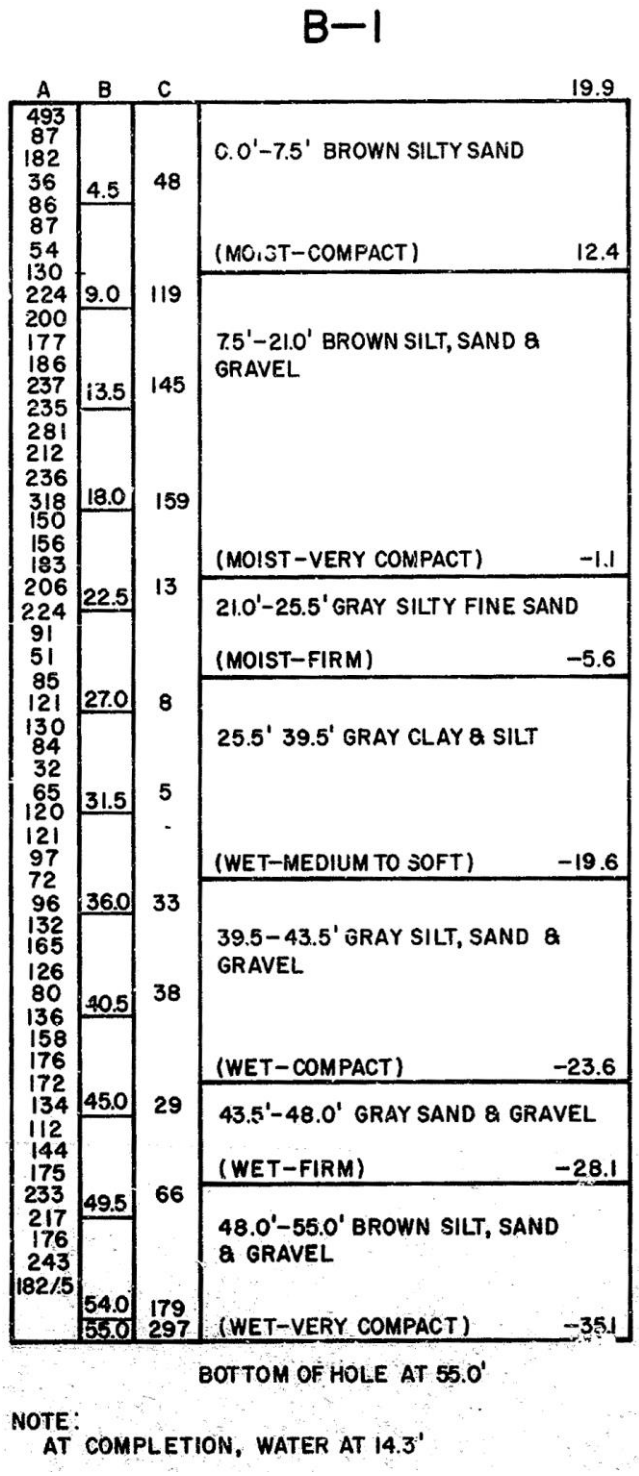

Figure 5-6: Subsurface profile at Ramp B Pier 7 location based on boring performed prior to construction of Betsy Ross Interchange in 1970. (Note: A = Blows/ft on 4 in Casing, B = Depth sampling spoon lower limit, and C = Blows/ft on spoon sampler).

(a)

(b)

Figure 5-7: Drilling operations at BR0: (a) Start of drilling, and (b) Typical running sands drilling spoils.

Figure 5-8: Roller-cone bit used for difficult drilling conditions.

Figure 5-9: Installation of PVC inside borehole at BR0.

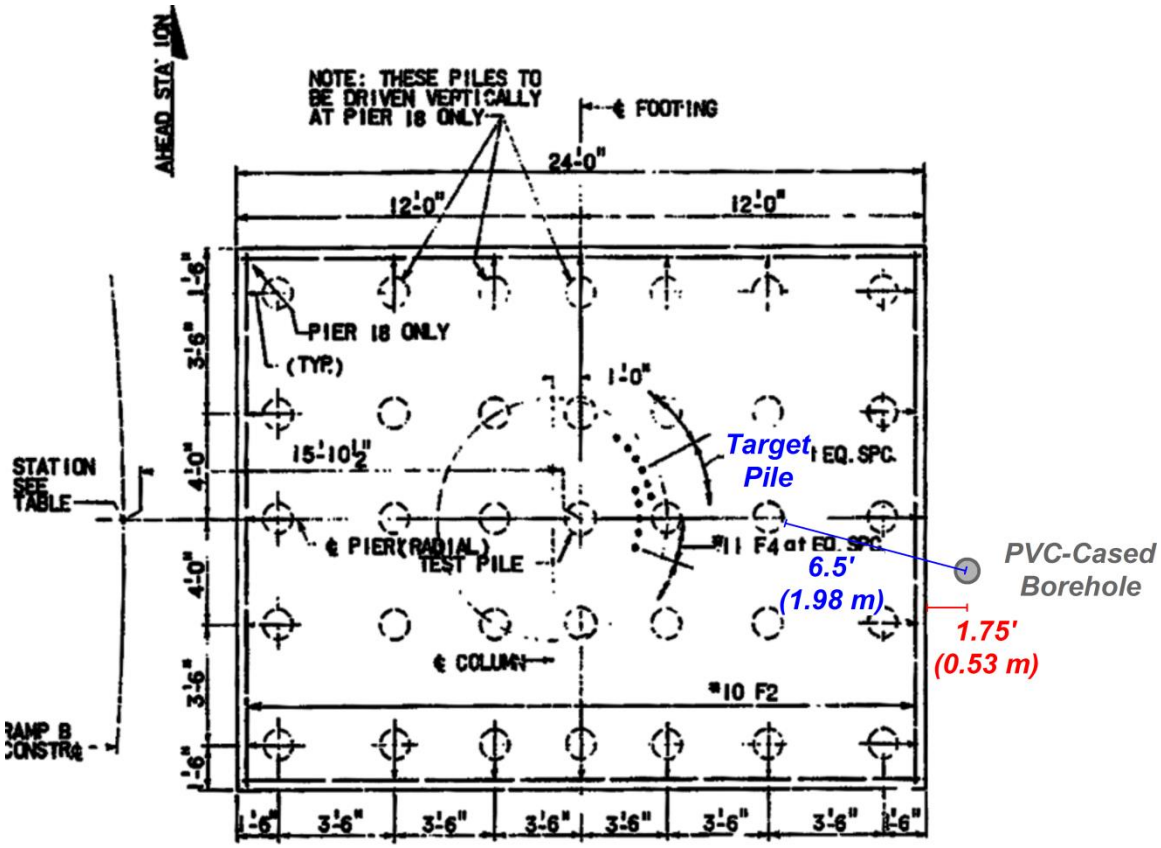

Figure 5-10: Approximate final location of cased borehole at BR0.

DEPTH (FT.)	SAMPLE NO./ TYPE/CORE RUN	BLOWS/0.5 FT. ON SAMPLER	RECOVERY (Ft.)	RECOVERY(%) / RQD (%)	POCKET PENT/ TORVANE (TSF)	USCS / AASHTO	H_2O CONTENT	DESCRIPTION	REMARKS
0.0		6				gm		0.0' to 1.5' Silty Gravel (gm), dark gray to black, dry, very dense, heterogeneous, (FILL)	
		13							
1.4	S-1	50/0.4	1.0	71	-	a-1-b	d	EL. 12.8	Gravel consists of rock fragments and brick
1.5		6				ml		1.5' to 5.2' Sandy Silt with mica (ml), dark brown, dry to moist, loose, homogeneous, (FILL)	
		4							
3.0	S-2	4	1.3	87	-		d		PID--OK
		3							
		3							
4.5	S-3	4	1.3	87	-		m		
		3				a-4		EL. 9.1	
		10				ml		5.2' to 11.3' Sandy Silt with coarse gravel (ml), dark brown to brown, dry to wet, loose to medium dense, mottled, (FILL)	
6.0	S-4	10	1.2	80	-		d		
		10							
		12							
7.5	S-5	12	1.1	73	-		m		PID--OK
		13							
		11							
9.0	S-6	12	1.0	67	-		w		
		3							
		4							
10.5	S-7	5	1.3	87	-		w		
		8				a-2-4		EL. 3.0	
		19				sm		11.3' to 13.5' Silty Medium Sand with mica (sm), dark brown to dark gray, wet, medium dense to dense, poorly graded, homogeneous, (ALLUVIUM)	
12.0	S-8	16	0.9	60	-		w		
		11							
		11							
13.5	S-9	9	1.1	73	-	a-2-4	w	EL. 0.8	
		3				ml		13.5' to 20.4' Micaceous Sandy Silt with coarse sand (ml), orangeish gray to dark gray, wet, loose to dense, laminated, (RESIDUUM)	Mud added
		5							PID--OK
15.0	S-10	5	1.0	67	-		w		
		4							
		6							
16.5	S-11	17	1.4	93	-		w		
		14							
		14							
18.0	S-12	13	1.0	67	-		w		
		4							
		6							
19.5	S-13	7	1.1	73	-		w		PID--OK
						a-4			

NOTE: DRAW STRATIFICATION LINES AT THE APPROXIMATE BOUNDARY BETWEEN SOIL TYPES FOR THIS BORING LOCATION AND SHOW DEPTHS

Figure 5-11: Previous boring log from Pier 18 NB at GR3.

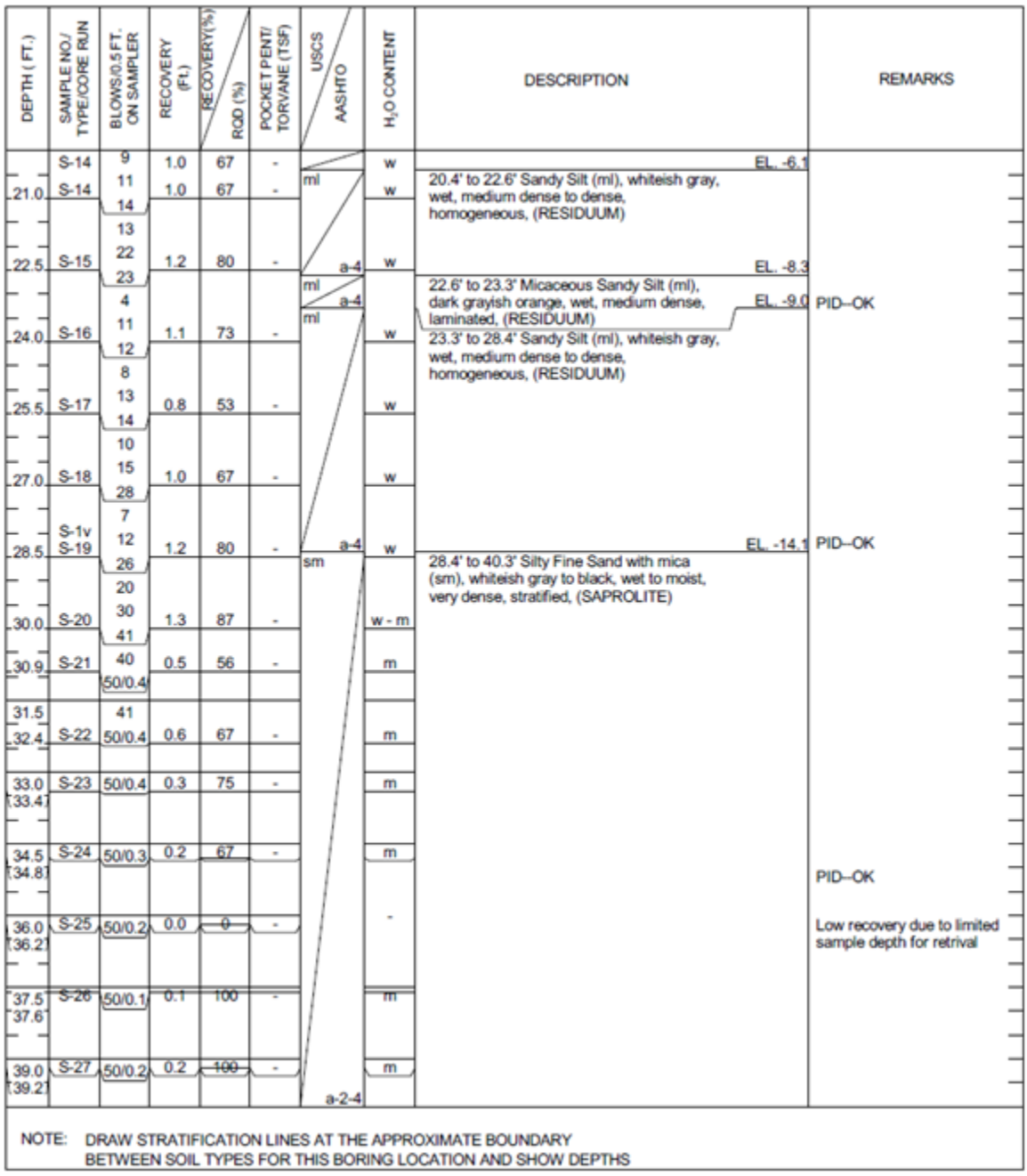

DEPTH (FT.)	SAMPLE NO./ TYPE/CORE RUN	BLOWS/0.5 FT. ON SAMPLER	RECOVERY (Ft.)	RECOVERY(%) / RQD (%)	POCKET PENT/ TORVANE (TSF)	USCS / AASHTO	H_2O CONTENT	DESCRIPTION	REMARKS
	S-14	9	1.0	67	-		w	EL. -6.1	
		11				ml		20.4' to 22.6' Sandy Silt (ml), whiteish gray, wet, medium dense to dense, homogeneous, (RESIDUUM)	
21.0	S-14	14	1.0	67	-		w		
		13							
		22							
22.5	S-15	23	1.2	80	-	a-4	w	EL. -8.3	
		4				ml / a-4		22.6' to 23.3' Micaceous Sandy Silt (ml), dark grayish orange, wet, medium dense, laminated, (RESIDUUM)	PID--OK
		11				ml		EL. -9.0	
24.0	S-16	12	1.1	73	-		w	23.3' to 28.4' Sandy Silt (ml), whiteish gray, wet, medium dense to dense, homogeneous, (RESIDUUM)	
		8							
		13							
25.5	S-17	14	0.8	53	-		w		
		10							
		15							
27.0	S-18	28	1.0	67	-		w		
		7							
	S-1v	12							
28.5	S-19	26	1.2	80	-	a-4	w	EL. -14.1	PID--OK
		20				sm		28.4' to 40.3' Silty Fine Sand with mica (sm), whiteish gray to black, wet to moist, very dense, stratified, (SAPROLITE)	
		30							
30.0	S-20	41	1.3	87	-		w - m		
		40							
30.9	S-21	50/0.4	0.5	56	-		m		
31.5		41							
32.4	S-22	50/0.4	0.6	67	-		m		
33.0	S-23	50/0.4	0.3	75	-		m		
33.4									
34.5	S-24	50/0.3	0.2	67	-		m		
34.8									PID--OK
36.0	S-25	50/0.2	0.0	0	-		-		Low recovery due to limited sample depth for retrival
36.2									
37.5	S-26	50/0.1	0.1	100	-		m		
37.6									
39.0	S-27	50/0.2	0.2	100	-		m		
39.2						a-2-4			

NOTE: DRAW STRATIFICATION LINES AT THE APPROXIMATE BOUNDARY BETWEEN SOIL TYPES FOR THIS BORING LOCATION AND SHOW DEPTHS

Figure 5-11 (cont.): Previous boring log from Pier 18 NB at GR3.

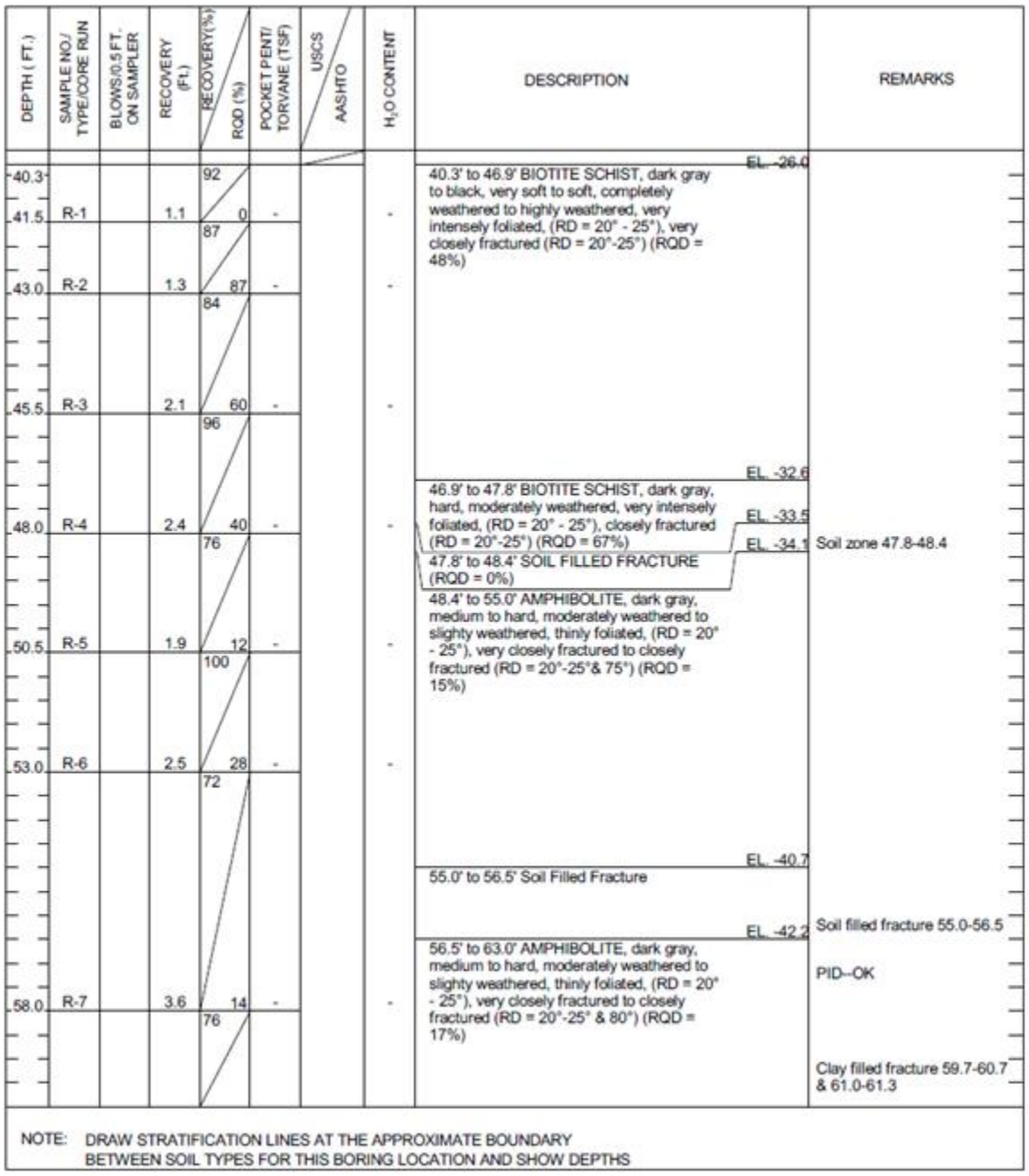

Figure 5-11 (cont.): Previous boring log from Pier 18 NB at GR3.

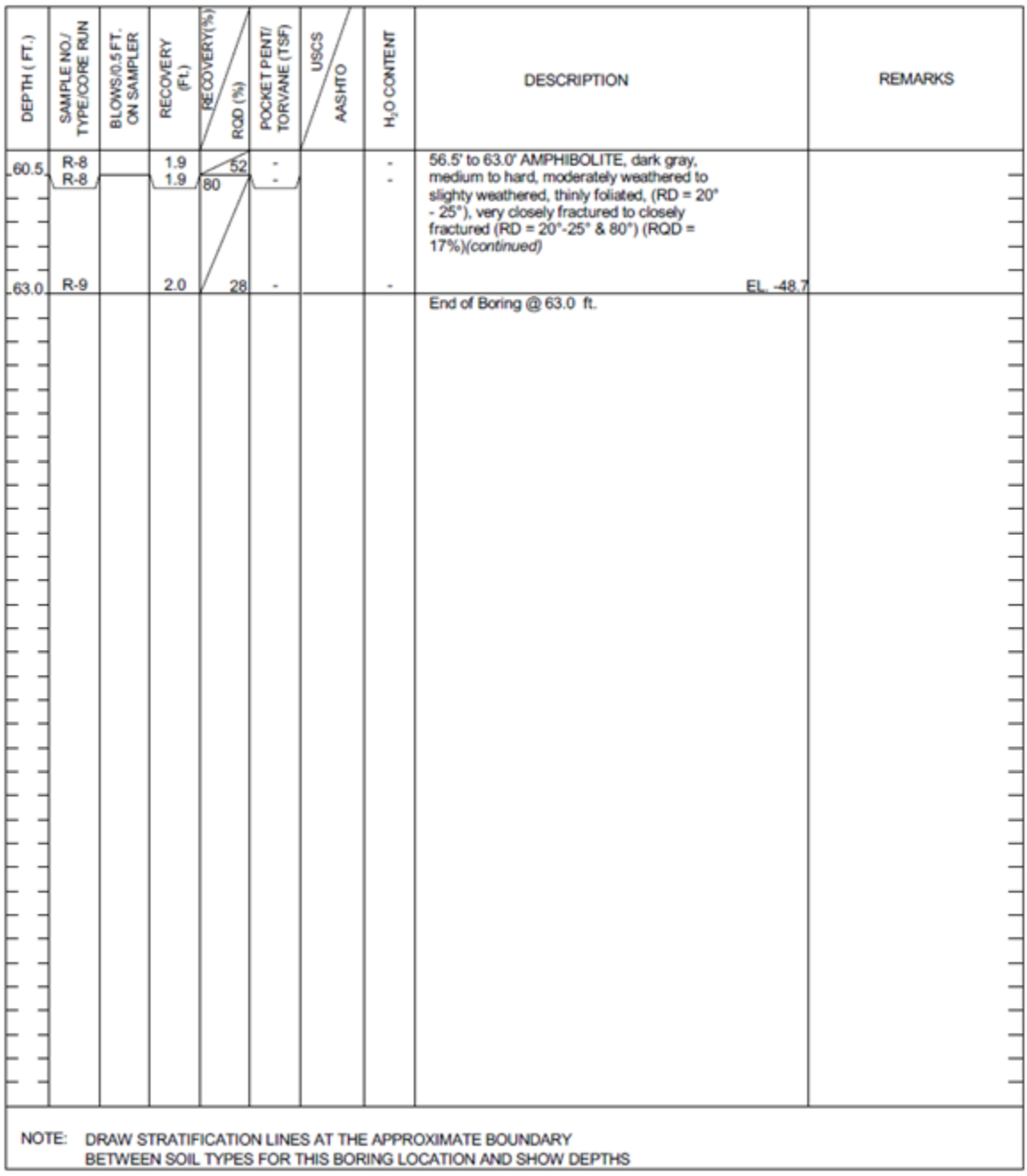

DEPTH (FT.)	SAMPLE NO./ TYPE/CORE RUN	BLOWS/0.5 FT. ON SAMPLER	RECOVERY (Ft.)	RECOVERY(%) / RQD (%)	POCKET PENT/ TORVANE (TSF)	USCS / AASHTO	H_2O CONTENT	DESCRIPTION	REMARKS
60.5	R-8 R-8		1.9 1.9	52 80	- -		- -	56.5' to 63.0' AMPHIBOLITE, dark gray, medium to hard, moderately weathered to slighty weathered, thinly foliated, (RD = 20° - 25°), very closely fractured to closely fractured (RD = 20°-25° & 80°) (RQD = 17%)*(continued)*	
63.0	R-9		2.0	28	-		-	EL. -48.7 End of Boring @ 63.0 ft.	

NOTE: DRAW STRATIFICATION LINES AT THE APPROXIMATE BOUNDARY BETWEEN SOIL TYPES FOR THIS BORING LOCATION AND SHOW DEPTHS

Figure 5-11 (cont.): Previous boring log from Pier 18 NB at GR3.

Figure 5-12: Sample taken at approximately 7.6 m (25 ft) depth at GR3.

Figure 5-13: Core barrel and rock sample after coring at GR3.

Figure 5-14: Installation of PVC inside borehole at GR3.

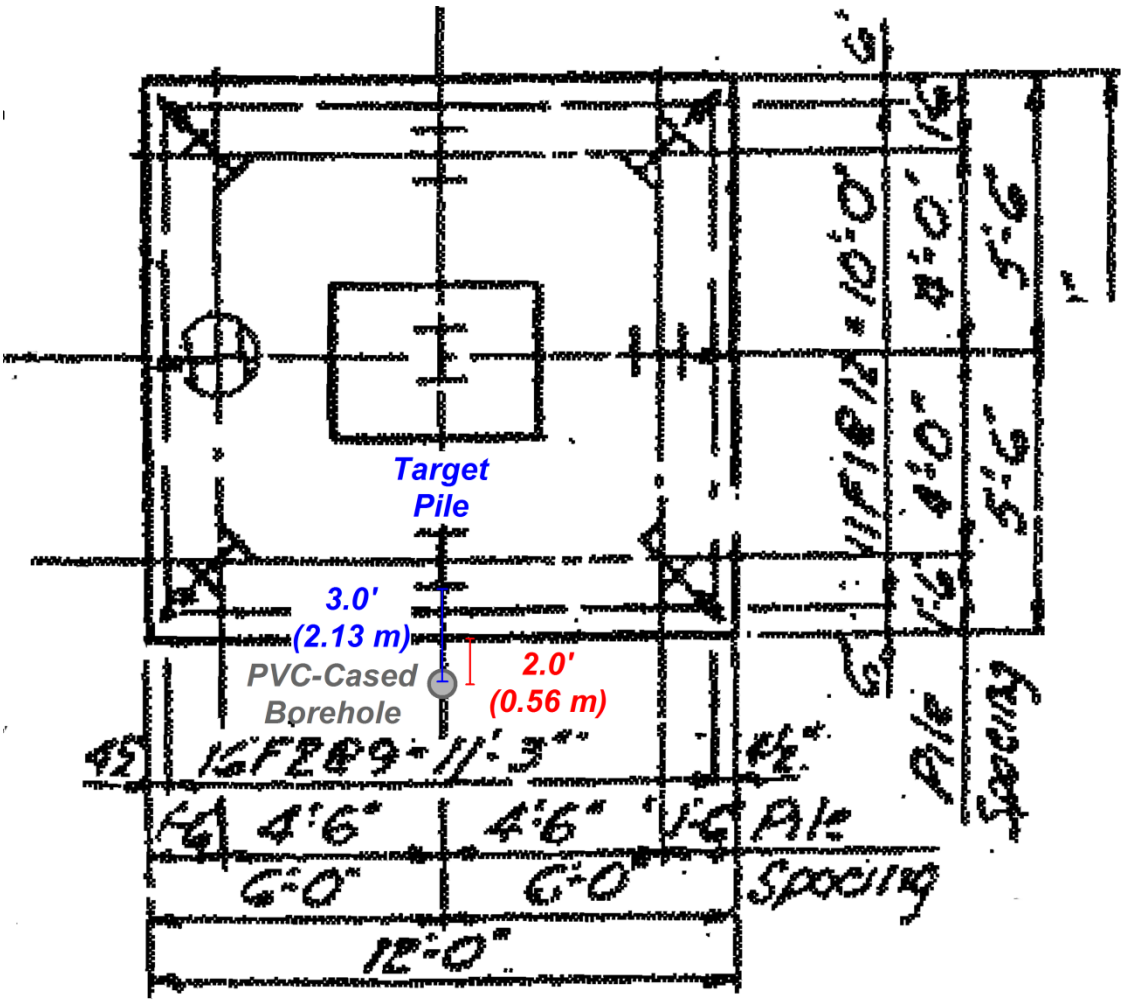

Figure 5-15: Approximate final location of cased borehole at GR3.

Figure 5-16: SubSurface Instruments BHG-1 Borehole Gradiometer used for BM method.

Figure 5-17: Data acquisition with BHG-1 and survey wheel tripod system.

Figure 5-18: AGI SuperSting R8/IP system used in ERI method.

(a)

(b)

Figure 5-19: Two ERI survey lines at BR0: (a) Perpendicular to ramp; and (b) Approaching parallel to ramp.

(a)

(b)

Figure 5-20: Two ERI survey lines at GR3: (a) Perpendicular to Ramp; and (b) Parallel to Ramp.

Figure 5-21: Pouring salt water near electrodes to ensure adequate electrical coupling with ground surface.

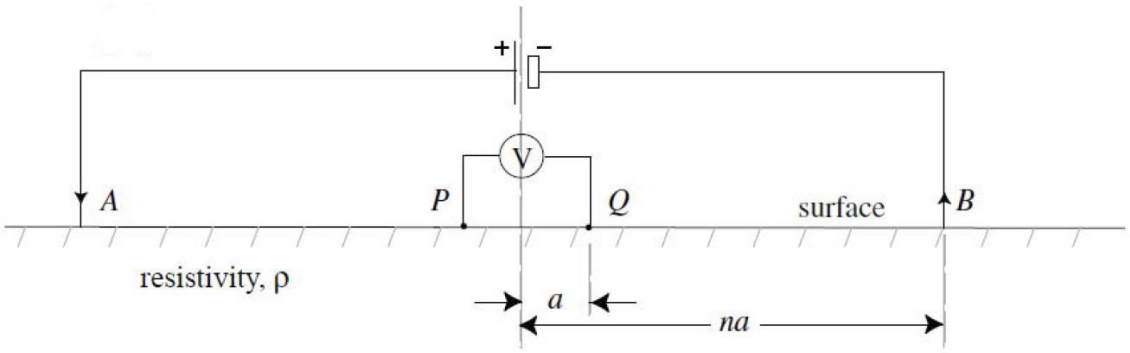

(a)

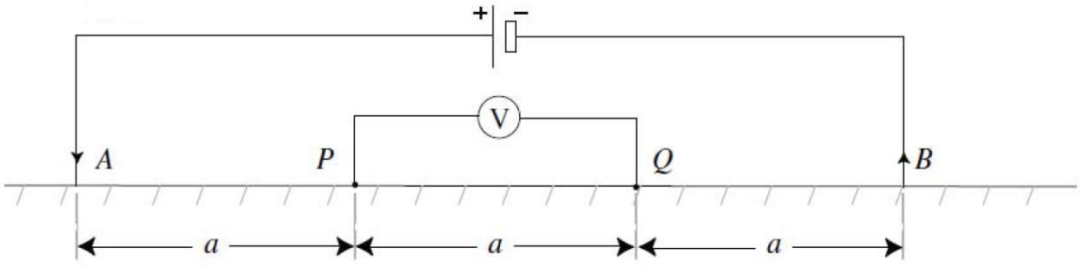

(b)

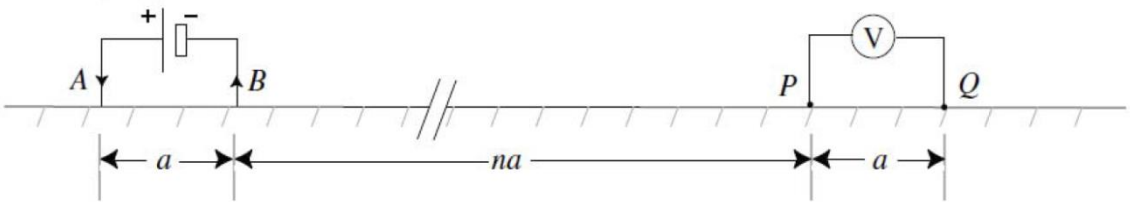

(c)

Figure 5-22: Traditional Four-Electrode Configurations: (a) Schlumberger; (b) Wenner; and (c) Dipole-Dipole (adapted from Briaud et al. 2012).

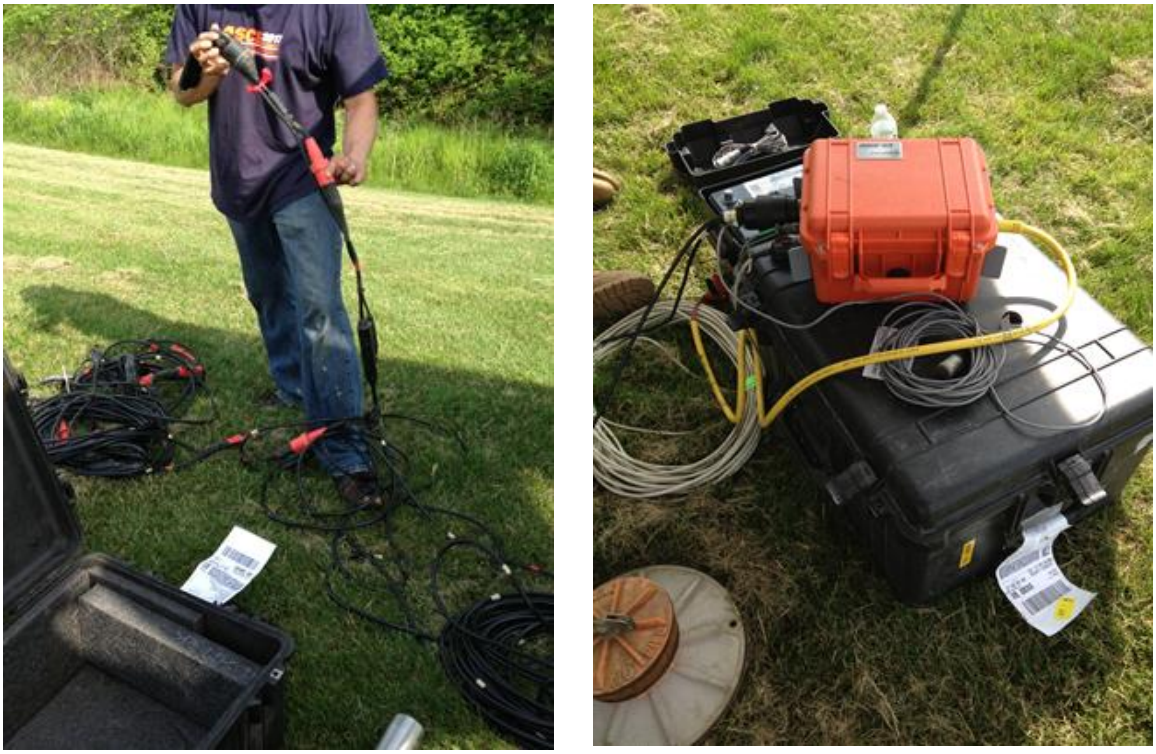

(a) **(b)**

Figure 5-23: PS Equipment: (a) OYO Geospace MP-25 Hydrophone String; and (b) Geometrics ES-3000 Seismograph and GISCO G-ST-01 piezoelectric hammer switch.

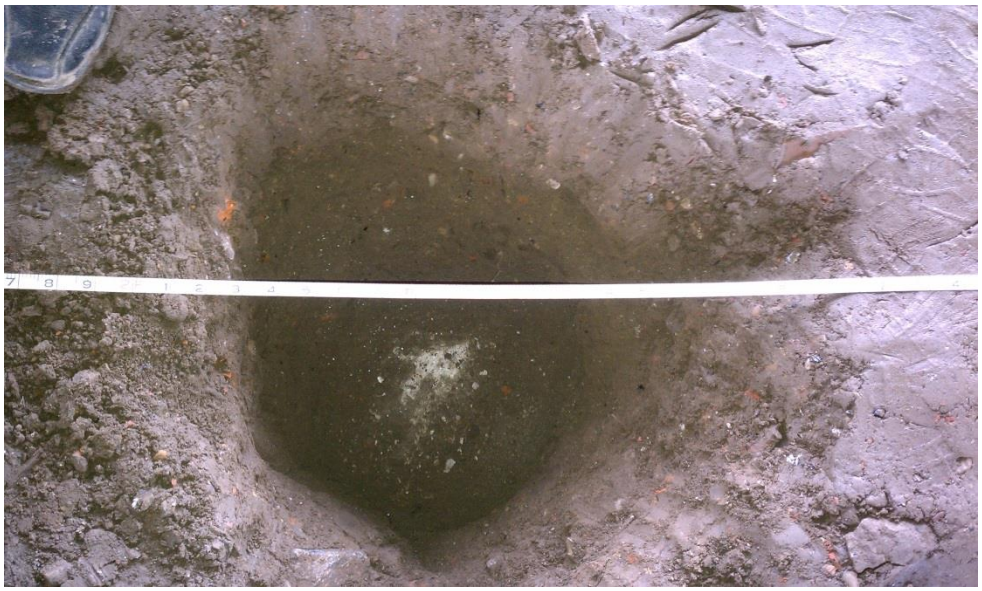

Figure 5-24: Pile cap at GR3 after hand augering and digging.

Figure 5-25: Direct impact to PVC casing during PS testing at GR3.

(a) **(b)**

Figure 5-26: Backfilling gaps between PVC casing and borehole wall: (a) Before; and (b) After.

Figure 5-27: Motorized winch, steel wire rope, and pulley system used to lower ultrasound probe and connecting rods.

Figure 5-28: Water-proofing at the probe end.

Figure 5-29: Pooling of water inside rods after testing with P-wave system.

Figure 5-30: MALA GPR equipment.

(a)

(b)

Figure 5-31: GPR test zone: (a) BR0; and (b) GR3.

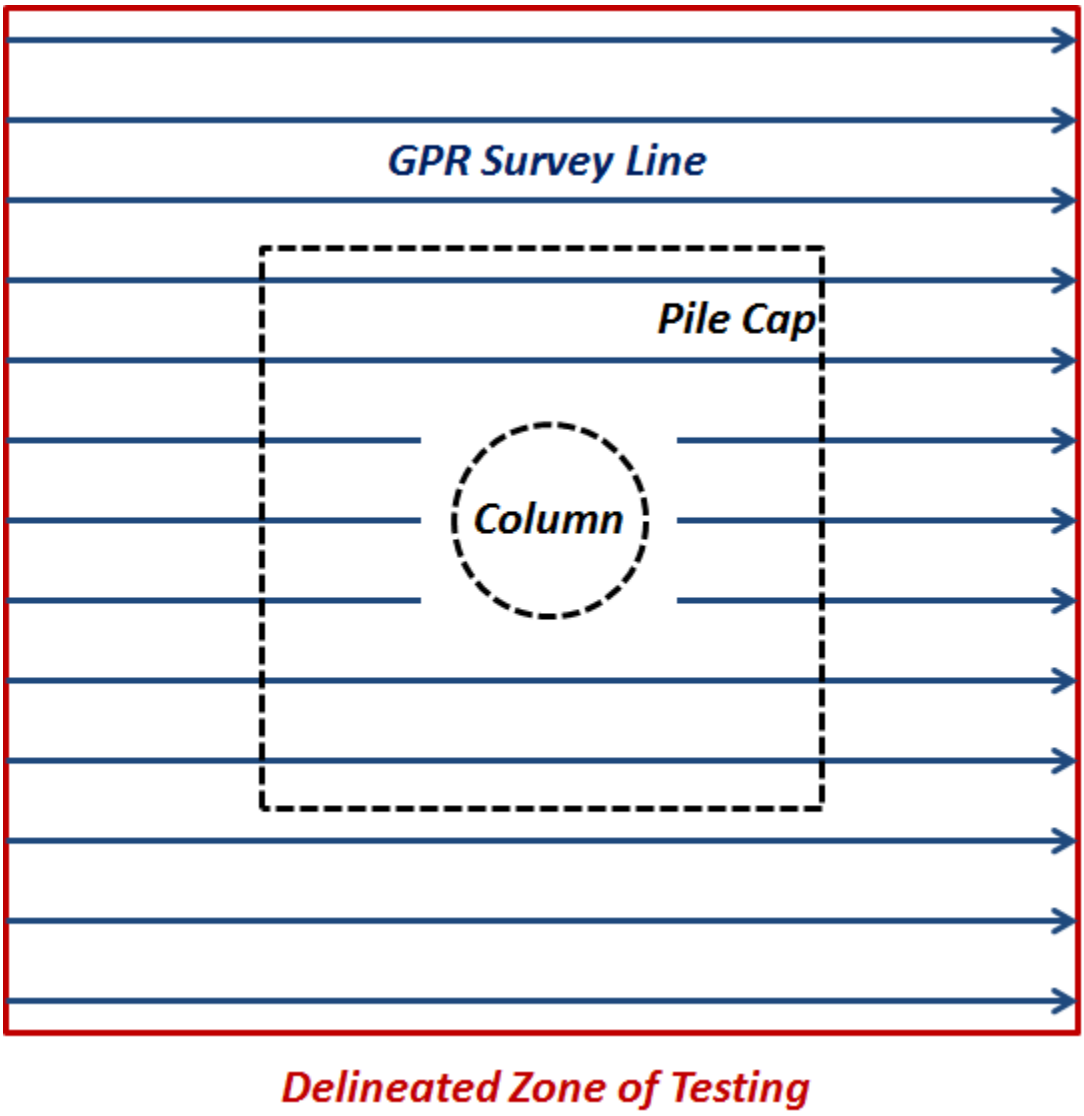

Figure 5-32: Typical GPR 2D survey scan lines and zone of testing.

Figure 5-33: GSSI BHR antenna and SIR-3000 controller for BHR testing.

6. DATA POST-PROCESSING AND PREDICTION OF FOUNDATION CHARACTERISTICS

As the suite of field tests described in previous reports was underway, post-processing and analysis of the data was also continuously performed. The concurrent analysis of data aided in highlighting potential difficulties with certain methods. Such information allowed the research team to prioritize field testing days and address deficiencies in data whenever possible. The following sections discuss the analysis of data collected during field testing at both Pennsylvania Department of Transportation (PennDOT) bridge test sites and at the Temple University Ambler (AMB) campus test site. Based on these results, an evaluation of the foundation characteristics is discussed for the two PennDOT bridge test sites.

6.1 SUBSURFACE METHODS

The substructures of interest were known to be complex deep foundations (i.e. steel piles on footings) based on design plans from their original construction. Thus, subsurface methods were more likely to allow direct interpretation of the depth to the foundation bottoms. The following sections highlight the quality of the data acquired and issues related to data interpretation for each of the subsurface methods performed in the field.

6.1.1 Borehole Magnetic (BM) Method

The BM method proved to provide a relatively quick and straightforward approach to evaluating the length of the foundations at both test sites. The data was highly repeatable and followed similar trends at all tested locations.

6.1.1.1 Temple Ambler (AMB) Test Site

As a means to aid in data interpretation, BM testing was performed at AMB immediately after completion of testing at BR0 and GR3. Figure 6-1 illustrates the results from the AMB BM test. The readings up to approximately 15 m (49 ft) are caused by the strong magnetic field produced by the steel casing. The large magnitudes are due to the close proximity of the gradiometer to the steel casing. Additionally, since it is extremely difficult to prevent the gradiometer from oscillating while it dangles in the borehole, the large fluctuations in the readings are a result of the gradiometer constantly moving away and towards the steel casing. When the steel casing

terminates at approximately 15 m (49 ft), the readings almost instantly diminish and stay in this range throughout the rest of the profile. At BR0 and GR3 the readings should exhibit a similar pattern at the depth where the steel piles terminate if indeed the boreholes extend beneath the bottom of the piles. Thus the test results from AMB give a better sense of the overall impact of metallic objects on gradiometer readings and define typical “zero” levels when such objects are no longer present.

6.1.1.2 Betsy Ross Bridge Interstate 95 (BR0) Test Site

Figure 6-2 illustrates the BM test results from BR0 and GR3. The initial readings within the first few meters are likely related to surficial metallic objects such as nearby embedded utilities. Even the survey tripod itself contains significant enough metal to alter the reading levels. For example, after the gradiometer was placed inside the borehole and flush with the ground surface, the close proximity of the tripod and other surficial metallic objects prevented use of the auto-range setting on the controller unit to re-zero the sensor. Note the non-zero reading at the top of the borehole in Fig. 6-2a. As the gradiometer was lowered in the borehole, the nearby pile elements began to increasingly affect the overall readings. The gradiometer essentially functions as two magnetometers inside the same sensor. The readings displayed on the control unit are the difference in the magnetic field at one end of the sensor from the other end. As the gradiometer is lowered deeper into the borehole, the major source of magnetic disturbance is caused by the steel pile elements, which are located at approximately the same distance away from either end of the gradiometer. Thus the readings tend to reach a plateau where very small fluctuations in magnetic strength are no longer prevalent. This is evident at approximately 5 m (16.4 ft) in Fig. 6-2 After 5 m (16.4 ft) there is a very gradual shift towards a zero reading. However, due to the abbreviated depth of the borehole at BR0, the gradiometer never truly reaches a zero reading because it does not extend past the pile bottom. Thus it is impossible to make an accurate prediction of the foundation depth at BR0. The best that can be offered is a lower bound estimate of foundation length equal to the length of the borehole. One interesting item to note is the distinct change in gradiometer readings (i.e. magnitude and polarity) present at the final three data points. It is at this location that the gradiometer is approaching the water-tight cap inserted at the bottom of the PVC. The metallic screw and wing nut that press the cap gasket against the PVC walls (see previous Fig. 5-9) quickly dominate the gradiometer readings and induce a large change in magnitude and polarity of the recorded magnetic flux values.

Though not directly relevant to foundation length determination, this observation allowed a greater sense of confidence in the experimental results since the signal fluctuation could be related to a known physical object.

6.1.1.3 Girard Avenue Interstate 95 (GR3) Test Site

Figure 6-2 also plots the gradiometer readings with depth at the GR3 test site. As at BR0, the readings near the top of the profile at GR3 are strongly affected by surficial metallic objects. In fact, both sites share a very similar shape with inflection points in the surficial data at nearly the same locations. However, at larger depths the profiles show some distinct differences. For example, the location of the peak reading at depth is separated by approximately 2.5 m (8.2 ft) between the two sites, with the peak arriving at a deeper location in the borehole at GR3. Moreover, at GR3 the magnetic field weakens much more quickly after the peak reading because the sensor has likely passed the bottom of the pile. The recorded magnetic field diminishes significantly at a little over 11 m (36 ft) in depth, which can be used as a good lower-bound estimate of the foundation bottom for GR3.

6.1.2 Ultrasonic P-wave Method

Based on the results from laboratory testing with the P-wave system, it was expected with reasonable certainty that reflections would be visible from the target steel H-pile at GR3 and not from the cast-in-place concrete pile at BR0. The 100 kHz ultrasonic P-waves proved capable of traveling up to a two-way distance of 1.8 m (6 ft) in saturated sand during laboratory testing. There was also some evidence to suggest that multiple reflections were recorded, meaning that the waves may have actually traversed this 1.8 m (6 ft) distance more than one time. It was anticipated that the target pile at GR3 was approximately located only 2.1 m (3 ft) from the ultrasound probe based on design plans. This distance was more than doubled for BR0 where the target pile was one of the vertical inside piles located approximately 2 m (6.5 ft) from the transducers. These distances lie within the range of potential acceptable distances based on the results of laboratory testing. However, depending on conditions in the field, it may be possible for the waves to travel farther or closer than the limits established in the laboratory under controlled conditions.

6.1.2.1 Betsy Ross Bridge Interstate 95 (BR0) Test Site

Figure 6-3 summarizes the recorded P-wave signals obtained at BR0. The traces in Fig. 6-3 have all been recovered based on a series of 1200 stacks. Stacking is a procedure to increase the signal-to-noise (S/N) ratio of an acquired data. Multiple records are obtained at the same location and added together. The correlated areas of the signal (e.g. reflections) reinforce each other while the high frequency noise is presumably random in nature and does not increase as quickly. Fast stacking (Brandenberg 2008) with 100 stacks was initially attempted at GR3 but the S/N ratio was poor and unsuitable for analysis of the foundation bottom locations. All subsequent tests were performed using traditional stacking techniques which require a period of "dead time" between subsequent source inputs into the domain. This appreciably increased data acquisition time to the point where obtaining data while retrieving the probe proved impractical. The signals in Fig. 6-3 have also been band-pass filtered at 50 kHz and 150 kHz to highlight the dominant frequency response of the 100 kHz transducers to the reflection signals.

The P-wave results from BR0 show some evidence of potential reflections from foundation elements. For example, note the strong reflector source located approximately 1.9 m (6.2 ft) from the transducers at an approximate depth of 6.5 m (21.3 ft). However, the reflections do not line up to form an obvious continuous reflector as should be the case with such a long vertically oriented element such as a pile. One obvious exception is the strong reflection signal in the initial segment of the record from the direct arrival and from multiple reflections off the PVC wall that lined the borehole. Another noticeable feature is the series of reflection signals starting at approximately 8 m (26 ft) below the ground surface that fall along a line of decreasing two-way travel time/distance to the transducers. Initially, this reflection signal is located at approximately 0.005 s two-way travel time [i.e. 3.75 m (12.3 ft) assuming a saturated soil P-wave velocity, V_p, of 1500 m/s (4920 ft/s)]. By a depth of approximately 10 m (33 ft), this two-way travel time has been reduced to about 0.002 s [i.e. 1.6 m (5.2 ft) with V_p = 1500 m/s (4920 ft/s)], which lies within the realm of possible reflection signals from the target pile. However, given the highly linear nature of the change in two-way travel time with depth, it could also be attributable to P-wave signals that strike the PVC interface and produce a downward traveling tube wave which reflects from the bottom of the casing and returns to the receiver transducer. Based on the computed depths and two-way travel times, the velocity of this potential tube wave can be approximated as 2 x (11.2 m – 8 m)/(0.005 s) = 1280 m/s. This value is reasonable assuming the tube wave energy is primarily carried by the water inside the

PVC casing. The velocity would generally be expected to approach 2400 m/s (7900 ft/s) if the tube wave energy was primarily carried by the PVC pipe itself.

Despite the evidence for reflection signals from distant sources, very little reflection data is recorded for a significant number of the traces. Additionally, what is visible is often noise and related artifacts from filtering the data. There are a number of potential reasons for these results. One major potential source of issues may be rotation of the probe within the borehole. Since the rods connected to the probe were held in place via a steel wire rope and hook, it was impossible to prevent some rotation of the probe as it was lowered into the borehole. To minimize the impact of these potential rotations, each new rod was marked with a line that represented the direction in which the transducers faced. However a better developed system would clamp the rods and prevent them from rotating, or better yet, would utilize omni-directional transducer components. This is especially crucial at BR0 since the steel casing for the cast-in-place concrete piles are circular in cross section and therefore tend to reflect any signals away from the transducer centerline. Another potential issue is that the borehole was simply not constructed in the appropriate location since foundation plans can sometimes vary from as-built conditions. Only a small amount of mismatch between the transducer location and the pile location could diminish signal quality from any reflectors. Finally, inadequate coupling between the PVC casing and borehole wall can lead to extra impedance mismatches and a resulting loss of signal amplitude at each interface. There may be some evidence to support this theory given the variations in PVC direct arrival signal amplitudes and durations across the traces in Fig. 6-3.

6.1.2.2 Girard Avenue Interstate 95 (GR3) Test Site

Figure 6-4 contains the reflection records for P-wave imaging at the GR3 site. As previously noted, the travel distance at GR3 was within the limits established during laboratory testing. Initially, testing at GR3 was performed using a linear string potentiometer to measure distance and allow triggering of the P-wave system as very small depth intervals. However, only 100 stacks were possible using fast stacking in this configuration. Instead, traditional stacking was employed which runs more slowly but allows easier post-processing of the signal. As with BR0, the P-wave results from GR3 show some evidence of potential reflections from foundation elements. Noticeable reflection traces are located approximately 0.75 m (2.5 ft) away from the transducers between depths of 2 m – 4m (6.6 ft – 13.1 ft). Again, the reflection signals do not

line up to form an obvious continuous reflector as should be the case with a long vertical element. As with the BR0 records, the direct arrival and multiple reflection signals off the PVC wall are clearly visible. Additionally, the series of reflection signals with decreasing two-way travel times is also evident in the GR3 data. Initially at approximately 11 m (36 ft) below the ground surface the reflection signal is located at approximately 0.004 s two-way travel time [i.e. 3.0 m (9.8 ft) assuming a saturated soil P-wave velocity, Vp, of 1500 m/s (4920 ft/s)]. By a depth of approximately 13.2 m (43.3 ft), this two-way travel time has been reduced to about 0.0012 s [i.e. 0.9 m (3.0 ft) with Vp = 1500 m/s (4920 ft/s)], which lies within the range of possible reflection signals from the target pile. However, given the repeatability of these results at both sites, the evidence suggests that these reflections indeed result from downward traveling tube waves that reflect from the PVC casing bottom. Based on the computed depths and two-way travel times, the velocity of this potential tube wave can be approximated as 2 x (13.8 m – 11 m)/(0.004 s) = 1400 m/s. This value approaches the P-wave velocity of water (i.e. 1500 m/s) which signifies that the tube wave is carried primarily by the water inside the PVC casing. The issues affecting data quality as discussed in section 6.1.2.1 are all equally as likely at GR3 given that very little was changed in test methodology at both sites. Moreover, issues related to borehole wall and PVC coupling may have been more prevalent at GR3 than BR0 since more gaps seemed to develop at GR3 at the end of drilling (see Fig. 5-26). A larger percentage of the backfill material at GR3 was also composed of drilling mud compared to what was used at the end of drilling at BR0.

6.1.3 Borehole Radar (BHR) Method

Despite the various issues with equipment, the BHR method proved to be extremely capable of generating high quality data and of and sending signals the farthest of the subsurface test methods. The data was highly repeatable and followed similar trends at all tested locations.

6.1.3.1 Betsy Ross Bridge Interstate 95 (BR0) Test Site

Figure 6-5 illustrates the resulting BHR data at BR0. Post-processing of the data was facilitated by the use of matGPR, a free MATLAB®-based software package available to the general public (Tzanis 2010). The data in Fig. 6-5 was filtered with a 160 MHz low-pass filter to remove high frequency noise in the recorded record. The raw data wiggle traces were plotted in front of the image generated when the traces are mapped to pixel color intensity on a Red-Green-Blue

(RGB) color scheme. Areas of darker pixel color represent locations of strong reflection energy. Note that the figure axes were rotated to allow easier interpretation with the vertical depth axis oriented in the vertical direction.

Evident in Fig. 6-5 is a series of multiple reflections likely from the pile cap near the surface. This extends down to approximately 4 m (13.1 ft) in depth, below which multiple reflections from pile elements are noticeable throughout the rest of the profile at a farther distance away from the antenna [i.e. 5+ m (16+ ft)]. The estimated distance to the pile cap and the target pile were very close to the antenna [i.e. within 1 m (3.3 ft)], and any corresponding reflection signals coincide with the direct arrival of the radar wave from source to receiver within the antenna. Note in Fig. 6-5 how the initial waveform in the immediate vicinity of the antenna (i.e. the direct arrival wave) is altered by another waveform, particularly closer to the top of the borehole. Such interference is likely caused by reflection energy from the target pile cap and pile elements. Therefore the strong signals seen at farther distances are likely reflections from other nearby foundations that are farther away from the antenna. The omni-directional nature of the borehole antenna allows it to record signals from all directions and there are multiple substructure units in the immediate vicinity of Pier 7 at BR0.

In terms of evaluating the depth to the bottom of the foundation, the pile reflections at depths greater than 4 m (13.1 ft) continue throughout the rest of the profile. No break is seen in the data which signifies the bottom is not visible at BR0. Again, these reflections are likely from nearby foundations rendering the results from BHR as inconclusive for the target foundation. Either a much higher frequency antenna must be utilized so that the direct wave arrival between source and receiver occurs more quickly, or the borehole should be constructed farther away from the target foundation to allow some settling time before reflections arrive at the antenna. However, the results do illustrate that the BHR method is highly capable of imaging embedded foundation elements, though care must be exercised in locating the borehole and interpreting the results. Additionally, the depth of the borehole could be used as a conservative estimate of the depth of the foundation if this substructure were truly unknown.

6.1.3.2 Girard Avenue Interstate 95 (GR3) Test Site

Figure 6-6 presents the BHR results at GR3. Post-processing of the data proceeded in a similar manner to BR0. It is notable how similar an image is generated from the recorded signals at both sites. Again a series of multiple reflections from what is likely the pile cap is recorded almost immediately in the signal trace. Evidence of these reflections in the received signals extends to a depth of approximately 1.5 m (5 ft). This depth agrees favorably with the fact that the top of the pile cap was directly unearthed during Parallel Seismic testing at approximately 0.5 m, which implies an approximate pile cap thickness of 1 m (3.3 ft). Below the depth of 1.5 m (5 ft), the reflection signals shift to slightly later in time (i.e. farther away from the antenna). This shift is noticeable in the later reflections as well as in the interference caused to the direct arrival at the beginning of the trace records. As was the case in BR0, the pile reflections seem to continually extend well past the bottom of the profile recorded by the borehole antenna. This implies that the borehole at GR3 may not have been drilled deep enough to pick out the break in the radar reflection records and therefore the foundation bottoms. This result contradicts the result from BM testing at GR3 which indicated that the foundation bottom was approximately 11 m (36 ft) beneath the ground surface. Based on the results of BHR at GR3, the foundation bottoms were located at least as deep as the bottom of the borehole [i.e. 13.6 m (45 ft)]. Final interpretation of the depth to the bottom of the foundation at GR3 will be discussed in a later section.

6.1.4 PARALLEL SEISMIC (PS) METHOD

Since PS is considered one of the most robust NDT methods for unknown foundations, it was important to perform this method to establish a baseline for comparison among the other subsurface methods. However, the conditions under which PS was performed in this study (i.e. urban environment, high traffic noise, embedded pile group with no direct access to pile) truly tested the limits for acquiring reasonable data. The following sections discuss the efforts by the research team to overcome the issues with the site conditions and evaluate the foundation lengths based on PS data.

6.1.4.1 Temple Ambler (AMB) Test Site

Prior to deployment at either of the PennDOT bridge sites, the PS equipment was utilized in preliminary investigations at the AMB site. The purpose of this testing was to verify system performance and ensure appropriate data acquisition settings for the seismograph. The

hydrophones were lowered into the steel casing until submerged below the water table. Unfortunately, due to the water table elevation several of the hydrophones were likely below the bottom of the steel casing and into open borehole in rock. Seismic traces were then recorded as the concrete surface surrounding the steel casing was directly impacted by a small sledgehammer. Figure 6-7 present the seismic traces from this initial testing at AMB. The records were band-pass filtered at 80 – 500 Hz to suppress high frequency noise and low frequency wave energy. Based on these results it is not too difficult to pick the arrival time of the main tube wave pulse resulting from impacting the concrete pad. However, there does seem to be a slight difference in velocity of this pulse as it passes by hydrophones 3 – 8 and 9 – 12. Based on picking first arrival times, the velocity of the wave seems to slow down at hydrophone 9 from a predicted velocity of 2000 m/s (6560 ft) to 500 m/s (1640 ft/s). It is possible that this marks the transition where the remaining hydrophones extended beneath the steel casing. In this particular record, the first two hydrophones were actually not submerged in the water which explains their overall lack of response. Another interesting feature to note is that there seem to be a couple of polarity changes for the wave as it travels down the steel casing and/or water (i.e. hydrophones 3 and 6). This test layout was not meant to mimic PS exactly. In fact, in some ways the hydrophones may be subjected to a much more complex signal inside the steel casing as it rings with several wave types long after the impact with the sledgehammer. It is possible that several waves are constructively and destructively interfering to produce the data acquired. Therefore this testing was not intended to obtain meaningful and complementary data; rather it was used as a basis for ensuring proper function of all equipment. However, interpretation of the acquired data was an indication that PS records would not be as straight forward as originally anticipated and the research team took extra care to verify appropriate system performance prior to all field tests as a result.

6.1.4.2 Betsy Ross Bridge Interstate 95 (BR0) Test Site

Figure 6-8 presents PS data that was collected at BR0. The hydrophone string was lowered into the PVC casing so that the string was just above the bottom of the casing and a 20 lb sledgehammer was used to impact the pier column. The noise levels were monitored to attempt to find a quiet period to impact the column and avoid any potential seismic waves from the surrounding environment. Each recorded seismic trace was band-pass filtered at 10 – 250 Hz and consisted of 16 stacks (i.e. the summation of data from 16 sledgehammer blows). There is

no discernible evidence of any seismic energy passing through the pier to the underlying pile and reaching the hydrophones in the PVC casing. There are simply too many factors that are degrading signal quality. For example, there is too much seismic noise in the environment (e.g. traffic) which prevents the low amplitude seismic traces from being interpreted above the noise floor. Moreover, there is a significant loss of wave energy at all the major interfaces in the wave path (e.g. between the pier column and pile cap, between the pile cap and underlying piles, and even likely between the PVC casing and surrounding soils).

Since the seismic noise at the site was so severe, the research team investigated whether such noise could be utilized within the context of the PS method. Perhaps the hydrophones that may be located below the bottom of the piles have a different response to the noise sources compared to those in line with the pile. Such passive surveys using noise sources are routinely utilized in geophysical studies and seismic profiling (e.g. Louie 2001), though little information was uncovered for applications to PS profiling for unknown foundations. The hydrophone string was left dangling inside the PVC casing and data was acquired of the ambient seismic noise for approximately 4 s. Figure 6-9 plots the Welch power spectral density (i.e. a measurement of the power of a signal at a given frequency component) for each hydrophone in response to the recorded noise data. There is very little difference in the overall power spectrum for each hydrophone. Any discernible differences would need to be discovered using much more sophisticated data processing techniques that outside the scope of this project. However, if such an approach could highlight differences in the hydrophone responses, there would be potential to extend PS to noisier environments and address one major limitation of the method. Based on the results at BR0 and the state-of-practice in PS signal interpretation and post-processing, PS proved unsuccessful at BR0. Note that this was expected in any case since the borehole at BR0 did not extend beneath the piles. However even if the borehole did extend below the pile caps, PS would still prove unsuccessful at BR0 since there was no discernible signal above the noise.

6.1.4.3 Girard Avenue Interstate 95 (GR3) Test Site

PS testing was continued at GR3 after the lessons learned at BR0. Since the piles were closer to the PVC casing and the research team had direct access to the top of the pile cap at GR3, the chances for success for PS were more favorable at that site. Prior to impacting the pile cap directly, the noise threshold was monitored with the hydrophones by performing a simple

experiment where the PVC itself was impacted by the sledgehammer. Figure 6-10 illustrates the resulting data from this small initial test of the equipment and noise levels. The seismic traces in Fig. 6-10 were band-pass filtered from 200 – 500 Hz and were assembled after 30 stacks. The tube wave generated by impacting the PVC is clearly visible in the resulting data. Based on picking first arrival times, the velocity of the wave can be estimated as approximately 1500 m/s (4920 ft/s) which corresponds to the acoustic velocity of water. However, based on the results of this initial test it was still evident that traffic noise would be a concern. The signal to noise ratio accomplished in Fig. 6-10 was only possible after 32 direct impacts to the PVC casing. Essentially, even under the most favorable impact conditions (i.e. directly to PVC) it was necessary to utilized a large number of stacks.

Based on the results from the initial impact testing on PVC, it was decided to forgo impacting the pier column with the 20 lb sledgehammer and to skip directly to striking the pile cap above the target pile. Figure 6-11 presents the seismic traces from testing with direct impact to the pile cap. The seismic traces in Fig. 6-11 have been band-pass filtered at 10 – 250 Hz and contain 25 stacks. Again, all traces are dominated by seismic noise from the environment. No first break time arrivals are discernible above the noise. The passive method previously discussed for BR0 was attempted as well at GR3. This time 30 s of environmental seismic noise was recorded by the hydrophones as they were suspended within the PVC casing alongside the foundation at GR3. Figure 6-12 presents the Welch power spectrum for each of the hydrophones in response to the seismic noise. As was the case at BR0, there is very little difference in the frequency response to noise for any of the hydrophones. Therefore, PS testing was unsuccessful as well at GR3. The sites selected for TEM002 just proved to be poorly suited for evaluating foundation lengths with PS.

6.2 SURFACE METHODS

The surface methods employed in TEM002 were originally intended to be supplemental in nature to the subsurface methods. It was clear from the literature review that several of the surface methods would not be able to image or determine the location of the foundation bottoms due to the overlying pile cap. For that reason, most of the methods attempted in this study were subsurface methods. However, in the case of Ground Penetrating Radar (GPR), the ability to image the pile cap was an invaluable tool. For a truly unknown foundation with no

design plans, Ground Penetrating Radar can provide an efficient method to start gathering information about the foundation and to plan a more effective NDT plan. The approach in this project was to investigate the level of detailed information that could be pulled from GPR data to aid in planning a subsurface NDT study. In the case of Electrical Resistivity Imaging (ERI), only a handful of studies had demonstrated its potential as an NDT tool for unknown foundations. The resulting ERI data would prove invaluable as to whether ERI is capable of imaging the bottoms of piles beneath pile caps. The following sections highlight the quality of the data acquired using both methods and issues related to data interpretation.

6.2.1 Electrical Resistivity Imaging (ERI) Method

The experiences of the research team with ERI for unknown foundations in this project highlighted the importance of appropriate site selection for a given NDT method. In general, ERI did provide information that would normally be impractical to obtain via other surface NDT methods such as Sonic Echo, Ultraseismic, and Spectral Analysis of Surface Waves. For example, conservative estimates of the foundation depths were obtained and a much more comprehensive image of the subsurface was possible. However, the extremely long survey lines required (i.e. typically 3 – 5 times the vertical depth of interest) proved problematic in a highly urbanized environment such as Philadelphia both in terms of space on the surface and the presence of multiple utilities in the subsurface. Noise in the data often prevented a more accurate evaluation of the foundation depths. Despite these issues ERI proves itself to be invaluable as one of the only methods to obtain foundation information at great depths without having to drill a boring or somehow have direct access to impact the substructure. The following sections discuss data acquisition with ERI at all test sites and the necessary efforts to post-process the resulting data.

6.2.1.1 Temple Ambler (AMB) Test Site

Prior to deployment at either of the PennDOT sites, ERI was initiated at the AMB site to familiarize the research team with appropriate procedures for data acquisition. A single line was setup with the 28 electrodes spaced at a 3 m interval alongside the soccer field at the AMB test site. The final electrode on the ERI line was located near the test well used for subsurface testing. Figure 6-13 illustrates the resulting cross section after inversion using the RES2DINV software (Geotomo Software, Penang, Malaysia) for Windows. RES2DINV is one of many

software codes available to compute the 2D resistivity model that agrees with the actual measurements recorded by the AGI SuperSting R8 resistivity meter used in this study. This process is an inversion that attempts to fit a model of the true resistivity to the measured apparent resistivity pseudosection. The accuracy of this inversion process depends on many factors, including the number of data points, the accuracy of the measured resistivity values, and even the optimization method used to determine the difference between model response and measured data (Loke 2010). Figure 6-13 was generated for measurements using a Schlumberger four-electrode configuration (as discussed in Chapter 5). In general, sandy soils have higher resistivity values than clayey soils, bedrock material tends to have higher resistivity than soils, and the resistivity of water varies based on salinity level (Loke 2010). The resistivity of reinforced concrete varies with a number of factors including microstructure of the cement matrix, the porosity, the pore-size distribution, corrosion, and moisture content (Briaud et al. 2012). Typical values range from 10^1 to 10^5 Ωm (Tuutti 1982). Metals, such as steel rebar, have very low resistivity values. Based on these trends for resistivity, a likely interpretation of the results in Fig. 6-13 is that the deeper materials at the AMB site are likely clayey and/or saturated relative to the sandy layer that exists on the other end of the survey line [i.e. after approximately 24 m (79 ft) and between 2 m (6.5 ft) and 12 m (39 ft)].

6.2.1.2 Betsy Ross Bridge Interstate 95 (BR0) Test Site

After testing at AMB, two ERI survey lines were arranged to evaluate the lengths of the foundation beneath Pier 7 at BR0. The two lines were arranged over two perpendicular cross sections centered approximately over the tested foundation. One line followed a path that was parallel to the pier cap and the other was more in line with the direction of traffic flow in the ramp overhead (i.e. perpendicular to the pier cap). Testing procedures were discussed in the Chapter 5. 2D resistivity sections were generated using the Advanced Geoscience Incorporated (AGI) EarthImager 2D software. The recorded data files for the Schlumberger and Wenner electrode configurations were combined into a single data file in EarthImager 2D for a given survey line. The resulting single set of data was inverted to generate the desired 2D cross section. This was performed in an effort to provide complementary information and increase the accuracy of the inversion process since each of the individual data files often contained excessive reciprocal/repeat errors. As part of the command files for each electrode configuration, a reciprocal measurement is taken in the opposite direction to ensure data

repeatability. For example, if the measurement was taken between electrode 1 and 2, the reciprocal would be taken from 2 to 1. The data recorded using the Dipole-Dipole configuration proved to have excessive inconsistencies with the reciprocal measurements due to electrical noise from embedded utilities on site. The Sclumberger and Wenner files were typically less affected, but often still had issues as well. Keeping these inconsistent data points in the inversion process can lead to significant errors in the results. However, the other approach is to remove these inconsistent readings from the data files. Removing data points from the apparent measured pseudosection often leads to less than ideal data coverage at larger depths of interest which limits the final depth of investigation.

Figures 6-14 and 6-15 present the inverted 2D cross sections for the two survey lines at BR0. Immediately evident in the cross sections is the large sections of blue (i.e. very low resistivity) in the center of the image towards the ground surface. These areas are very low in overall magnitude and are likely measurements of the steel piles and the reinforcement in the pile cap. Thus both cross sections highlight the location of the pile cap and are also able to capture the batter in the outer row of piles. In fact, the lateral extent of the pile cap can be estimated based on Fig. 6-14. The minimum length for the darkest blue zones is approximately 5.5 m (18 ft) wide, while taking into account any of the blue shades leads to an upper bound estimate of 9.25 m (30 ft). These estimates agree reasonably well with the 7.3 m (24 ft) dimension in the design plans. Unfortunately, the increase in survey line length (and therefore survey depth) in Fig. 6-15 introduced more inconsistent data that was removed prior to inversion. In fact very few data points existed below about 15 m (49 ft) for the inversion that generated Fig. 6-15 and little confidence can be placed on the results below that depth. Unfortunately, this implies that only a conservative (i.e. possibly short) estimate of 15 m (49 ft) can be made regarding the length of the foundations. Also apparent on Fig. 6-15 is the presence of stiff sandy materials with higher resistivity values (i.e. red shades) near the ground surface throughout most of the site. This is also noticeable in Fig. 6-14. Also, at approximately 5.5 m (18 ft) in Fig. 6-15 the high resistivity zone transitions to a very low resistivity zone at the beginning of the survey line. This could signify the presence of water and can help estimate the approximate location of the water table on site. This estimate agrees reasonably well with the measurements of the water table within the borehole [3.4 m (11.2 ft)].

6.2.1.3 Girard Avenue Interstate 95 (GR3) Test Site

ERI testing was performed at GR3 in much the same manner as BR0. Two sets of perpendicular survey lines were arranged at the GR3 site. The long survey line ran parallel to I-95 alongside several of the northbound pier foundations. The short survey ran perpendicular to I-95 along Pier 17 NB and SB. Figures 6-16 and 6-17 illustrate the 2D resistivity cross sections that resulted from ERI testing. As with BR0, the 2D cross sections were generated based on data obtained using the Schlumberger and Wenner configurations. Data interpretation is more difficult at GR3 due to the larger number of targets in the subsurface. Multiple foundations were crossed by each of the survey lines and both Figs. 6-16 and 6-17 contain a series of low resistivity zones (i.e. blue shades). The blue zones near the center of each survey line represent the foundation for Pier 17 NB Column A. Other areas of blue also correspond to different substructure units along the survey line throughout the site. Unfortunately, as with BR0, this site had issues with electrical noise at greater depths. Figure 6-17 in particular is the long survey line meant to allow determination of the foundation bottom for Pier 17 NB Column A. Based on the location of the blue shade in the center of the profile this foundation length can be estimated at approximately 10 m (33 ft). However, an examination of the original raw data shows that several data point were removed prior to inversion due to issues with reciprocal errors as described previously. The end result is that very few real data was used in the inversion for anything below about 11 m (36 ft). It is not clear then whether the blue pixel shades terminate at 10 m (33 ft) because the piles stop at that depth or because there was no accurate information from which to pick up the piles at that depth. So again a conservative estimate of 10 m (33 ft) can be established with the understanding that there is some probability that the piles actually extend farther. One final notable item in the results is the zone of relatively higher resistivity (i.e. red shades) in Fig. 6-17 towards the end of the survey line. The implication is that the shallow bedrock on site may actually get closer to surface as one move closer to Aramingo Avenue along the site.

6.2.2 Ground Penetrating Radar (GPR) Method

As previously mentioned, the use of GPR was studied within the context of providing an accurate assessment of the lateral foundation dimensions. In general, GPR proved capable of providing a good image of the pile cap and relatively accurate estimates of the pile cap dimensions provided the site was not rich in clay soils. The following sections describe data acquisition with GPR and the corresponding analysis of foundation dimensions.

6.2.2.1 Betsy Ross Bridge Interstate 95 (BR0) Test Site

A series of 2D survey lines were arranged within a 15.2 m by 15.2 m (i.e. 50 ft by 50 ft) square surrounding Pier 7 at BR0. Each line was spaced at a 0.3 m (1 ft) interval from the previous line. No lines were arranged to pass through the pier column. Along each survey line, data was acquired at a 3 cm (1.2 in) interval. This resulted in a total of 40 scans slices each with approximately 520 traces. This allowed the generation of a 3D image of the foundation by arranging the series of 2D slices in their appropriation location based on the local coordinate system (Fig. 6-18). However, though a 3D image allows a more comprehensive understanding of the general subsurface conditions, 2D slices are typically easier to view to discover finer detail regarding each individual slice of data. Figures 6-19 and 6-20 are 2D scans along two perpendicular survey lines at BR0. This approach is the simplest way to determine the lateral extent of a given pile cap since each survey line contains complementary information about the other dimension. Based on interpretation of the locations of reflection signals from the pile cap, the overall dimensions can be estimated as approximately 8 m (26.2 ft) by 8.5 m (27.9 ft). These estimates compare somewhat favorably with the dimensions of 5.5 m (18 ft) by 7.3 m (24 ft) noted on the design plans, particularly in one direction. One potential explanation for the discrepancy is that the GPR antennas have a broad enough directivity pattern that they "see" the edges of the cap too early when approaching the cap and for too long after passing over the cap. This demonstrates that the dimensions obtained with GPR should not be used without some context such as old design plans or results from another surface method (e.g. Spectral Analysis of Surface Waves, Seismic Reflection, etc.). However, there is some overall agreement with the estimated dimensions which shows that GPR is a valuable tool in evaluating subsurface conditions. One particular item to note is the appearance of diffraction hyperbolas from point sources at one end of the pile cap. This likely represents reflections from a slender element relative to the survey distance (i.e. one of the steel piles). The GPR antenna seems to be able to pick up reflections from a couple of battered piles on the outer row of the pile cap. Finally, the initial large reflection signal from the pile cap occurs at approximately 70 - 80 ns in the profile. Based on an estimated radar velocity of 0.07 m/ns, the pile cap can be estimated to be embedded at approximately 2.45 m – 2.8 m (8 ft – 9.2 ft). This seems to generally agree with other estimates of the pile cap depth based on other test methods.

6.2.2.2 Girard Avenue Interstate 95 (GR3) Test Site

GPR testing at GR3 focused on acquiring data at two 2D perpendicular cross sections after this approach proved sufficient to estimate the lateral extent of the pile cap at BR0. However, an added complication was incorporated by running each survey line over several foundations to determine how well GPR could distinguish multiple targets within a given cross section. Data was also compared between the 250 MHz and 500 MHz antennas. In the first survey line the 250 MHz antenna was run parallel to I-95 northbound along column B for Piers 18, 19, and 20 (Fig. 6-21). For the second survey line the 500 MHz was dragged perpendicular to I-95 along the foundations at Pier 19 (Fig. 6-22). Pier 19 was utilized instead of Pier 18 due to inclement weather and accumulation of standing water along most of Pier 18. However, the foundations at Piers 18 and 19 share the same design plans and should be identical. Testing proceeded as if Pier 18 NB Column B was the foundation of interest. Along each survey line, data was acquired at a 3 cm (1.2 in) interval as was the case at BR0. As can be noted in Fig. 6-21, the presence of multiple foundations along the survey line complicates data interpretation. Additionally, there are more diffraction hyperbolas (signifying point source reflectors) in the 250 MHz profile due to the smaller size of the pile caps at GR3. Each pile cap edge is essentially imaged as a diffraction hyperbola [i.e. at approximately 5 m (16.4 ft), 10 m (32.8 ft), 16 m (52.5 ft), 22 m (72.2 ft), 28 m (91.8 ft), and 34 m (111.5 ft)]. This phenomenon makes the pile cap edges fuzzier and less distinct, which complicates estimates of the pile cap dimensions. For example, the first two point sources actually represent the edges of the first pile cap. Based on Fig. 6-21 the distance of the pile cap between these two points is approximately 5 m (16.4 ft). This overestimates the true foundation dimension of 3.4 m (11 ft). The point source visualization is less of an issue with the 500 MHz antennas based on Fig. 6-22. Reflection signals from all five pile caps are present in Fig. 6-22. The final two sets of reflection signals represent the northbound columns A and B for Pier 19. The foundation dimension in this direction can be estimated as approximately 3 m (9.8 ft). This compares very well with the 3.4 m (11 ft) indicated in the foundation plans. A subtle feature in Fig. 6-22 is that the northbound pile caps seem to be slightly shallower than the southbound pile caps. Based on an estimated radar velocity of 0.07 m/ns, the pile cap can be estimated to be embedded at approximately 0.2 m – 0.25 m (0.7 ft – 0.8 ft). This agreed reasonably well with the 0.45 m (1.5 ft) observed at Pier 18 NB Column A after excavating the top of the pile cap for PS testing. Overall, GPR performed reasonably well in characterizing some key features of the pile cap geometry at GR3. Further refinement of the 250 MHz results using

migration techniques could slightly decrease the uncertainty in the pile cap edges for that survey direction. This illustrates the need to select proper operating frequencies for the antennas so that the highest quality data is collected for each scan. In this case, use of the 500 MHz antenna resulted in poor data quality and limited depth of radar wave penetration along the perpendicular survey line, which was why the 250 MHz antenna was favored. The likely culprit for the 500 MHz antenna was surficial clayey soils (e.g. leftover bentonite drilling mud) which are highly conductive and decrease radar signals.

6.3 PREDICTION OF FOUNDATION CHARACTERISTICS

Based on analysis of all the acquired data, it was possible to generate predictions of some of the characteristics of the foundations at both BR0 and GR3. Whenever possible, conservative estimates were made based on the limited availability of data.

6.3.1 BETSY ROSS BRIDGE INTERSTATE 95 (BR0) TEST SITE

Table 6-1 summarizes the predicted foundation dimensions at BR0 from each of the methods utilized in this study. Unfortunately, difficult drilling conditions forced drilling operations to be terminated prior to the desired depth at BR0. As a result, none of the subsurface methods were truly capable of estimating the location of the foundation bottom at BR0. However, conservative estimates (i.e. likely shorter predictions) were made based on the results of BHR [11 m (36 ft)] and BM [11.5 m (37.7 ft)]. ERI was also capable of making a similar estimate [15 m (49 ft)] based on the confidence level of the inversion performed to generate the 2D cross section in Fig. 6-15. GPR was capable of providing the clearest estimate of the depth to the pile cap [2.45 m – 2.8 m (8 ft – 9.2 ft)], though some agreement can be noted with this estimate and the location inferred in the 2D ERI cross sections in Figs. 6-14 and 6-15. Finally, GPR provided estimates for the lateral extent of the foundation [8 m (26.2 ft) by 8.5 m (27.9 ft)] that were relatively reasonable given the foundation design plans. ERI results also were capable of providing a rough estimate of the lateral extent of the foundation, though not as sharply defined as GPR. No useful information regarding foundation dimensions were obtained using PS testing. P-wave testing showed reflections from likely pile elements, but was too inconsistent to make any accurate predictions of foundation characteristics. Therefore, based on all the available information it is predicted (trivially, of course) that the depth to the bottom of the foundation at BR0 must be at least 15 m.

6.3.2 GIRARD AVENUE INTERSTATE 95 (GR3) TEST SITE

Table 6-2 summarizes the foundation dimension predictions at GR3. The information obtained from GR3 proved just as difficult to interpret as BR0. At GR3 it was assumed that the borehole extended deep enough beneath the target pile since coring of bedrock material was performed for approximately 1.5 m (5 ft) during borehole construction. However, given the large variation in bedrock location and engineering properties across a typical site in Pennsylvania, it is possible that a saprolite layer was reached rather than schist and that the piles were actually driven a little deeper than the bottom of the borehole. Nevertheless, BM estimated a depth to foundation bottom of 11 m (36 ft) (Table 6-2). This contradicted BHR, which showed no distinct foundation bottom and therefore yielded a conservative estimate of 13.6 m (45 ft) for the foundation bottom (i.e. at least as deep as the borehole). However, care must be exercised in interpreting the BHR data too strictly as the reflections may have come from other nearby foundations. PS and P-wave testing provided no meaningful additional information. Issues with noise in the ERI data led to a conservative estimate of 10 m (33 ft) for the length of the GR3 foundations. Together with the subsurface test methods, the depth to the foundation bottom at GR3 can be predicted to be 11 m (36 ft). GPR provided estimates of the lateral extent of the foundation (i.e. Pier 18 NB Column B which is assumed the same as Pier 17 NB Column A) at GR3. The overall dimension was interpreted to be 5 m (16.4 ft) by 3 m (9.8 ft) and it was estimated that the pile cap was embedded at approximately 0.2 m – 0.25 m (0.7 ft – 0.8 ft) below the ground surface.

6.4 CONCLUDING REMARKS

In many ways, the sites selected for this testing proved to be extremely difficult from the viewpoint of geophysical and NDT techniques. Seismic and electro-magnetic methods were impacted by the strong noise levels, variable soil conditions caused issues with radar waves, and the presence of several other foundations as well as embedded utilities made data interpretation difficult. It is evident that relying on a single NDT method as a panacea for the issue of unknown foundations is not a recommended approach. Moreover, multiple items need to be addressed for the ultrasonic P-wave system before it can be recommended for future long term implementation as an unknown foundation NDT tool. Potential improvements include the use of omni-directional transducers to diminish the highly directional nature of the current

transducers. Other improvements include a pulser rated for higher power so that the source transducer is excited with higher energy and inputs that more effectively into the domain of interest. If possible, a mudded open borehole should be tested to note the effects on signal amplitude. However, despite these shortcomings with the P-wave system and the lack of consistent agreement with the various NDT methods, a lot of high quality data was generated and each of the methods was carefully vetted in order to provide PennDOT engineers guidance for evaluation of unknown foundations given the current state-of-the-art and state-of-practice. Such feedback is provided in Chapter 7 of this report.

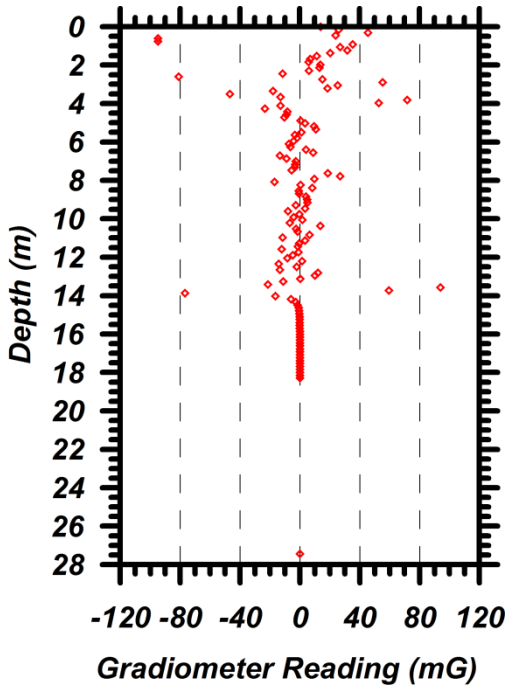

Figure 6-6: BM test results from AMB test site.

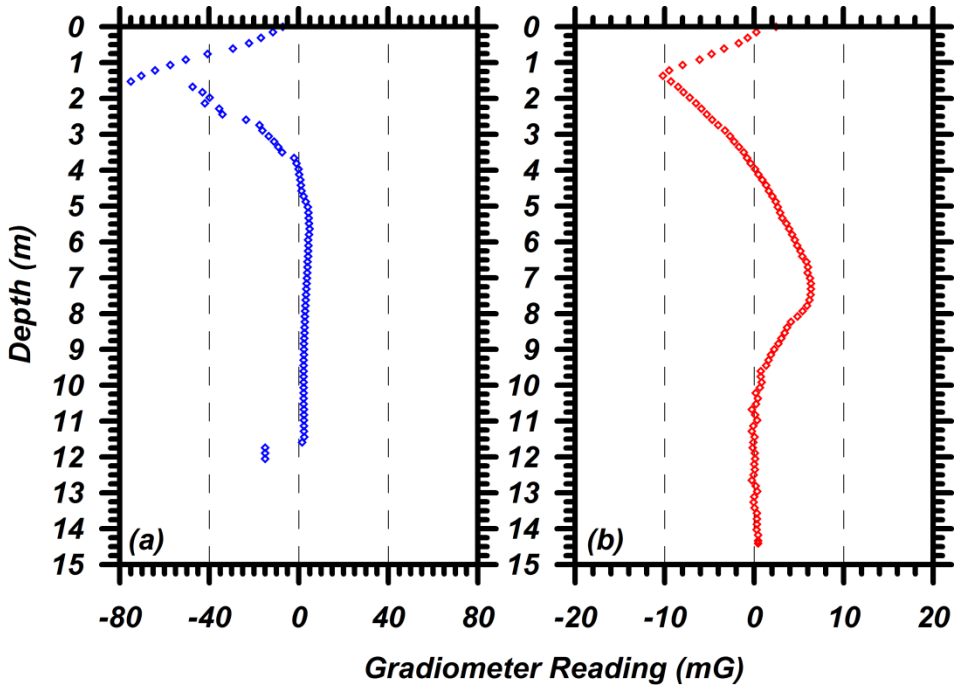

Figure 6-2: BM test results: (a) BR0; and (b) GR3.

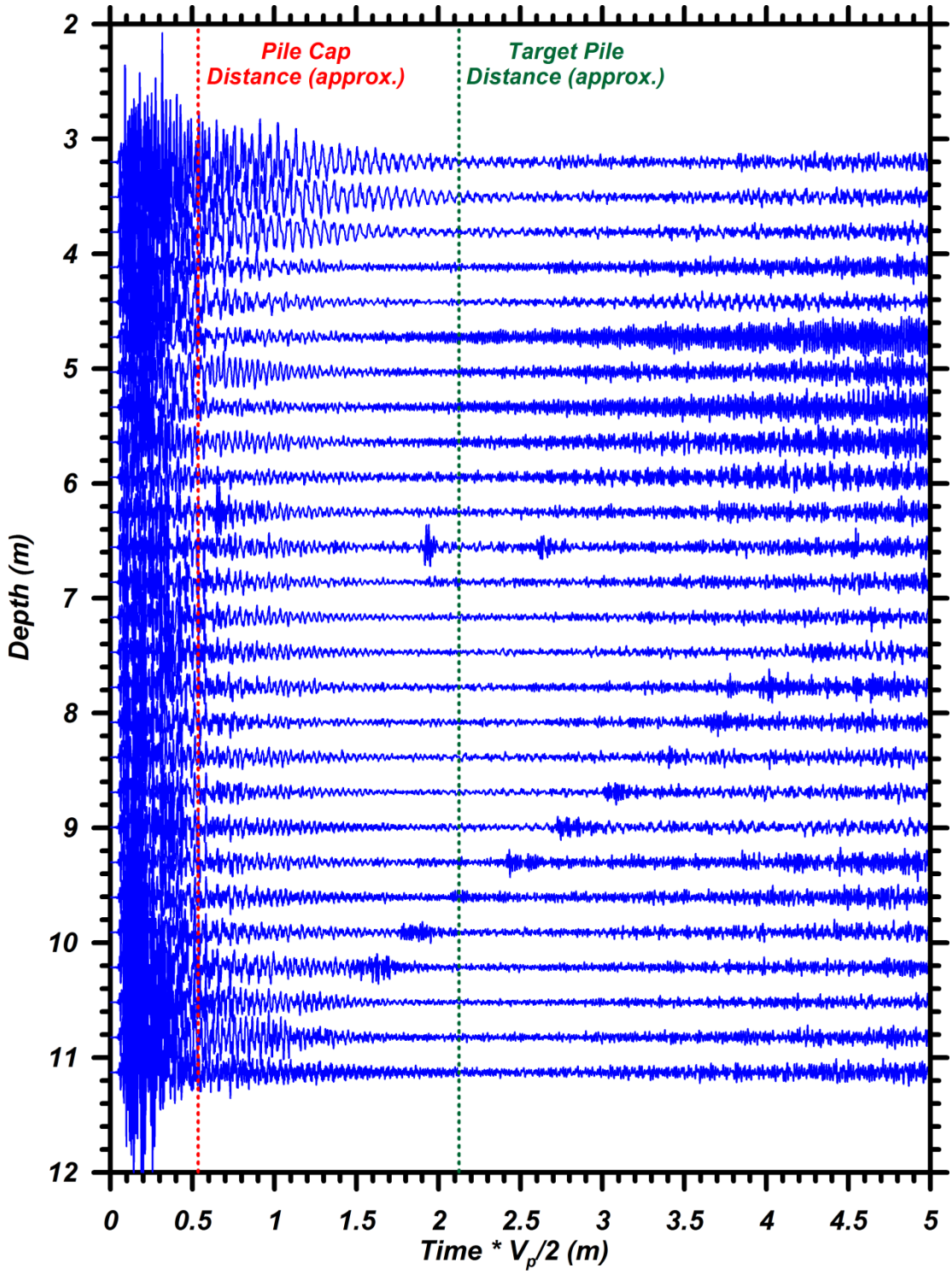

Figure 6-3: BR0 Ultrasonic P-wave test results

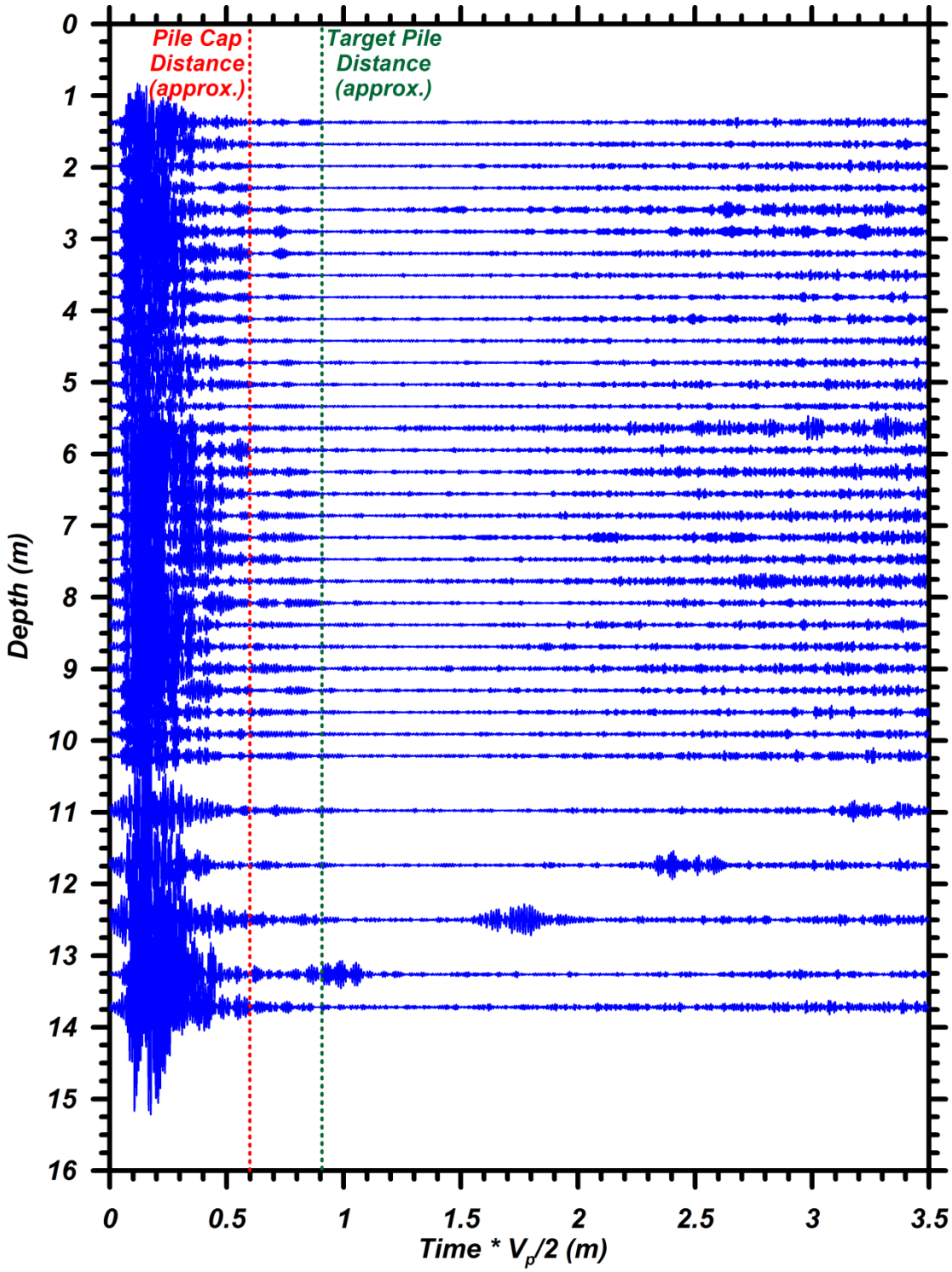

Figure 6-4: GR3 Ultrasonic P-wave test results.

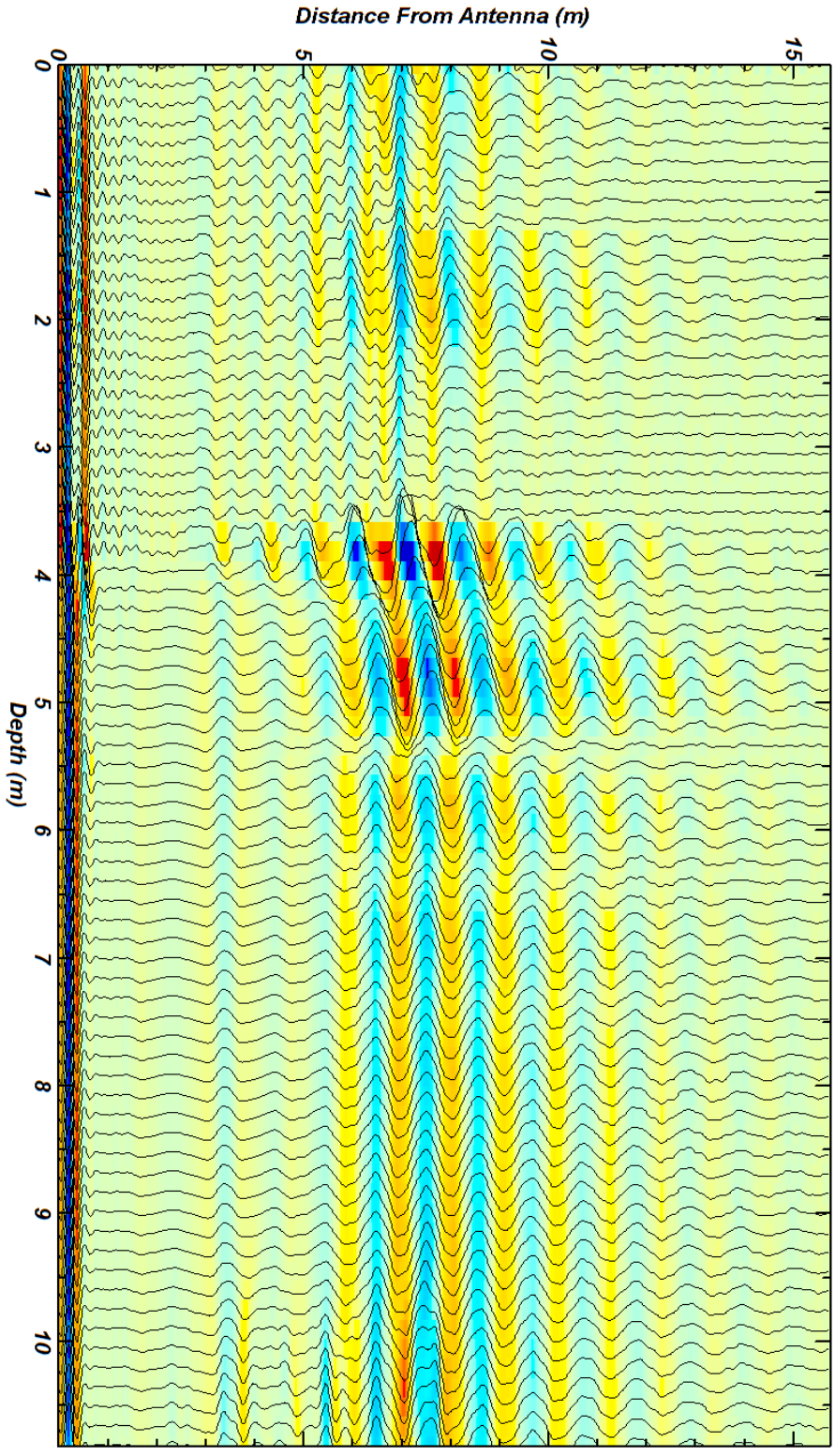

Figure 6-5: BR0 BHR test results.

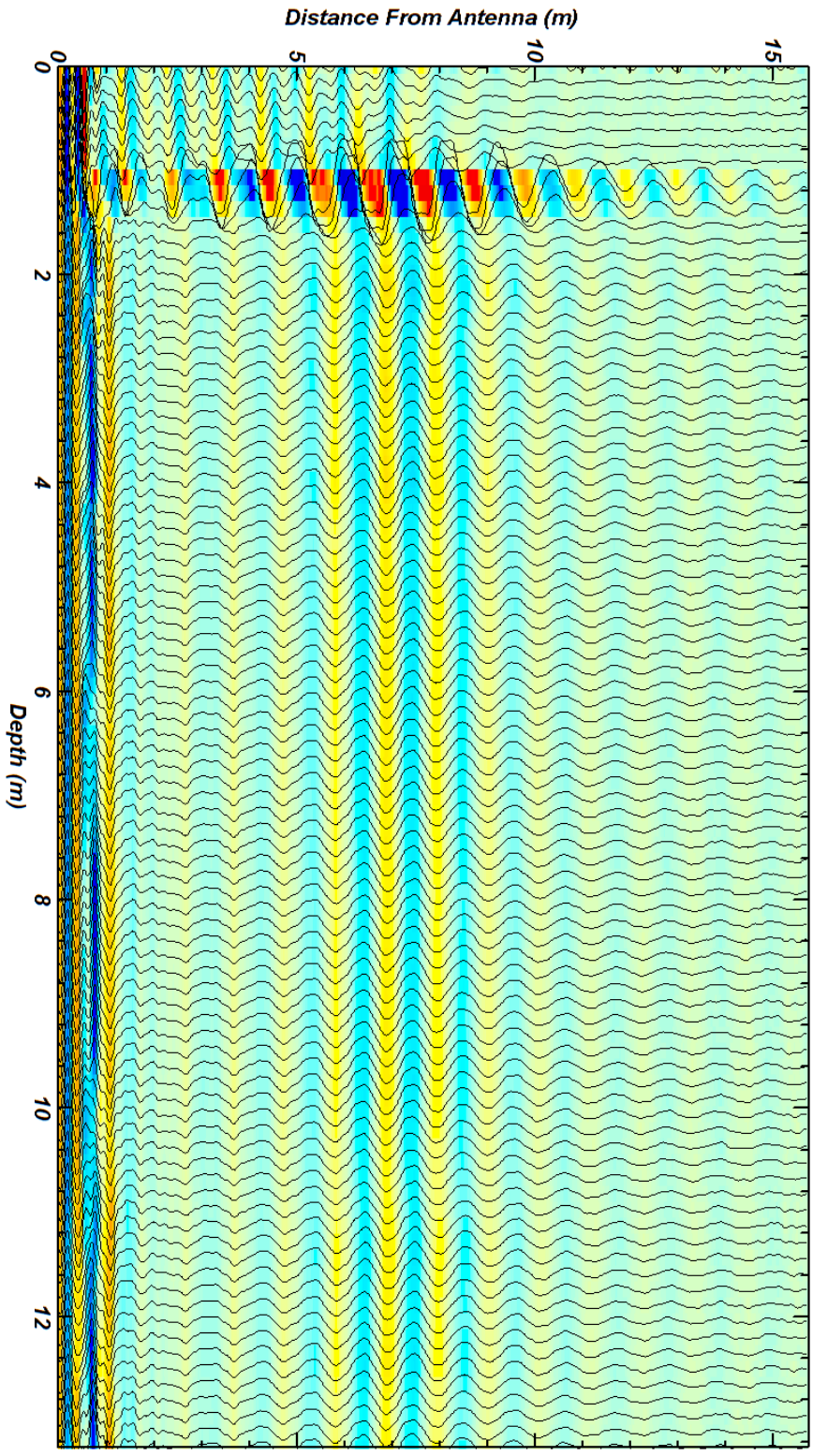

Figure 6-6: GR3 BHR test results.

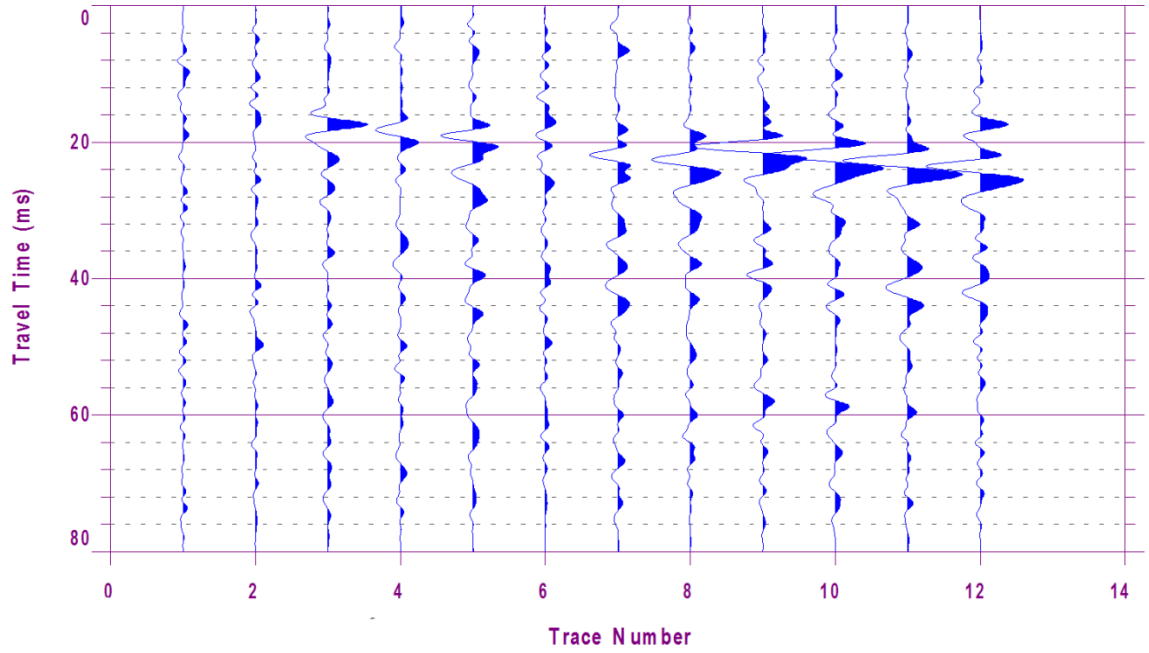

Figure 6-7: Seismic traces from testing at AMB.

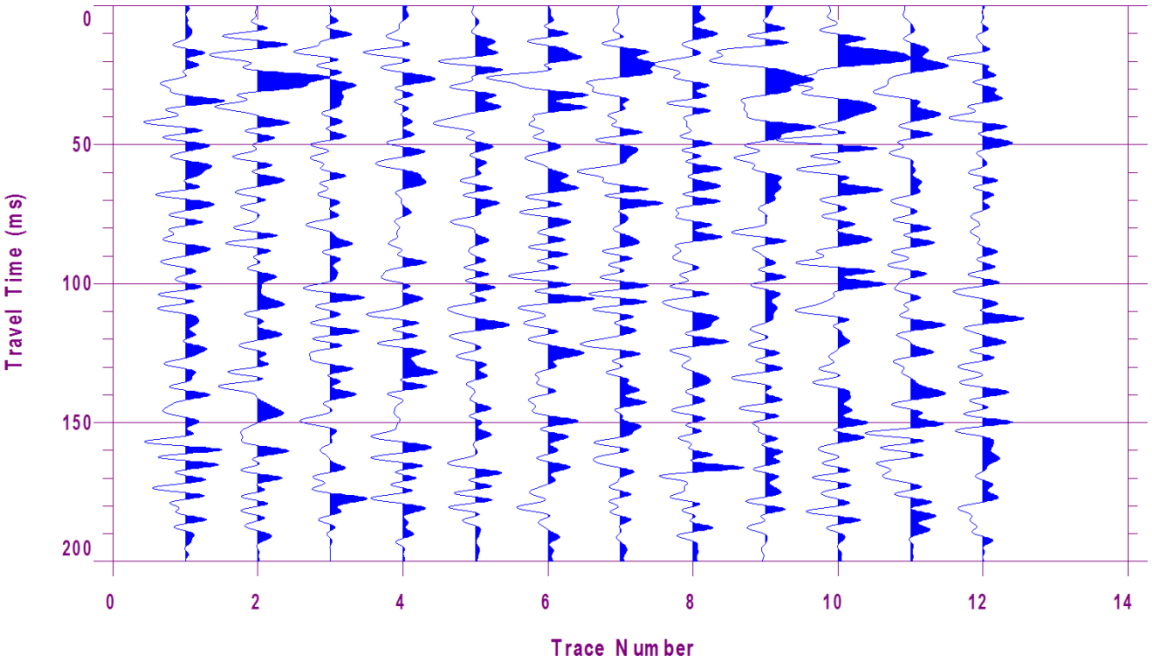

Figure 6-8: Seismic traces from direct impacts to pier column at BR0. 10 – 250 Hz

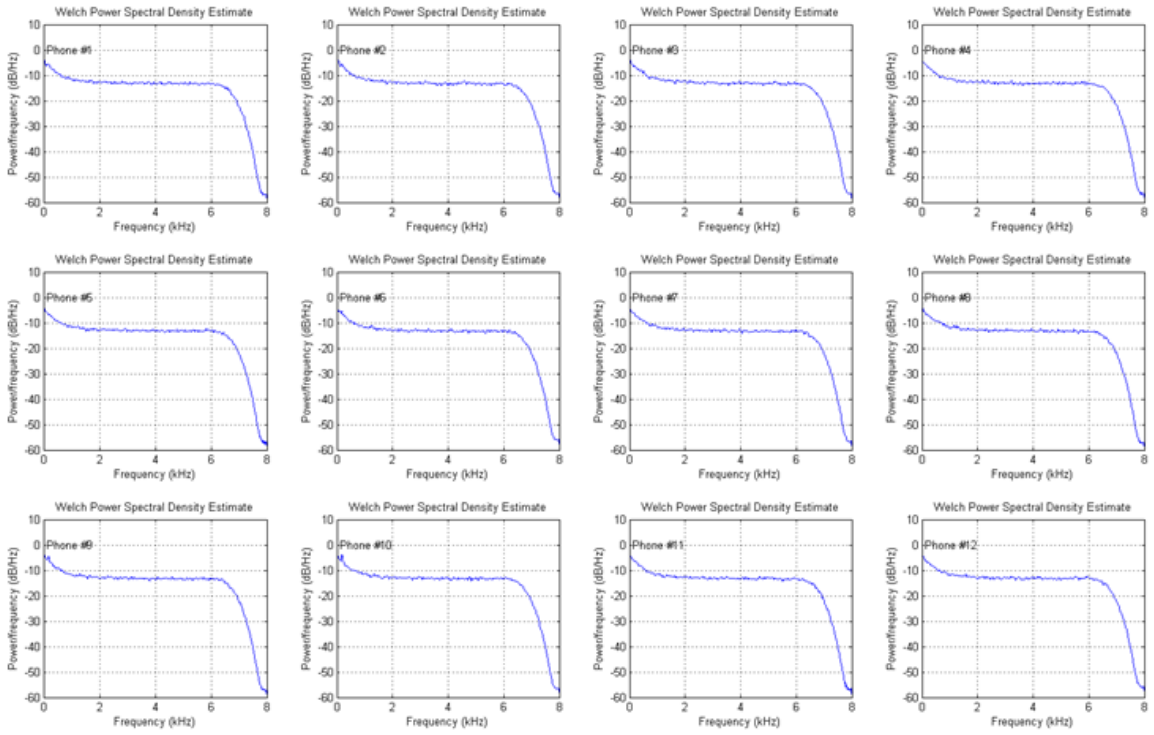

Figure 6-9: Comparison of individual hydrophone Welch's power spectrum for passive noise seismic traces acquired at BR0.

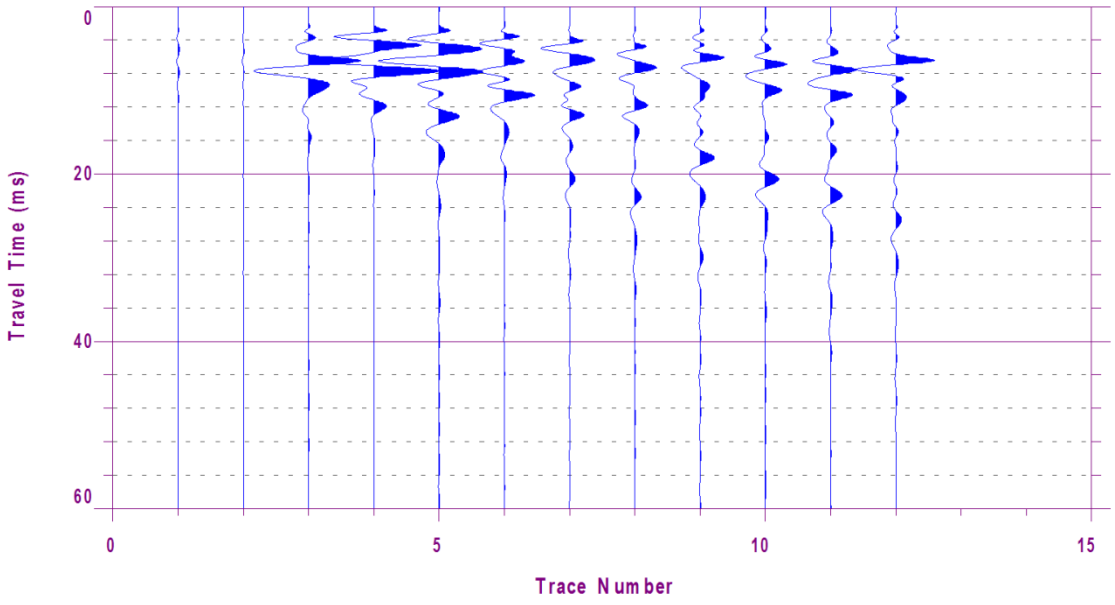

Figure 6-10: Seismic traces from direct impacts to PVC at GR3. 200 – 500 Hz

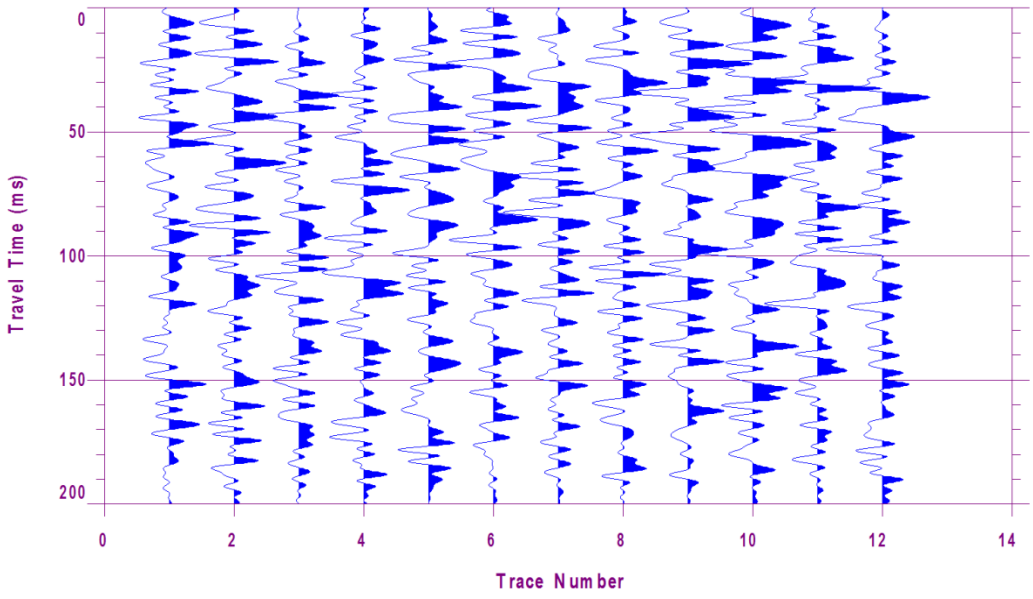

Figure 6-11: Seismic traces from direct impacts to pile cap at GR3. 10 – 250 Hz

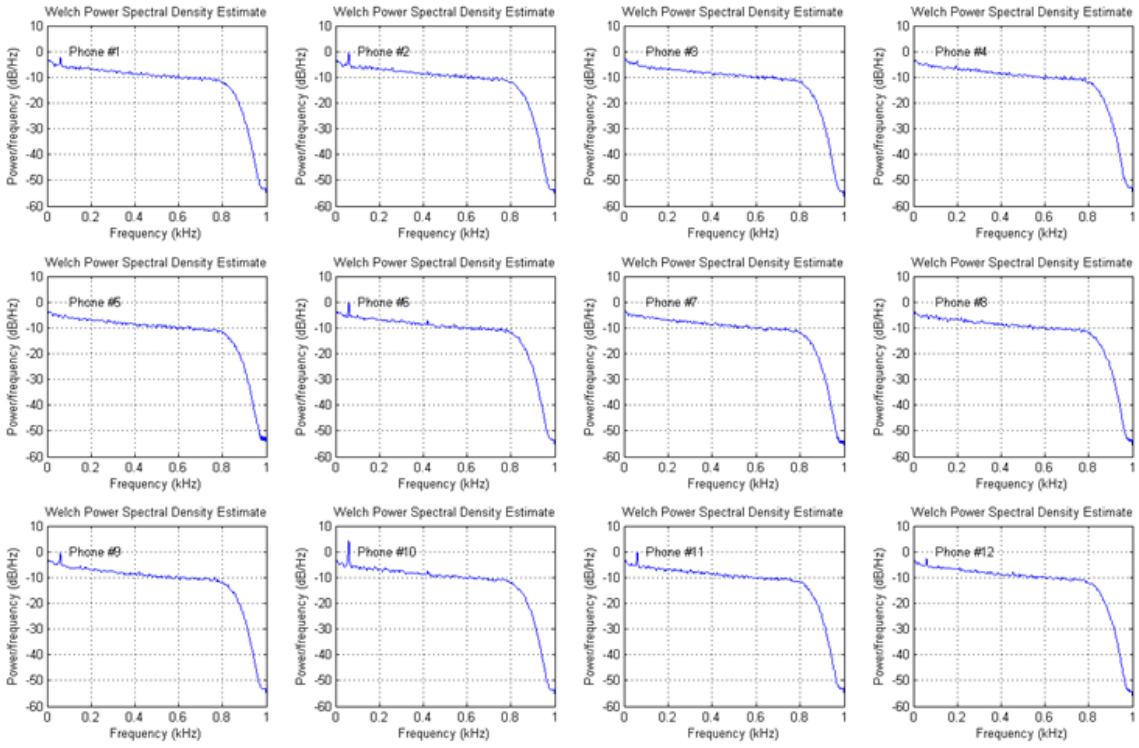

Figure 6-12: Comparison of individual hydrophone Welch's power spectrum for passive noise seismic traces acquired at GR3.

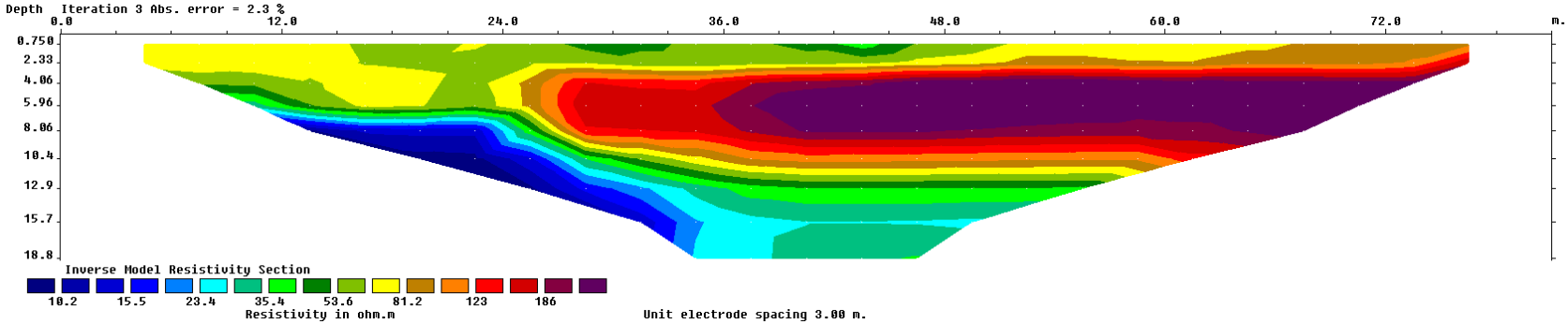

Figure 6-13: ERI-2D image for test at AMB.

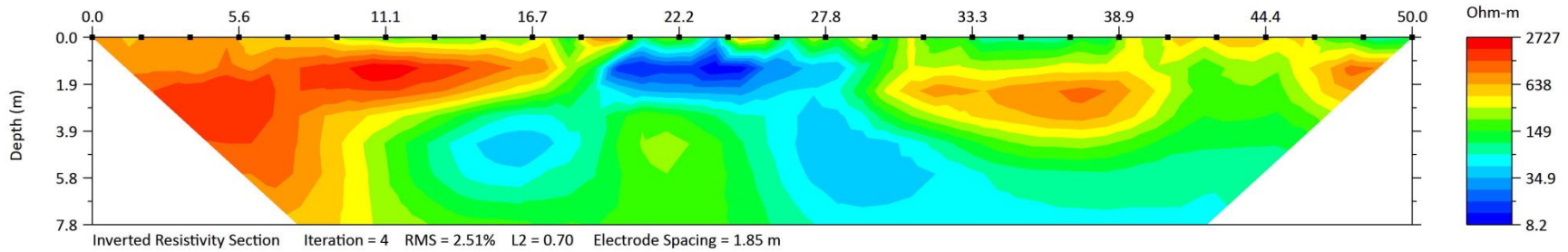

Figure 6-14: ERI-2D image for survey line parallel to pier cap at BR0.

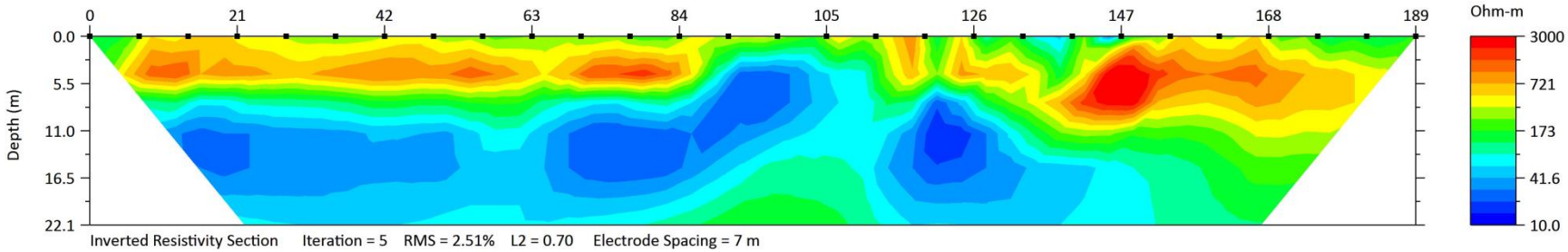

Figure 6-15: ERI-2D image for survey line approaching perpendicular to pier cap at BR0.

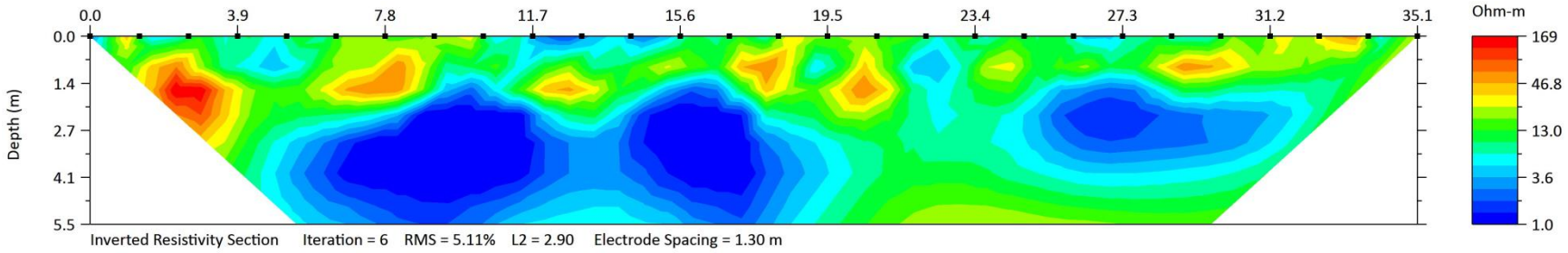

Figure 6-16: ERI-2D image for survey line parallel to pier cap at GR3.

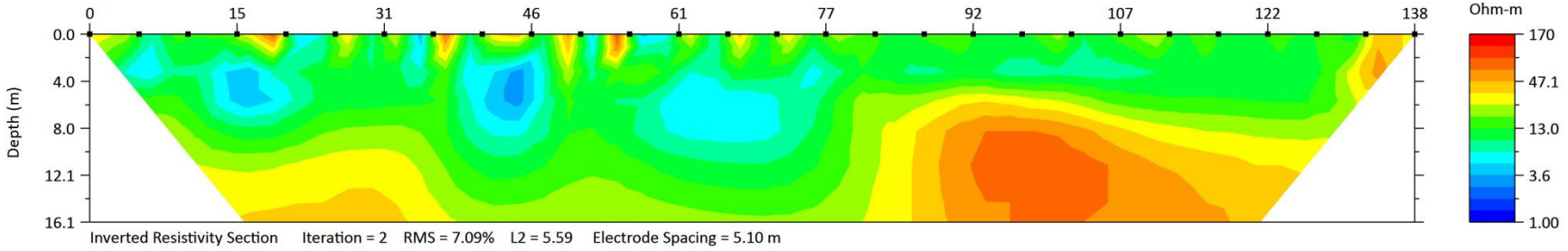

Figure 6-17: ERI-2D image for survey line perpendicular to pier cap at GR3.

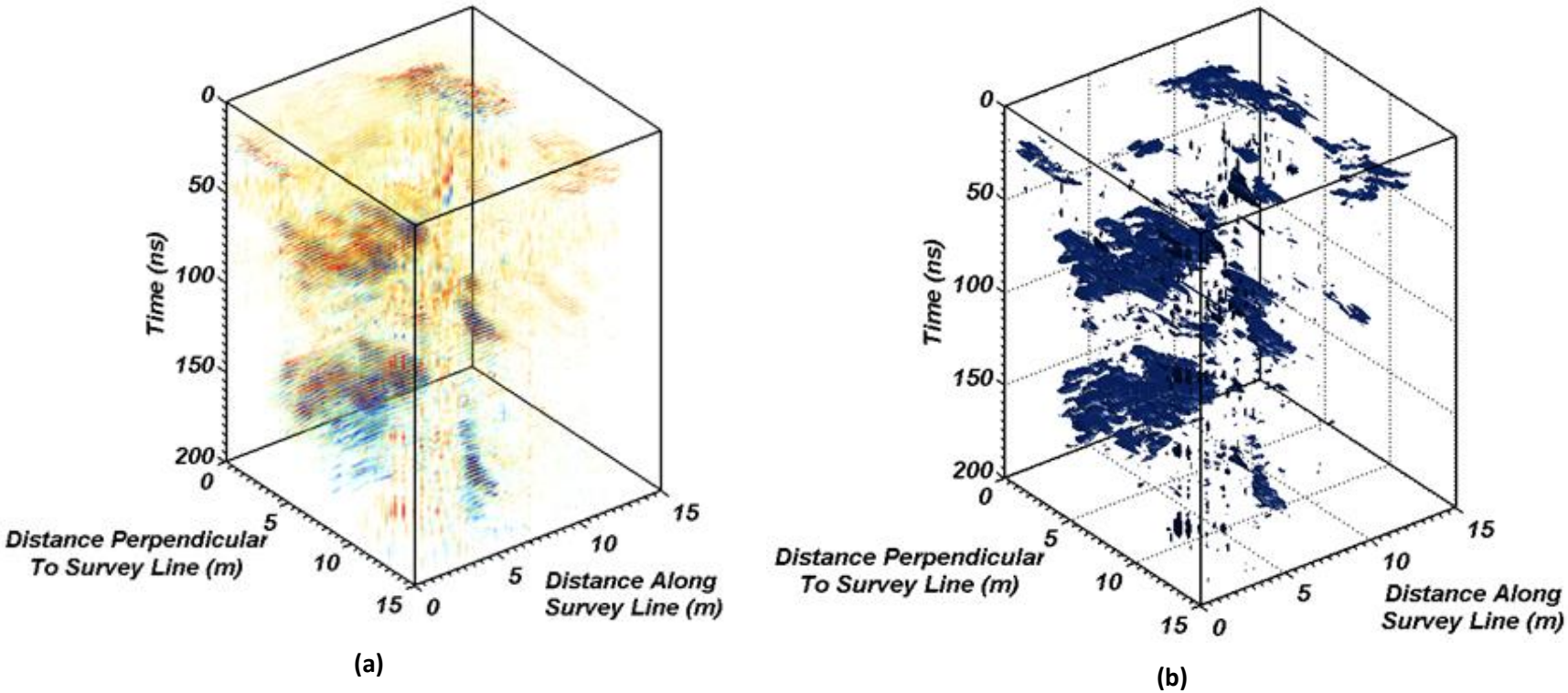

Figure 6-18: 3D GPR image of BR0 foundation: (a) 3D slices; and (b) Isosurface display (i.e. surfaces of equal signal amplitude).

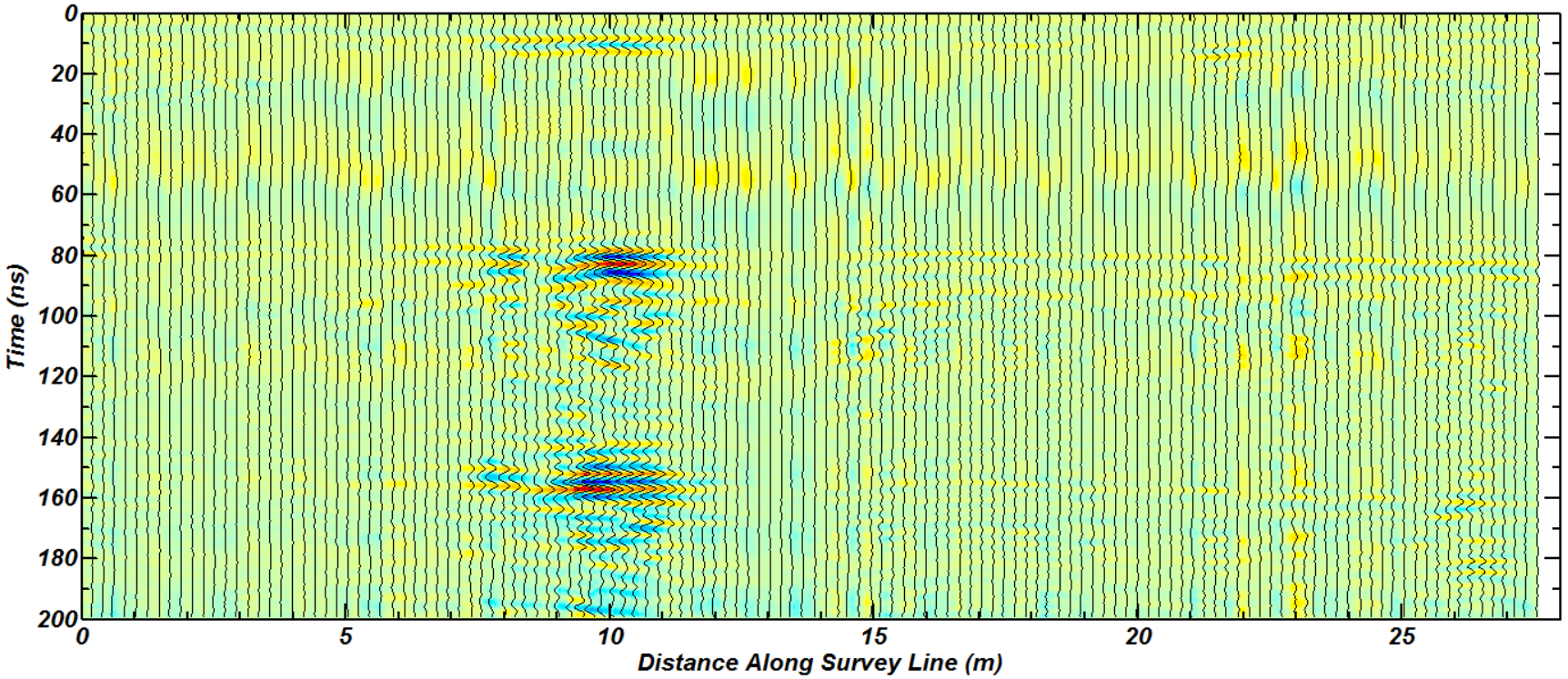

Figure 6-19: 2D GPR scan along line perpendicular to pier cap (i.e. parallel to direction of traffic on overhead ramp) at BR0.

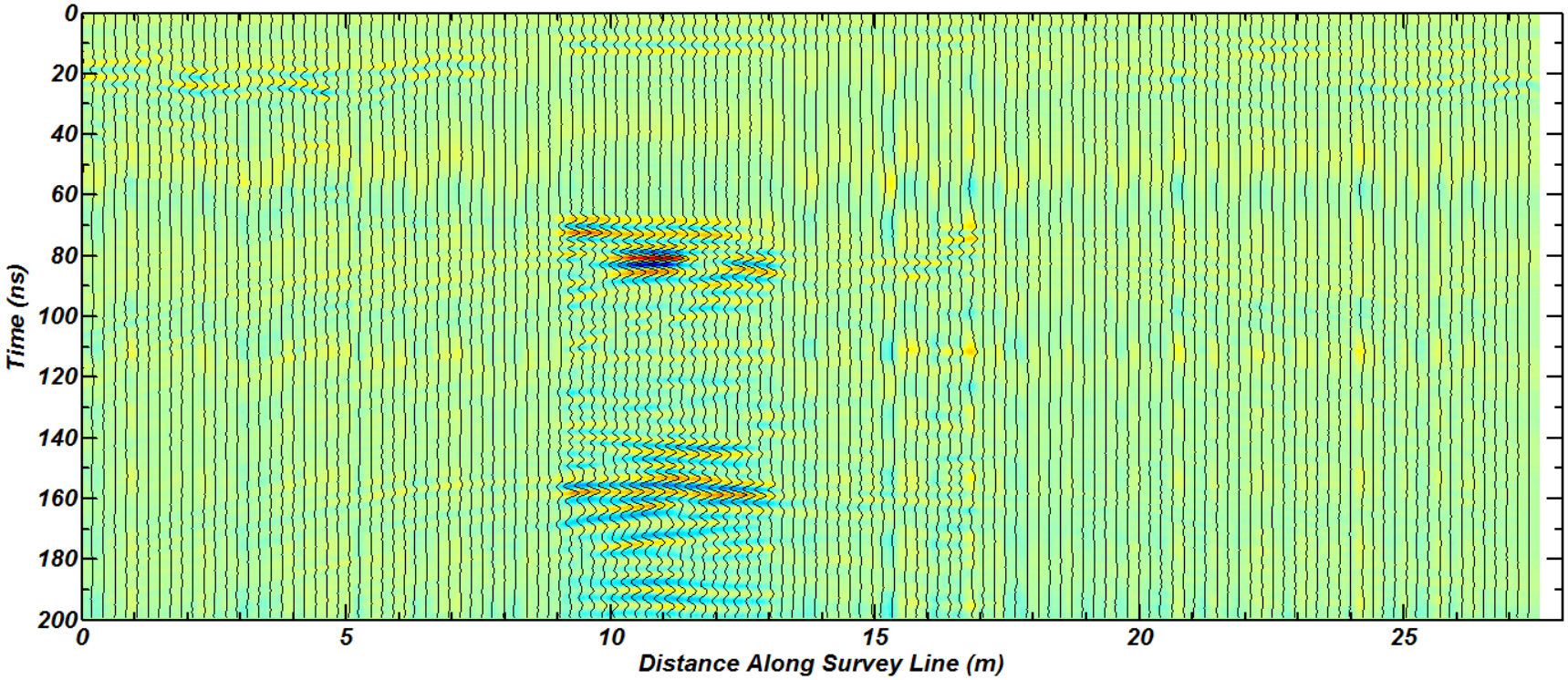

Figure 6-20: 2D GPR scan along line parallel to pier cap (i.e. perpendicular to direction of traffic on overhead ramp) at BR0.

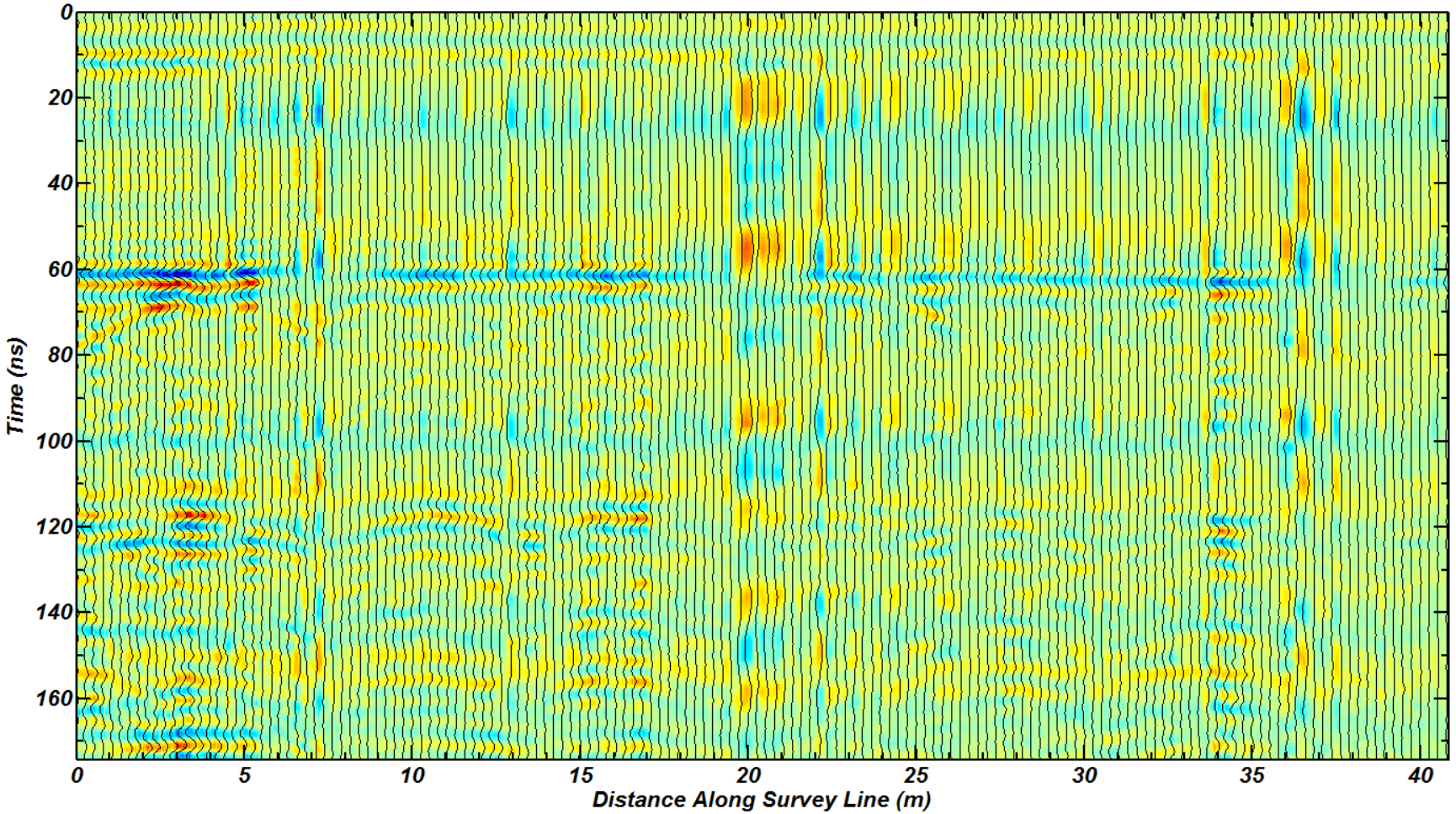

Figure 6-21: 2D GPR scan along line perpendicular to pier cap (i.e. parallel to direction of traffic on overhead ramp) at GR3.

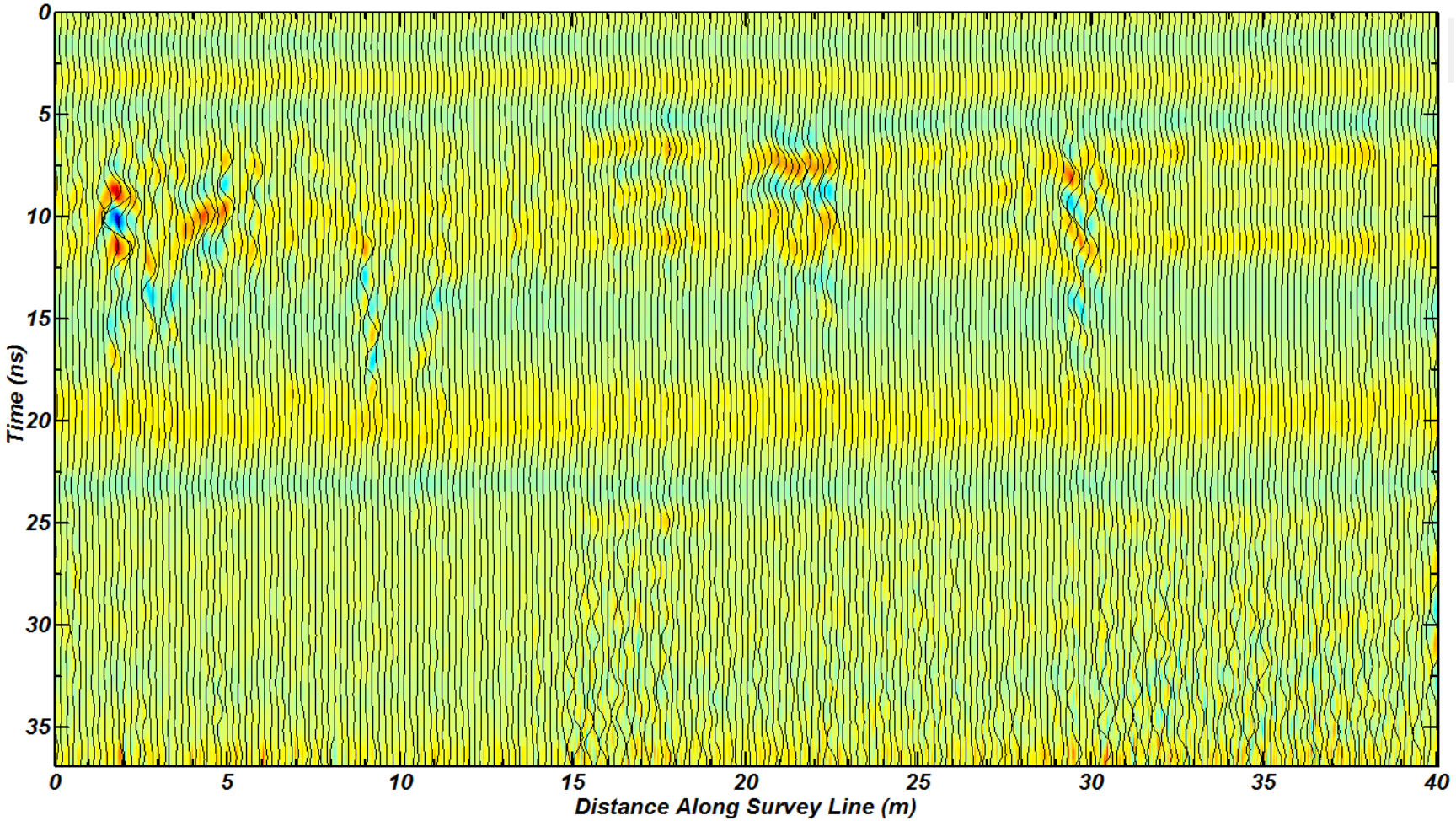

Figure 6-22: 2D GPR scan along line parallel to pier cap (i.e. perpendicular to direction of traffic on overhead ramp) at GR3.

Betsy Ross (BR0) Test Site				
Method	***Depth to Foundation Bottom***	***Depth to Pile Cap***		***Dimensions of Pile Cap***
BM	> 11.5 m (> 38 ft)	Top: Bottom:	N/S	N/A
Ultrasonic P-wave	N/S	Top: Bottom:	N/S	N/A
BHR	> 11 m (> 36 ft)	Top: Bottom:	N/S 4.0 m (13 ft)	N/A
PS	N/S	Top: Bottom:	N/S	N/A
ERI	> 15 m (> 49 ft)	Top: Bottom:	1.0 m (3 ft) 3.0 m (10 ft)	7.4 m x 7 m (24 ft x 23 ft)
GPR	N/A	Top: Bottom:	2.45 m – 2.8 m (8 ft – 9 ft) N/A	8 m x 8.5 m (26 ft x 28 ft)

Note: N/S = Unsuccessful; N/A = Not Applicable

Table 6-1: Summary of foundation dimension estimates based on field testing at BR0.

Girard (GR3) Test Site				
Method	***Depth to Foundation Bottom***	***Depth to Pile Cap***		***Dimensions of Pile Cap***
BM	11 m (36 ft)	Top: Bottom:	N/S	N/A
Ultrasonic P-wave	N/S	Top: Bottom:	N/S	N/A
BHR	> 13.6 m (> 45 ft)	Top: Bottom:	N/S 1.6 m (5 ft)	N/A
PS	N/S	Top: Bottom:	N/S	N/A
ERI	> 10 m (> 33 ft)	Top: Bottom:	N/S	N/S
GPR	N/A	Top: Bottom:	0.2 m – 0.25 m (0.7 ft – 0.8 ft) N/A	5 m x 3 m (16 ft x 10 ft)

Note: N/S = Unsuccessful; N/A = Not Applicable

Table 6-2: Summary of foundation dimension estimates based on field testing at GR3.

7. APPLICATION OF RESEARCH RESULTS TO DISTRICT 6 BRIDGES WITH UNKNOWN FOUNDATIONS

The results obtained from field testing in TEM002 contain a wealth of information regarding various Non-Destructive Testing (NDT) approaches to the unknown foundation issue. The following sections provide feedback and guidelines for a practical, methodical approach to evaluate unknown foundations based on these field results. The document will focus primarily on PennDOT District 6-0, but many of the findings and discussions will be equally applicable to various districts spread out throughout the Commonwealth of Pennsylvania.

7.1 PENNSYLVANIA DEPARTMENT OF TRANSPORTATION (PENNDOT) DISTRICT 6-0

PennDOT District 6-0 is one of eleven regional engineering districts in the Commonwealth of Pennsylvania. It is home to the greater Philadelphia metropolitan region and over three million people in Bucks, Montgomery, Chester, and Delaware counties and the city of Philadelphia (Fig. 7-1). The district office is located in King of Prussia, PA in Montgomery county. District 6-0 is responsible for 3,600 roadway miles and 2,800 bridges in the region. As home to the city of Philadelphia and the surrounding areas, many of the issues faced by District 6-0 are unique to the transportation needs of a large area comprised of a highly urbanized city core and wide range of transportation infrastructure. The following discussions regarding the work performed in TEM002 will relate to this aspect of District 6-0, particularly in relation to applicability of various NDT methods for evaluation of unknown foundations.

7.1.1 UNKNOWN BRIDGE FOUNDATIONS IN DISTRICT 6-0

Based on information provided by District 6-0, there are 31,645 bridges in the Commonwealth of Pennsylvania (Abboud and Kaiser 2012). Of these bridges 27,036 are located over water and 11,409 are considered scour critical. Of the scour critical bridges, 11,201 have insufficient information regarding bridge substructure and can be classified as unknown foundation bridges. For example, in District 6-0 there are 1,087 bridges with unknown foundations (325 in Bucks county, 339 in Chester County, 268 in Montgomery County, and 28 in Philadelphia County) (Abboud and Kaiser 2012). Thus unknown foundation bridges pose a significant concern for PennDOT in light of the FHWA policies to treat unknown foundations as scour critical.

7.2 DISCUSSION OF RESEARCH RESULTS

The issue of unknown foundations and scour vulnerability of bridges in District 6-0 formed the motivation for this research project. The main purpose of TEM002 was to examine an innovative NDT method (ultrasound P-wave) developed by the PI to visualize embedded structural elements and to compare its performance in evaluating unknown foundations against other available NDT methods. The comparison to other NDT methods based on field testing was a critical aspect of the research which served two purposes: (1) validation of new innovative method against current state-of-practice; and (2) development of guidelines for PennDOT District 6-0 regarding use of various NDT methods based on their field performance. Prior to field work with the system, it was subjected to a suite of laboratory tests to ensure adequate behavior for the field studies.

Overall, the field work demonstrated the potential applicability of the ultrasound P-wave system to unknown foundations. Though still under development, the P-wave system proved capable of reflecting off interfaces as far away as 2 m. However, much work must be initiated if the system is to be implemented more fully because the conditions under which the system can provide high quality data are extremely limited. Three other subsurface NDT methods were employed in the field, including Parallel Seismic (PS), Borehole Magnetometer (BM), and Borehole Radar (BHR). Of these methods, PS proved the least useful due to the high traffic noise. BM and BHR provided more promising results. BM proved to be the most straightforward of the tests with highly reproducible results. BHR was capable of imaging foundations that were much farther than the one immediately adjacent to the PVC-cased borehole. Surface methods were also performed in the field. Ground Penetrating Radar was examined as a supplemental method to determine the lateral dimensions of a footing prior to the implementation of subsurface methods. GPR provided estimates of the foundation dimensions that were reasonable but not as accurate as had been anticipated. Finally, ERI showed tremendous promise as the only surface method that proved capable of imaging the deep into the subsurface below the pile cap. Based on these field test results, the foundation dimensions and depth were estimated.

7.3 RECOMMENDATIONS REGARDING NDT FOR UNKNOWN BRIDGE FOUNDATIONS IN DISTRICT 6-0

Based on the results from field testing, it was clear that certain methods were better suited for the field conditions typically encountered in District 6-0. The following sections provide a more detailed discussion of which NDT methods are recommended for unknown foundation field investigations in District 6-0 and the rationale for their selection. These recommendations are summarized in Table 7-1.

7.3.1 Suitability of Selected NDT Methods

The most problematic of the field methods implemented in TEM002 proved to be PS. P-wave had its share of issues and was not fully successful. However, the ultrasound P-wave system is still in its infancy and under continual development. PS is a robust and well-established investigation method. The primary issue in this case was the amount of seismic noise present in the field. As a result, none of the seismic methods (PS, Sonic Echo, Ultraseismic, etc.) are suitable for the highly trafficked locations in District 6-0 unless there is direct contact to an individual pile element at the ground surface. Even in such cases, great care must be exercised to ensure an adequate number of stacks is utilized to improve signal to noise ratio.

If the foundation in question is known to contain metal (e. g. reinforced concrete, steel piles, etc.), BM proved highly suitable for this application. As the majority of deep foundations in District 6-0 contain steel (i.e. steel H-piles are very common), use of BM is highly recommended as an efficient approach to profile a potential unknown foundation.

BHR is recommended in situations where access to a given foundation is limited and a borehole must be drilled with a significant setback from the foundation to be tested. For example, in District 6-0 there are a number of seasonal or tidal waterways that have restrictions on access. In such cases, it may be more cost effective to consider placing the borehole in an area outside of the waterway. Note that the presence of clay soils will drastically reduce the signal amplitude since clay is highly conductive. It is not recommended to focus on any radar-based methods in soil profiles rich in clay content.

Based on the current revision of the hardware and software package, use of the ultrasound P-wave system is not recommended for field testing of an unknown foundation outside an academic research setting. The system is still undergoing revisions to improve its long term

robustness. Once some of the main issues are resolved, it is recommended that such a P-wave system be considered in lieu of other seismic systems because it will address the major shortcoming associated with seismic energy transfer. Since a large number of bridge sites in District 6-0 will be subjected to considerable seismic noise in the form of traffic, it is always necessary to ensure the maximum level of seismic energy is imparted across all boundaries to combat the seismic noise. By locating the seismic source in the same hole as the receiver, locations of seismic energy loss are avoided (e.g. pier column and pile cap junction) and it may still be possible to rely on the propagation of seismic waves to identify the foundation bottom. For soil profiles with considerable clays, seismic methods will likely be well-suited and radar waves should be avoided.

ERI proved to be a versatile test method able to detect foundation lengths even beneath pile caps. However, it may not be as well suited for District 6-0 where bridge sites are often sharing space with significant subsurface utilities, rail lines, and other substructure and surface units (e.g. trees, fences, guard rails, other roads, etc.). The large amount of space necessary to string out a line for deep ERI surveys combined with its susceptibility to electrical noise make for a frustrating experience in losing deeper data points prior to inversion. One way to avoid this is to utilize a high power external transmitter to drive more current into the ground during ERI testing.

Finally, GPR is not recommended for clayey profiles. Moreover, radar waves run into similar issues with embedded utilities which can be a concern at District 6-0 bridge sites. However, GPR was able to provide a reasonably accurate picture of the subsurface and estimate of the pile cap dimensions at the selected field sites. The importance of this method increases if there are truly no foundation plans available and the goal is to construct boreholes that run immediately adjacent to an unknown foundation to perform subsurface testing.

7.3.2 Implementation of Research Results

Given the preceding discussion of suitable testing techniques, the following suggestions discuss ways to implement the results of TEM002 across District 6-0 and the broader PennDOT community:

1. The lessons learned from the field work in TEM002 and the previous discussion on suitable NDT methods can be utilized to develop a series of guidelines to inform bridge engineers about the potential issues related to unknown foundation NDT techniques.
2. A short webinar can be developed which highlights the major findings of TEM002 and discusses the challenges of NDT field work for unknown foundations.

7.3.3 FUTURE WORK

There are a number of areas that can be explored to improve the suitability of many of the NDT methods utilized in this study and the quality of data obtained during testing. The following topics include ideas that may address some of the shortcomings of various methods attempted in TEM002 or to generally improve PennDOT's ability to evaluate unknown foundations:

1. The ultrasonic P-wave system should be redeveloped to address the issues that presented themselves during field testing in TEM002. For example, omni-directional transducer components should be explored as a viable means of introducing the p-wave energy. The directional nature of the current transducers simplifies data interpretation but decreases the ability of the system to record reflections from off-line targets. Other improvements include a pulser rated for higher power so that the source transducer is excited with higher energy and inputs that more effectively into the domain of interest. Finally, the P-wave system should be tested in a mudded open borehole to note the effects on signal amplitude.
2. Consideration should be given to studying traffic noise as a passive source of seismic energy that can be used to identify substructure behavior. For example, in Dynamic Foundation Response (DFR) accelerometers are attached throughout a bridge substructure and then impacts are generated to record seismic traces. With such high environmental noise at various District 6-0 sites, it may be possible to effectively harness this noise as a means of generating an appropriate input function to learn more information about the domain of interest. In addition, the PS method should be re-explored to study the potential for traffic noise to serve as a passive source for PS testing.
3. The continued use of ERI should be studied as a potential quick assessment for whether a foundation is deep or shallow. Moreover, ERI can be explored as a method to detect the corrosion potential for either unknown or known foundations.

4. The use of inferential methods should be explored as a means to quickly diminish the number of unknown foundation (and therefore scour critical) bridges from the PennDOT database. Reverse engineering and Artificial Neural Network methods have been previously utilized by others to develop region-specific models to estimate the length of unknown foundations with a reasonable degree of accuracy, all without any necessary field testing.

7.4 CONCLUDING REMARKS

The ultrasonic P-wave system studied in this project proved only partially successful in obtaining reflection signals from the target foundations at two test sites. There are still a few issues to address before it can serve as a viable NDT tool for unknown foundations. However, field testing also showed that even well-established methods such as PS and GPR are subject to potential site-specific issues that diminish their capabilities to resolve unknown foundations. Ultimately, the evaluation of an unknown foundation becomes challenging very quickly once variable site parameters are introduced. Only through careful research and systematic characterization of all the tools available will the evaluation of unknown foundations continue to improve. Research with the ultrasound P-wave system will continue to contribute to that improvement over time.

Figure 7-7: Map graphic of PennDOT District 6-0.

Method	*Confidence Level* [1]	*Expected Foundation Type*	*Expected Foundation Material*	*Recommended Soil Type*	*Water Table Depth*	*Site Access*	*Presence of Utilities*
BM	High	Piles	Steel	All	No Major Effect	Limited	Limited
Ultrasonic P-wave	Low	Shallow Footings, Piles, Drilled Shafts	Steel, Reinforced Concrete	Fine Sands, Clays	Shallow	Moderate	No Major Effect
BHR	Medium-High	Shallow Footings, Piles, Drilled Shafts	Steel, Reinforced Concrete	Sands	Deep	Limited	Limited
PS	Low [2]	Piles, Drilled Shafts	Steel, Reinforced Concrete, Timber	All	No Major Effect	Limited	No Major Effect
ERI	Medium	Shallow Footings, Piles, Drilled Shafts	Steel, Reinforced Concrete	Clays	Shallow	Extensive	Limited
GPR	Medium-Low	Shallow Footings	Steel, Reinforced Concrete	Sands	Deep	Moderate	Limited

[1] Confidence level reflects field studies in this project and may change depending on anticipated site conditions

[2] Confidence level increases to Medium-High if direct access to deep foundation element is possible

Table 7-1: Summary of recommendations regarding selection of NDT methods for unknown foundations based on field testing experiences in this project.

REFERENCES

Abboud, B., and Kaiser, S. (2012). “Selection and Design of Scour Countermeasures for Pennsylvania Bridges.” Report No. FHWA-PA-2012-001-TEM 001, The Pennsylvania Department of Transportation, Harrisburg, PA.

ACI Committee 228 (1998) “Nondestructive Test Methods for Evaluation of Concrete in Structures.” Report No. ACI 228.2R-98, American Concrete Institute (ACI), Farmington Hills, MI.

Aki, K. and Richards, P. G. (1980). Quantitative Seismology – Theory and Methods. Vols. 1 & 2, Freeman Company, San Francisco, CA.

American Society for Testing and Materials (ASTM) (2007). “Standard Test Method for Low Strain Impact Integrity Testing of Deep Foundations.” ASTM D5882-07, West Conshohocken, PA.

American Society for Testing and Materials (ASTM) (2007). “Standard Test Methods for Crosshole Seismic Testing.” ASTM D4428/D4428M-07, West Conshohocken, PA.

American Society for Testing and Materials (ASTM) (2008) “Standard Test Method for Integrity Testing of Concrete Deep Foundations by Ultrasonic Crosshole Testing.” ASTM D6760-08, West Conshohocken, PA.

Anderson, N.L., Ismael, A.M., and Thitimakorn, T. (2007). “Ground-Penetrating Radar: A Tool for Monitoring Bridge Scour.” Environmental & Engineering Geoscience, Vol. 13, No. 1, 1-10.

Arneson, L.A., Zevenbergen, L.W., Lagasse, P.F., and Clopper, P.E. (2012). “Evaluating Scour at Bridges," Hydraulic Engineering Circular No. 18, Fifth Edition, Publication No. FHWA-HIF-12-003, Federal Highway Administration, Washington, D.C.

Baker, B. B. (1987). The Mathematical Theory of Huygens' Principle. 3rd Ed. Ams Chelsea Publishing, New York, NY.

Bateni, S.M., Borghei, S.M., and Jeng, D.S. (2007). “Neural Network and Neuro-Fuzzy Assessments for Scour Depth around Bridge Piers.” Engineering Applications of Artificial Intelligence, Vol. 20, 401-414.

Beard, J. (2005). “NCDOT Unknown Bridge Foundations.” Proceedings of Federal Highway Administration 2005 Unknown Foundation Summit, Lakewood, CO.

Beattie, G. J. (1982). "Pile Length Determination - Induction Field Method." Technical Note 5-3, Works Consultancy Services, Central Laboratories, Lower Hutt, New Zealand.

Biot, M. A. (1956b). “Theory of Propagation of Elastic Waves in Fluid Saturated Porous Solid. II. High-Frequency Range.” Journal of the Acoustical Society of America, Vol. 28, No. 2, 179–191.

Bolt, B. A. (2002). Earthquakes. 4th Ed. W.H. Freeman and Company, New York, NY.

Bolton, R., Sikorsky, C., Park, S., Choi, S., and Stubbs, N. (2005). ”Modal Property Changes of a Seismically Damaged Concrete Bridge.” Journal of Bridge Engineering, Vol. 10, No. 4, 415–428.

Brandenberg, S. J., Kutter, B. L., and Wilson, D. W. (2008). "Fast Stacking and Phase Corrections of Shear Wave Signals in a Noisy Environment." Journal of Geotechnical & Geoenviromental Engineering, Vol. 134, No. 8, 1154-1165.

Briaud, J., Ballouz, M., and Nasr, G. (2002) “Defect And Length Predictions By NDT Methods For Nine Bored Piles.” Proceedings of the International Deep Foundations Congress 2002, Orlando, FL.

Briaud, J., Medina-Cetina, Z., Hurlebaus, S., Everett, T., Tucker, S., Yousefpour, N., and Arjwech, R. (2012). “Unknown Foundation Determination for Scour.” Report No. FHWA/TX-12/0-6604-1, Texas Department of Transportation, Austin, TX.

Butler, D. K. (ed.) (2005) Near Surface Geophysics. Society of Exploration Geophysicists, Tulsa, OK.

Cawley, P., and Adams, R.D. (1979). “The Location of Defects in Structures from Measurements of Natural Frequencies,” Journal of Strain Analysis, Vol. 4, No. 2, 49-57.

Coe, J. T. (2010). “Ultrasonic P-Wave Reflection Imaging of Laboratory Soil Models and Application to Deep Foundations in the Field.” Ph.D. Dissertation, University of California, Los Angeles, CA.

Coe, J. T. and Brandenberg, S. J. (2010). “P-wave Reflection Imaging of Submerged Soil Models Using Ultrasound.” Journal of Geotechnical & Geoenviromental Engineering, Vol. 136, No. 10, 1358-1367.

Coe, J.T. and Brandenberg, S.J. (2012). “Cone Penetration Test–Based Ultrasonic Probe for P-Wave Reflection Imaging of Embedded Objects.” Journal of Bridge Engineering, Vol. 17, No. 6, 940-950.

Comina, C., Foti, S., Boiero, D. and Socco, L.V. (2011). “Reliability of VS,30 Evaluation From Surface-Wave Tests.” Journal of Geotechnical and Geoenvironmental Engineering, Vol. 137, No. 6, 579-586.

Deng, L. and Cai, C.S. (2010). “Bridge Scour: Prediction, Modeling, Monitoring, and Countermeasures – Review.” Practice Periodical on Structural Design and Construction, Vol. 15, No. 2, 125-134.

Descour, J.M., and Kabir, J.J. (2010). “Imaging Piles in Bridge Foundations Using Tomography and Horizontal Seismic Reflector Tracing.” Proceedings Geo-Florida 2010, West Palm Beach, FL.

DeWolf, J., Bagdasarian, D.A., and O’Leary, P.N. (1992). “Bridge Condition Assessment Using Signatures.” Nondestructive Evaluation of Civil Structures and Materials Conference, Boulder, CO.

Doll, H. G. (1949). “Introduction to Induction Logging and Application to Logging of Wells Drilled With Oil Based Mud.” Journal of Petroleum Technology, Vol. 1, No. 6, 148-162.

Douglas, R.A., and Holt, J.D. (1994). “Determining Length of Installed Timber Pilings by Dispersive Wave Propagation Methods.” North Carolina State University Center for Transportation Engineering Studies, North Carolina Department of Transportation, Federal Highway Administration, Washington, D.C.

Douglass, S.L. and Krolak, J. (2008). "Highways in the Coastal Environment," Hydraulic Engineering Circular No. 25, Second Edition, Publication No. FHWA-NHI-07-096, Federal Highway Administration, Washington, D.C.

Farid, A., Martinez-Lorenzo, J.A., Alshawabkeh, A.N., and Rappaport, C.M. (2012). “Experimental Validation of a Numerical Forward Model for Tunnel Detection Using Cross-Borehole Radar.” Journal of Geotechnical and Geoenvironmental Engineering, Vol. 138, No. 12, 1537-1541.

Federal Highway Administration (1988). "Scour at Bridges." Technical Advisory T5140.20, updated by Technical Advisory T5140.23, October 28, 1991, "Evaluating Scour at Bridges." U.S. Department of Transportation, Washington, D.C.

Federal Highway Administration (1995). "Recording and Coding Guide for the Structure Inventory and Appraisal of the Nation's Bridges.” Report No. FHWA-PD-96-001, U.S. Department of Transportation, Washington, D.C.

Federal Highway Administration (2004). "National Bridge Inspection Standards." Federal Register, Volume 69, No. 239, 23CFR Part 650, FHWA Docket No. FHWA-2001-8954, Final Rule, December 14, 2004, effective January 13, 2005, U.S. Department of Transportation, Washington, D.C.

Finno, R.J. and Gassman, S.L. (1998). "Impulse Response Evaluation of Drilled Shafts," Journal of Geotechnical Engineering, Vol. 124, No. 10, 965-975.

Gee, K.W. (2008) "ACTION: Technical Guidance for Bridges over Waterways with Unknown Foundations." Technical Guidance for Bridges over Waterways with Unknown Foundations - Policy & Memos - Scour - FHWA. Web. 01 February 2013. <http://www.fhwa.dot.gov/engineering/hydraulics/policymemo/20080109.cfm>.

Geo-Institute (GI) Deep Foundations Committee Task Force (2000) “Nondestructive Evaluation of Drilled Shafts.” Journal of Geotechnical and Geoenvironmental Engineering, Vol. 126, No. 1, 92-95.

Gomm, T. J. and Mauseth, J. A. (1999) “State of the Technology: Ultrasonic Tomography.” Materials Evaluation, Vol. 57, No. 7, 747-752.

Grandjean, G. (2006). "A Seismic Multi-Approach Method for Characterizing Contaminated Sites." Journal of Applied Geophysics, Vol. 58, 87-98.

Grègoire, C., and Joesten, P. K. (2006). “Use of Borehole Radar Tomography to Monitor Steam Injection in Fractured Limestone.” Near Surface Geophysics, Vol. 4, No. 6, 355–365.

Gregory, A.E., N.C. Yang, and R.C.Y. Young (1985) “Bridge Inspection by Dynamic Loading Technique,” Proceedings of the ASCE National Convention, Denver, CO.

Haas, C., Weissman, J., and Groll, T. (1999). “Remote Bridge Scour Monitoring – A Prioritization and Implementation Guideline.” Report No. TX-00/0-3970-1, Texas Department of Transportation, Austin, TX.

Haeni, F.P., Halleux, L., Johnson, C.D., and Lane, J.W., (2002). “Detection and Mapping of Fractures and Cavities Using Borehole Radar.” Proceedings Fractured Rock 2002, Denver, CO.

Haeni, F.P., Placzek, G., and Trent, R.E. (1992). “Use of Ground-Penetrating Radar to Investigate Infilled Scour Holes at Bridge Foundations.” Proceedings: Geological Survey of Finland Special Paper 16, Fourth International Conference on Ground Penetrating Radar, Rovaniemi, Finland.

Heisey, J.S., Stokoe, K.H., Hudson, W.R., and Meyer A.H. (1982). "Determination of In Situ Shear Wave Velocity from Spectral Analysis of Surface Waves." Research Report 256-2, Center for Transportation Research, The University of Texas, Austin, TX.

Hertlein, B.H., and Walton, W.H. (2000). “Assessment and Reuse of Old Foundations.” Transportation Research Record 1736, Paper No. 00-0792, Transportation Research Board, Washington, D.C.

Hertlein, B.H., and Walton, W.H. (2007). “Project Experience in Assessment and Reuse of Old Foundations.” Proceedings of Geo-Denver 2007, Denver, CO.

Hiltunen, D.R. and Roth, M.J.S. (2003). “Investigation of Bridge Foundation Sites in Karst Terrane via Multri-Electrode Electrical Resistivity.” 2003 Highway Geophysics NDE Conference. Orlando, FL.

Holt, J.D., and Douglas, R.A. (1994). “A Field Test Procedure for Finding the Overall Lengths of Installed Timber Piles by Dispersive Wave Propagation Methods.” UNC Institute for Transportation Research and Education, North Carolina Department of Transportation, Federal Highway Administration, Washington, D.C.

Holt, J.D., and Hardy, C. (2005). “Dispersive Methods For Unknown Foundations.” Proceedings of Federal Highway Administration 2005 Unknown Foundation Summit, Lakewood, CO.

Hossain, M. S., Khan, M. S., Hossain, J., Kibria, G., and Taufiq, T. (2011). “Evaluation of Unknown Foundation Depth using Different NDT Method.” Journal of Performance of Constructed Facilities, Vol. 27, No. 2, 209-214.

Hsieh, K.H., Halling, M.W., and Barr, P.J. (2006) “Overview of Vibrational Structural Health Monitoring with Representative Case Studies.” Journal of Bridge Engineering, Vol. 11, No. 6, 707-715.

Huang, D., and Chen, L. (2007). “3-D Finite Element Analysis of Parallel Seismic Testing for Integrity Evaluation of In-Service Piles.” Proceedings of Geo-Denver 2007, Denver, CO.

Huisman, J. A., Hubbard, S. S., Redmanc, J. D., and Annanc A. P. (2003). “Measuring Soil Water Content with Ground Penetrating Radar: A Review.” Vadose Zone Journal, Vol. 2, No. 4, 476-491.

Indiana Department of Transportation (INDOT) (2010) “Bridge Inspection Manual.” Paquin, L.A., and Gilliland, K. (eds.), Indiana Department of Transportation, Indianapolis, IN.

Jalinoos, F., Gibson, A., Diehl, J., Hadfield, P. and Gordon, G. (2006). “Determination of Unknown Length of Sheet Piles Using Three Geophysical Logging Methods” 2006 Highway Geophysics NDE Conference, St. Louis, MO.

Jo, C.H., Cha, Y.H., and Choi, J.H. (2003). “A Borehole Magnetic Logging Tool for Estimating Unknown Foundation Depths.” 2003 Highway Geophysics NDE Conference, Orlando, FL.

Jo, C.H., Jung, H.K., and Cho, K.H. (1999). “Borehole Magnetics for the Estimation of Unknown Foundation Pile Depth” (in Korean), Journal of the Korea Institute for Structural Maintenance Inspection, 3, 161-167.

Kase, E. J., and Ross, T. A. (2004). "Seismic Imaging to Characterize Subsurface Ground Conditions in Civil Construction." Proceedings of Geo-Trans 2004. ASCE Special Publication No. 126, 1823-1831.

Kaya, A. (2010). “Artificial Neural Network Study of Observed Pattern of Scour Depth around Bridge Piers.” Computers and Geotechnics, Vol. 37, 413-418.

Khan, M.S. Hossain, M.S., Hossain, J., and Kibria, G. (2012). “Determining Unknown Bridge Foundation Depth by Resistivity Imaging Method.” Proceedings Geo-Congress 2012, Oakland, CA.

Kim, J.H., Cho, S.J., and Yi, M.J. (2004). “Borehole Radar Survey to Explore Limestone Cavities For the Construction of a Highway Bridge.” Exploration Geophysics (Sydney), Vol. 35, No. 1, 80-87.

Kim, J.H., Yi, M.J., Song, Y., Cho, S.-J., Chung, S.-H., and Kim, K.S. (2002). “DC Resistivity Survey to Image Faults Beneath a Riverbed.” Symposium on the Application of Geophysics to Engineering and Environmental Problems (SAGEEP), Las Vegas, NV.

Kramer, S. L. (1996). Geotechnical Earthquake Engineering. Prentice Hall, Upper Saddle River, NJ.

Lagasse, P. F., Richardson, E. V., Schall, J. D., and Price, G. R. (1997). “Instrumentation for Measuring Scour at Bridge Piers and Abutments.” National Cooperative Highway Research Program (NCHRP) Report No. 396, Transportation Research Board (TRB), Washington, D.C.

Lee, J. S. (2003). “High Resolution Geophysical Techniques For Small-Scale Soil Model Testing.” Ph.D. Dissertation, Georgia Institute of Technology, Atlanta, GA.

Lee, J. S., and Santamarina, J. C. (2005). “P-wave reflection imaging.” ASTM Geotechnical Testing Journal, Vol. 28, No. 2, 197–206.

Lee, S., Feng, M., Kwon, S., and Hong, S. (2011). ”Equivalent Modal Damping of Short-Span Bridges Subjected to Strong Motion.” Journal of Bridge Engineering, Vol. 16, No. 2, 316–323.

Lee, T.L., Jeng, D.S., Zhang, G.H., and Hong, J.H. (2007). “Neural Network Modeling for Estimation of Scour Depth around Bridge Piers.” Journal of Hydrodynamics, Ser. B 19, 378-386.

Leng, Z., Al-Qadi, I.L., Baek, J., and Lahouar, S. (2009). “Selection of Antenna Type and Frequency for Pavement Surveys Using Ground Penetrating Radar (GPR)” Paper #09-1541, Transportation Research Board 88th Annual Meeting, Washington, D.C.

Li, Z., Swanson, J., Helmicki, A., and Hunt, V. (2005). ”Modal Contribution Coefficients in Bridge Condition Evaluation.” Journal of Bridge Engineering, Vol. 10, No. 2, 169–178.

Likins, G. E., Webster, S., Saavedra, M. (2004). “Evaluations of Defects and Tomography for CSL.” Proceedings of the Seventh International Conference on the Application of Stress Wave Theory to Piles 2004, Petaling Jaya, Selangor, Malaysia.

Loke, M.H. (2010). Tutorial: 2D and 3D Electric Imaging Surveys. Geoelectric Company.

Loke, M.H., and J.W. Lane, J. (2004). “Inversion of Data from Electrical Resistivity Imaging Surveys in Water Covered Areas.” Exploration Geophysics, Vol. 35, No. 4, 266-71.

Louie, J. N. (2001). “Faster, Better: Shear-Wave Velocity to 100 Meters Depth From Refraction Microtremor Arrays.” Bulletin of the Seismological Society of America, Vol. 91, No. 2, 347-364.

Luke, B. and Stokoe, K.H. (1998). ”Application of SASW Method Underwater.” Journal of Geotechnical and Geoenvironmental Engineering, Vol. 124, No. 6, 523-531.

Lwin, M.M. (2009a) "Additional Guidance for Assessment of Bridges Over Waterways with Unknown Foundations." Additional Guidance for Assessment of Bridges Over Waterways with Unknown Foundations - Unknown Foundations - FHWA. Web. 01 February 2013. <http://www.fhwa.dot.gov/unknownfoundations/091029.cfm>.

Lwin, M.M. (2009b) "Frequently Asked Questions - Bridges Over Waterways with Unknown Foundations.” Frequently Asked Questions - Bridges Over Waterways with Unknown Foundations - Unknown Foundations – FHWA. Web. 01 February 2013. <http://www.fhwa.dot.gov/unknownfoundations/090603.cfm>.

Marosi, K.T., and Hiltunen, D.R. (2004). “Characterization of Spectral Analysis of Surface Waves Shear Wave Velocity Measurement Uncertainty.” Journal of Geotechnical and Geoenvironmental Engineering, Vol. 130, No. 10, 1034-1041.

Maser, K.R., Sanayei, M., Klimkewicz, L., Abedi, H. and Edgers, L. (2001). “Unknown Foundation Identification Using Stiffness Data From Field Measurements.” Paper Number 01-3388, Transportation Research Board (TRB), Washington, D.C.

Maser, K.R., Sanayei, M., Lichtenstein, A., Chase, S.B. (1998). “Determination of Bridge Foundation Type From Structural Response Measurements.” Nondestructive Evaluation Techniques for Aging Infrastructure & Manufacturing, SPIE, 3400, 55-67.

Matasovie, N., and Kavazanjian, E. (1998). “Cyclic Characterization of Landfill Solid Waste.” Journal of Geotechnical and Geoenvironmental Engineering, Vol. 124, No.3, 197-210.

McLemore, S., Zendegui, S., Whiteside, J., Sheppard, M., Gosselin, M., Demir, H., Passe, P., and Hayden, M. (2010). “Unknown Foundation Bridges Pilot Study.” Federal Highway Administration & Florida Department of Transportation.

Mclntire, P. (1991). Nondestructive Testing Handbook - Ultrasonic Testing. 2nd Ed., American Society of Nondestructive Testing, Columbus, OH.

Melville, B.W. and Coleman, S.E. (2000). Bridge Scour, Water Resources Publications, Highlands Ranch, CO.

Mercado, E.J., and O’Neill, M.W. (2000). “Geophysical Survey Techniques to Determine Lengths of Piles and Drilled Shafts.” Use of Geophysical Methods in Construction, Geotechnical Special Publication 108, Proceedings of Sessions of Geo-Denver 2000, Denver, CO.

Meyer, C., Burkard, U., and Barlieb, C. (2007). “Archaeological Questions and Geophysical Solutions: Ground-Penetrating Radar and Induced Polarization Investigations in Munigua, Spain.” Archaeological Prospection, Vol. 14, No. 3, 202-11.

Molnar, S., Cassidy, J.F., Monahan, P.A., and Dosso, S.E. (2007). “Comparison of Geophysical Shear-Wave Velocity Methods.” Ninth Canadian Conference on Earthquake Engineering, Ottawa, Ontario, Canada.

Morse, M.S., Lu, N., Godt, J.W., Revil, A., and Coe J.A. (2012). “Comparison of Soil Thickness in a Zero-Order Basin in the Oregon Coast Range Using a Soil Probe and Electrical Resistivity Tomography.” Journal of Geotechnical and Geoenvironmental Engineering, Vol. 138, No. 12, 1470-1482.

Nazarian, S., and Stokoe, K.H. (1984). "Nondestructive Testing of Pavements Using Surface Waves." Transportation Research Record 993, Transportation Research Board (TRB), Washington, D. C.

Nichols, T. C., King, K. W., Collins, D. S., and Williams, R. A. (1987). "Seismic-Reflection Technique Used to Verify Shallow Rebound Fracture Zones in the Pierre Shale of South Dakota." Canadian Geotechnical Journal, Vol. 25, 369-374.

Niederleithinger, E. and Fritsche, M. (2010). “Measurement of Sheet Pile Length by Pile Integrity Testing and the Parallel Seismic Method.” Symposium on the Application of Geophysics to Engineering and Environmental Problems (SAGEEP), Keystone, CO.

Niederleithinger, E., and Taffe, A. (2006) “Improvement and Validation of Foundation NDT Methods”. Proceedings 2006 NDE Conference on Civil Engineering (NDT-CE), St. Louis, MO.

Niederleithingher, E. (2006). “Numerical Simulation of Non-Destructive Foundation Pile Tests.” European Federation For Non-Destructive Testing (ECNDT) 2006 Conference, Berlin, Germany.

Niederleithingher, E. (2013) “Two In One: Parallel Seismic For Foundation Length Determination and Downhole Seismic For Soil Properties Using a Single Borehole.” Geotechnical and Geophysical Site Characterization 4, Coutinho, R.Q. and Mayne, P.W. (eds.), Taylor & Francis Group, London, United Kingdom.

Novak, M. (1976). "Dynamic Stiffness and Damping of Piles." Canadian Geotechnical Journal, Vol. 11, No. 4, 574-598.

Novak, M. and Aboul-Ella, F. (1978). "Impedance Functions of Piles in Layered Media." Journal of Engineering Mechanics, Vol. 104, No. 3, 643-661.

Olson L.D., Aouad M.F., and Sack D.A. (1998). “Nondestructive Diagnosis of Drilled Shaft Foundations.” Transportation Research Record No. 1633, Transportation Research Board (TRB), Washington, D.C.

Olson, L., Jalinoos, F., and Aouad, M.F. (1998). “Determination of Unknown Subsurface Bridge Foundations: A Summary of the NCHRP 21-5 Interim Report.” Geotechnical Engineering Notebook, Geotechnical Guideline No. 16, Federal Highway Administration, Washington, D.C.

Olson, L.D. (2005a). “Dynamic Bridge Substructure Evaluation and Monitoring.” Publication No. FHWA-RD-03-089, Federal Highway Administration, Washington, D.C.

Olson, L.D. (2005b). “NCHRP 21-5 Research Results: Unknown Subsurface Bridge Foundation Testing for Depth Determination.” Proceedings of Federal Highway Administration 2005 Unknown Foundation Summit, Lakewood, CO.

Olson, L.D., and Aouad, M.F. (2001). “Unknown Subsurface Bridge Foundation Testing, NCHRP Project 21-05(2) Final Report.” National Cooperative Highway Research Program (NCHRP), Transportation Research Board, Washington, D.C.

Parrillo, R., Roberts, R.L., and Haggan, A. (2005). “Bridge Deck Condition Assessment Using Ground Penetrating Radar.” International Bridge Conference 2005, Pittsburgh, PA.

Priddy, K.L., and Keller, P.E. (2005) Artificial Neural Networks: An Introduction. The International Society of Photo-Optical Instrumentation Engineers. Bellingham, WA.

Qiu, T. (2010). “Analytical Solution For Biot Flow Induced Damping in Saturated Soil During Shear Wave Excitations.” Journal of Geotechnical and Geoenvironmental Engineering, Vol. 136, No. 11, 1501–1509.

Rausche, F., Likins, G.E., Hussein, M.H. (1988) “Pile Integrity By Low And High Strain Impacts.” Third International Conference on the Application of Stress-Wave Theory to Piles, Ottawa, Canada, 44-55.

Rinaldi, V., Guichon, M., Ferrero, V., Serrano, C., and Ponti, N. (2006). “Resistivity Survey of the Subsurface Conditions in the Estuary of the Rio de la Plata.” Journal of Geotechnical and Geoenvironmental Engineering, Vol. 132, No. 1, 72-79.

Robinson, B., and Webster, S. (2008). “Successful Testing Methods for Unknown Bridge Foundations.” Proceedings of The Fifth Highway Geophysics NDE Conference, Charlotte, NC.

Sack, D.A., and Olson, L.D. (2009). “Combined Parallel Seismic and Cone Penetrometer Testing of Existing Foundations for Foundation Length and Evaluation” Proceedings 2009 International Foundation Congress and Equipment Expo, Orlando, FL.

Samouëlian, A., Cousin, I., Tabbagh, A., Bruand, A., and Richard, G. (2005). “Electrical Resistivity Survey in Soil Science: A Review.” Soil & Tillage Research, Vol. 83, No. 2, 173-193.

Santamarina, J. C., Klein, K. A., and Fam, M. A. (2001). Soils and waves: Particulate materials behavior, characterization and process monitoring. Wiley, Chicester, U.K.

Sayed, S.M., Sunna, H.N., and Moore, P.R. (2012). “Rational Alternative to Positive Discovery of Pile-Supported Bridges with Unknown Foundation Depth.” Journal of Bridge Engineering, Vol. 17, No. 1, 173-181.

Scott, J.H., and Olson, G.G. (1985). “Three-Component Borehole Magnetometer Probe For Mineral Investigations and Geologic Research.” Transactions of the Society of Professional Well Log Analysts (SPWLA) Annual Logging Symposium, Dallas, TX.

Shaari, A., Millard, S.G. and Bungey, J.H. (2003). “GPR Antenna Medium Coupling Effects: Experimental and 2D FDTD Modeling Results.” BB 85-CD International Symposium, Non-Destructive Testing in Civil Engineering (NDT-CE), Berlin, Germany.

Shahin, M., & Jaksa, M. (2008). “State of the Art of Artificial Neural Networks in Geotechnical Engineering.” Electronic Journal of Geotechnical Engineering, Vol. 8, 1-26.

Sheriff, R. E. and Geldart, L. P. (1995). Exploration Seismology. 2nd Ed., Cambridge University Press, New York, NY.

Shirhole, A. M., and Holt, R. C. (1991). “Planning For A Comprehensive Bridge Safety Program.” Transportation Research Record No. 1290, Transportation Research Board (TRB), National Research Council, Washington, D.C.

Splitstone, D.E., Stonecheck, S.A., Dodson, R.L., and Fuller, J.A. (2010). “Birmingham Bridge Emergency Repairs: Micropile Foundation Retrofit.” Proceedings Geo-Florida 2010, West Palm Beach, FL.

Stegman, B.G., and Holt, J.D. (2000). “Determining the Capacity of Unknown Foundations.” Use of Geophysical Methods in Construction, Geotechnical Special Publication 108, Proceedings of Sessions of Geo-Denver 2000, Denver, CO.

Stein, S., and Sedmera, K. (2006). “Risk-Based Management Guidelines for Scour at Bridges with Unknown Foundations.” Web-Only Document-107, National Cooperative Highway Research Program (NCHRP), Transportation Research Board, Washington, D.C.

Stokoe, K.H., and Woods, R.D. (1972). “In Situ Shear Wave Velocity by Cross-Hole Method.” Journal of the Soil Mechanics and Foundations Division, Vol. 98, No. 5, 443-460.

Stokoe, K.H., Nazarian, S., Rix, G. J., Sanchez-Salinero, I., Sheu, J.C., and Mok, Y.J. (1988). "In Situ Seismic Testing of Hard-to-Sample Soils by Surface Wave Method." Proceedings Earthquake Engineering and Soil Dynamics II, Park City, Utah.

Stokoe, K.H., Wright, S.G., Roesset, J.M., Gauer, R.C., and Sedighi-Manesh, M. (1990). "In-Situ Measurement of Stiffness Profiles in Ocean Bottom Materials Using the SASW Method", 22nd Annual Offshore Technology Conference, Houston, TX.

Tuutti, K. 1982. Corrosion of Steel in Concrete. In: Polder R.B., 2001. Test Methods for on Site Measurement of Resistivity of Concrete-a Rilem Tc-154 Technical Recommendation. Construction and Building Materials 15, 125-31.

Tzanis, A. (2010). “matGPR Release 2: A freeware MATLAB® package for the analysis & interpretation of common and single offset GPR data.” FastTimes, Vol. 15, No. 1, 17-43.

Von Quintus, H.L., Chetana, R., Minchin Jr., R.E., Nazarian, S., Maser, K., and Prowell, B. (2009). “NDT Technology for Quality Assurance of HMA Pavement Construction.” National Cooperative Highway Research Program (NCHRP) Report No. 626, Transportation Research Board, Washington, D.C.

Wardhana, K. & Hadipriono, F.C. (2003). “Analysis of Recent Bridge Failures in the United States.” Journal of Performance of Constructed Facilities, Vol. 17, No. 3, 144-150.

Waters, K. H. (1992). Reflection Seismology: A Tool for Energy Resource Exploration. 3rd Ed., John Wiley & Sons, New York, NY.

Wightman, W.E., Jalinoos, F., Sirles, P., and Hanna, K. (2003) “Application of Geophysical Methods to Highway Related Problems.” Federal Highway Administration, Central Federal Lands Highway Division, Lakewood, CO.

Wright P.D. (1979). "Rangitaiki River Bridge, Te Teko, Pile Length Investigations", Report 5-79/9, Ministry of Works and Development, Central Laboratories, Lower Hutt, New Zealand.

Yang, C., Wang, T., and Liu, H. (2010). “Application of BGPR Logging: Two Case Studies.” Journal of Geotechnical and Geoenvironmental Engineering, Vol. 136, No. 5, 755-758.

Yousefpour, N., Medina-Cetina, Z., Jahedkar, K., Delphia, J., Briaud, J., Hurlebaus, S., Tucker, S., Everett, M. and Arjwech, R. (2011) “Determination of Unknown Foundation of Bridges for Scour Evaluation Using Artificial Neural Networks.” Proceedings of Geo-Frontiers 2011, Dallas, TX.

Yu, X., Fang, J., Zhang, B., Adams, J. and Lin, G. (2007). “Unknown Foundation Testing: A Case Comparison of Different Geophysical Methods.” FMGM 2007: Seventh International Symposium on Field Measurements in Geomechanics, Boston, MA.

Zonge, K., Wynn, J., and Urquhart, S. (2005). “Resistivity, Induced Polarization and Complex Resistivity.” Near-Surface Geophysics, Society of Exploration Geophysics Press, Tulsa, OK.

Zounemat-Kermani, M., Beheshti, A.A., Ataie-Ashtiani, B., and Sabbagh-Yazdi, S.R. (2009). “Estimation of Current-Induced Scour Depth around Pile Groups Using Neural Network and Adaptive Neuro-Fuzzy Inference System.” Applied Soft Computing, Vol. 9, 746-755.